CLIMATIC AND ASSOCIATED CRYOSPHERIC AND HYDROSPHERIC CHANGES ON THE THIRD POLE

EDITED BY: Lei Wang, Chunqiao Song, Tobias Conradt, Mohamed Rasmy and Xiuping Li

PUBLISHED IN: Frontiers in Earth Science

frontiers Research Topics

frontiers

ISSN 1664-8714
ISBN 978-2-88966-582-2
DOI 10.3389/978-2-88966-582-2

About Frontiers

Frontiers is more than just an open-access publisher of scholarly articles: it is a pioneering approach to the world of academia, radically improving the way scholarly research is managed. The grand vision of Frontiers is a world where all people have an equal opportunity to seek, share and generate knowledge. Frontiers provides immediate and permanent online open access to all its publications, but this alone is not enough to realize our grand goals.

Frontiers Journal Series

The Frontiers Journal Series is a multi-tier and interdisciplinary set of open-access, online journals, promising a paradigm shift from the current review, selection and dissemination processes in academic publishing. All Frontiers journals are driven by researchers for researchers; therefore, they constitute a service to the scholarly community. At the same time, the Frontiers Journal Series operates on a revolutionary invention, the tiered publishing system, initially addressing specific communities of scholars, and gradually climbing up to broader public understanding, thus serving the interests of the lay society, too.

Dedication to Quality

Each Frontiers article is a landmark of the highest quality, thanks to genuinely collaborative interactions between authors and review editors, who include some of the world's best academicians. Research must be certified by peers before entering a stream of knowledge that may eventually reach the public - and shape society; therefore, Frontiers only applies the most rigorous and unbiased reviews.
Frontiers revolutionizes research publishing by freely delivering the most outstanding research, evaluated with no bias from both the academic and social point of view. By applying the most advanced information technologies, Frontiers is catapulting scholarly publishing into a new generation.

What are Frontiers Research Topics?

Frontiers Research Topics are very popular trademarks of the Frontiers Journals Series: they are collections of at least ten articles, all centered on a particular subject. With their unique mix of varied contributions from Original Research to Review Articles, Frontiers Research Topics unify the most influential researchers, the latest key findings and historical advances in a hot research area! Find out more on how to host your own Frontiers Research Topic or contribute to one as an author by contacting the Frontiers Editorial Office: frontiersin.org/about/contact

CLIMATIC AND ASSOCIATED CRYOSPHERIC AND HYDROSPHERIC CHANGES ON THE THIRD POLE

Topic Editors:
Lei Wang, Institute of Tibetan Plateau Research (CAS), China
Chunqiao Song, Nanjing Institute of Geography and Limnology (CAS), China
Tobias Conradt, Potsdam Institute for Climate Impact Research (PIK), Germany
Mohamed Rasmy, National Graduate Institute for Policy Studies, Japan
Xiuping Li, Institute of Tibetan Plateau Research (CAS), China

Citation: Wang, L., Song, C., Conradt, T., Rasmy, M., Li, X., eds. (2021). Climatic and Associated Cryospheric and Hydrospheric Changes on the Third Pole. Lausanne: Frontiers Media SA. doi: 10.3389/978-2-88966-582-2

Table of Contents

frontiers in Earth Science

EDITORIAL
published: 03 February 2021
doi: 10.3389/feart.2020.638371

Editorial: Climatic and Associated Cryospheric and Hydrospheric Changes on the Third Pole

Lei Wang[1,2]*, *Chunqiao Song*[3], *Tobias Conradt*[4], *Mohamed Rasmy*[5] and *Xiuping Li*[1]

[1]Institute of Tibetan Plateau Research, Chinese Academy of Sciences (CAS), and CAS Center for Excellence in Tibetan Plateau Earth Sciences, Beijing, China, [2]University of Chinese Academy of Sciences, Beijing, China, [3]Key Laboratory of Watershed Geographic Sciences, Nanjing Institute of Geography and Limnology (CAS), Nanjing, China, [4]Potsdam Institute for Climate Impact Research (PIK), Potsdam, Germany, [5]International Centre for Water Hazard and Risk Management (ICHARM) and National Graduate Institute for Policy Studies, Tokyo, Japan

Keywords: the third pole, river, lake, glacier, snow, permafrost

Editorial on the Research Topic

Climatic and Associated Cryospheric and Hydrospheric Changes on the Third Pole

The Third Pole (TP), known as the "Asian Water Tower," is a high-elevation region of Asia centered on the Tibetan Plateau. The TP is home to around 100,000 km^2 of glaciers, comprising the largest volume of ice outside the Antarctic and Arctic. The TP lies at the headwaters of many large Asian rivers (e.g., Ganges, Brahmaputra, Indus, Yangtze, Yellow, Mekong, Salween, Amu Darya, and Syr Darya) and serves as the main water supply for millions of inhabitants in downstream countries. The high-elevation region is widely covered by snow, glaciers, lakes, permafrost, and seasonally frozen ground, and exerts a profound climatic influence on adjacent and distant regions.

The TP has been getting warmer and wetter during the past several decades, as indicated by significant air temperature rises, and spatiotemporally, heterogeneous precipitation increases–particularly since the 1980s. The TP warming, which is above the global average rate, could be associated with variations in precipitation and decreases in snow depth, extent, and persistence. The warming and wetting climate has been closely associated with glacier retreat, lake expansion, permafrost thawing, and thickening of the active layers over the permafrost.

This research topic aims to cover recent climate changes over the TP and its associated impacts on the cryosphere and hydrosphere. The studies address changes in surface air temperature, precipitation, seasonal snow cover, mountain glaciers, permafrost, lakes, and river runoff, and examine how these changes are linked to climate change across different spatial scales (from a catchment to the whole TP). Results from these studies will improve our understanding of cryosphere–hydrosphere–atmosphere interactions over the TP.

This research topic includes three comprehensive reviews in TP cryohydrology (one about the discipline as a system, and two about permafrost), which describe research progress in these topics and provide insightful perspectives on the recent advancement of *in situ* observations, satellite remote sensing, as well as process-based modeling. This is a multidisciplinary special issue bridging the gaps in climatology, hydrology, cryosphere, geochemistry, and remote sensing sciences.

Dai et al. suggest that a large alpine lake (Lake Nam Co.) can be an important regulator of regional climate (e.g., precipitation) over the TP, based on the WRF (weather research forecasting model) sensitivity experiments for the year 2008. Their study indicates that the lake cooling effect can cause a reduction in the over-lake summer precipitation by 45–70%, while the lake warming effect can enhance the autumn precipitation by 60% over the lake and surroundings.

OPEN ACCESS

Edited and reviewed by:
Nick Van De Giesen,
Delft University of Technology,
Netherlands

***Correspondence:**
Lei Wang
wanglei@itpcas.ac.cn

Specialty section:
This article was submitted to Hydrosphere, a section of the journal Frontiers in Earth Science

Received: *06 December 2020*
Accepted: *30 December 2020*
Published: *03 February 2021*

Citation:
Wang L, Song C, Conradt T, Rasmy M and Li X (2021) Editorial: Climatic and Associated Cryospheric and Hydrospheric Changes on the Third Pole. Front. Earth Sci. 8:638371. doi: 10.3389/feart.2020.638371

Wood et al. demonstrate that glacier retreat and snowpack loss threaten high-altitude communities that rely upon seasonal melting water for domestic water resources. They indicate that 34–90% of water comes from ice and snow melt during the dry pre-monsoon season, accounting for an average discharge contribution of 65% in the Khumbu Valley, Nepal (a highly glaciated catchment with elevations ranging from 2,000 to 8,848 m). With as much as two-thirds of the dry-season domestic water supply at risk, the communities of the Khumbu Valley are extremely vulnerable to the cryospheric effects of climate change.

Chevallier et al. examine the headwater geochemistry of Mount Everest (Upper Dudh Koshi River, Nepal). They aim to address three parallel topics: 1) the dynamics of the water geochemistry, major ions, and trace elements; 2) the stable water isotopes of precipitation and rivers; and 3) water use by the inhabitants.

Chen et al. illustrate an atmospheric bridge that connects the Barents Sea ice and snow depth in the midwest Tibetan Plateau. They reveal that a positive anomaly of the Barents Sea ice can enhance the meridional air temperature gradient to the south and hence accelerate the polar front westerly jet. Consequently, an anomalous Rossby wave propagating upward and equatorward is generated, resulting in a dipole pattern of the atmospheric circulation anomaly over the polar region and Eurasian continent.

Different from previous studies on the TP snow using coarse-resolution microwave data (25 km × 25 km), Smith and Bookhagen assess multi-temporal snow–volume trends in the TP from 1987 to 2016 with high-resolution (3.125 km × 3.125 km) passive microwave data from the special sensor microwave imager (SSM/I) instrument family at refined spatial details. They find that changes in the high percentile monthly snow–water volume exhibit steeper trends than changes in low percentile snow–water volume, which suggests a reduction in the frequency of high snow–water volumes in much of TP. Regions with positive snow–water storage trends generally correspond to regions of positive glacier mass balances.

Under accelerated warming on the TP, permafrost degradation is dramatically altering regional hydrological regimes. Jiang et al. review the progress and challenges in studying the TP permafrost, with a focus on remote sensing approach, while Gao et al. review the state-of-the-art understanding of permafrost hydrological processes in hydrological models of varying complexity. They both emphasize the importance of long-term field measurements and recommend the integration of satellite remote sensing retrievals together with process-based permafrost-hydrology models to deepen the understanding of permafrost hydrological processes and to enhance the ability to predict the future response of permafrost hydrology to climate change.

Finally, Ding et al. review the evolution of the concept of cryohydrology, and analyzes its hydrological basis and discipline system. Three points are concluded in this study. 1) Cryohydrology was developed based on traditional hydrology for a single element of the cryosphere, focusing on the hydrological functions of the cryosphere and their impacts on the water cycle and water supply to other spheres. 2) The hydrological function of cryohydrology is further subdivided into water conservation, runoff recharge and hydrological regulation. 3) The key research issues of cryohydrology include the principal research method, hydrological process, watershed function, and regional impact. Cryohydrology aims to deepen the theoretical and cognitive levels of the associated mechanisms and processes, to accurately quantify the hydrological functions of the basin, and to promote the understanding of the ecological and environmental impacts of the cryosphere.

AUTHOR CONTRIBUTIONS

All authors listed have made a substantial, direct, and intellectual contribution to the work, and approved it for publication.

FUNDING

This study was supported by the National Natural Science Foundation of China (Grant Nos. 91747201 and 41971403), the Second Tibetan Plateau Scientific Expedition and Research Program (2019QZKK020604), and the "Strategic Priority Research Program" of the Chinese Academy of Sciences (XDA20060202 and XDA23100102).

ACKNOWLEDGMENTS

We warmly appreciate the Editorial Board and Editorial Office of Frontiers in Earth Science for the kind invitation to edit this Research Topic and their timely support during organizing and managing the topic.

Conflict of Interest: The authors declare that the research was conducted in the absence of any commercial or financial relationships that could be construed as a potential conflict of interest.

frontiers in Earth Science

ORIGINAL RESEARCH
published: 29 April 2020
doi: 10.3389/feart.2020.00128

Melting Himalayan Glaciers Threaten Domestic Water Resources in the Mount Everest Region, Nepal

Leah R. Wood[1], Klaus Neumann[2], Kirsten N. Nicholson[2], Broxton W. Bird[1], Carolyn B. Dowling[2] and Subodh Sharma[3]*

[1] Department of Earth Sciences, Indiana University-Purdue University Indianapolis, Indianapolis, IN, United States, [2] Department of Environment, Geology, and Natural Resources, Ball State University, Muncie, IN, United States, [3] Department of Environmental Science and Engineering, Kathmandu University, Kathmandu, Nepal

Retreating glaciers and snowpack loss threaten high-altitude communities that rely upon seasonal melt for domestic water resources. But the extent to which such communities are vulnerable is not yet understood, largely because melt contribution to water supplies is rarely quantified at the catchment scale. The Khumbu Valley, Nepal is a highly glaciated catchment with elevations ranging from 2,000 to 8,848 m above sea level, where more than 80% of annual precipitation falls during the summer monsoon from June to September. Samples were collected from the rivers, tributaries, springs, and taps along the major trekking route between Lukla and Everest Base Camp in the pre-monsoon seasons of 2016–2017. Sources were chosen based upon their use by the communities for drinking, cooking, bathing, and washing, so the sample suite is representative of the local domestic water supply. In addition, meltwater samples were collected directly from the base of the Khumbu Glacier, and several rain samples were collected throughout the study site. Meltwater contribution was estimated from $\delta^{18}O$ isotopic data using a two-component mixing model with the Khumbu glacial melt and pre-monsoon rain as endmembers. Results indicate between 34 and 90% of water comes from melt during the dry, pre-monsoon season, with an average meltwater contribution of 65%. With as much as two-thirds of the dry-season domestic water supply at risk, the communities of the Khumbu Valley are extremely vulnerable to the effects of climate change as glaciers retreat and snowpack declines.

Keywords: climate change, drinking water, meltwater, glaciers, isotopes, two-component mixing model, Himalayas, high-altitude

OPEN ACCESS

Edited by:
Chunqiao Song, Nanjing Institute of Geography and Limnology (CAS), China

Reviewed by:
Qianggong Zhang, Institute of Tibetan Plateau Research (CAS), China
Xander Wang, University of Prince Edward Island, Canada

****Correspondence:***
Leah R. Wood
leahwood@iupui.edu

Specialty section:
This article was submitted to Interdisciplinary Climate Studies, a section of the journal Frontiers in Earth Science

Received: *13 January 2020*
Accepted: *03 April 2020*
Published: *29 April 2020*

Citation:
Wood LR, Neumann K, Nicholson KN, Bird BW, Dowling CB and Sharma S (2020) Melting Himalayan Glaciers Threaten Domestic Water Resources in the Mount Everest Region, Nepal. Front. Earth Sci. 8:128. doi: 10.3389/feart.2020.00128

INTRODUCTION

High-elevation communities are some of the most susceptible to the effects of climate change (Salerno et al., 2008), and a recent report concluded that even if global warming is kept below 1.5°C, a third of the glaciers in the Hindu Kush-Himalayan region and more than half of those in the eastern Himalaya will likely be lost by the end of this century (Bolch et al., 2019). Yet significant questions remain regarding the contribution of melt from glaciers and snow to water resources in mountain regions (Immerzeel et al., 2010; Bocchiola et al., 2011). Answering them requires catchment-scale study in order to quantify the role of meltwater and gauge the vulnerability of these communities to the effects of climate change (La Frenierre and Mark, 2014).

The sensitivity and vulnerability of high-altitude regions to the effects of a shifting climate make them ideal long-term sites for monitoring climate change (Salerno et al., 2008). The Hindu Kush-Himalayan Region and Tibetan Plateau are often referred to as the Earth's "Third Pole" (e.g., Yao et al., 2012) as they contain the greatest number of glaciers outside of polar regions. They are also referred to as the "Water Tower of Asia" (e.g., Viviroli et al., 2007), because they are the headwaters for some of the continent's largest rivers, including the Indus, Ganges, Brahmaputra, Yangtze, and Yellow rivers.

Previous related studies from the Himalaya have primarily focused on river discharge, rather than specifically sampling water sources that are used for domestic purposes including drinking, cooking, bathing, cleaning, laundry, and other daily necessities by local communities (e.g., Balestrini et al., 2014; Wilson et al., 2016); or they have estimated meltwater contributions at large, basin scales (e.g., Immerzeel et al., 2010). Analysis of surface waters by Balestrini et al. (2014) in the upper Khumbu Valley revealed relatively low ionic concentrations and indicated that surface water composition did not entirely reflect precipitation composition. This suggests that another source, or sources, made significant contributions to the local water resources. Despite the modest contribution of meltwater to total Ganges River Basin discharge, high-altitude communities may rely much more heavily on seasonal melting, and annual recharge of glaciers, snow, and ice since regional precipitation decreases with increasing altitude (Asahi, 2010). Similar work in the Langtang Basin, a comparable catchment *c.* 100 km west of the Khumbu Valley, concluded that meltwater dominated the hydrograph outside of the monsoon season (Wilson et al., 2016).

Likewise, our research concludes that in the Khumbu Valley, Nepal, up to two-thirds of water comes from glacial and snow melt during the dry season. This indicates that communities there are especially vulnerable to the retreat and eventual disappearance of glaciers and permanent snow fields in response to continued warming trends. By developing a baseline of the hydrologic cycle for the Khumbu Valley, this study benefits future monitoring of these critical water resources and provides a snapshot of pre-monsoon domestic water resources in the Khumbu Valley against which the effects of climate change can be observed. Predicting climate-driven changes before they occur, and quantifying how the contribution of meltwater to domestic water resources will change will allow the high-altitude Nepali communities to be better prepared. In addition, the approach implemented in this project may be applied to other high-altitude environments where snow and glaciers contribute to valuable water resources.

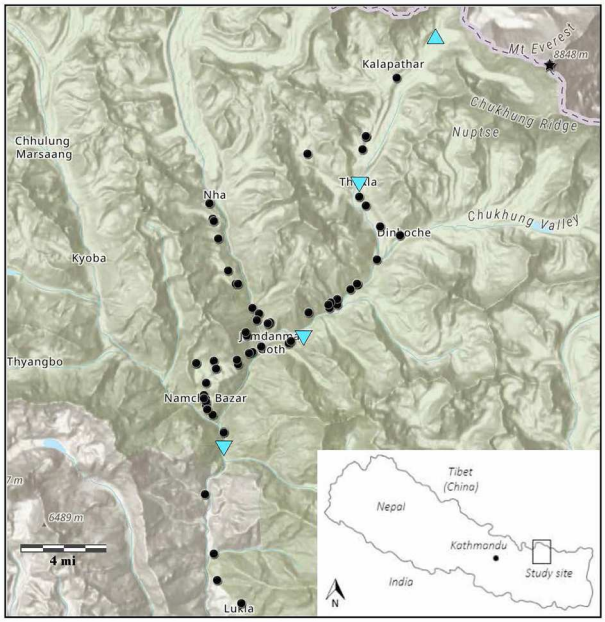

FIGURE 1 | Map of Khumbu Valley; point-up triangle represents glacial melt sample; point-down triangles represent rain samples; circles represent all other sampling locations; inset map shows location of study area within Nepal.

MATERIALS AND METHODS

Site Background

The Khumbu Valley is located in the upper catchment of the Dudh Kosi river basin, in the Sagarmatha National Park, and Buffer Zone (SNPBZ) of northeastern Nepal, ∼140 km northeast of the capital city of Kathmandu (**Figure 1**). The park was established in 1976 (Panzeri et al., 2013), and it was designated a World Heritage Site in 1979 due to its unique geological, ecological, cultural, and aesthetic value. In 2002, a 275 km^2 Buffer Zone was added on the southern border of the 1,148 km^2 park to further protect the region (UNESCO [United Nations Educational Scientific and Cultural Organization], 2009). The Dudh Kosi river drains the Mt. Everest Massif to the south, which makes it the highest-elevation river system in the world, along with the Yarlung Tsangpo river in Tibet, which drains the Mt. Everest Massif to the north. The Dudh Kosi river begins near the Gokyo lakes in the western portion of the study area, flows southward past Namche Bazar, and then west of Lukla and out of the study area. The Imja Khola and Lobuche rivers originate at the glaciers of the eastern portion of the study site, including the Khumbu and Imja glaciers. They flow southward, joining the Dudh Kosi river below Phortse. The Dudh Kosi river is one of the seven tributaries of the Sapta Koshi river, which is part of the greater Ganges river system (Xiang et al., 2018). Elevations within the study area ranges from *c.* 2,000 m where the Dudh Kosi River flows southward out of the Buffer Zone just southwest of Lukla to 8,848 m above sea level (asl) at the summit of Mt. Everest on the northern border of the park.

The climate of the Khumbu Valley is temperate, characterized by strong seasonality with dry, cold winters and warm, wet summers (Nicholson et al., 2016). Due to its location within the Subtropical Asian Monsoon zone, more than 80% of annual precipitation to the region falls between the months of June and September (Mani, 1981; Barry and Chorley, 1982; Byers, 2005; Salerno et al., 2008). This precipitation is delivered via the South Asian Monsoon System, which carries warm, moist air out of the south, or southwest from the Bay of Bengal across the Indian

Subcontinent and as far north as the Tibetan Plateau (Müller, 1980; Salerno et al., 2015).

Regional vegetation varies with altitude. The majority of samples were collected below the local tree line at *c.* 4,000 m asl. The landscape here is dominated by lush rhododendron forests punctuated by small, terraced, subsistence agricultural fields. Above the tree line, much of the ground is bare, and juniper and other hardy shrubs replace rhododendrons. From *c.* 5,500–6,000 m asl, only low-growing mats of cushion plants thrive. The nival zone above *c.* 6,000 m asl is glaciated or snow-covered for much of the year and vegetation is extremely limited. Local fauna includes the snow leopard, musk deer, and red panda, all of which are either endangered or threatened species (Van Geldern and Barth, 2012; Balestrini et al., 2014).

Despite concerns since the 1970s regarding the tourism-related pollution increase in the region, the first systematic study of drinking water quality in the Khumbu Valley was not undertaken until 2014. In that year, Nicholson et al. (2016) sampled community water sources with a focus on fecal contamination of drinking water. The study concluded that there were higher counts of *E. coli* and other coliform bacteria associated with fecal contamination in samples collected from lower elevation, higher population areas, and that surface water was more highly contaminated than groundwater-fed springs. Accurate census data for the region are scarce; however, recent estimates place the population of the Khumbu Valley between 3,500 and 6,000 people (e.g., Byers, 2005; UNESCO [United Nations Educational Scientific and Cultural Organization], 2009; Nicholson et al., 2016).

The Khumbu Valley, and the SNPBZ in general, is considered a data-poor region. The paucity of research is largely due to the location's geographic remoteness and ruggedness; historically, it has been difficult and expensive to access (Salerno et al., 2013). Increasing tourism over the past few decades has boosted the local economy and infrastructure, making access to the region for scientific endeavors more feasible, and there has been a marked increase in published research of the region since the turn of the century, and this study represents the first to attempt to evaluate local vulnerability to climate change with respect to domestic water resources.

Objectives

The objectives of this study were to: (1) collect a suite of samples representing community domestic water supplies in the Khumbu Valley as well as the sources that contribute to them, (2) to analyze the samples for $\delta^{18}O$ and $\delta^{2}H$ isotope values, and (3) to identify source endmembers and estimate the overall contribution of melt from glaciers, snow, and ice (hereafter "meltwater" or "melt") vs. precipitation using a two-component mixing equation. The results have been used to evaluate the vulnerability of community domestic water resources in the Khumbu Valley to the observed and anticipated effects of climate change.

Methods

Two field campaigns were conducted: the first in spring 2016, when samples were collected between April 21 and May 06; and the second in spring 2017, when samples were collected between April 21 and May 05. These campaigns took place during the dry, pre-monsoon season. Sampling was carried out within the Khumbu Valley along the main Everest Base Camp Trekking Route between the town of Lukla and Everest Base Camp. Sampling locations included large rivers, small streams, natural springs, numerous community standpipes, and several indoor taps Locations were selected to reflect community drinking water sources—primarily standpipes and taps—as well as the waterways that supply them—rivers, tributaries, and springs. Collectively, the samples represent the water used for drinking by local residents and tourists alike. In addition, a glacial melt sample was taken directly from the terminus of the Khumbu Glacier in 2016, and precipitation samples were collected on April 22, April 28, and May 1, 2017 (**Figure 1**).

Samples for ion analysis were collected with a syringe, then passed through a 0.45-μm filter into pre-washed 60 or 125-mL high-density polyethylene bottles with screw-on polypropylene caps. Bottles were then sealed with paraffin sealing film. Samples for isotope analysis were collected, unfiltered, by syringe, or directly from the water source in 2-mL glass vials with plastic screw-on caps with no visible bubbles or headspace, then sealed with paraffin sealing film.

Temperature, pH, conductivity, and total dissolved solids (TDS) were measured in the field via Fisher Scientific Accumet AP85 portable waterproof meter. When possible, the instrument probes were inserted directly in the uncollected water for measurements. In case of insufficient flow—at standpipes and taps, for example—it was necessary to collect whole water in a plastic 1-L bottle into which the probes were inserted.

Ion Analysis

Analysis for cations (Ca^{2+}, K^{+}, Li^{+}, Mg^{2+}, Na^{+}, and NH_4^{+}) was conducted at Ball State University via ion chromatography (IC) using a Dionex ICS-2000 with a Dionex AS40 Automated Sampler and processed through Chromeleon Chromatography Data System software. Analysis for anions (Cl^{-}, NO_3^{-}, and SO_4^{2-}) was conducted at Ball State University via IC using a Dionex ICS-5000+ with a Dionex EGC for potassium hydroxide eluent generation, a Dionex IonPac AS15 analytical column, and an Anion Self-Regenerating Suppressor 300. HCO_3^{-} concentrations were calculated at Ball State University using AquaChem groundwater software. All measured and calculated ion concentrations are reported in μEq/L.

Isotope Analysis

$\delta^{18}O$ and $\delta^{2}H$ isotopes were measured directly from water vapor using infrared spectroscopy (Kerstel et al., 1999; Kerstel and Gianfrani, 2008) at Indiana University Purdue University Indianapolis using a Picarro L2130-i Cavity Ringdown Spectrometer according to the methods described by Van Geldern and Barth (2012).

Isotope values are reported in standard delta notation (δ) in per mille units (‰), comparing heavy-to-light isotope ratios in the sample with the reference, Vienna Standard Mean Ocean

Water (VSMOW). The following equations are used:

$$\delta^{18}O = \left(\frac{(^{18}O/^{16}O)_{sample}}{(^{18}O/^{16}O)_{VSMOW}} - 1 \right) \cdot 1{,}000‰$$

$$\delta^{2}H = \left(\frac{(^{2}H/^{1}H)_{sample}}{(^{2}H/^{1}H)_{VSMOW}} - 1 \right) \cdot 1{,}000‰$$

The VSMOW abundance ratio for $^{2}H/^{1}H$ is 1.5575×10^{-4} and 2.0052×10^{-3} for $^{18}O/^{16}O$ (Clark, 2015). The global meteoric water line (GMWL), defined by Craig (1961) is a linear equation expressing the global average linear relationship between $\delta^{18}O$ and $\delta^{2}H$ ratios in terrestrial waters:

$$\delta^{18}O = 8 \cdot \delta^{2}H + 10‰$$

where 8 is the slope of the line and 10‰ is the deuterium intercept, or value of $\delta^{2}H$ at $\delta^{18}O = 0$. A local meteoric water line (LMWL) can be defined by the same equation for a set of samples according to $\delta^{18}O$ and $\delta^{2}H$ values, slope, and deuterium intercept. The intercept of any given sample, termed *deuterium excess* by Dansgaard (1964), is calculated according to the following equation:

$$d = \delta^{2}H - 8 \cdot \delta^{18}O$$

For the purposes of this study, deuterium excess is calculated using Dansgaard's equation, and all LMWLs are compared to the GMWL observed by Craig (1961).

Estimating Meltwater Contribution

Meltwater contribution estimates were calculated using the following two-component mixing equation:

$$x_m = \frac{c_s - c_p}{c_m - c_p} \cdot 100$$

where x_m is the contribution of meltwater to the sample in percent, c_s is the $\delta^{18}O$ value of the sample, c_p is the $\delta^{18}O$ value of the precipitation endmember, and c_m is the $\delta^{18}O$ value of the melt endmember (Mark and Seltzer, 2003).

RESULTS AND DISCUSSION

Water Chemistry

Ion analysis revealed domestic water resources in the study site were primarily of the calcium-bicarbonate water-type. HCO_3^- was the most abundant ion overall, with an average concentration of 234.12 μEq/L. SO_4^{2-} exceeds HCO_3^- as the dominant anion in only six samples. The average SO_4^{2-} concentration is 84.56 μEq/L. Ca^{2+} is the dominant cation in the majority of samples, with an average concentration of 207.41 μEq/L. Na^+ is the second-most abundant cation, with an average concentration of 71.69 μEq/L. Overall, the following trends are observed regarding concentrations of cations and anions, respectively: $Ca^{2+} > Na^+ > Mg^{2+} > K^+ > NH_4^+ > Li^+$; $HCO_3^- > SO_4^{2-} > Cl^- > NO_3^+$ (**Table 1**).

All samples were undersaturated with respect to any mineral. Ionic strength ranged from 0.14 to 0.91 mM/L with an average of 0.50 mM/L. Considering the abundant feldspar minerals in the lithology of the study site, the relatively low concentrations of Ca^{2+}, Na^+, and K^+ may be indicative of a short groundwater residence time and little water-rock interaction (Ako et al., 2011; Nganje et al., 2017). And although the dissolution-resistant local metamorphic bedrock would not be expected to drastically increase ionic strength even given substantial groundwater residence time, samples collected from springs were chemically indistinguishable from other surface water samples. These observations collectively suggest there may be relatively little water-rock interaction within the region.

Local Meteoric Water Lines

All collected waters plot close to the Global Meteoric Water Line (GMWL; **Figure 2**), and the Local meteoric water line (LMWL) for 2017 is defined as follows:

$$\delta^{18}O = 8.27 \cdot \delta^{2}H + 12.7‰$$

The deuterium excess of 12.7‰ is slightly higher than for the GMWL (10‰), and is similar to the results of Balestrini et al. (2014) and Florea et al. (2017). This increase suggests a slightly greater kinetic component to primary evaporation than the global mean. This is consistent with the northward migration of the thermal equator with the Intertropical Convergence Zone (ITCZ) during the months of April and May (Kump et al., 2014). This is only a slight observed deviation from the deuterium excess of the GMWL, however, and it would be anticipated to be stronger during the warmer monsoon months, and weaker during the cooler winter months.

In **Figure 2**, the sample that is most depleted in heavy oxygen and hydrogen isotopes compared with VSMOW has a $\delta^{18}O$ value of −20.27‰ and a $\delta^{2}H$ value of −152.46‰. This sample was collected directly from the base of the Khumbu Glacier at Everest Base Camp during the 2016 field campaign, and it serves as the melt endmember for the purposes of this study. The three precipitation samples collected during the 2017 campaign are the most enriched in the heavy isotopes with $\delta^{18}O$ values of at least −2.09‰ and $\delta^{2}H$ values of at least 2.19‰. Excluding the precipitation samples and meltwater endmember, all samples fell between a range of −8.25 to −18.39‰ for $\delta^{18}O$ and −52.37 to −135.44‰ for $\delta^{2}H$. Within these samples, there was no clear trend based upon source. Specifically, there was no characteristic isotopic signature for samples sourced from springs vs. streams. Because of this, groundwater is not included as an endmember in this study. Considering the high topographic relief and dense metamorphic rocks of the study site, the lack of a groundwater signal from springs is not surprising. The water produced by springs is likely interflow with a short residence time below the surface. This is not to say that there is no groundwater in the region, but rather that deep groundwater does not seem to be a significant component in current domestic water resources.

Contribution of Meltwater

The estimated melt contribution to each sample was calculated based on isotopic composition using a two-component mixing equation with meltwater from the Khumbu Glacier and local

TABLE 1 | Summary of results from ion analysis; all concentrations expressed in μEq/L; <DL indicates concentration was below instrument detection limit.

	Ca^{2+}	Na^{+}	Mg^{2+}	K^{+}	NH_4^{+}	Li^{+}	HCO_3^{-}	SO_4^{2-}	Cl^{-}	NO_3^{-}
Min.	31.54	10.46	5.32	4.07	<DL	<DL	49.21	1.14	1.16	<DL
Max.	515.22	201.97	86.87	31.4	5.91	0.76	442.2	359.11	32.18	62.25
Range	483.68	191.5	81.55	27.33	5.91	0.76	392.99	357.96	31.03	62.25
Avg.	207.41	71.69	39.43	14.61	0.66	0.07	234.12	84.56	7.44	6.97
Stdev.	137.65	40.15	18.18	7.51	0.98	0.14	106.2	81.24	7.77	13.12

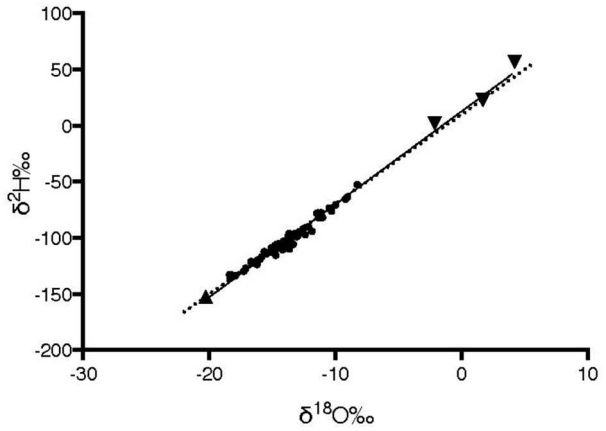

FIGURE 2 | Local meteoric water line, represented by solid line, calculated from isotopic ratios of collected samples; LMWL is $\delta^{18}O = 8.27\ \delta^{2}H + 12.7‰$; point-up triangle represents glacial melt sample; point-down triangles represent rain samples; circles represent all other sampling locations; global meteoric water line ($\delta^{18}O = 8\ \delta^{2}H + 10‰$) is represented by dotted line.

precipitation as endmembers (Mark and Seltzer, 2003). The glacial melt sample was collected during the 2016 field campaign directly from the base of the Khumbu Glacier. The precipitation samples were collected during the 2017 field campaign from three separate rain events at a range of latitudes and altitudes. The most depleted of the precipitation samples is used as the precipitation endmember since it is known to be 100% rain. Using the other precipitation samples as endmembers or averaging them would skew the calculations so that the most depleted precipitation sample would appear to be <100% precipitation. If future work yields pre-monsoon-season rain samples more depleted than those in this study, the upper endmember would be further constrained, facilitating more accurate melt contribution estimates. Likewise, more enriched meltwater samples would constrain the lower endmember and alter melt contribution estimates. The use of rain samples from the pre-monsoon season assumes that only recent rain contributes to the rain component of samples. This is likely true as long as the residence time for surface water in the catchment is short. The majority of annual rainfall to the catchment occurs during the summer monsoon and is much more depleted in $\delta^{18}O$ than pre-monsoon rain. But this water likely moves through the catchment very quickly, and therefore doesn't significantly contribute to pre-monsoon-season samples. Future work should focus on collecting additional rain and melt samples to improve endmember data quality as well as verifying or disproving the assumption that only pre-monsoon season rain contributes to the pre-monsoon season water supply.

Melt contribution estimates ranged from *c.* 34–90% (10–66% rain) with an average contribution of *c.* 65% (35% rain; **Table S1**). This far exceeds estimates that meltwater contributes *c.* 10% to the greater Ganges River Basin, the majority (*c.* 85%) of which area is located below 2,000 m asl, and is therefore supplied primarily by monsoonal precipitation rather than meltwater (Immerzeel et al., 2010). **Figure 3** shows a strong positive relationship between altitude and meltwater contribution regardless of source. This relationship indicates that vulnerability to water scarcity from climate change increases with altitude.

For the purposes of this study, there is no differentiation between melt from glaciers and that from other snow and ice. Because they are derived from the same vapor bodies, snowmelt from a mountain peak should isotopically match glacial melt from an adjacent valley, with any slight differences between them due to fractionation during melting. Analysis of fresh snow from the northeast face of Mt. Everest yielded isotopic values indistinguishable from those of Khumbu Glacier melt from this study (Kang et al., 2002). Furthermore, a study from the Eastern Himalaya determined glacial samples were isotopically similar to fresh snow samples from the same glacier (Nijampurkar and Bhandari, 1984). Likewise, a more recent study from the Bhutan Himalaya found that $\delta^{18}O$ values for glacier ice, glacial outflow, and snow were all similar (Williams et al., 2016). Because glacial melt can only contribute to a sample if there is a glacier upslope of the sampling site, the contribution of melt from snow vs. glaciers can be rudimentarily evaluated by "looking uphill." The region's glaciers are located primarily in valley bottoms at elevations higher than 4,500 m. As a general rule, melt contribution from samples collected downstream of these locations, such as river samples, can be assumed to have a significant glacial component. On the other hand, hillside springs and small streams do not generally have glaciers above them, so the melt component from those samples must be assumed to derive from snowmelt from the nival zone.

Implications for Climate Change Vulnerability

The SNPBZ is known for being the location of Mt. Everest. The Himalayas, containing the world's largest freshwater reserve outside of polar regions and known as Earth's "Third Pole" and the "Water Tower of Asia," are particularly sensitive and

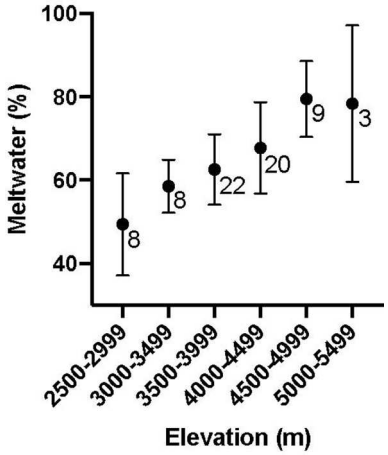

FIGURE 3 | Comparison of the relationship between percent of meltwater contribution and elevation; for each elevation group, circle represents mean, bars represent one standard deviation, and number represents number of samples.

vulnerable to climate change. The first study of glaciers in the region was conducted by Müller in 1956, just 3 years after the first successful ascent of Mt. Everest (Müller, 1959). In 2007, Bajracharya et al. (2011) mapped 3,808 glaciers across Nepal. They concluded that glaciers at elevations below 5,800 m above sea level are retreating, and in general, the number of individual glaciers in Nepal is increasing as larger ones break up. According to Salerno et al. (2008), there are *c.* 29 glaciers in the Sagarmatha National Park, which are primarily summer accumulation, debris-covered (D-type) "black glaciers." The melting and retreat of these glaciers, which feed the Indus, Ganges, Brahmaputra, Yangtze, and Yellow Rivers, has the potential to impact over 1.4 billion people. Nearly half a billion live in the Ganges River Basin alone, where snow and glacial melt are estimated to contribute 10% of the basin's total discharge (Immerzeel et al., 2010).

Despite the significance of the Himalayan glaciers, catchment scale studies are almost non-existent. Previous studies from the Himalaya have primarily focused on river discharge (e.g., Balestrini et al., 2014; Wilson et al., 2016) and the large basin scale (e.g., Immerzeel et al., 2010). Yet, catchment-scale studies quantifying the role of melt are critical to assessing regional variability and vulnerability (La Frenierre and Mark, 2014). The results of this study, using geochemistry and $\delta^{18}O$ and $\delta^{2}H$ isotope analyses, indicate a reliance on meltwater to supply domestic drinking water sources in the Khumbu Valley. An average of 65% of the volume of domestic water resources in the Khumbu Valley during the dry, pre-monsoon season, can be attributed to meltwater contribution, with the remaining 35% coming from rain. The results are supported by work in the Langtang Valley where Wilson et al. (2016) conclude that meltwater dominates the hydrograph throughout most of the year, except during the monsoon season when precipitation dominates. The similarities between the Langtang Valley and the Khumbu Valley suggests that meltwater plays a significant role for the streams in the Khumbu region.

Given these results, along with the observation that Himalayan glaciers are rapidly receding (Bolch et al., 2019), high-altitude communities within the SNPBZ are likely to be particularly vulnerable to climate change and receding glaciers; extrapolating these results indicates that all high-altitude communities in the Himalaya may also be vulnerable. In addition, the low ionic strength of the samples in this study suggest little water-rock interaction, an indication that there is no long-term reservoir to buffer communities against even short-term shortages of water from precipitation or melt. In the long-term these results indicate that surface water availability during the pre-monsoon season will increase as rapid melting of alpine glaciers and snow contributes to streamflow in the short-term future, followed by eventual pre-monsoon water scarcity as the glaciers and permanent snow disappear. Because the samples used in this study were collected in 2016 and 2017, they reflect the relative contribution of meltwater and rain at that time. As global temperatures continue to rise (NOAA National Centers for Environmental Information, 2020), the meltwater contributions presented here can reasonably be considered minimum estimates, making these results even more important for local communities' efforts in resource management in the face of continued warming. The contribution of meltwater to community water supply in the Khumbu Valley and other high-altitude Himalayan catchments should continue to be monitored in order to refine and update meltwater estimates. Although not directly addressed in this study, future research may provide a detailed long-term timeline of Khumbu Valley domestic water supply through modeling of changing glacier, snow, and monsoon dynamics.

This study highlights the importance of understanding the high-altitude catchment basins, in order to predict the impact of climate change at both high and low altitudes in a river basin. Understanding climate-driven changes before they occur and quantifying the contribution of meltwater to domestic water resources will allow the high-altitude Nepali communities to be better prepared. These concepts may be applied to other high-altitude environments where snow and glaciers contribute to valuable water resources. In addition, the implications of this research can be used for long-term planning and climate hazard mitigation throughout the entire region.

SUMMARY OF CONCLUSIONS

(1) Domestic water resources in the Khumbu Valley are of low ionic strength and are primarily of the calcium-bicarbonate water- type, and less commonly, calcium-sulfate, sodium-bicarbonate, and sodium-sulfate.

(2) The LMWL calculated from 2016 to 2017 isotopic data is $\delta^{18}O = 8.27\ \delta^{2}H + 12.7‰$. Long- term monitoring will yield a more accurate LMWL.

(3) A two-component mixing equation using meltwater from the Khumbu Glacier and local precipitation as endmembers reveals that meltwater contributes an average of 65% of the

volume of domestic water resources in the Khumbu Valley during the dry, pre-monsoon season, and there is a strong positive correlation between altitude and meltwater contribution.

(4) It is likely that meltwater contribution to pre-monsoon domestic water resources in the Khumbu Valley will increase in the short-term future as glaciers, snow, and ice melt, and that water scarcity will follow when these sources have melted and are no longer recharged annually.

(5) Water resources in the Khumbu Valley should continue to be monitored in future years to further confirm or to update the findings of this study with the ultimate goal of making the communities of the Khumbu Valley and other high-altitude communities more resilient in the face of climate change.

DATA AVAILABILITY STATEMENT

All datasets generated and analyzed for this study are included in the article/**Supplementary Material** or are available from the authors upon request, without undue reservation, to any qualified researcher.

AUTHOR CONTRIBUTIONS

LW, KNe, KNi, BB, CD, and SS contributed conception and design of the study. LW organized the database. LW, KNe, and BB performed the statistical analysis. LW wrote the first draft of the manuscript. KNe and KNi wrote sections of the manuscript. All authors contributed to manuscript revision, read, and approved the submitted version.

ACKNOWLEDGMENTS

We would like to acknowledge Ball State University for financially supporting this research. We also thank the Nepal National Park Service, Kathmandu University, and Ang Nurbu Sherpa of Holiday Namche for making this work possible.

SUPPLEMENTARY MATERIAL

The Supplementary Material for this article can be found online at: https://www.frontiersin.org/articles/10.3389/feart.2020.00128/full#supplementary-material

REFERENCES

Ako, A. A., Shimada, J., Hosono, T., Ichiyanagi, K., Nkeng, G. E., Fantong, W. Y., et al. (2011). Evaluation of groundwater quality and its suitability for drinking and agricultural uses in the banana plain (mbanqa, njombe, penja) of cameroon volcanic line. *Environ. Geochem. Health* 33, 559–575. doi: 10.1007/s10653-010-9371-1

Asahi, K. (2010). Equilibrium-line altitudes of the present and last glacial maximum in the eastern nepal himalayas and their implications for SW monsoon climate. *Quat. Int.* 212, 26–34. doi: 10.1016/j.quaint.2008.08.004

Bajracharya, S., Maharajan, S., and Shrestha, F. (2011). "Climate change – geophysical foundations and ecological effects," ed Blanco, J. (InTech), 445–458. Available online at: http://www.intechopen.com/books/climate-change-~geophysical-foundations-and-ecological-effects/glaciers-shrinking-in-nepal-himalaya

Balestrini, R., Polesello, S., and Sacchi, E. (2014). Chemistry and isotopic composition of precipitation and surface waters in Khumbu valley (Nepal himalaya): N dynamics of high elevation basins. *Sci. Tot. Environ.* 485–486, 681–692. doi: 10.1016/j.scitotenv.2014.03.096

Barry, R. G., and Chorley, R. J. (1982). *Atmosphere, Weather and Climate*, *4th Edn*. London; New York, NY: Methuen.

Bocchiola, D., Diolaiuti, G., Soncini, A., Mihalcea, C., D'Agata, C., Mayer, C., et al. (2011). Prediction of future hydrological regimes in poorly gauged high altitude basins: the case study of the upper Indus, Pakistan. *Hydrol. Earth Syst. Sci.* 15, 2059–2075. doi: 10.5194/hess-15-2059-2011

Bolch, T., Shea, J. M., Liu, S., Azam, F. M., Gao, Y., Gruber, S., et al. (2019). "Status and change of the Cryosphere in the extended Hindu Kush Himalaya region," in *The Hindu Kush Himalaya Assessment*, eds P. Wester, A. Mishra, A. Mukherji, and A. Shrestha (Cham: Springer).

Byers, A. (2005). Contemporary human impacts on alpine ecosystems in the sagarmatha (Mt. Everest) national park, Khumbu, Nepal. *Ann. Assoc. Am. Geograp.* 95, 112–140. doi: 10.1111/j.1467-8306.2005.00452.x

Clark, I. (2015). *Groundwater Geochemistry and Isotopes*. Boca Raton, FL: CRC Press; Taylor & Francis Group.

Craig, H. (1961). Isotopic variation in meteoric waters. *Science* 133, 1702–1703. doi: 10.1126/science.133.3465.1702

Dansgaard, W. (1964). Stable isotopes in precipitation. *Tellus* 16, 436–468. doi: 10.3402/tellusa.v16i4.8993

Florea, L., Bird, B., Lau, J. K., Wang, L., Lei, Y., Yao, T., et al. (2017). Stable isotopes of river water and groundwater along altitudinal gradients in the high himalayas and the eastern nyainqentanghla mountains. *J. Hydrol.* 14, 37–48. doi: 10.1016/j.ejrh.2017.10.003

Immerzeel, W. W., van Beek, L. P. H., and Bierkens, M. F. P. (2010). Climate change will affect the Asian water towers. *Science* 328, 1382–1385. doi: 10.1126/science.1183188

Kang, S., Kreutz, K. J., Mayewski, P. A., Qin, D., and Yao, T. (2002). Stable-isotopic composition of precipitation over the northern slope of the central himalaya. *J. Glaciol.* 48, 519–526. doi: 10.3189/172756502781831070

Kerstel, E., and Gianfrani, L. (2008). Advances in laser-based isotope ratio measurements: selected applications. *Appl. Phys. B* 92, 439–449. doi: 10.1007/s00340-008-3128-x

Kerstel, E., Van Trigt, R., Dam, N., Reuss, J., and Meijer, H. A. J. (1999). Simultaneous determination of the $^{2}H/^{1}H$, $^{17}O/^{16}O$, and $^{18}O/^{16}O$ isotope abundance ratios in water by means of laser spectrometry. *Anal. Chem.* 71, 5297–5303. doi: 10.1021/ac990621e

Kump, L. R., Kasting, J. F., and Crane, R. G. (2014). *The Earth System*, 3rd Edn. Harlow: Pearson Education. ISBN-13: 978-0321597793

La Frenierre, J., and Mark, B. G. (2014). A review of methods for estimating the contribution of glacial meltwater to total watershed discharge. *Prog. Phys. Geograp.* 38, 173–200. doi: 10.1177/0309133313516161

Mani, A. (1981). "The climate of the himalaya," in *The Himalaya: the Aspects of Change,* eds R. Lall, and A. D. Moddie (New Delhi: Oxford University Press), 3–15.

Mark, B., and Seltzer, G. (2003). Tropical glacier meltwater contribution to stream discharge: a case study in the Cordillera Blanca, Peru. *J. Glaciol.* 49, 271–281. doi: 10.3189/172756503781830746

Müller, F. (1959). "Eight months of glacier and soil research in the Everest region." in *The Mountain World 1958/59*, ed. M. Barnes, (London: George Allen & Unwin Ltd), 191–208.

Müller, F. (1980). "Present and late pleistocene equilibrium line altitudes in the Mt. Everest region – an application of the glacier inventory," in *Riederalp Workshop 1978 – World Glacier Inventory*, Vol. 126 (IAHS Publisher), 75–94. Available online at: https://iahs.info/uploads/dms/iahs_126_0075.pdf

Nganje, T. N., Hursthouse, A. S., Aniekan, E., Stirling, D., and Adamu, C. I. (2017). Hydrochemistry of surface water and groundwater in the shale bedrock, cross river Basin and Niger Delta region, Nigeria. *Appl. Water Sci.* 7, 961–985. doi: 10.1007/s13201-015-0308-9

Nicholson, K., Hayes, E., Neumann, K., Dowling, C., and Sharma, S. (2016). Drinking water quality in the Sagarmatha national park, Nepal. *J. Geosci. Environ. Protect.* 4, 43–53. doi: 10.4236/gep.2016.44007

Nijampurkar, V. N., and Bhandari, N. (1984). Oxygen isotopic ratios of some himalayan glaciers. *Tellus* 36B, 300–302. doi: 10.1111/j.1600-0889.1984.tb00250.x

NOAA National Centers for Environmental Information (2020). *State of the Climate: Global Climate Report for Annual 2019*. Available online at: https://www.ncdc.noaa.gov/sotc/global/201913 (accessed March 20, 2020).

Panzeri, D., Caroli, P., and Haack, B. (2013). Sagarmatha park (Mt Everest) porter survey and analysis. *Tour. Manage.* 36, 26–34. doi: 10.1016/j.tourman.2012.11.003

Salerno, F., Buraschi, E., Bruccoleri, G., Tartari, G., and Smiraglia, C. (2008). Glacier surface-area changes in Sagarmatha national park, Nepal, in the second half of the 20th century, by comparison of historical maps. *J. Glaciol.* 54, 738–752. doi: 10.3189/002214308786570926

Salerno, F., Guyennon, N., Thakuri, S., Viviano, G., Romano, E., Vuillermoz, E., et al. (2015). Weak precipitation, warm winters and springs impact glaciers of south slopes of Mt. Everest (central himalaya) in the last 2 decades (1994–2013). *Cryosphere* 9, 1229–1247. doi: 10.5194/tc-9-1229-2015

Salerno, F., Viviano, G., Manfredi, E. C., Caroli, P., Thankuri, S., and Tartari, G. (2013). Multiple carrying capacities from a management-oriented perspective to operationalize sustainable tourism in protected areas. *J. Environ. Manage.* 128, 116–125. doi: 10.1016/j.jenvman.2013.04.043

UNESCO [United Nations Educational Scientific and Cultural Organization] (2009). *Case Studies on Climate Change and World Heritage*. Paris.

Van Geldern, R., and Barth, J. A. C. (2012). Optimization of instrument setup and post-run corrections for oxygen and hydrogen stable isotope measurements of water by isotope ratio infrared spectroscopy (IRIS). *Limnol. Oceanograp. Methods* 10, 1024–1036. doi: 10.4319/lom.2012.10.1024

Viviroli, D., Dürr, H. H., Messerli, B., Meybeck, M., and Weingartner, R. (2007). Mountains of the world, water towers for humanity: typology, mapping, and global significance. *Water Resour. Res.* 47:W07447. doi: 10.1029/2006WR005653

Williams, M. W., Wilson, A., Tshering, D., Thapa, P., and Kayastha, R. B. (2016). Using geochemical and isotopic chemistry to evaluate glacier melt contributions to the Chamkar Chhu (river), Bhutan. *Ann. Glaciol.* 57, 339–348. doi: 10.3189/2016AoG71A068

Wilson, A. M., Williams, M. W., Kayastha, R. B., and Racoviteanu, A. (2016). Use of a hydrologic mixing model to examine the roles of meltwater, precipitation and groundwater in the Langtang river basin, Nepal. *Ann. Glaciol.* 57, 155–168. doi: 10.3189/2016AoG71A067

Xiang, Y., Yao, T., Gao, Y., Zhang, G., Wang, W., and Tian, L. (2018). Retreat rates of debris-covered and debris-free glaciers in the Koshi river basin, central Himalayas, from 1975 to 2010. *Environ. Earth Sci.* 77:285. doi: 10.1007/s12665-018-7457-8

Yao, T., Thompson, G., Mosbrugger, V., Zhang, F., Ma, Y., Luo, T., et al. (2012). The Third Pole Environment (TPE). *Environ. Dev.* 3, 52–64. doi: 10.1016/j.envdev.2012.04.002

Conflict of Interest: The authors declare that the research was conducted in the absence of any commercial or financial relationships that could be construed as a potential conflict of interest.

frontiers in Earth Science

ORIGINAL RESEARCH
published: 07 July 2020
doi: 10.3389/feart.2020.00265

Atmospheric Bridge Connecting the Barents Sea Ice and Snow Depth in the Mid-West Tibetan Plateau

Yuhang Chen[1,2], *Anmin Duan*[1,2]* *and Dongliang Li*[1]*

[1] College of Atmospheric Science, Collaborative Innovation Center on Forecast and Evaluation of Meteorological Disasters, Nanjing University of Information Science and Technology, Nanjing, China, [2] State Key Laboratory of Numerical Modeling for Atmospheric Sciences and Geophysical Fluid Dynamics, Institute of Atmospheric Physics, Chinese Academy of Sciences, Beijing, China

In contrast to the rapid warming of the climate, there is growing evidence to indicate that no significant trend exists in the snow cover/depth over the western Tibetan Plateau in recent decades. Here, by analyzing multiple sources of observational and reanalysis data, we address the possible interannual connection between the mid-west Tibetan Plateau (MWTP) snow depth and Arctic sea ice. Results indicate that a robust and coherent variation exists between the winter Barents Sea ice concentration and the MWTP snow depth; that is, a positive anomaly of the former can enhance the meridional air temperature gradient to the south and hence accelerate the polar-front westerly jet. As a result, an anomalous Rossby wave propagating upward and equatorward generates, resulting in a dipole pattern of the atmospheric circulation anomaly over the polar region and the Eurasian continent. The anticyclonic circulation anomaly, corresponding to the south center of the dipole pattern, weakens the subtropical westerly jet and forms a southeast wind climbing the MWTP, which enhances the zonal advection and meridional convergence of the atmospheric moisture flux over the MWTP, and hence facilitates the MWTP snowfall. The interannual variation of the Barents Sea ice and the MWTP snow depth are therefore closely connected through the atmospheric bridge effect of the westerly jet and Rossby wave.

Keywords: Arctic sea ice, Barents Sea, Rossby wave, Tibetan Plateau, snow depth

OPEN ACCESS

Edited by:
Lei Wang,
Institute of Tibetan Plateau Research (CAS), China

Reviewed by:
Seong-Joong Kim,
Korea Polar Research Institute, South Korea
Jiping Liu,
University at Albany, United States

***Correspondence:**
Anmin Duan
amduan@lasg.iap.ac.cn
Dongliang Li
lidl@nuist.edu.cn

Specialty section:
This article was submitted to Interdisciplinary Climate Studies, a section of the journal Frontiers in Earth Science

Received: *01 May 2020*
Accepted: *12 June 2020*
Published: *07 July 2020*

Citation:
Chen Y, Duan A and Li D (2020) Atmospheric Bridge Connecting the Barents Sea Ice and Snow Depth in the Mid-West Tibetan Plateau. Front. Earth Sci. 8:265. doi: 10.3389/feart.2020.00265

INTRODUCTION

The Tibetan Plateau is often referred to as the "third pole of the world" owing to its high-altitude terrain in the mid-latitudes (Yao et al., 2012). Driven by orographic effects, a freshwater resource exists on the Tibetan Plateau in the form of glaciers, snow cover, lakes, and permafrost (Lu et al., 2005; Bookhagen and Burbank, 2010; Yao et al., 2012; Zhang et al., 2017; Li et al., 2018), the surface runoff of which is sufficient to form major rivers such as the Yellow, Yangtze, Brahmaputra, Mekong, and Indus, which is sufficient to provide water for Asia's agricultural activities and ecosystems (Bookhagen and Burbank, 2010; Immerzeel et al., 2010; Singh et al., 2014; Li et al., 2018). In particular, the snow cover serves as the foundation for the glacial mass balance (Kumar et al., 2019), and snowmelt can supply the runoff of Asian rivers (Bookhagen and Burbank, 2010;

Singh et al., 2014; Li et al., 2018). The increased soil moisture from the melting of snow cover during the spring can induce localized thermal anomalies over the Tibetan Plateau and increase the precipitation in summer over the middle and lower reaches of the Yangtze River basin through snow-related hydrological effects (Chow et al., 2008; Xiao and Duan, 2016). Moreover, the snow-related albedo effect enables the Tibetan Plateau snow cover to give an indication of the onset of the Indian summer monsoon and the occurrence of the autumn Indian Ocean Dipole pattern (Senan et al., 2016; Yuan et al., 2019).

Recently, the snow cover and glaciers distributed in the western part of the Tibetan Plateau have shown different characteristics of climate change compared with the eastern part (Kapnick et al., 2014; Guo et al., 2020). Model projections under all greenhouse gas emission scenarios suggest a continuous reduction in low-elevation mountain snow cover by the end of the 21st century (Hock et al., 2019). However, at high elevation, the climate trend of winter snow cover tends to be generally less clear, and snowfall is projected to increase over the western Tibetan Plateau in particular (Kapnick et al., 2014; Song and Liu, 2017; Guo et al., 2019; Hock et al., 2019). The glaciers and snow cover of the whole Tibetan Plateau are retreating and declining (Yao et al., 2012; Zhang et al., 2017; Li et al., 2018). However, there is no significant declining trend of snow depth in the western Tibetan Plateau (Kapnick et al., 2014; Guo et al., 2019), and the Karakoram glaciers even show an increasing trend (albeit a statistically non-significant one) (Gardelle et al., 2012; Yao et al., 2012). All these results suggest unique characteristics of the snow cover/depth over the west Tibetan Plateau, which might be related to the different atmospheric influences on snowfall from those of the eastern Tibetan Plateau.

As one of the most important components of the cryosphere, the Arctic sea ice is also undergoing tremendous changes. The sea ice loss in summer mainly happens over the perennial ice-covered area, with the East Siberian Sea ice holding the largest fraction of loss (22%) in September. Meanwhile, the decline of ice in wintertime mostly occurs in the seasonally dependent sea ice area, with the Barents Sea ice contributing the largest fraction of loss (27%) in March (Onarheim et al., 2018). Recently, it was found that the decline of the Arctic sea ice contributes greatly to wintertime snowfall change in the high latitudes, as bare seas with reduced sea ice are capable of providing rich sources of water vapor. The reduction in sea ice strengthens the atmospheric circulation meridionally and promotes the transport of water vapor to Eurasia, resulting in more winter snowfall over that region (Cohen et al., 2012; Ghatak et al., 2012; Liu et al., 2012; Wegmann et al., 2015). As simulated by multi-model ensemble mean results, a significant role of the decline in autumn Arctic sea ice in the growing climate change of Eurasian winter snowfall and snow cover has been proposed during the 21st century (Song and Liu, 2017).

In addition, the feedback effect of the autumn and winter Arctic sea ice on the large-scale circulation has been verified by statistical analysis and model simulations (Honda et al., 2009; Mori et al., 2014; Sun et al., 2016; Zuo et al., 2016; Blackport and Screen, 2019). The reduction in Arctic sea ice can stimulate an upward stationary Rossby wave, amplifying the Siberian high and transferring the westerly wind equatorward (Honda et al., 2009; Kim et al., 2014; Cohen et al., 2018, 2020; Blackport and Screen, 2019, imposing an influence on the climate of East Asia (Sun et al., 2016; Zuo et al., 2016). In fact, the mid-latitude westerly winds are considered as a critical factor for TP snow because they serve as a Rossby waveguide transmission medium, along which small troughs can propagate and guide water vapor north to cause TP snowfall (Bao and You, 2019; Song et al., 2019; Zhang et al., 2019b). Although the long-term change and climate impact of the Arctic sea ice and snow cover over the Tibetan Plateau has quite rightly been a primary focus among scientists, the potential connection between them on the interannual time scale and the underlying mechanisms involved remain unclear.

In the above context, the aim of this work is to investigate the possibility that the winter Barents Sea ice regulates the mid-west Tibetan Plateau (MWTP) snow depth on the interannual timescale by considering the non-significant trend in the west Tibetan Plateau snow cover and significant trend in the Arctic sea ice. The mechanism involved will be elucidated through emphasizing the feedback effect of the Arctic sea ice on the Asian westerly jet and Rossby wave. The data and methods are introduced in Section "Materials and Methods." The interannual relationship between the Barents Sea ice and western TP snow and the role played by the atmospheric bridge in this relationship are analyzed in Section "Results." Finally, a summary and some further discussion are presented in Section "Discussion and Conclusion."

MATERIALS AND METHODS

The datasets utilized in this study include:

1. Snow depth, from 1979 to 2015, derived from passive microwave data with a spatial resolution of 0.25° × 0.25°, which can be downloaded from the Big Earth Data Platform for Three Poles (available at http://poles.tpdc.ac.cn/zh-hans/). The dataset has been corrected based

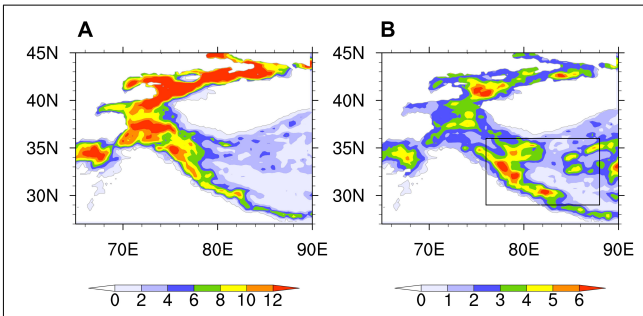

FIGURE 1 | (A) Boreal winter (DJF) mean snow depth over the western Tibetan Plateau and **(B)** its standard deviation during the period 1979–2015 (units: cm). The gray line outlines the 2-km topography of the Tibetan Plateau.

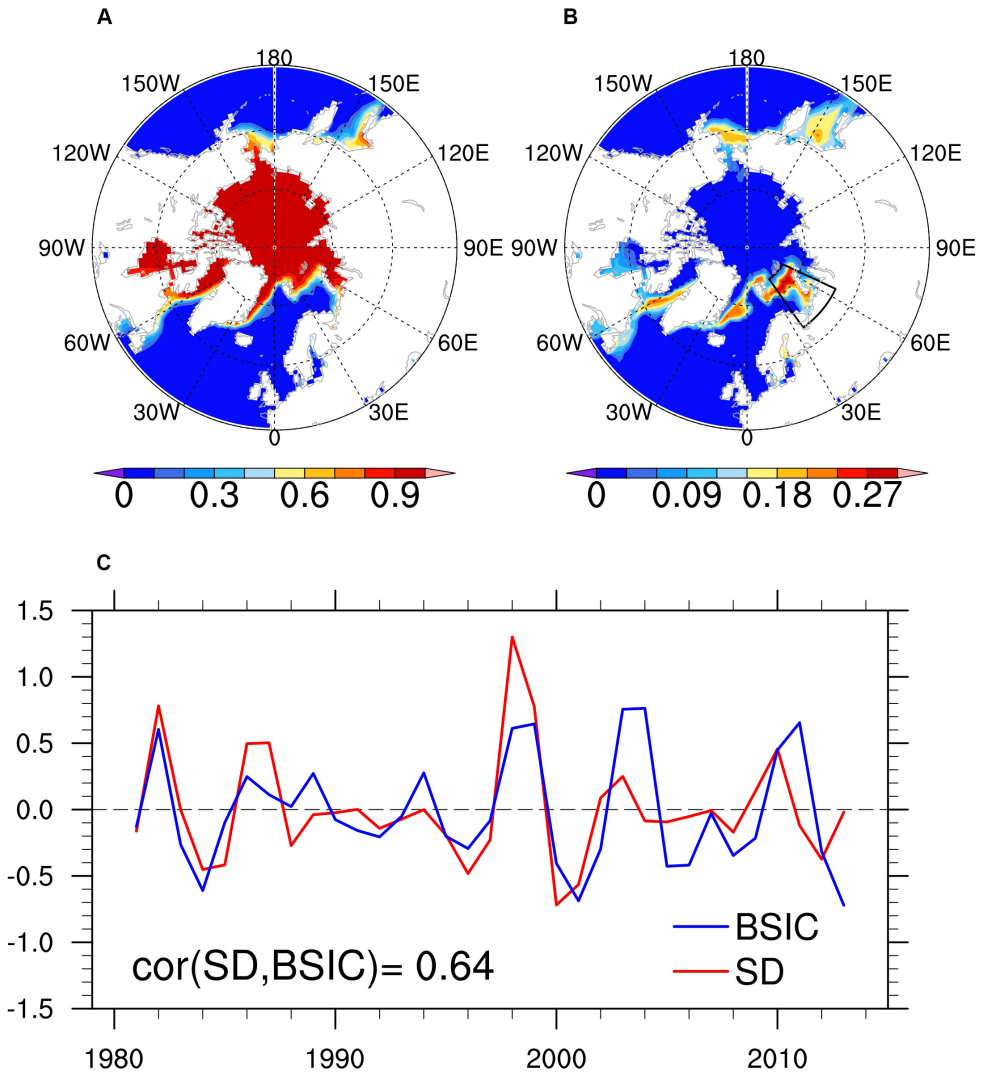

FIGURE 2 | (A) Boreal winter mean Arctic sea ice concentration; **(B)** the corresponding standard deviation during the period 1979–2015; and **(C)** the normalized time series of the domain-averaged snow depth (SD, red) over the MWTP (29°–36°N, 76°–88°E) and the Barents Sea ice concentration (BSIC, blue) in the area of (65°–80°N, 35°–65°E) as marked by the black box in **B**.

on *in situ* station snow depth and the optimized Chang algorithm according to TP vegetation and snow characteristics. More details regarding the improved temporal consistency of different satellite sensors and the suitability of the algorithm for the derivation of snow depth across the whole of China can be found in Che et al. (2008). These data have been widely used to investigate snow-related climate characteristics (Xiao and Duan, 2016; Zhang et al., 2017; Bao and You, 2019). The monthly sea-ice concentration data are provided by the Hadley Center (Rayner et al., 2003).

2. ERA-Interim reanalysis data with a spatial resolution of 0.5° × 0.5° are utilized in this study (Dee et al., 2011), which include the spatial geopotential height, winds, specific humidity, and temperature. Surface sensible and latent heat fluxes and pressure are also from ERA-Interim. The monthly means of daily forecast accumulated snowfall are used to analyze the snow depth contributed by the snowfall.

All data were calculated for the average of December, January, and February (DJF) as the winter mean from 1978/1979 to 2014/2015, and the linear trend was removed. To filter the low frequency of the MWTP snow depth and Barents Sea ice, Lanczos bandpass filtering was used to extract the 3–9-year interannual signal in all data (Duchon, 1979). Pearson correlation analysis and regression analysis were used to investigate the relationship between the Arctic sea ice and MWTP snow depth. The level of statistical significance was estimated using the two-sided Student's *t*-test.

To diagnose the moisture transport, we calculated the water vapor flux $\frac{1}{g}q\vec{V}$ following Banacos and Schultz (2005).

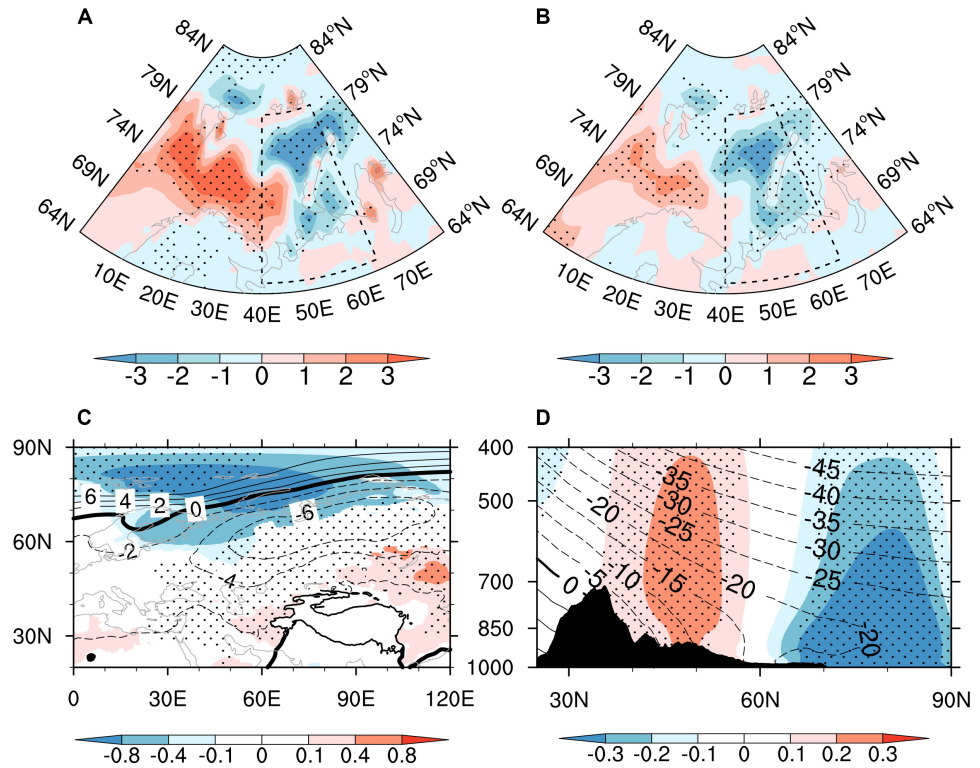

FIGURE 3 | Regression fields of **(A)** the winter surface sensible heat flux (units: W/m^2), **(B)** the winter surface latent heat flux (units: W/m^2), **(C)** the 1000-hPa air temperature (shaded; units: ℃) and surface pressure (contours; units: Pa), and **(D)** the 50°–120°E-averaged air temperature (shaded; units: ℃; contours are the climate mean air temperature) against the BSICI. The shading and contour values of the stippled areas in **A, B, D,** and **C** exceed the p = 0.1 confidence level. The shaded values in **C** exceed the p = 0.1 confidence level. The dashed box in **A** and **B** denotes the Barents Sea region (65°–80°N, 35°–65°E). The black line over the region (25°–45°N, 60°–110°E) in **C** outlines the 2-km topography of the Tibetan Plateau.

The precipitation can be estimated by the water vapor flux divergence D as follows:

$$Pre \approx -\frac{1}{g}\int_{300}^{ps}\left(\nabla \bullet q\vec{V}\right)dp = -\int_{300}^{ps} Ddp = -\int_{300}^{ps}\left(D_{xy}+D_p\right)dp, \quad (1)$$

$$D = \frac{1}{g}\left(u\frac{\partial q}{\partial x}+v\frac{\partial q}{\partial y}+\omega\frac{\partial q}{\partial p}+q\frac{\partial u}{\partial x}+q\frac{\partial v}{\partial y}+q\frac{\partial \omega}{\partial p}\right), \quad (2)$$

where Pre is the estimated precipitation, $\vec{V}(u, v,\omega)$ present the three dimensions of the atmospheric wind component, and q is the specific humidity. Parameter g represents gravitational acceleration, while ps refers to the surface pressure. The 300-hPa level is used to represent the tropopause because the specific humidity above it is negligible. The horizontal and vertical components of D are D_{xy} and D_p. The six terms on the right-hand side of Eq. 2 stand for the contributions from the zonal advection, meridional advection, vertical advection, zonal convergence, meridional convergence, and vertical convergence, respectively. With the complexity of the MWTP topography, the D at 400 hPa was calculated and used to estimate the MWTP winter precipitation.

The atmospheric Rossby wave activity involved in the effect of sea ice on the atmosphere was diagnosed by the TN Rossby wave activity flux $\vec{W}$ (Takaya and Nakamura, 2001):

$$\vec{W} = \frac{P}{2000\left|\vec{U}\right|}\begin{Bmatrix} U\left(v'^2-\psi' v'_x\right)+V\left(-u'v'+\psi' u'_x\right) \\ U\left(-u'v'+\psi' u'_x\right)+V\left(u'^2+\psi' u'_y\right) \\ \frac{fR_a}{N^2H_0}\left[U\left(v'T'-\psi' T'_x\right)+V\left(-u'T'-\psi' T'_y\right)\right] \end{Bmatrix}, \quad (3)$$

where ψ is the quasi-geostrophic stream function, $\vec{U}$ (U, V) is the zonally inhomogeneous basic flow, P and T are the pressure and temperature of the atmosphere, $\left(u', v', T'\right)$ is a perturbation from the basic flow, the subscript of the parameter indicates the partial derivatives, f is the Coriolis parameter, R_a is the gas constant of dry air, N is the buoyancy frequency, and H_0 is a constant scale height.

RESULTS

In winter, the west Tibetan Plateau snow maintains an extensive coverage in the mountain area, where snow covers throughout the whole year. The largest amount of snow mainly covers the mountain ranges including the Karakoram, Pamir, and western Himalayan mountains (**Figure 1A**). The variance in the snow depth displays two centers. One center presents considerable

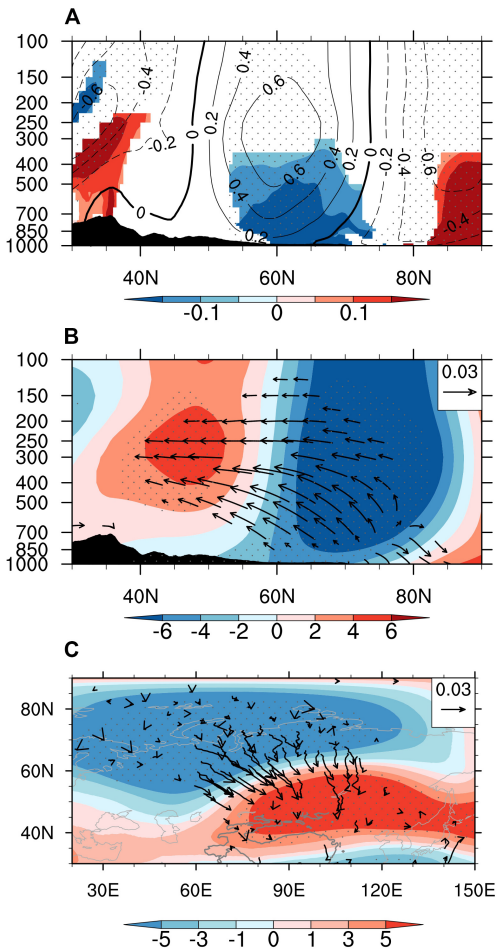

FIGURE 4 | Regression fields of the **(A)** winter 50°–120°E-averaged temperature gradient (shaded; units: 10^{-6} K/m) and zonal wind (contours; units: m/s), **(B)** 50°–120°E-averaged geopotential height (shaded; units: m) and the TN Rossby wave activity flux in the vertical (vectors; units: m^2/s^2), and **(C)** 250-hPa geopotential height (shaded; units: m) and the TN Rossby wave activity flux (black vectors; units: m^2/s^2) in the horizontal, against the BSICI. The contour and shaded values of the stippled area in **A** and **B, C** exceed the $p = 0.1$ confidence level. The shaded value in **A** exceeds the $p = 0.1$ confidence level. The gray line over the (25°–45°N, 60°–110°E) in **C** outline the 2-km topography of the Tibetan Plateau.

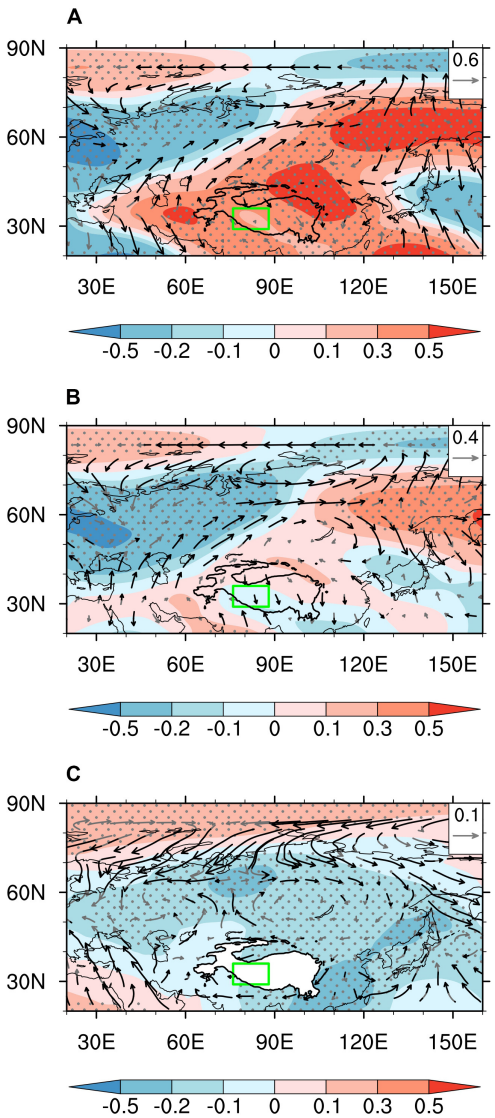

FIGURE 5 | Regression fields of the divergent wind (vectors; units: m/s) and velocity potential (shaded; units: 10^6 m^2/s) at **(A)** 250, **(B)** 500, and **(C)** 1000 hPa, against the BSICI. Black arrows indicate vector values above the $p = 0.1$ confidence level. The shaded values of the stippled areas exceed the $p = 0.1$ confidence level. The green box represents the MWTP region. The black line over the region (25°–45°N, 60°–110°E) outlines the 2-km topography of the Tibetan Plateau.

variation of snow depth in the Pamirs, while the other exists in the MWTP (black box in **Figure 1B**), which is a transition zone from high to low snow values (**Figure 1A**). As for the spatial pattern of the winter climatology of Arctic sea ice, there are large quantities of stable sea ice in the polar region (**Figure 2A**). At the fringes of the Arctic sea ice, the marginal sea ice exhibits a large interannual fluctuation, especially in the Barents Sea (**Figure 2B**). Taking the region (29°–36°N, 76°–88°E) as the snow depth study area, the areal mean snow depth was calculated and the time series shows a distinct interannual variation (**Figure 2C**). Taking the region (65°–80°N, 35°–65°E) of the Arctic sea ice as the Barents Sea ice, the regional-averaged Barents Sea ice was calculated. It is worth noting that the time series of areal mean snow depth over the MWTP and the Barents Sea ice present a robust and coherent interannual variation, with a correlation coefficient of 0.64 ($p < 0.01$) (**Figure 2C**). This correlation illustrates a significantly correlated cryosphere between the Arctic and Tibetan Plateau. Therefore, we selected (65°–80°N, 35°–65°E) as the key study region of the Arctic, and the domain-averaged sea-ice concentration defined the Barents Sea Ice Concentration Index (BSICI) that is used in the following parts. The cause for this prominent link on the interannual time scale will be the main point of discussion below.

As the main source of cold air in the Northern Hemisphere, Arctic sea ice can form large-scale Eurasian cold events, which

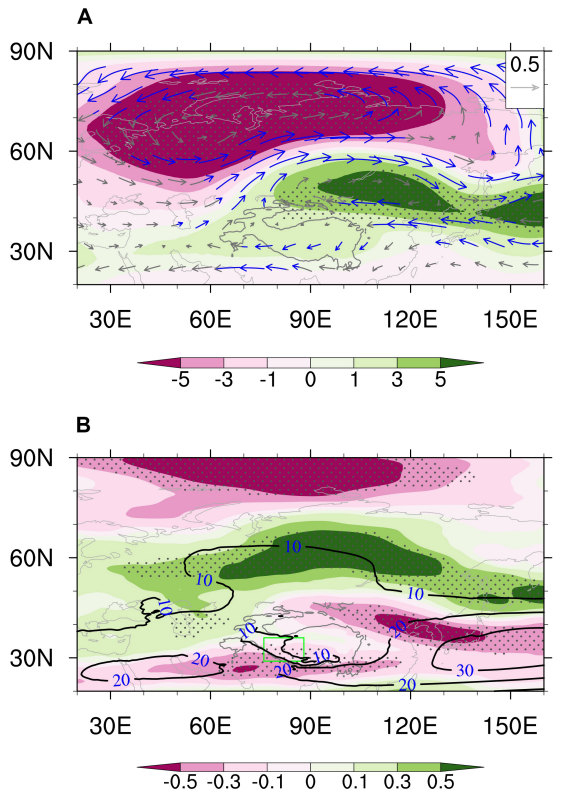

FIGURE 6 | Regression fields of **(A)** the winter geopotential height (shaded; units: m) and horizontal wind vector (units: m/s), and **(B)** zonal wind speed (shaded; units: m/s) at 500 hPa, against the BSICI. Blue arrows in **A** indicate vector values above the $p = 0.1$ confidence level. The black contours in **B** represent the climatology of the zonal wind speed with intensity larger than 10 m/s. The shaded values of the stippled areas exceed the $p = 0.1$ confidence level. The black box in **B** represents the MWTP region. The gray line over the region (25°–45°N, 60°–110°E) outlines the 2-km topography of the Tibetan Plateau.

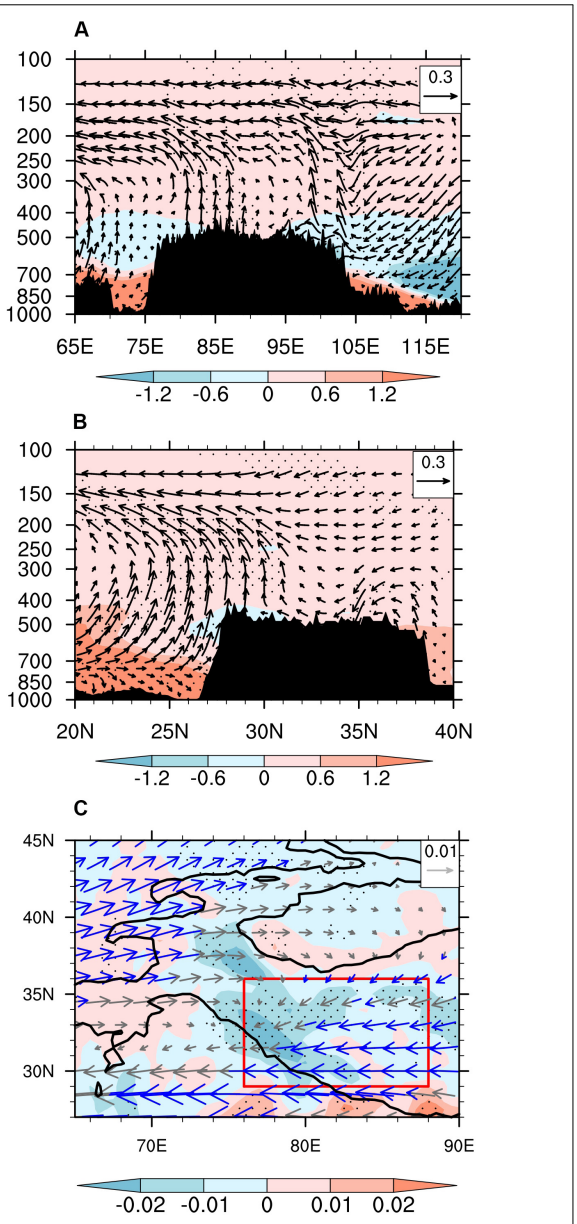

FIGURE 7 | Regression fields of the **(A)** cross sections of zonal-vertical circulation (vectors; zonal wind speed in m/s, and vertical velocity in Pa/s, multiplied by −57) and specific humidity (shaded; units: 10^{-2} g/kg) averaged over 25°–32°N, and **(B)** cross sections of meridional-vertical circulation (vectors; zonal wind speed in m/s, and vertical velocity in Pa/s, multiplied by −71) and specific humidity (shaded; units: 10^{-2} g/kg) averaged over 80°–88°E, and **(C)** water vapor flux (vectors; units: g/cm•s•hPa) and convergence at 400 hPa (shaded; units: 10^{-8} g/cm^2•s•hPa), against the BSICI. The vectors of the stippled areas in **A** and **B** exceed the $p = 0.1$ confidence level. Blue arrows in **C** indicate vector values above the $p = 0.1$ confidence level. The red box in **C** represents the MWTP region. The black line over the region (25°–45°N, 60°–110°E) in **C** outlines the 2-km topography of the Tibetan Plateau.

are closely related to the survival of human beings both directly and indirectly through their effects on agricultural production (Cohen et al., 2014; Kim and Son, 2016; Shi et al., 2018). As demonstrated by simulation of the feedback effect of the Arctic sea ice, the decline of the Barents Sea ice can produce the upward propagation of planetary wave energy because of the anomalous meridional heat flux transition, and stimulate a Rossby wave that spreads horizontally from the Arctic to Eurasia, by which the westerly winds may attain some influence (Honda et al., 2009; Mori et al., 2014; Cohen et al., 2018, 2020; Kim and Kim, 2018; Blackport and Screen, 2019). When the BSICI is above normal, the presence of more sea ice will prevent the transmission of heat from ocean to atmosphere, and weaken the planetary wave activity (Cohen et al., 2020). This point can be verified by the negative upward surface turbulent heat flux in the Barents Sea (**Figures 3A,B**). When the Barents Sea ice extends, the surface sensible and latent heat flux are reduced. The weakened surface heat source reduces temperatures in the lower atmosphere, leading to a cold center over the Barents Sea (**Figure 3C**). A vertical profile averaged from 50°E to 120°E of the boreal winter mean air temperature and the corresponding regressed field against the BSICI is shown in **Figure 3D**. Clearly, the lower tropospheric atmosphere from 70°N to 80°N becomes

colder because of the reduced oceanic heat. As a result, the temperature gradient from south to north over the Eurasian continent turns to be increased (shaded in **Figure 4A**).

As in the model simulation, the change of the Barents Sea ice is partially responsible for the shift of the eddy-driven westerly jet, forming a meridional dipole circulation pattern in the mid-troposphere (Mori et al., 2014; Sorokina et al., 2016; Blackport and Screen, 2019). According to thermal wind theory, the increased meridional temperature gradient (shaded in **Figure 4A**) strengthens the zonal wind as height increases (contours in **Figure 4A**), which enhances the intensity of the polar-front jet. Such zonal wind anomalies contribute to the baroclinicity of the lower troposphere and trigger an upward propagation of the Rossby waves from 850 to 200 hPa (**Figure 4B**). These Rossby waves propagate from north to south in the horizontal direction, forming a dipole circulation distributed over the Eurasian continent in winter (**Figure 4C**). To the north of the anomalous polar-front jet, the height is reduced and a convergence forms from 1000 to 250 hPa (**Figures 5A–C**), which can weaken the Siberian high and reduce the delivery of Arctic cold air to Eurasia (**Figure 3C**). Therefore, in contrast to the colder temperatures over the Barents Sea, a positive air temperature anomaly is evident over the mid-latitudes (**Figure 3D**), which might be due to the weakened Siberian high linked with the abnormal Barents Sea ice (Honda et al., 2009; Overland et al., 2015; Sorokina et al., 2016; Cohen et al., 2018, 2020; Kim and Kim, 2018).

The MWTP experiences frequent snowfall in the cold season (Lu et al., 2005; Bookhagen and Burbank, 2010). This abundant snowfall is often modulated by the subtropical westerly jet, which may provide moisture transport toward the Tibetan Plateau (Norris et al., 2015; Bao and You, 2019). Considering the high topography of the MWTP, the regression fields of 500 hPa (near the surface over the TP) atmospheric circulation and zonal wind against the winter BSICI are exhibited in **Figure 6**. One can see a salient meridional dipole pattern in the geopotential height anomaly over the Eurasian continent because of the horizontal propagation of the Rossby wave in **Figures 4B,C**. The low center occupies the north part of the Eurasian continent and another high center in the belly of Eurasia with the Tibetan Plateau included (**Figure 6A**). The south center of the dipole pattern can generate anticyclonic circulation near the Tibetan Plateau, which can directly influence the subtropical westerly jet that is concerned as the regulator of the Tibetan Plateau snow depth.

Generally, the subtropical westerly jet and polar-front westerly jet coexist in the mid-troposphere over the Eurasian continent, with the larger intensity in the former, and these two jets converge into one in the east of East Asia. Synergistic changes in the north–south jet often induce the Tibetan Plateau and Eurasian climate change (Zhang et al., 2019a). With above-normal BSICI, the zonal wind is strengthened around 60°N and weakened around the polar region and Tibetan Plateau (**Figure 6B**). The south center of the dipole pattern, i.e., the anticyclonic circulation anomaly, leads to the decelerated subtropical westerly jet, especially over the southwestern MWTP (**Figure 6B**). These changes imposed on the westerly wind may have some influence on the moisture transport associated with the snowfall over the MWTP. The anticyclonic circulation can cause anomalous southeasterly wind to climb the MWTP, and the regression fields of the wind and specific humidity show that the anomalous southeasterly winds at the south part of the anticyclonic circulation facilitate the moisture convergence in the mid-high troposphere over the MWTP (**Figures 7A,B**). As indicated by the divergent wind, there is a large-scale atmospheric divergence at 250 hPa and convergence at 1000 hPa around the TP region (**Figures 5A–C**). At 500 hPa, the surface circulation converges to the TP, especially in the MWTP. Considering the steep terrain of the MWTP, the 400-hPa horizontal water vapor flux ($\frac{1}{g}qu$, $\frac{1}{g}qv$) and divergence D_{xy} were estimated. The water vapor flux converges and forms a negative center over the MWTP (**Figure 7C**), which is conducive to the MWTP snowfall.

To reveal the respective contributions of the moisture transport to the MWTP snowfall related to the Barents Sea ice concentration anomaly, in **Figure 8**, we plot the regression fields of the winter precipitation, snow depth, the 400-hPa moisture convergence indicated on the left-hand side of Eq. 2, and the six terms of the water vapor convergence indicated on the right-hand side of Eq. 2. It is clear that, with the favorable circulation as shown in **Figures 6**, **7**, more winter precipitation appears over the MWTP (**Figure 8A**) when the BSICI has a positive anomaly, bringing about more snowfall and greater snow depth over the MWTP (**Figure 8B**), which are largely contributed by the moisture convergence (**Figure 8C**). The diagnosis of the six terms of water vapor transport indicates that the moisture convergence anomaly over the MWTP is contributed mainly by the zonal advection (**Figure 8D**), which should be directly related to the weakened westerly in the downstream regions as shown in **Figure 6B**, and the vertical advection and meridional convergence of moisture flux (**Figures 8F,H**) as a result of the anomalous southeasterly winds climbing the MWTP. The meridional advection has relatively less influence on the snowfall (**Figure 8E**), and the contribution from the zonal (**Figure 8G**) and vertical (**Figure 8I**) convergence terms are not conducive to the snowfall.

DISCUSSION AND CONCLUSION

As the world's highest topography, the snow depth over the MWTP shows an inconspicuous trend but strong interannual variation during recent decades, which inspired us to study the possible driving force behind its interannual variation. Satellite snow and sea ice data and ERA-Interim reanalysis data were utilized to address this issue. The main conclusions can be summarized as follows:

1) A coherent interannual variation between MWTP snow depth and the Barents Sea ice concentration is robust in the observations. Above-normal Barents Sea ice cools the air temperature aloft by reducing the transmission of heat between ocean and atmosphere, thus enhancing the temperature gradient between the polar region and mid-latitudes over the Eurasian continent.

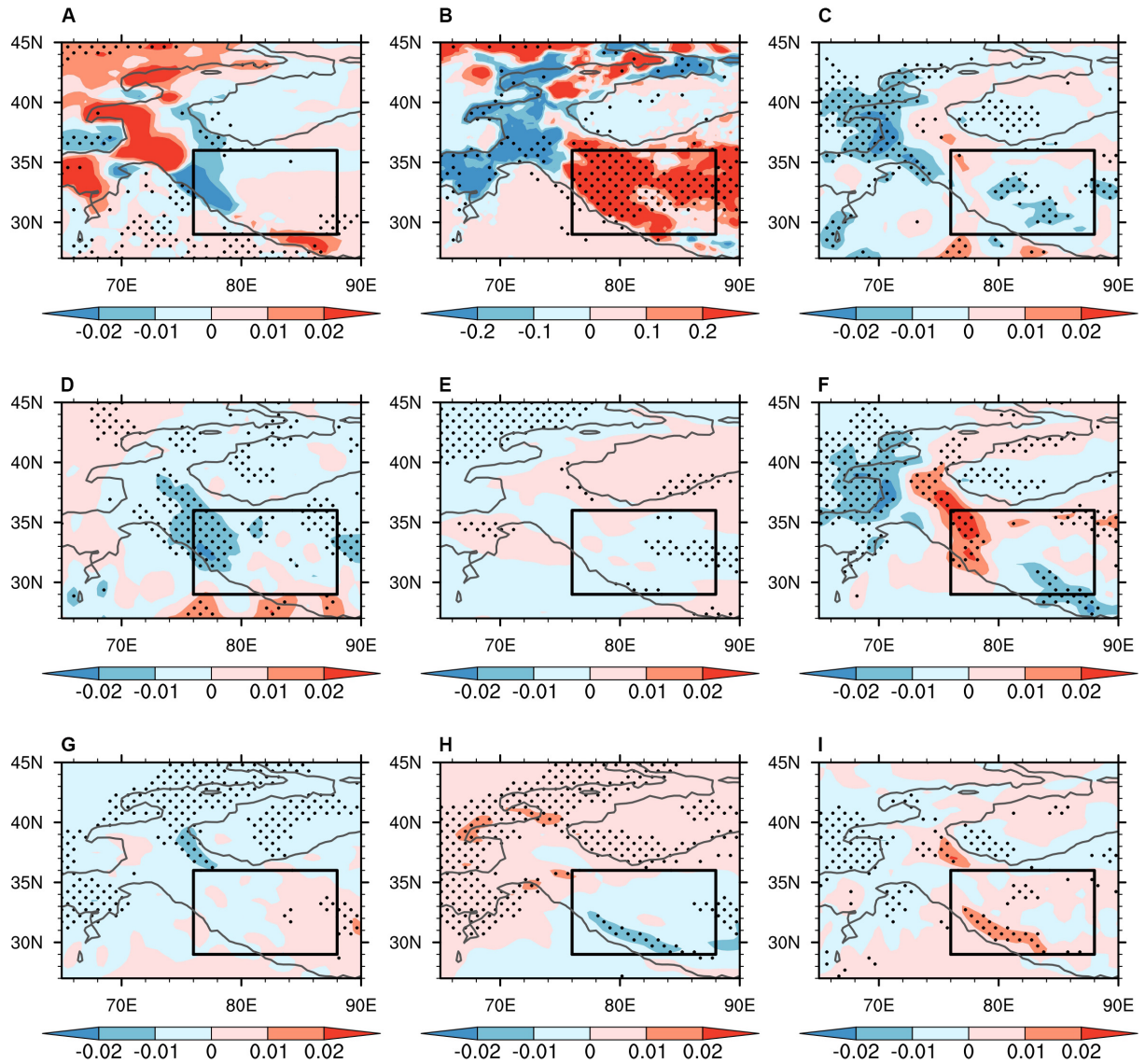

FIGURE 8 | Regression fields of **(A)** the winter snowfall (units: mm/day), **(B)** snow depth (units: cm), and **(C)** the moisture divergence *D* at 400 hPa (units: 10^{-8} g/cm^2•s•hPa); and the **(D)** zonal advection, **(E)** meridional advection, **(F)** vertical advection, **(G)** zonal convergence, **(H)** meridional convergence, and **(I)** vertical convergence (units: 10^{-8} g/cm^2•s•hPa) of moisture flux at 400 hPa, against the BSICI. The stippled areas exceed the $p = 0.1$ confidence level. The black box (29°–36°N, 76°–88°E) represents the MWTP region. The gray line over the region (25°–45°N, 60°–110°E) outlines the 2-km topography of the Tibetan Plateau.

2) With the increased temperature gradient, the polar-front westerly jet is enhanced, which increases the atmospheric baroclinicity and stimulates a Rossby wave propagating upward and equatorward, producing an anomalous anticyclone in the mid-troposphere of the subtropics with the Tibetan Plateau included to influence the subtropical westerly jet.
3) As a result, the zonal advection of moisture flux and the meridional convergence of moisture flux over the MWTP are intensified significantly, bringing about more moisture from surrounding areas and a resultant above-normal snowfall and snow depth in the MWTP. Therefore, the westerly jet and anomalous Rossby wave serve as an efficient atmospheric bridge in connecting the winter Arctic sea ice and snow depth over the MWTP.

This paper emphasizes the role of the westerly jet and Rossby wave in connecting the interannual variation between the Barents Sea ice and MWTP snow depth, but some other processes might also be important. The westerly wind anomalies can also be influenced by El Niño–Southern Oscillation (Matsumura and Kosaka, 2019) and Atlantic sea surface temperature (Jung et al., 2017; Sung et al., 2018). The Arctic sea ice aside from that in the Barents Sea also vary greatly and can impose some influence on the mid-latitude climate (Screen, 2017; Cohen et al., 2020); plus, the lagged impact of the autumn Arctic sea ice and continental

snow cover also play a role in the winter atmospheric circulation (Cohen et al., 2012; Furtado et al., 2015; Handorf et al., 2015). In addition, the combination effect of internal variability and external forcing on the relationship between sea ice change and Eurasia continent climate is still under debate (Overland et al., 2015; Park et al., 2015; Kim and Son, 2016; Cohen et al., 2018, 2020; Ye et al., 2018; Ye and Jung, 2019). Therefore, a comprehensive picture of the relationship between Arctic sea ice and snow depth over the Tibetan Plateau needs to be further explored in future. Moreover, owing to the imperfect physical schemes and coarse resolutions (Rahimi et al., 2019), existing climate models fail to simulate the observed spatiotemporal variation of snowfall and snow depth over the mid-west Tibetan Plateau, meaning a more complete model is therefore needed in future work to understand the mechanism involved in the variation of Tibetan Plateau snow depth.

DATA AVAILABILITY STATEMENT

The datasets presented in this study can be found in online repositories. The names of the repository/repositories and accession number(s) can be found below: http://poles.tpdc.ac.cn/zh-hans/, https://www.metoffice.gov.uk/hadobs/index.html, and https://www.ecmwf.int/en/forecasts/datasets/reanalysis-datasets/era-interim.

AUTHOR CONTRIBUTIONS

YC wrote the initial manuscript and calculated the data analysis. AD designed the structure of the manuscript and revised the manuscript. DL checked the manuscript and proposed comments. All authors contributed to the article and approved the submitted version.

FUNDING

This work was supported by the Strategic Priority Research Program of the Chinese Academy of Sciences (Grant No. XDA19070404) and the National Natural Science Foundation of China (Grant Nos. 41725018 and 91637312).

REFERENCES

Banacos, P. C., and Schultz, D. M. (2005). The use of moisture flux convergence in forecasting convective initiation: historical and operational perspectives. *Weather Forecast.* 20, 351–366. doi: 10.1175/waf858.1

Bao, Y., and You, Q. (2019). How do westerly jet streams regulate the winter snow depth over the Tibetan Plateau? *Clim. Dyn.* 53, 353–370. doi: 10.1007/s00382-018-4589-1

Blackport, R., and Screen, J. A. (2019). Influence of Arctic sea ice loss in autumn compared to that in winter on the atmospheric circulation. *Geophys. Res. Lett.* 46, 2213–2221. doi: 10.1029/2018GL081469

Bookhagen, B., and Burbank, D. W. (2010). Toward a complete Himalayan hydrological budget: spatiotemporal distribution of snowmelt and rainfall and their impact on river discharge. *J. Geophys. Res. Earth Surf.* 115:F03019. doi: 10.1029/2009JF001426

Che, T., Li, X., Jin, R., Armstrong, R., and Zhang, T. J. (2008). Snow depth derived from passive microwave remote-sensing data in China. *Ann. Glaciol.* 49, 145–154. doi: 10.3189/172756408787814690

Chow, K. C., Chan, J. C., Shi, X., Liu, Y., and Ding, Y. (2008). Time-lagged effects of spring Tibetan Plateau soil moisture on the monsoon over China in early summer. *Int. J. Climatol.* 28, 55–67. doi: 10.1002/joc.1511

Cohen, J., Screen, J. A., Furtado, J. C., Barlow, M., Whittleston, D., Coumou, D., et al. (2014). Recent Arctic amplification and extreme mid-latitude weather. *Nat. Geosci.* 7, 627–637. doi: 10.1038/ngeo2234

Cohen, J., Zhang, X., Francis, J., Jung, T., Kwok, R., Overland, J., et al. (2018). "Arctic change and possible influence on mid-latitude climate and weather," in *A US CLIVAR white paper (No. 2018-1)*, ed. K. Uhlenbrock (Washington, DC: U.S. CLIVAR Project Office), 41. doi: 10.5065/D6TH8KGW

Cohen, J., Zhang, X., Francis, J., Jung, T., Kwok, R., Overland, J., et al. (2020). Divergent consensuses on Arctic amplification influence on midlatitude severe winter weather. *Nat. Clim. Chang.* 10, 20–29. doi: 10.1038/s41558-019-0662-y

Cohen, J. L., Furtado, J. C., Barlow, M. A., Alexeev, V. A., and Cherry, J. E. (2012). Arctic warming, increasing snow cover and widespread boreal winter cooling. *Environ. Res. Lett.* 7, 14007–14014. doi: 10.1088/1748-9326/7/1/014007

Dee, D. P., Uppala, S. M., Simmons, A. J., Berrisford, P., Poli, P., Kobayashi, S., et al. (2011). The ERA-Interim reanalysis: configuration and performance of the data assimilation system. *Q. J. R. Meteorol. Soc.* 137, 553–597. doi: 10.1002/qj.828

Duchon, C. E. (1979). Lanczos filtering in one and two dimensions. *J. Appl. Meteor.* 18, 1016–1022. doi: 10.1175/1520-045019790182.0.CO;2

Furtado, J. C., Cohen, J. L., Butler, A. H., Riddle, E. E., and Kumar, A. (2015). Eurasian snow cover variability and links to winter climate in the cmip5 models. *Clim. Dyn.* 45, 2591–2605. doi: 10.1007/s00382-015-2494-4

Gardelle, J., Berthier, E., and Arnaud, Y. (2012). Slight mass gain of Karakoram glaciers in the early twenty-first century. *Nat. Geosci.* 5, 322–325. doi: 10.1038/ngeo1450

Ghatak, D., Deser, C., Frei, A., Gong, G., Phillips, A., Robinson, D. A., et al. (2012). Simulated Siberian snow cover response to observed Arctic sea ice loss, 1979–2008. *J. Geophys. Res.* 117:D23108. doi: 10.1029/2012jd018047

Guo, D., Sun, J., Yang, K., Pepin, N., Xu, Y., Xu, Z., et al. (2019). Satellite data reveal southwestern Tibetan Plateau cooling since 2001 due to snow-albedo feedback. *Int. J. Climatol.* 40, 1644–1655. doi: 10.1002/joc.6292

Guo, H., Li, X., and Qiu, Y. (2020). Comparison of global change at earth's "three poles" using spaceborne earth observation. *Sci. Bull.* doi: 10.1016/j.scib.2020.04.031

Handorf, D., Jaiser, R., Dethloff, K., Rinke, A., and Cohen, J. (2015). Impacts of Arctic sea ice and continental snow cover changes on atmospheric winter teleconnections. *Geophys. Res. Lett.* 42, 2367–2377. doi: 10.1002/2015GL063203

Hock, R., Rasul, G., Adler, C., Cáceres, B., Gruber, S., Hirabayashi, Y., et al. (2019). "High mountain areas," in *IPCC Special Report on the Ocean and Cryosphere in a Changing Climate*, eds H.-O. Pörtner, D. C. Roberts, V. Masson-Delmotte, P. Zhai, M. Tignor, E. Poloczanska, et al. (Geneva: IPCC).

Honda, M., Inoue, J., and Yamane, S. (2009). Influence of low Arctic sea ice minima on anomalously cold Eurasian winters. *Geophys. Res. Lett.* 36, 262–275. doi: 10.1029/2008GL037079

Immerzeel, W. W., Van Beek, L. P., and Bierkens, M. F. (2010). Climate change will affect the Asian water towers. *Science* 328, 1382–1385. doi: 10.1126/science.1183188

Jung, O., Sung, M. K., Sato, K., Lim, Y. K., Kim, S. J., Baek, E. H., et al. (2017). How does the sst variability over the western North Atlantic ocean control arctic warming over the barents-kara seas? *Environ. Res. Lett.* 12:034021. doi: 10.1088/1748-9326/aa5f3b

Kapnick, S. B., Delworth, T. L., Ashfaq, M., Malyshev, S., and Milly, P. C. (2014). Snowfall less sensitive to warming in Karakoram than in Himalayas due to a unique seasonal cycle. *Nat. Geosci.* 7, 834–840. doi: 10.1038/ngeo2269

Kim, B. M., Son, S. W., Min, S. K., Jeong, J. H., Kim, S. J., Zhang, X., et al. (2014). Weakening of the stratospheric polar vortex by Arctic sea ice loss. *Nat. Commun.* 5:4646. doi: 10.1038/ncomms5646

Kim, K. Y., and Son, S. W. (2016). Physical characteristics of eurasian winter temperature variability. *Environ. Res. Lett.* 11:044009. doi: 10.1088/1748-9326/11/4/044009

Kim, S. J., and Kim, B. M. (2018). Arctic warming and its influence on east Asian winter cold events: a brief recap. *Adv. Polar Sci.* 29, 3–12. doi: 10.13679/j.advps.2018.1.00003

Kumar, P., Saharwardi, M. S., Banerjee, A., Azam, M. F., Dubey, A. K., and Murtugudde, R. (2019). Snowfall variability dictates glacier mass balance variability in himalaya-karakoram. *Sci. Rep.* 9:18192. doi: 10.1038/s41598-019-54553-9

Li, C., Su, F., Yang, D., Tong, K., Meng, F., and Kan, B. (2018). Spatiotemporal variation of snow cover over the Tibetan Plateau based on MODIS snow product, 2001–2014. *Int. J. Climatol.* 38, 708–728. doi: 10.1002/joc.5204

Liu, J., Curry, J. A., Wang, H., Song, M., and Horton, R. M. (2012). Impact of declining Arctic sea ice on winter snowfall. *PNAS* 109, 4074–4079. doi: 10.1073/pnas.1114910109

Lu, C., Ge, Y., and Xie, G. (2005). "Tibetan plateau serves as a water tower," in *Proceedings 2005 IEEE International Geoscience and Remote Sensing Symposium, 2005*, Seoul, 3120–3123.

Matsumura, S., and Kosaka, Y. (2019). Arctic–Eurasian climate linkage induced by tropical ocean variability. *Nat. Commun.* 10:3441. doi: 10.1038/s41467-019-11359-7

Mori, M., Watanabe, M., Shiogama, H., Inoue, J., and Kimoto, M. (2014). Robust Arctic sea ice influence on the frequent Eurasian cold winters in past decades. *Nat. Geosci.* 7, 869–873. doi: 10.1038/ngeo2277

Norris, J., Carvalho, L. M., Jones, C., and Cannon, F. (2015). WRF simulations of two extreme snowfall events associated with contrasting extratropical cyclones over the western and central Himalaya. *J. Geophys. Res. Atmos.* 120, 3114–3138. doi: 10.1002/2014JD022592

Onarheim, I. H., Eldevik, T., Smedsrud, L. H., and Stroeve, J. C. (2018). Seasonal and regional manifestation of Arctic sea ice loss. *J. Clim.* 31, 4917–4932. doi: 10.1175/JCLI-D-17-0427.1

Overland, J., Francis, J. A., Hall, R., Hanna, E., Kim, S. J., and Vihma, T. (2015). The melting arctic and midlatitude weather patterns: are they connected? *J. Clim.* 28, 7917–7932. doi: 10.1175/JCLI-D-14-00822.1

Park, H. S., Lee, S., Son, S. W., Feldstein, S. B., and Kosaka, Y. (2015). The impact of poleward moisture and sensible heat flux on arctic winter sea ice variability. *J. Clim.* 28, 5030–5040. doi: 10.1175/JCLI-D-15-0074.1

Rahimi, S. R., Wu, C., Liu, X., and Brown, H. (2019). Exploring a variable-resolution approach for simulating regional climate over the Tibetan Plateau using VR-CESM. *J. Geophys. Res. Atmos.* 124, 4490–4513. doi: 10.1029/2018JD028925

Rayner, N., Parker, D. E., Horton, E., Folland, C. K., Alexander, L. V., Rowell, D., et al. (2003). Global analyses of sea surface temperature, sea ice, and night marine air temperature since the late nineteenth century. *J. Geophys. Res. Atmos.* 108:D14. doi: 10.1029/2002jd002670

Screen, J. A. (2017). Simulated atmospheric response to regional and pan-Arctic sea ice loss. *J. Clim.* 30, 3945–3962. doi: 10.1175/jcli-d-16-0197.1

Senan, R., Orsolini, Y. J., Weisheimer, A., Vitart, F., Balsamo, G., Stockdale, T. N., et al. (2016). Impact of springtime Himalayan–Tibetan Plateau snowpack on the onset of the Indian summer monsoon in coupled seasonal forecasts. *Clim. Dyn.* 47, 2709–2725. doi: 10.1007/s00382-016-2993-y

Shi, N., Wang, X., and Tian, P. (2018). Interdecadal variations in persistent anomalous cold events over Asian mid-latitudes. *Clim. Dyn.* 52, 3729–3739. doi: 10.1007/s00382-018-4353-6

Singh, S. K., Rathore, B. P., and Bahuguna, I. M. (2014). Snow cover variability in the Himalayan–Tibetan region. *Int. J. Climatol.* 34, 446–452. doi: 10.1002/joc.3697

Song, L., Wu, R., and An, L. (2019). Different sources of 10 to 30 day intraseasonal variations of autumn snow over Western and Eastern Tibetan Plateau. *Geophys. Res. Lett.* 46, 9118–9125. doi: 10.1029/2019GL083852

Song, M., and Liu, J. (2017). The role of diminishing Arctic sea ice in increased winter snowfall over northern high-latitude continents in a warming environment. *Acta Oceanol. Sin.* 36, 34–41. doi: 10.1007/s13131-017-1021-3

Sorokina, S. A., Li, C., Wettstein, J. J., and KvamstÃ, N. G. (2016). Observed atmospheric coupling between Barents Sea ice and the warm-Arctic cold-Siberian anomaly pattern. *J. Clim.* 29, 495–511. doi: 10.1175/JCLI-D-15-0046.1

Sun, C., Yang, S., Li, W., Zhang, R., and Wu, R. (2016). Interannual variations of the dominant modes of East Asian winter monsoon and possible links to Arctic sea ice. *Clim. Dyn.* 47, 481–496. doi: 10.1007/s00382-015-2851-3

Sung, M. K., Kim, S. H., Kim, B. M., and Choi, Y. S. (2018). Interdecadal variability of the warm Arctic and cold Eurasia pattern and its North Atlantic origin. *J. Clim.* 31, 5793–5810. doi: 10.1175/JCLI-D-17-0562.1

Takaya, K., and Nakamura, H. (2001). A formulation of a phase-independent wave-activity flux for stationary and migratory quasigeostrophic eddies on a zonally varying basic flow. *J. Atmos. Sci.* 58, 608–627. doi: 10.1175/1520-0469(2001)058<0608:afoapi>2.0.co;2

Wegmann, M., Orsolini, Y., Vázquez, M., Gimeno, L., Nieto, R., Bulygina, O., et al. (2015). Arctic moisture source for Eurasian snow cover variations in autumn. *Environ. Res. Lett.* 10:054015. doi: 10.1088/1748-9326/10/5/054015

Xiao, Z., and Duan, A. (2016). Impacts of Tibetan Plateau snow cover on the Interannual variability of the east asian summer monsoon. *J. Clim.* 29, 8495–8514. doi: 10.1175/JCLI-D-16-0029.1

Yao, T., Thompson, L., Yang, W., Yu, W., Gao, Y., Guo, X., et al. (2012). Different glacier status with atmospheric circulations in Tibetan Plateau and surroundings. *Nat. Clim. Change* 2, 663–667. doi: 10.1038/nclimate1580

Ye, K., and Jung, T. (2019). How strong is influence of the tropics and midlatitudes on the Arctic atmospheric circulation and climate change? *Geophys. Res. Lett.* 46, 4942–4952. doi: 10.1029/2019GL082391

Ye, K., Jung, T., and Semmler, T. (2018). The influences of the Arctic troposphere on the midlatitude climate variability and the recent Eurasian cooling. *J. Geophys. Res. Atmos.* 123, 162–184. doi: 10.1029/2018JD028980

Yuan, C., Li, W., Guan, Z., and Yamagata, T. (2019). Impacts of april snow cover extent over Tibetan Plateau and the central Eurasia on Indian Ocean Dipole. *Int. J. Climatol.* 39, 1756–1767. doi: 10.1002/joc.5888

Zhang, G., Yao, T., Shum, C. K., Yi, S., Yang, K., Xie, H., et al. (2017). Lake volume and groundwater storage variations in Tibetan Plateau's endorheic basin. *Geophys. Res. Lett.* 44, 5550–5560. doi: 10.1002/2017GL073773

Zhang, Y., Yan, P., Liao, Z., Huang, D., and Zhang, Y. (2019a). The winter concurrent meridional shift of the East Asian Jet streams and the associated thermal conditions. *J. Clim.* 32, 2075–2088. doi: 10.1175/JCLI-D-18-0085.1

Zhang, Y., Zou, T., and Xue, Y. (2019b). An Arctic-Tibetan connection on subseasonal to seasonal time scale. *Geophys. Res. Lett.* 46, 2790–2799. doi: 10.1029/2018GL081476

Zuo, J., Ren, H. L., Wu, B., and Li, W. (2016). Predictability of winter temperature in China from previous autumn Arctic sea ice. *Clim. Dyn.* 47, 2331–2343. doi: 10.1007/s00382-015-2966-6

Conflict of Interest: The authors declare that the research was conducted in the absence of any commercial or financial relationships that could be construed as a potential conflict of interest.

frontiers in Earth Science

ORIGINAL RESEARCH
published: 03 September 2020
doi: 10.3389/feart.2020.00358

Contrasting Roles of a Large Alpine Lake on Tibetan Plateau in Shaping Regional Precipitation During Summer and Autumn

Yufeng Dai[1], Tandong Yao[1,2,3], Lei Wang[1,2,3]*, Xiangyu Li[4] and Xiaowen Zhang[1]*

[1] Institute of Tibetan Plateau Research, Chinese Academy of Sciences, Beijing, China, [2] CAS Center for Excellence in Tibetan Plateau Earth Sciences, Chinese Academy of Sciences, Beijing, China, [3] University of Chinese Academy of Sciences, Beijing, China, [4] Institute of Atmospheric Physics, Chinese Academy of Sciences, Beijing, China

OPEN ACCESS

Edited by:
Nick Van De Giesen, Delft University of Technology, Netherlands

Reviewed by:
Hongkai Gao, East China Normal University, China
Lijuan Wen, Northwest Institute of Eco-Environment and Resources (CAS), China

***Correspondence:**
Yufeng Dai
yufengdai@itpcas.ac.cn
Lei Wang
wanglei@itpcas.ac.cn

Specialty section:
This article was submitted to Hydrosphere, a section of the journal Frontiers in Earth Science

Received: *05 January 2020*
Accepted: *04 August 2020*
Published: *03 September 2020*

Citation:
Dai Y, Yao T, Wang L, Li X and Zhang X (2020) Contrasting Roles of a Large Alpine Lake on Tibetan Plateau in Shaping Regional Precipitation During Summer and Autumn. Front. Earth Sci. 8:358. doi: 10.3389/feart.2020.00358

Lakes have important influence on local temperature and precipitation and are also regulators of regional climate. Using satellite and climate reanalysis datasets and a regional weather research forecasting (WRF) model, we carried out two WRF sensitivity experiments: one including the lake (WRF_lake) and the other with lake replaced by land surface (WRF_nolake). The comparison between the two sensitivity WRF experiments revealed that, in summer, the lake was strong heat sink in the daytime and heat source at night. In autumn, the lake was weak heat sink in the daytime and strong heat source at night. Correspondingly, the precipitation was reduced by about 45–70% over the lake because of the cooling effect in summer of 2008, and the precipitation over the lake and to the east of the lake was enhanced by 60% because of the warming effect of 2008.

Keywords: cooling effect, warming effect, Nam Co Lake, WRF model, Tibetan Plateau

INTRODUCTION

The landscape of the Tibetan Plateau (TP) is characterized by extremely complex topography. The local climate varies greatly. Lake represents a significant feature of the surface because its thermal inertia has a large potential impact on the climate (Bonan, 1995; Laird et al., 2009; Xu et al., 2009; Zhou et al., 2015; Kirillin et al., 2017; Wang et al., 2018; Zhan et al., 2019). The lake system of the TP is also closely linked to local climate (Haginoya et al., 2009; Tsujimoto and Koike, 2013; Huang et al., 2017; Wang et al., 2017; Song et al., 2019). The contribution of lake effects to local or regional climate is becoming more and more important. Due to the lake-air temperature difference in different seasons, there are different seasonal distribution characteristics of lake effect precipitation. To understand the seasonal characteristics of lake effect precipitation in the lake area is conducive to further understanding the regional water cycle characteristics.

Seasonal contributions of lake effects have attracted broad research attention given their dramatic impacts on local precipitation. In summer, the precipitation in Lake Ladoga and Great Lakes reduces 20–70% of convective precipitation because of lake effect (Scott and Huff, 1996;

Samuelsson et al., 2010). In winter, the lake effect increases the precipitation. For example, Lake Ladoga in Russia can increase convective precipitation by up to 20–40% (Samuelsson et al., 2010). The Great Lakes in the United States, which are unfrozen and induces large lake effect precipitation (more than 100%) in the winter (Umek and Gohm, 2016; Welsh et al., 2016). The effect is different from Ngoring Lake and Gyaring Lake on the TP in summer. Both of these two lakes cause an increase of precipitation in early summer (Wen et al., 2015). The increase precipitation was attributed to the hollowness of these two lakes, which allows them to easily warm in the early summer.

To our knowledge, up to now few quantitative studies have been done regarding the seasonal contributions of lake effects to local precipitation in such cold and high-mountain environment.

Nam Co Lake is one of the largest lakes on the TP, with an area of more than 2000 km^2. The maximum and average depths of Nam Co Lake are 98 and 45 m, respectively. The shape of Nam Co Lake is in the East-West direction, and the length of the fetch distance is about 73 km (**Figure 1**). The south area of the lake is the Nianqing Tanggula Mountains. Previous studies have demonstrated the role of Nam Co Lake in local climate (Lazhu et al., 2016; Huang et al., 2017; Dai et al., 2018a,b). Based on station meteorological data and reanalysis data, we analyzed the qualitative characteristics of lake effect precipitation in the Nam Co basin and identified the lake cooling effect during July–August and lake heating effect during November–December (Dai et al., 2018b). With weather research forecasting (WRF) model simulation and station meteorological data, we pointed out that the lake effect could contribute more than half of the precipitation to the downwind heavy precipitation events around Nam Co Lake during October to November (Dai et al., 2018a). However, the impact of the lake cooling effect of Nam Co on the regional climate during summer hasn't been quantitatively evaluated. The diurnal character of lake effect of Nam Co on regional climate hasn't been well-explored. In this paper, we focus on the lake effect of Nam Co on regional climate during daytime and nighttime, and its seasonal variations of the diurnal character of lake effect of Nam Co in summer and autumn.

MATERIALS AND METHODS

Multiple Data Products

We used MODIS Land Surface Temperature Data Product (MOD11A2) collected during the daytime (10:30 Local Time; 04:30 UTC) and at night (22:30 Local Time; 16:30 UTC), and we calculated diurnal surface temperatures separately by using Modis_day and Modis_night. We then used these surface temperatures to calculate the monthly averages of surface temperature. More detailed information of MOD11A2 data can be found in the MODIS Products Users' Guide[1].

[1]https://icess.eri.ucsb.edu/modis/LstUsrGuide/usrguide_8dtil.html

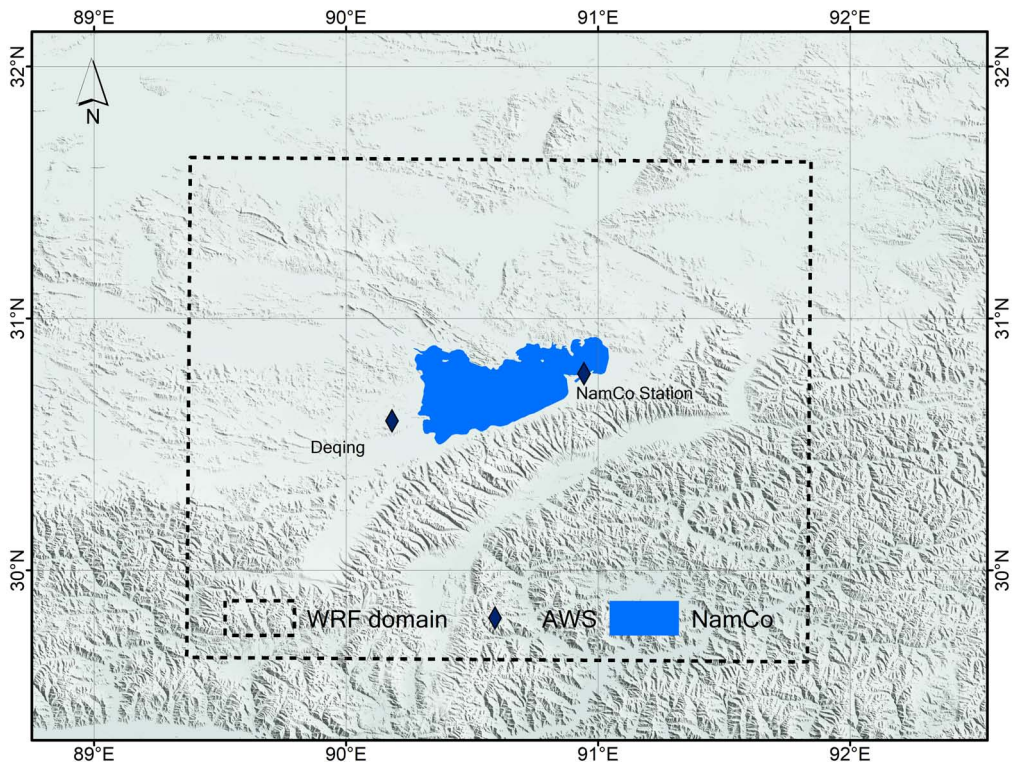

FIGURE 1 | Location and topography of Nam Co Lake and the two nearby meteorological stations (Nam Co and Deqing stations). The black dash box denotes the position of the simulation domain. The AWS is the abbreviation of Automatic Weather Station.

We used 10 m wind speed and 2 m air temperature data in 2008 from ERA 5 monthly reanalysis datasets, with a horizontal resolution of 0.25° × 0.25° (Copernicus Climate Change Service (C3S), 2017). We also used 2 m air temperature, and precipitation data (0.1° × 0.1° resolution) in 2008 from the China Meteorological Forcing Dataset (CMFD; Yang et al., 2010; He et al., 2020) that combines *in-situ* observations of TP, provided by the National Tibetan Plateau Data Center. Finally, we used monthly Tropical Rainfall Measuring Mission (TRMM; Kummerow et al., 2000) data in 2008.

WRF Model

WRF model is a useful tool to study regional lake-effect precipitation (Zhao et al., 2012; Nicholls and Toumi, 2014;

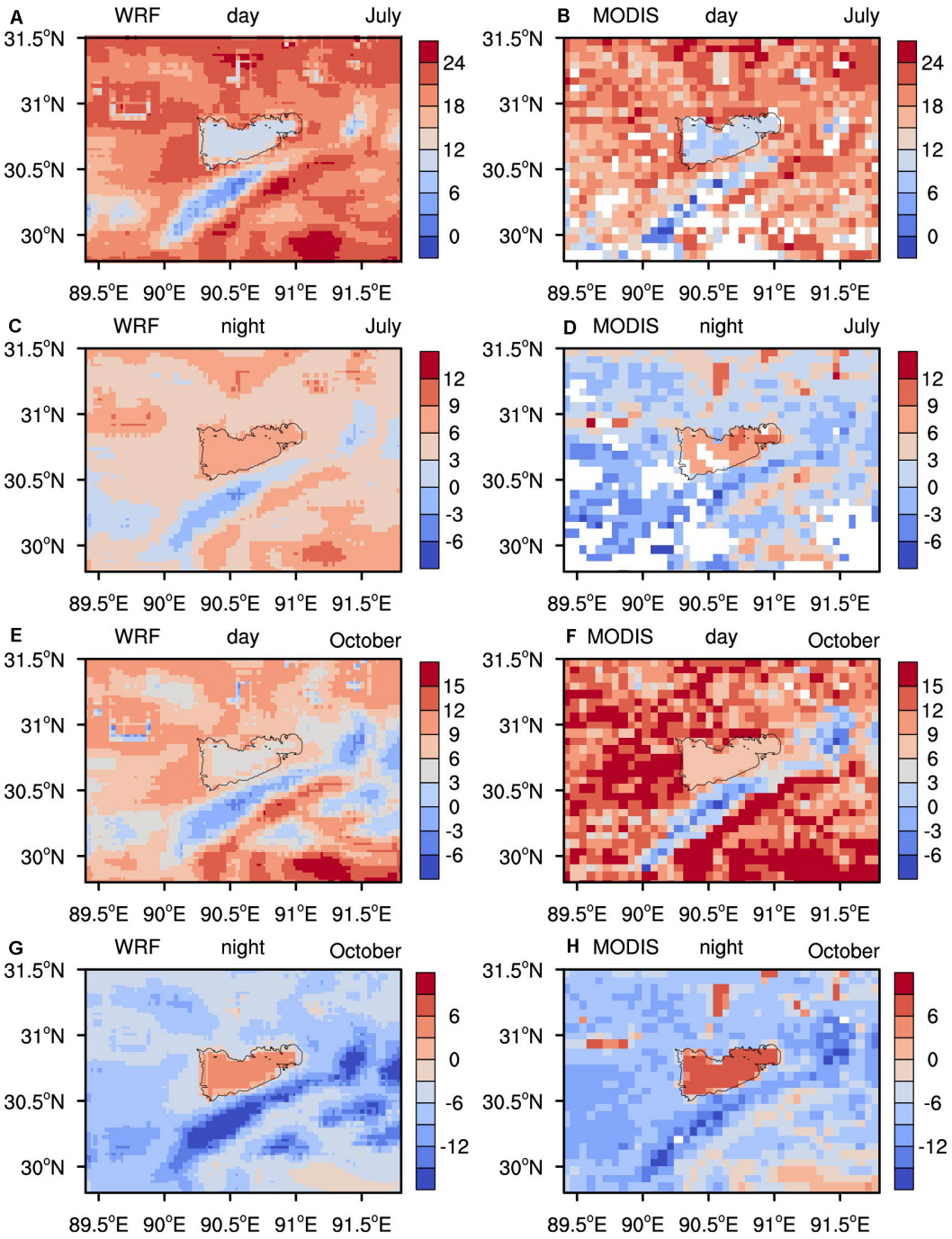

FIGURE 2 | Diurnal spatial pattern of temperature of skin surface (TSK, units: °C) of WRF_lake simulation in July **(A,C)** and October **(E,G)**, and the TSK from MODIS data in July **(B,D)** and October **(F,H)**. The gridded squares with missed MODIS value are filled by white color.

Sun et al., 2015; Wen et al., 2015; Dai et al., 2018a; Shi and Xue, 2019). Using the WRF-Lake model to simulate the regional climate of Nam Co in October of 2006, we showed that Nam Co causes lake-effect precipitation in October (Dai et al., 2018a). Similar to the study of Dai et al. (2018a), in this study we used the WRF model to simulate the impact of Nam Co Lake on local climate, with same physics options choices and similar boundary configuration. Please see more details in Dai et al. (2018a). The simulation start time was 0000 UTC 1 May 2008, and the end time was 0000 UTC 1 December 2008, and the model produced output every 3 h. The averages of the simulated data at two times during the day (03:00 and 06:00 UTC) and at two times during the night (15:00 and 18:00 UTC) are reported here to compare with the corresponding MODIS daytime (04:30 UTC) and nighttime (16:30 UTC) data. We carried out two WRF experiments: one including lake (WRF_lake) and the other with lake replaced by land surface (WRF_nolake). Comparison of WRF_lake and WRF_nolake showed the influence of the lake on the regional climate.

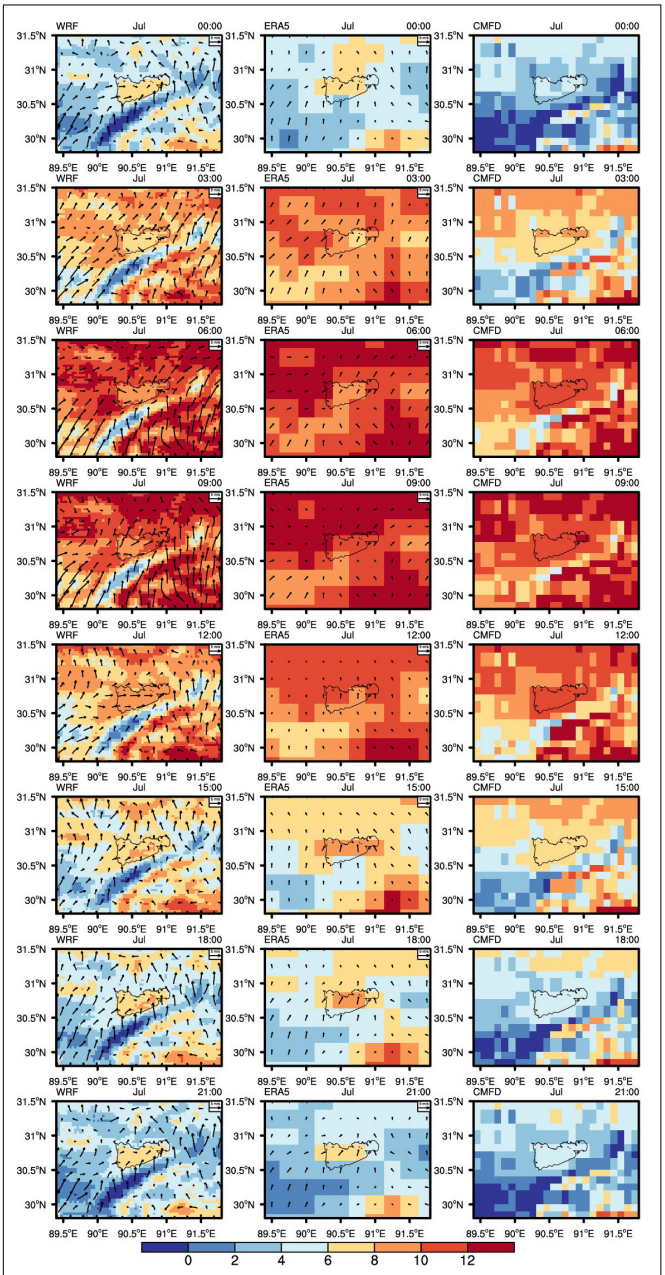

FIGURE 3 | Comparison of the monthly mean 3-h 2 m temperature (shading, units: °C) and 10 m wind (vector, units: mm/s) between the WRF_lake simulation, the ERA5 and the CMFD data in July 2008.

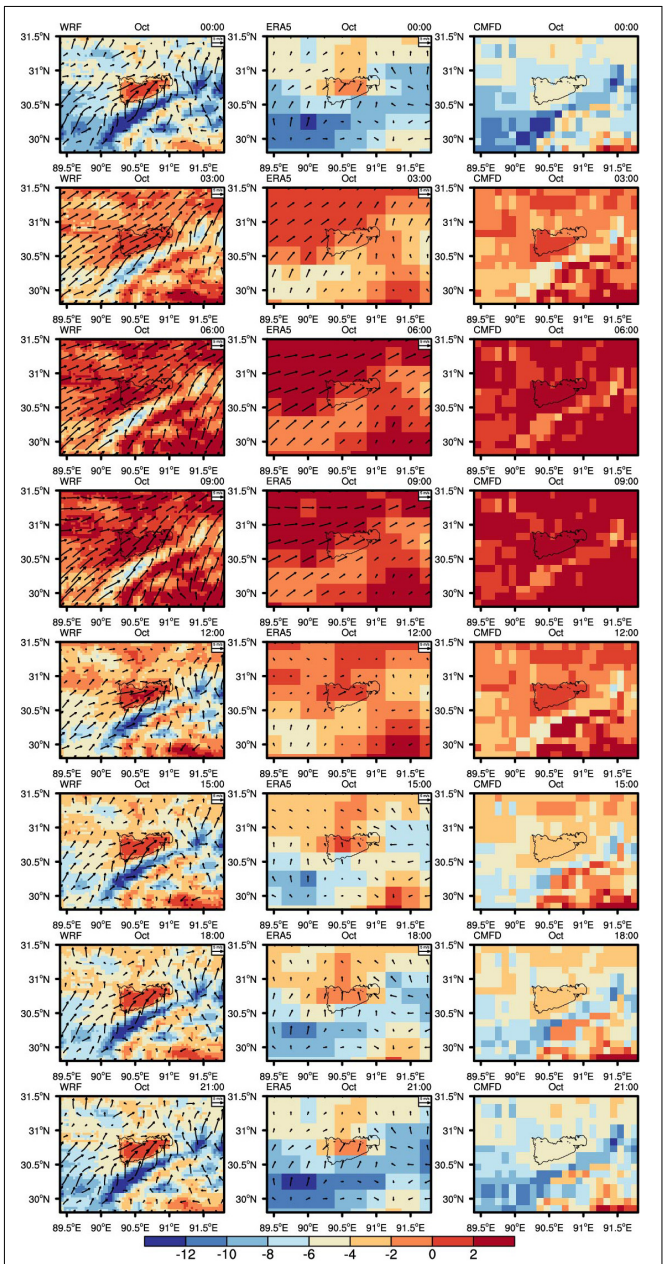

FIGURE 4 | Same as **Figure 3**, but for October 2008.

The aim of this study was to investigate the seasonal variety of Nam Co lake effects in summer and autumn using observations, reanalysis data, and numerical modeling. The key factor to understand the lake effect is lake-air temperature difference (Lavoie, 1972). In this study, we verified and analyzed the factors such as lake temperature, air temperature and precipitation. An observation station located in the Nam Co area since 2005, in the watershed of the southeastern part of the lake, 2 km away from the lake shore, where lake effect precipitation occurs in October and November (Dai et al., 2018a). The precipitation measurements of the west part of the lake (Deqing station) have been carried out in 2008 (Zhou et al., 2013). We therefore chose to analyze the characteristics of the lake effect in 2008. Nam Co Lake is ice-covered for about 5 months and ice free for about 7 months per year (Kropacek et al., 2013). From December to April, as the complex influence of lake ice and the total precipitation over the lake and surrounding is few to negligible. In our analysis we therefore focused on the period from May to November. According to the seasonal variations in the simulated latent and sensible heat fluxes of Nam Co (Lazhu et al., 2016), the result indicate that the evaporation is small in summer and reaches a peak in October. We chose July in summer and October in autumn for detailed analysis.

EVALUATION OF WRF SIMULATIONS: TEMPERATURE AND PRECIPITATION

Comparison of the Skin Surface Temperatures Between WRF and MODIS

The diurnal changes of MODIS lake surface temperature were relatively small compared to the corresponding temperature changes of the surrounding land surface. We first obtained the temperature of surface skin (TSK) over the lake by WRF simulation and by MODIS data. The spatial pattern of the WRF simulated TSK was in agreement with the MODIS data, though the simulated TSK over land is slightly higher with WRF than MODIS data in July and lower in October (**Figure 2**). In particular, the TSK difference between the lake and land and its diurnal variety are well-captured by WRF. Based on MODIS data, the TSK over Nam Co Lake was cooler (warmer) than the TSK in surrounding land during daytime (nighttime) (**Figure 2**). In July (**Figures 2A–D**), the TSK difference between the lake surface temperature and land surface temperature was −16°C in the daytime and 5°C at nighttime according to MODIS data. The simulated TSK difference between the lake and land with WRF was −12°C in the daytime and 3°C at nighttime. In October (**Figures 2E–H**), the TSK difference between the lake and land was −6°C in the daytime and 15°C at nighttime according to MODIS data. The simulated TSK difference between the lake and land with WRF was −3°C in the daytime and 12°C at nighttime. The simulated TSK difference between the lake surface temperature and land surface temperature was consistent with that based on MODIS data, which the deviation was about 4°C in the daytime and 3°C at nighttime. Therefore, WRF simulation was able to mimic the characteristics of diurnal variety the TSK difference between the lake and land in July and October.

Comparison of 2 m Temperatures and 500 hPa Temperatures Between WRF, ERA5, and CMFD

We also used the ERA 5 and CMFD data in July (**Figure 3**) and October (**Figure 4**) of 2008 to compare with the WRF simulation in terms of two varieties: 2 m air temperature

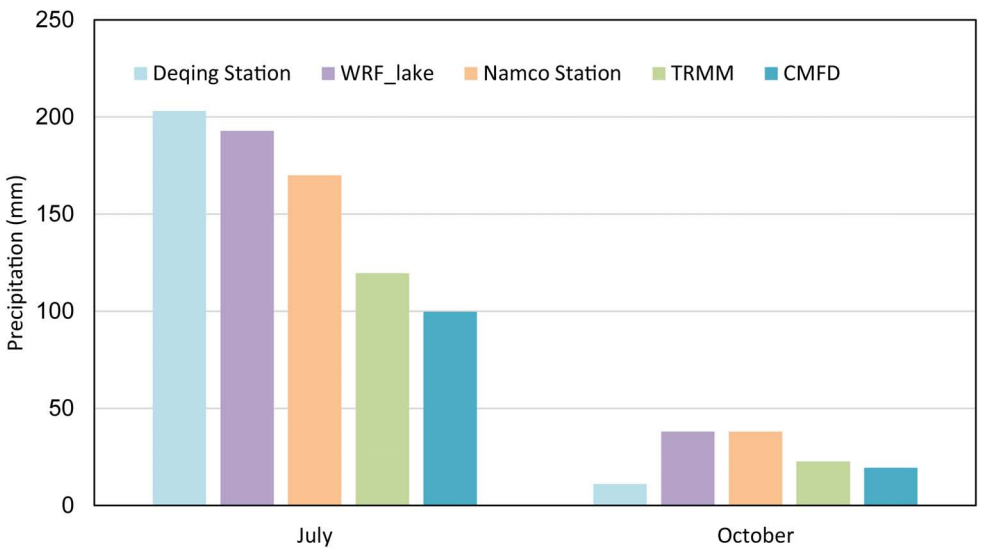

FIGURE 5 | The monthly precipitation at the upwind Deqing station (blue), and the downwind Nam Co station (orange), as well as the monthly precipitation averaged over the Nam Co Lake by the WRF simulation (purple) and from the TRMM product (green) and CMFD (dark blue), in July and October, respectively.

and 10 m wind speed. The resolutions of WRF, ERA 5, and CMFD were 0.06° × 0.06°, 0.25° × 0.25°, and 0.1° × 0.1°, respectively. Nearly at each 3-h time slices, the WRF reasonably reproduced the spatial pattern of CMFD 2 m temperature. It is also noticed that the WRF-simulated temperature over the lake was closer to the ERA5 data. The WRF-simulated wind pattern was also consistent with the ERA5 wind. The WRF generally well-simulated both the

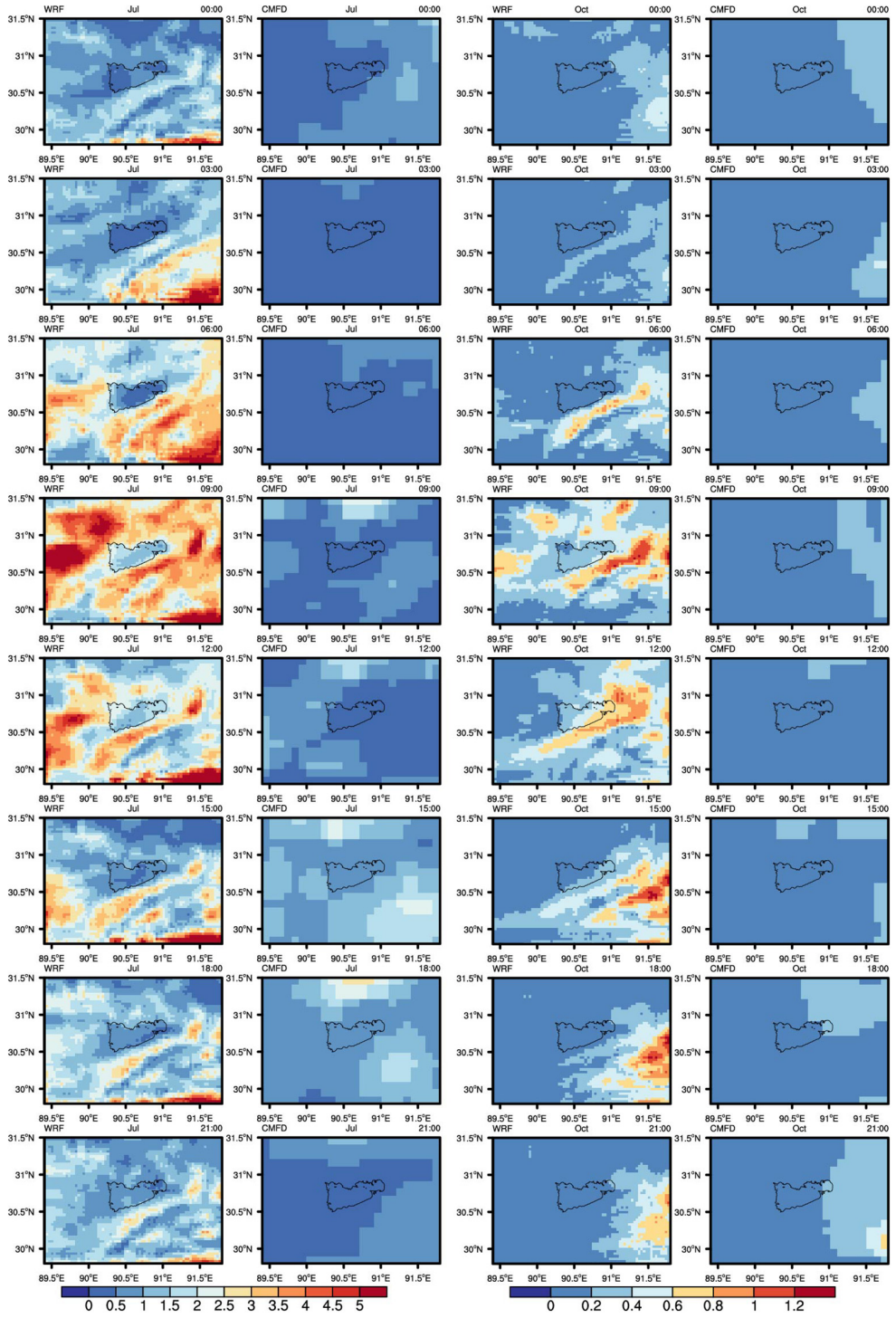

FIGURE 6 | Spatial distribution of monthly mean 3-h precipitation (shading, units: mm) from the WRF_lake simulation and the CMFD data in July (left two panels) and October (right two panels) of 2008.

wind in July and in October based on reanalysis data and gave more details.

Precipitation Comparison: Spatial and Temporal Distribution

The Nam Co Lake is a relatively gentle terrain in the basin. The simulated precipitation over the lake was larger than the TRMM and CMFD data (**Figure 5**). The deviation between the WRF simulation and the satellite data also appears in previous study on the TP (Gao et al., 2015). Compared with two stations on the east and west side of the lake, in July, the WRF-simulated precipitation was higher than the precipitation at the Nam Co station on the east coast and lower than the precipitation at the Deqing station on the west coast. In contrary, the WRF-simulated precipitation in October was

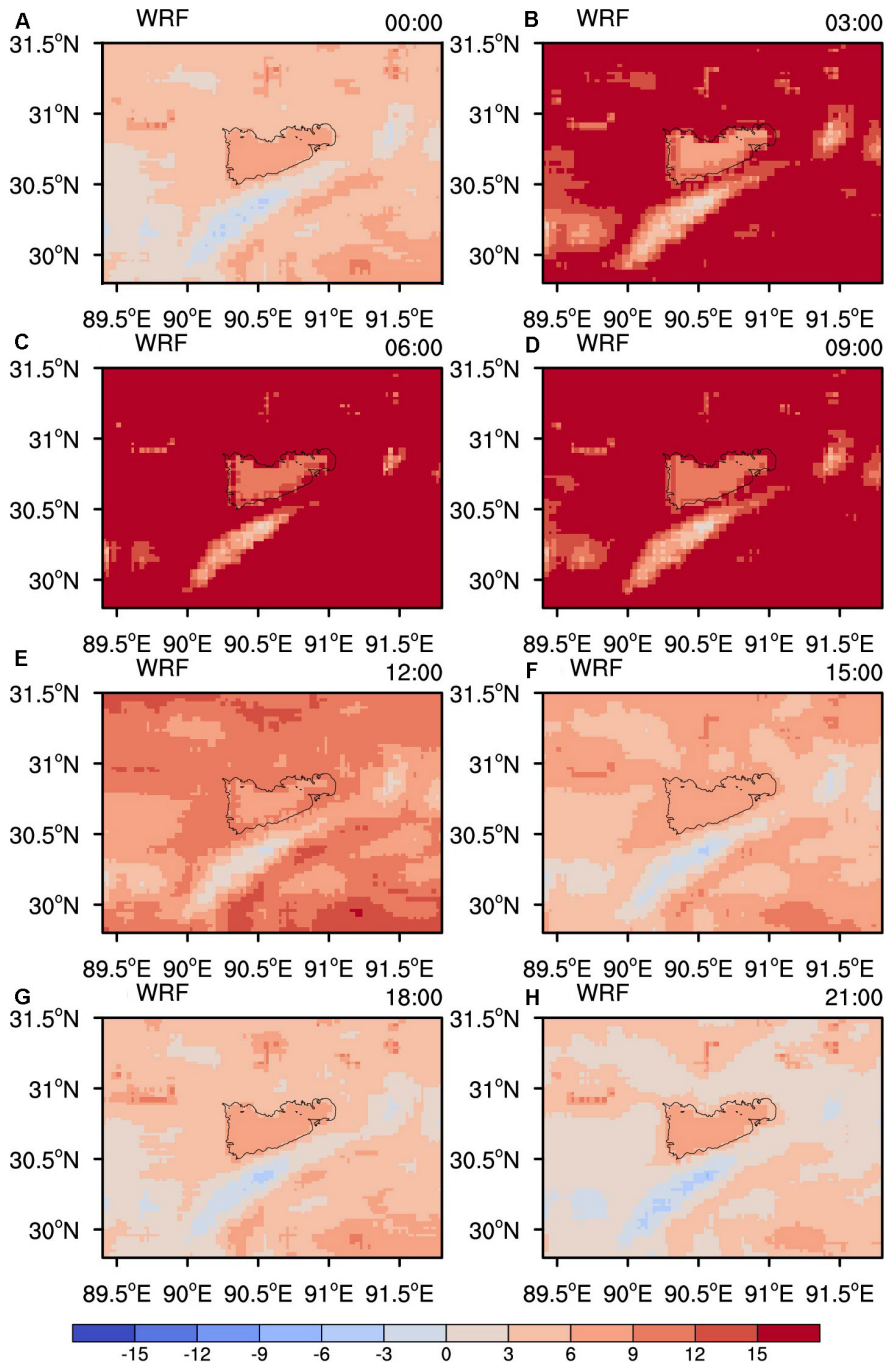

FIGURE 7 | Spatial pattern of monthly mean 3-h TSK (**A–H**, shading, units: °C) of WRF_lake simulation in July 2008.

slightly lower than the precipitation at the Nam Co station and higher than the precipitation at the Deqing station. However, WRF reasonably reproduced the seasonal rainfall amount in July and October. Regarding the spatial patterns, nearly at each 3 h time interval, the WRF produced a comparable spatial pattern of precipitation to that of the CMFD (**Figure 6**). We also found discrepancies between the WRF simulation and the CMFD data from 0:00 to 6:00 UTC, which may be attributed to their different 2 m temperature over the lake. In general, the WRF can reasonably depict the lake effect on the regional precipitation.

RESULTS AND DISCUSSION

Heat Sinks and Sources

Because the temperature difference between the lake and land is very different during the day and night, we analyzed the diurnal

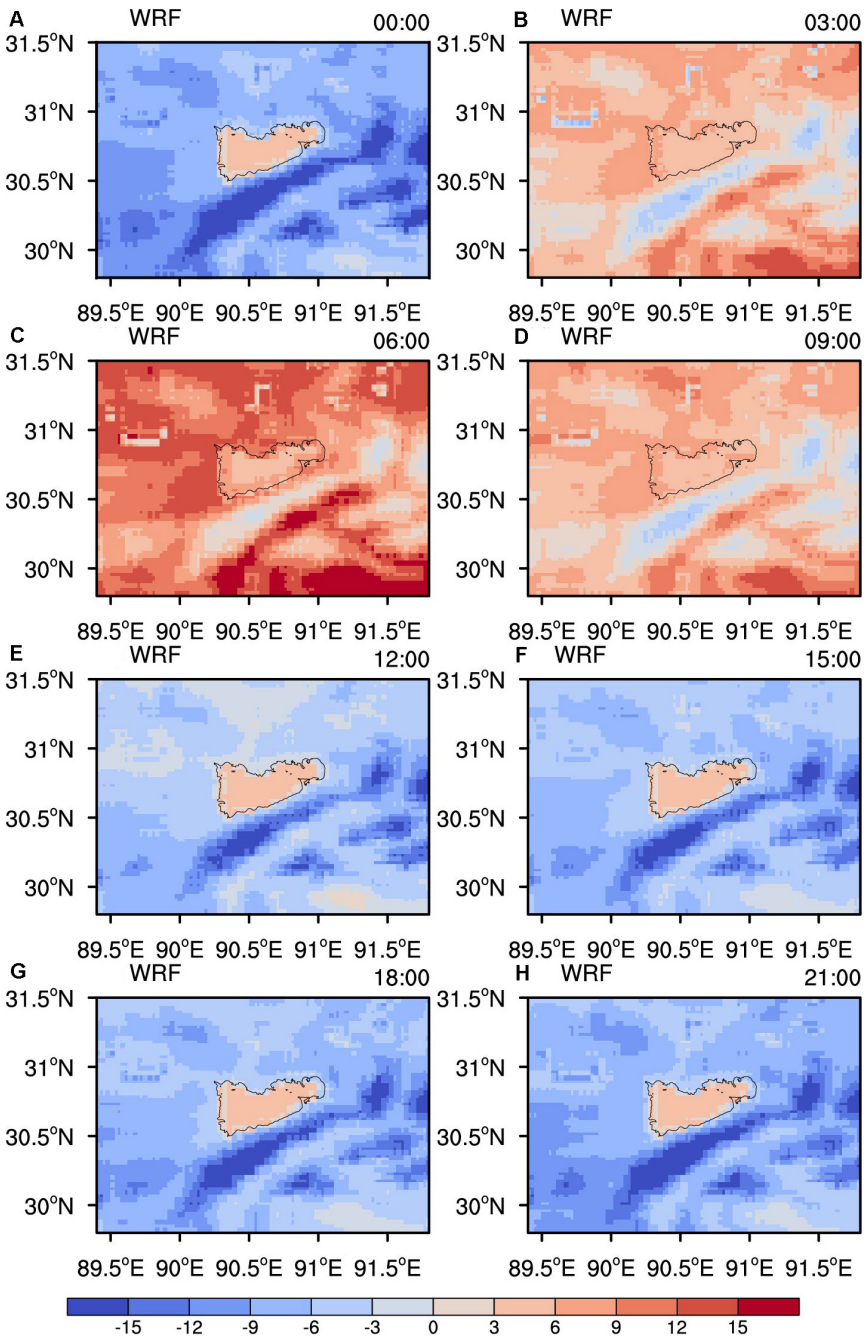

FIGURE 8 | Same as **Figure 7**, but for October 2008.

variety of the temperature difference between the lake and land during different seasons based on the WRF-simulated TSK. After the sun rises in the daytime (03:00–09:00 UTC) during July, the TSK of the land rises faster than the TSK of the lake, which is about 9°C cooler than the land TSK at 09:00 UTC (**Figure 7**). Six hours after sunset (15:00–18:00 UTC), the TSK difference between the lake and land reaches a minimum. The land cools faster at night (21:00–00:00 UTC), and the lake TSK is about

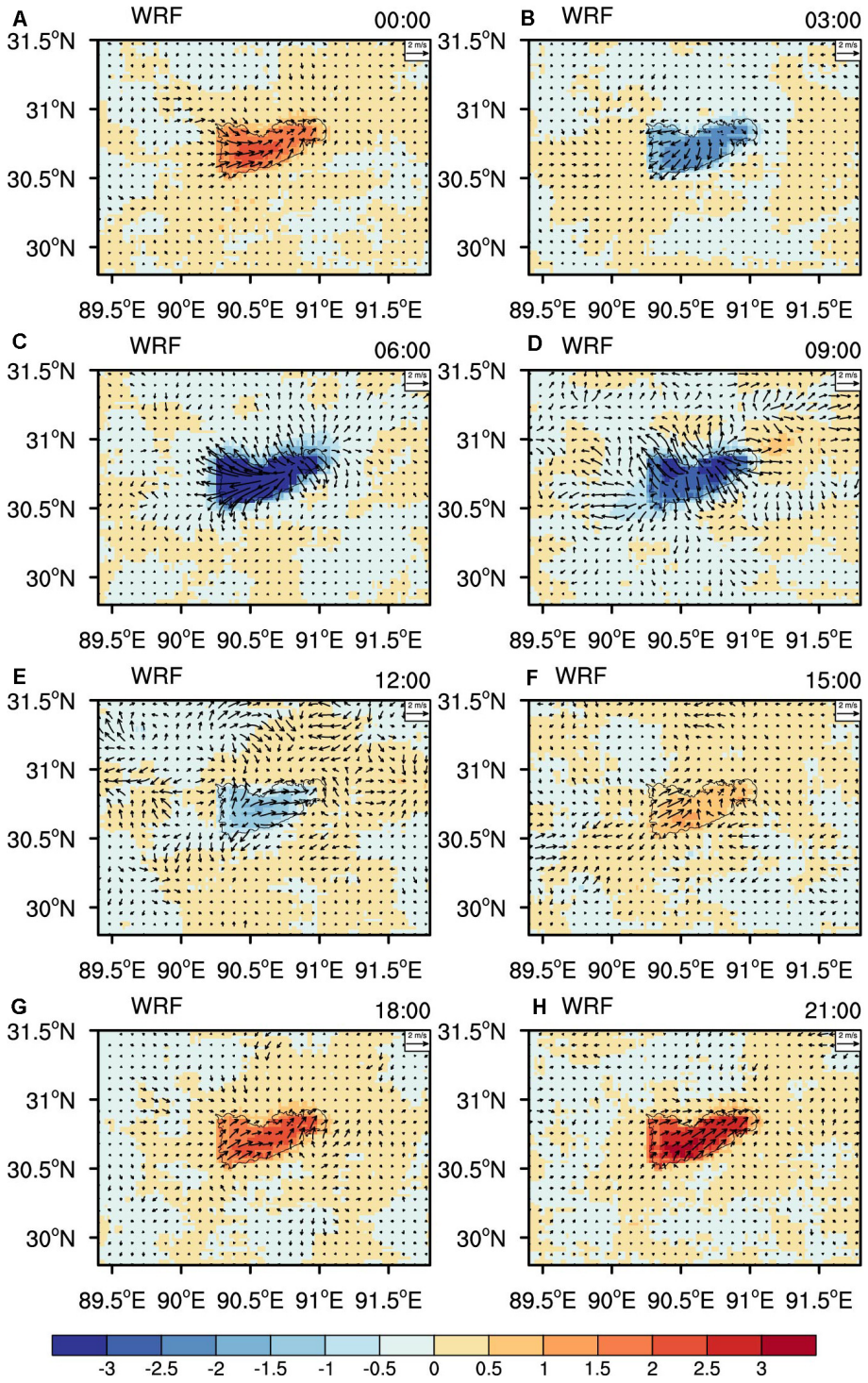

FIGURE 9 | Spatial pattern of simulated of monthly mean 3-h 2 m air temperature (**A–H**, shading, units: °C) and 10 m wind (**A–H**, vector, units: m/s) anomaly (difference between WRF_lake and WRF_nolake simulations) in July 2008.

6°C warmer than the land TSK. The maximum temperature difference between the lake and land can be as low as −17°C during the day, whereas the temperature difference is about 10°C at night. The lake is a strong heat sink during the day, and a source of heat at night in the summer.

In October, during the 6 h after the sun rises (03:00–09:00 UTC), the TSK of the land rises faster than the TSK of the lake (**Figure 8**). During evening and early morning (12:00–00:00 UTC), the TSK of the land decreases much faster than the TSK of the lake. The maximum TSK difference between the lake and land

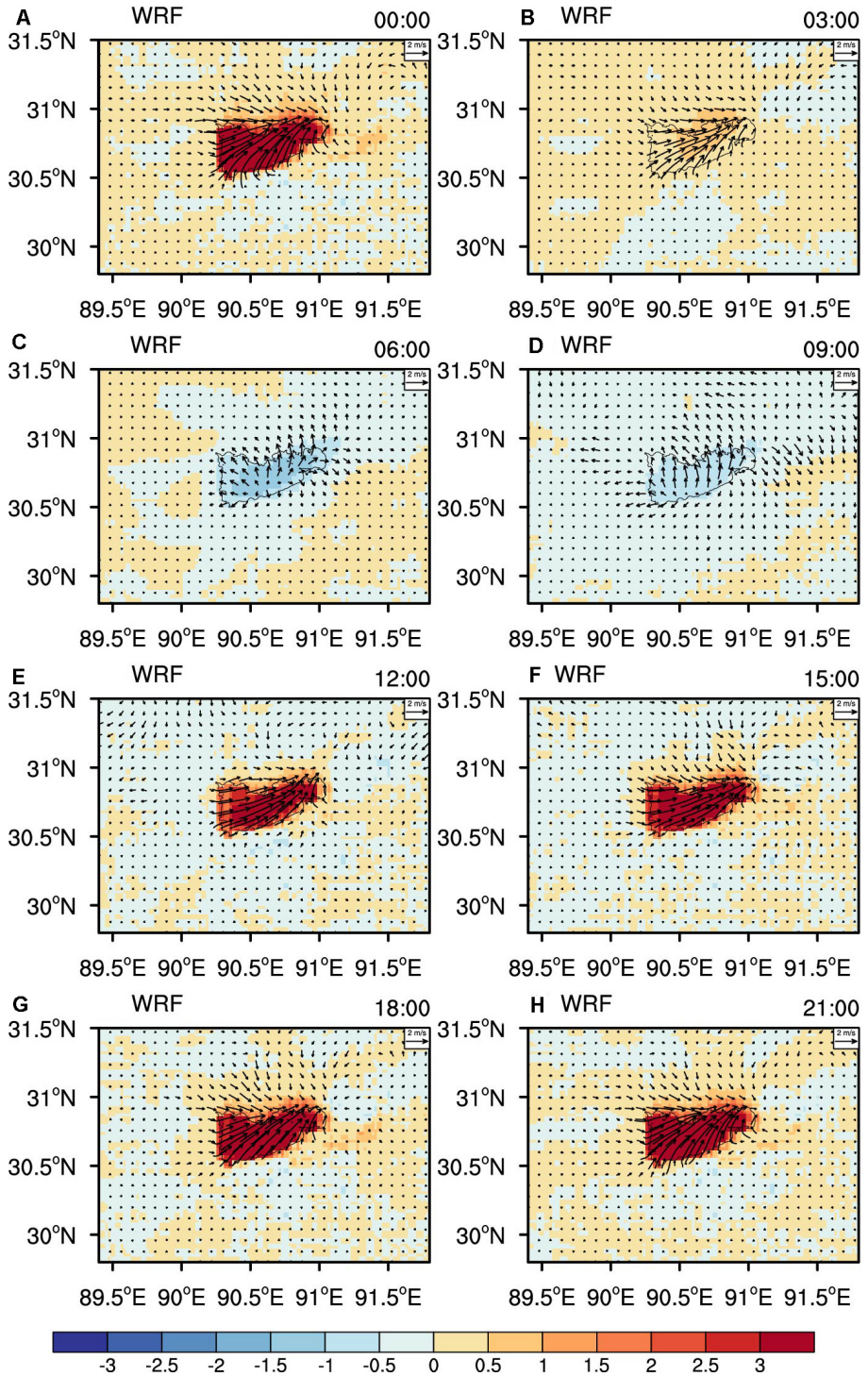

FIGURE 10 | Same as **Figure 9**, but for October 2008.

is greater than 18°C at night, whereas the difference between the land and lake temperature is less than 5°C during the daytime. The lake acted mainly as a strong heat source in the autumn.

Cooling and Warming Effects on 2 m Temperatures

The comparison of WRF_lake and WRF_nolake showed that the lake had a cooling effect in July, whereas the lake had a warming effect in October, in terms of 2 m air temperature. Due to the air temperature varies more diurnally than the lake temperature, we analyzed the temperatures during the daytime and night with WRF_lake and WRF_nolake models to determine the influence of the lake on the daily maximum and daily minimum air temperatures.

The lake effect was essentially limited to the immediate vicinity of the lake (**Figure 9**). In July, the lake was characterized by a negative temperature anomaly of up to 3°C during the day and by the positive anomalies of up to 3°C during the night. The presence of the lakes reduces the 2 m temperature within a distance of 10 km around the lake by an average of 0.4°C during the day (03:00–12:00 UTC), and increased it by about 0.3°C at night (18:00–03:00 UTC). The diurnal temperature difference around the lake was reduced by 0.7°C because of the lake effect. In July, there was still a warming effect of Nam Co Lake that could be explained by its relatively warm surface water at night.

In October, Nam Co Lake is characterized by a negative temperature anomaly of up to 1°C during the day and by the positive temperature anomalies of up to 4°C at night. According to the spatial pattern of simulated diurnal 2 m

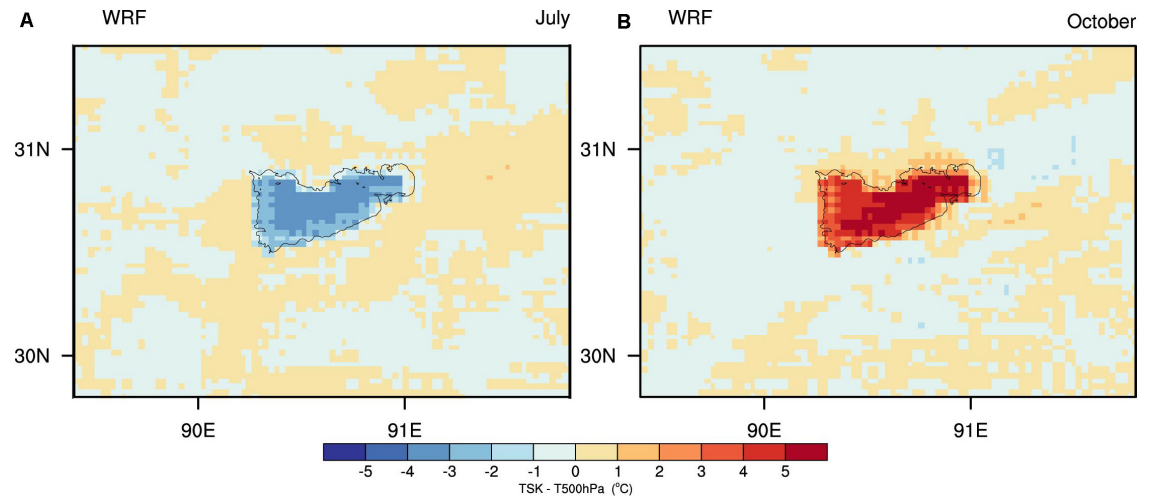

FIGURE 11 | Spatial pattern of the difference between the simulated results by the WRF_lake and the WRF_nolake, which is the gap between the lake surface and 500 hPa temperatures (units: °C) in July **(A)** and October **(B)** of 2008.

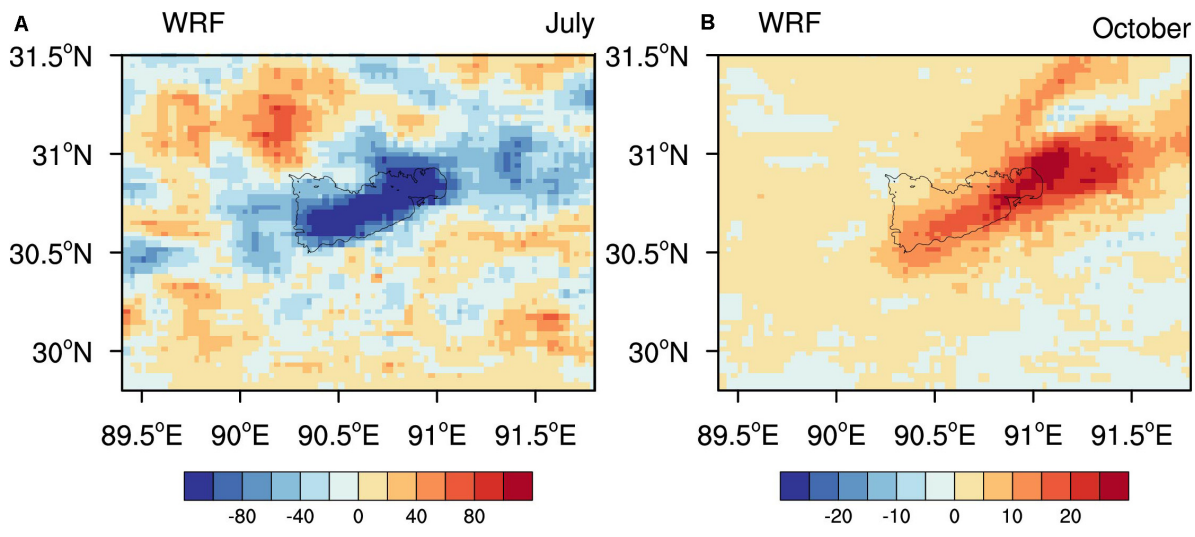

FIGURE 12 | Precipitation difference (mm) between the WRF_lake and the WRF_nolake simulations in July **(A)** and October **(B)** of 2008.

air temperature anomaly (difference between WRF_lake and WRF_nolake simulations) in October (**Figure 10**), The presence of the lakes reduced the temperature around the lake by 0.6°C in the daytime (06:00–12:00 UTC), and its influence extended from the shore for as much as 50 km to the east. In the middle of the night (21:00–06:00 UTC), the temperature within 10 km of the lake increased by an average of 0.4°C. The diurnal temperature difference around the lake was reduced by 1°C.

The cooling effect during the day led to a decrease of the daily maximum temperature in areas adjacent to the lake, and the warming effect at night led to an increase of the daily minimum temperature in the region. The lake therefore reduced the amplitude of the daily temperature difference cycle. Previous studies of Ngoring Lake and Gyaring Lake on the TP have also revealed that most lakes reduce the maximum temperature all year round and increase the minimum temperature, except in March (Wen et al., 2015). This temperature effect has an impact on the flora of the region.

Examination of the spatial pattern of the 10 m wind field (**Figures 9**, **10**) revealed that during the day (06:00–12:00 UTC) the presence of the lake caused a strong lake breeze around the lake, which was strongest in the afternoon (15:00–18:00 Local Time) in July. The Lake breeze emanated from the lake to the surrounding area and transported water vapor to the land and increased the humidity. The lake breeze not only changed the temperature but also caused the formation of low clouds and fogs. A land breeze, which blew from the land over the lake, was apparent during 1200–0000 UTC (18:00–06:00 Local Time) in October.

We compared the temperature difference between the surface and 500 hPa simulated by WRF_lake and WRF_nolake models to calculate the influence of the lake on the temperature difference between lake and 500 hPa. During the period from May to August, the lake-500 hpa temperature difference was less than 6°C based on the WRF_lake simulation, whereas lake-500 hPa temperature difference exceeded 12°C according to the WRF_nolake simulation. In July, the presence of the lakes reduced the lake-500 hPa temperature difference over Nam Co Lake by about 5°C (**Figure 11**). In September, the presence of the lake caused a slight increase in the lake-500 hPa temperature difference. In October and November, the lake-500 hPa temperature difference exceeded 12°C according to the WRF_lake simulation, whereas the lake-500 hPa temperature difference was less than 12°C based on the WRF_nolake simulation. In October, the presence of the lake increased the lake-500 hPa temperature difference by about 7°C (**Figure 11**). Theoretically, changes of the lake effect are reflected by changes of lake-500 hPa temperature difference.

Lake Effect: Enhancement and Suppression on Precipitation

The WRF_lake and WRF_nolake simulations indicated that there was no significant change in the distribution of large scale precipitation. Because of the cooling effects of the lake, there was characterized by much less precipitation over the lake during May to August. The presence of the lake reduced precipitation over the lake and thereby increased the spatial differences of regional precipitation. The precipitation over the lake simulated by the WRF_lake model was less than the simulated precipitation in the absence of the lake (WRF_nolake). The difference was greatest in July (**Figure 12A**). There was no significant change in May and September. During May to August, the presence of the lake reduced precipitation over the lake by about 45–70%.

The WRF_lake and WRF_nolake simulation showed that there was no significant change in the distribution of large scale precipitation from October to November too. At a smaller scale, parts of the basin east of 90.25°E were dominated by lake-effect precipitation. The precipitation over the lake simulated by WRF_lake model exceeded the precipitation simulated in the absence of the lake (WRF_nolake) by more than 60% (**Figure 12B**). Furthermore, precipitation was greater in the eastern than in the western part of the basin because of the lake.

The precipitation over Nam Co Lake is suppressed in summer and increased in autumn as a result of the lake effect. Although the Nam Co lake effect did not change the large-scale distribution of precipitation, it significantly affected the temporal pattern of precipitation locally. Specifically, the lake effect reduced precipitation in the wet season and increased precipitation in the dry season.

CONCLUSION

Although the monthly mean lake–land temperature difference was small in summer, the surface WRF-simulated temperature showed that in July the lake was a heat sink during the day and a source of heat during the night. The monthly mean lake–land temperature difference was significant in October and November, when the lake temperature was higher than the land temperature. In October, the lake was mainly a source of heat, especially between midnight and early morning. The distribution of precipitation in the Nam Co basin was characterized by two patterns. the precipitation was less over the lake than over the surrounding land in summer; and the precipitation was greater in the eastern than in the western part of the Nam Co basin in autumn.

A comparison of two WRF sensitivity experiments, one including the lake (WRF_lake) and the other with lake replaced by land surface (WRF_nolake), showed that the lake cooled the air during the day and warmed the air at night by up to several degrees, depending on the large-scale meteorological conditions. The cooling effect of the lake was manifested by lower air temperatures in the summer, and the warming effect of the lake was manifested by higher air temperatures in autumn. Both the cooling and warming effects were limited to the immediate vicinity of the lake and were normally not apparent more than a few kilometers from the shore. The presence of the lake reduced the lake–500-hPa temperature difference over Nam Co Lake by up to 6°C from May to August in 2008. In October and November of 2008, the presence of the lake increased the lake–500-hPa temperature difference by up to 7°C. The lake effect did not change the large-scale distribution of precipitation, but it affected local precipitation significantly. In 2008, from June

through August, the lake reduced precipitation over the lake by about 45–70%; while from October through November in 2008, the WRF-simulated precipitation was 60% greater than the precipitation in the absence of the lake.

DATA AVAILABILITY STATEMENT

Publicly available datasets were analyzed in this study. This data can be found here: https://e4ftl01.cr.usgs.gov/MODIS_Dailies_E/MOLT/MOD11A1.005/; https://disc2.gesdisc.eosdis.nasa.gov/opendap/TRMM_L3/; http://data.tpdc.ac.cn; https://reanalyses.org/atmosphere/era5-references.

AUTHOR CONTRIBUTIONS

YD designed the study and led the drafting of the manuscript. LW and TY contributed to the interpretation of results and the overall framing of the study. XL and XZ performed data analysis and prepared figures. All authors contributed to the article and approved the submitted version.

FUNDING

This study was funded by the National Natural Science Foundation of China (Grants 41801049 and 91747201).

ACKNOWLEDGMENTS

We would like to acknowledge the U.S. Geological Survey (USGS) and U.S. National Aeronautics and Space Administration (NASA) for providing MODIS data (https://e4ftl01.cr.usgs.gov/MODIS_Dailies_E/MOLT/MOD11A1.005/) and TRMM data (https://disc2.gesdisc.eosdis.nasa.gov/opendap/TRMM_L3/), the National Tibetan Plateau Data Center providing CMFD data (http://data.tpdc.ac.cn), and the European Center for Medium-Range Weather Forecasts for providing the ERA 5 data (https://reanalyses.org/atmosphere/era5-references).

REFERENCES

Bonan, G. B. (1995). Sensitivity of a gcm simulation to inclusion of inland water surfaces. *J. Clim.* 8, 2691–2704. doi: 10.1175/1520-0442(1995)008<2691:soagst>2.0.co;2

Copernicus Climate Change Service (C3S) (2017). ERA5: Fifth generation of ECMWF atmospheric reanalyses of the global climate. Copernicus Climate Change Service Climate Data Store (CDS). Available online at: https://cds.climate.copernicus.eu/cdsapp#!/home

Dai, Y., Wang, L., Yao, T., Li, X., Zhu, L., and Zhang, X. (2018a). Observed and simulated lake effect precipitation over the tibetan plateau: an initial study at nam co lake. *J. Geophys. Res. Atmos.* 123, 6746–6759. doi: 10.1029/2018jd028330

Dai, Y., Yao, T., Li, X., and Ping, F. (2018b). The impact of lake effects on the temporal and spatial distribution of precipitation in the nam co basin, tibetan plateau. *Quat. Int.* 475, 63–69. doi: 10.1016/j.quaint.2016.01.075

Gao, Y., Xu, J., and Chen, D. (2015). Evaluation of wrf mesoscale climate simulations over the tibetan plateau during 1979-2011. *J. Clim.* 28, 2823–2841. doi: 10.1175/jcli-d-14-00300.1

Haginoya, S., Fujii, H., Kuwagata, T., Xu, J., Ishigooka, Y., Kang, S., et al. (2009). Air-lake interaction features found in heat and water exchanges over nam co on the tibetan plateau. *Sola* 5, 172–175. doi: 10.2151/sola.2009-044

He, J., Yang, K., Tang, W., Lu, H., Qin, J., Chen, Y. Y., et al. (2020). The first high-resolution meteorological forcing dataset for land process studies over China. *Sci. Data* 7:25. doi: 10.1038/s41597-020-0369-y

Huang, L., Wang, J., Zhu, L., Ju, J., and Daut, G. (2017). The warming of large lakes on the tibetan plateau: evidence from a lake model simulation of nam co, china, during 1979-2012. *J. Geophys. Res. Atmos.* 122, 13095–13107. doi: 10.1002/2017jd027379

Kirillin, G., Wen, L., and Shatwell, T. (2017). Seasonal thermal regime and climatic trends in lakes of the tibetan highlands. *Hydrol. Earth Syst. Sci.* 21, 1895–1909. doi: 10.5194/hess-21-1895-2017

Kropacek, J., Maussion, F., Chen, F., Hoerz, S., and Hochschild, V. (2013). Analysis of ice phenology of lakes on the tibetan plateau from modis data. *Cryosphere* 7, 287–301. doi: 10.5194/tc-7-287-2013

Kummerow, C., Simpson, J., Thiele, O., Barnes, W., Chang, A. T. C., Stocker, E., et al. (2000). The status of the tropical rainfall measuring mission (trmm) after two years in orbit. *J. Appl. Meteorol.* 39, 1965–1982.

Laird, N., Sobash, R., and Hodas, N. (2009). The frequency and characteristics of lake-effect precipitation events associated with the New York state finger lakes. *J. Appl. Meteorol. Climatol.* 48, 873–886. doi: 10.1175/2008jamc2054.1

Lavoie, R. L. (1972). A mesoseale numerical model of lake-fffect storms. *J. Atmos. Sci.* 29, 1025–1040. doi: 10.1175/1520-0469(1972)029<1025:amnmol>2.0.co;2

Lazhu, Y. K., Wang, J., Lei, Y., Chen, Y., Zhu, L., Ding, B., et al. (2016). Quantifying evaporation and its decadal change for Lake Nam Co, central Tibetan Plateau. *J. Geophys. Res. Atmos.* 121, 7578–7591. doi: 10.1002/2015JD024523

Nicholls, J. F., and Toumi, R. (2014). On the lake effects of the caspian sea. *Q. J. R. Meteorol. Soc.* 140, 1399–1408. doi: 10.1002/qj.2222

Samuelsson, P., Kourzeneva, E., and Mironov, D. (2010). The impact of lakes on the european climate as simulated by a regional climate model. *Boreal Environ. Res.* 15, 113–129.

Scott, R. W., and Huff, F. A. (1996). Impacts of the Great Lakes on regional climate conditions. *J. Gt. Lakes Res.* 22, 845–863. doi: 10.1016/S0380-1330(96)71006-7

Shi, Q., and Xue, P. F. (2019). Impact of lake surface temperature variations on lake effect snow over the Great Lakes region. *J. Geophys. Res. Atmos.* 124, 12553–12567. doi: 10.1029/2019JD031261

Song, C., Sheng, Y., Zhan, S., Wang, J., Ke, L., and Liu, K. (2019). Impact of amplified evaporation due to lake expansion on the water budget across the inner Tibetan Plateau. *Int. J. Climatol.* 40, 2091–2105. doi: 10.1002/joc.6320

Sun, X., Xie, L., Semazzi, F., and Liu, B. (2015). Effect of lake surface temperature on the spatial distribution and intensity of the precipitation over the lake victoria basin. *Mon. Weather Rev.* 143, 1179–1192. doi: 10.1175/mwr-d-14-00049.1

Tsujimoto, K., and Koike, T. (2013). Land-lake breezes at low latitudes: the case of tonle sap lake in cambodia. *J. Geophys. Res. Atmos.* 118, 6970–6980. doi: 10.1002/jgrd.50547

Umek, L., and Gohm, A. (2016). Lake and orographic effects on a snowstorm at lake constance. *Mon. Weather Rev.* 144, 4687–4707. doi: 10.1175/mwr-d-16-0032.1

Wang, B., Ma, Y., Ma, W., and Su, Z. (2017). Physical controls on half-hourly, daily, and monthly turbulent flux and energy budget over a high-altitude small lake on the tibetan plateau. *J. Geophys. Res. Atmos.* 122, 2289–2303. doi: 10.1002/2016jd026109

Wang, W., Lee, X., Xiao, W., Liu, S., Schultz, N., Wang, Y., et al. (2018). Global lake evaporation accelerated by changes in surface energy allocation in a warmer climate. *Nat. Geosci.* 11, 410–414. doi: 10.1038/s41561-018-0114-8

Welsh, D., Geerts, B., Jing, X., Bergmaier, P. T., Minder, J. R., Steenburgh, W. J., et al. (2016). Understanding heavy lake-effect snowfall: The vertical structure of radar reflectivity in a deep snowband over and downwind of lake ontario. *Mon. Weather Rev.* 144, 4221–4244. doi: 10.1175/mwr-d-16-0057.1

Wen, L., Lv, S., Li, Z., Zhao, L., and Nagabhatla, N. (2015). Impacts of the two biggest lakes on local temperature and precipitation in the yellow river source region of the tibetan plateau. *Adv. Meteorol.* 2015:248031. doi: 10.1155/2015/248031

Xu, J., Yu, S., Liu, J., Haginoya, S., and Yasunari, T. (2009). The implication of heat and water balance changes in a lake basin on the tibetan plateau. *Hydrol. Res. Lett.* 3, 1–5. doi: 10.3178/hrl.3.1

Yang, K., He, J., Tang, W. J., Qin, J., and Cheng, C. C. K. (2010). On downward shortwave and longwave radiations over high altitude regions: observation and modeling in the Tibetan Plateau. *Agric. Forest Meteorol.* 150, 38–46. doi: 10.1016/j.agrformet.2009.08.004

Zhan, S., Song, C., Wang, J., Sheng, Y., and Quan, J. (2019). A global assessment of terrestrial evapotranspiration increase due to surface water area change. *Earth's Future* 7, 266–282. doi: 10.1029/2018EF001066

Zhao, L., Jin, J., Wang, S.-Y., and Ek, M. B. (2012). Integration of remote-sensing data with wrf to improve lake-effect precipitation simulations over the great lakes region. *J. Geophys. Res. Atmos.* 117:D09102. doi: 10.1029/2011jd016979

Zhou, J., Wang, L., Zhang, Y., Guo, Y., Li, X., and Liu, W. (2015). Exploring the water storage changes in the largest lake (selin co) over the tibetan plateau during 2003-2012 from a basin-wide hydrological modeling. *Water Resour. Res.* 51, 8060–8086. doi: 10.1002/2014wr015846

Zhou, S., Kang, S., Chen, F., and Joswiak, D. R. (2013). Water balance observations reveal significant subsurface water seepage from lake nam co, south-central tibetan plateau. *J. Hydrol.* 491, 89–99. doi: 10.1016/j.jhydrol.2013.03.030

Conflict of Interest: The authors declare that the research was conducted in the absence of any commercial or financial relationships that could be construed as a potential conflict of interest.

frontiers in Earth Science

ORIGINAL RESEARCH
published: 04 September 2020
doi: 10.3389/feart.2020.00351

Headwater Flow Geochemistry of Mount Everest (Upper Dudh Koshi River, Nepal)

Pierre Chevallier[1], Jean-Luc Seidel[1], Jean-Denis Taupin[1] and Ornella Puschiasis[2,3]*

[1] Laboratoire HydroSciences Montpellier, Centre National de la Recherche Scientifique, Institut de Recherche pour le Développement, Université de Montpellier, Montpellier, France, [2] Centre d'Etudes en Sciences Sociales sur les Mondes Africains, Américains et Asiatiques, l'Institut National des Langues et Civilisations Orientales, l'Institut de Recherche pour le Développement, Université de Paris, Paris, France, [3] Centre d'Etudes Himalayennes, Centre National de la Recherche Scientifique, Paris-Villejuif, France

The aim of this work, conducted in the upper valley of the Khumbu on the southern part of Mount Everest, is to approach in parallel three topics: (i) the dynamics of the water geochemistry, major ions and trace elements; (ii) the stable water isotopes of precipitation and rivers; and (iii) the water uses by the inhabitants. As in most mountain environments, the Khumbu area is threatened by climate change, which impacts the cryosphere and consequently the people and the landscapes. Moreover, changes in water use are also related to new needs stemming from tourism, which strongly affect local livelihood. For the first two topics, new results are presented. They provide details on the global chemical quality of the river water and show how certain elements are seasonally influenced and how other elements allow us to distinguish the water origins within the study zone. Beside the use of stable isotopes to determine mainly the origin of the water flow in the rivers, the isotopic patterns confirm the double climatic influence of the westerly fluxes in the winter season and of the Asian monsoon in the summer season. Regarding water use, the study does not conclude on the potability of the water resource, because microbiologic and organic components have not been investigated; however it confirms that the chemical quality is good. In conclusion, we attempt to predict the future of the geochemistry patterns submitted to the double pressure of climate change and the surge in tourism.

Keywords: major ions, trace elements, stable isotopes, precipitation, river flow, water use, Central Himalaya

OPEN ACCESS

Edited by:
Xiuping Li,
Institute of Tibetan Plateau Research (CAS), China

Reviewed by:
Andre Banning,
Ruhr University Bochum, Germany
Yan Bai,
Center for Excellence in Tibetan Plateau Earth Sciences (CAS), China

****Correspondence:***
Pierre Chevallier
pierre.chevallier@ird.fr

Specialty section:
This article was submitted to Hydrosphere, a section of the journal Frontiers in Earth Science

Received: *24 April 2020*
Accepted: *28 July 2020*
Published: *04 September 2020*

Citation:
Chevallier P, Seidel J-L, Taupin J-D and Puschiasis O (2020) Headwater Flow Geochemistry of Mount Everest (Upper Dudh Koshi River, Nepal). Front. Earth Sci. 8:351. doi: 10.3389/feart.2020.00351

INTRODUCTION

The future of the cryosphere (glacier and snow cover) in the Hindu Kush Himalaya high mountains is a major concern (Pörtner et al., 2019; Wester et al., 2019); it is threatened not only by global warming due to greenhouse gas emissions, but also by local air pollution due to the atmospheric brown cloud, and especially the transportation and deposition of black carbon aerosol (Bonasoni et al., 2010; Kaspari et al., 2011; Jacobi et al., 2015) from human activities in the densely inhabited regions of the south and southwest of the Central Himalaya mountain range as well as the rapid increase of tourist activity (Jacquemet, 2018).

In this context, the Paprika and Preshine projects (see section "Funding") joined the efforts of Nepalese, French, and Italian research teams (see section "Acknowledgments") to explore the

impact of these anthropogenic constraints on the water cycle dynamics in the Dudh Koshi River Basin (**Figure 1**) on the south side of Mount Everest (8847 m). Several reasons justified the choice of this study zone that is characterized by two confluent watercourses, the Imja River and the Khumbu River, respectively, originating from the southern and western faces of the main range of Mount Everest and its satellite summits.

Among these reasons, the following are particularly important in the context of this article:

- Relative facility of access with the Everest Base Camp Trail;
- Settlements at high altitude (above 3500 m) where inhabitants are facing a wide range of changes beside climatic one as a more tourism-centered economy involving integration to global markets, agropastoral and lifestyles changes, and new migration patterns (Puschiasis, 2019);
- Presence of a high-altitude scientific laboratory, the Pyramid of Lobuche (5050 m), administrated by the Italian Ev-K2/CNR association in agreement with the Nepalese Academy of Science and Technology (NAST).

In this framework, a working task of the Paprika and Preshine projects has been devoted to the identification of water resources and the perception of this held by the local inhabitants. In the preliminary exchanges with the scientists of the Paprika and Preshine projects, the Khumbu valley inhabitants manifested a deep concern regarding their water resource and its future. They were acutely aware that climate and economic changes will have a direct impact on the environment in which they live. As a consequence, it appears as a necessity to also aboard the climate processes and the water balance through the geochemical angle, even though this was not the primary route chosen for these projects.

The village of Pangboche, which includes several settlements, was chosen as the most convenient. The main settlement is located at an elevation of approximately 3950 m on the right bank of the Imja River, 4 km after the confluence of its two main branches: the Khumbu River flowing from the north and the Upper Imja River flowing from the west. An important concern of the local population is the future of the water resources, not only in quantity, but also in quality. Considering the latter point, it was also stated that the water quality could be a substantial indicator of the water flow processes, especially regarding the different origins of these flows: glacier melt, snowmelt, groundwater, or direct surface flow. The emergence of deep water is not documented, but is unlikely or negligible. This hypothesis is supported by the absence of local hot springs and by the water temperatures observed in springs or slope streams, which are directly influenced by air temperature (**Figure 2**), confirming a surface or a shallow origin.

During the past decade, geochemistry studies have been conducted of the Himalaya water flows (e.g., Jeelani et al., 2011; Ghezzi et al., 2017), but no study has been undertaken in the context of very high altitudes covering dynamically an entire year. This issue underlines the exploratory character of the current study, which, however, does not aim to address all the questions raised in this exceptional framework.

Numerous isotopic precipitation and river studies have been carried out in Himalaya at the local or regional scale in the past few years (Garzione et al., 2000; Wen et al., 2012; Jeelani et al., 2013, 2017; Balestrini et al., 2014, 2016; He and Richards, 2016; Ren et al., 2017; Florea et al., 2017; Jeelani and Deshpande, 2017; Guo et al., 2017; Li and Garzione, 2017; Kumar et al., 2018; Verma et al., 2018; Shen and Poulsen, 2019; Singh et al., 2019). The main aim of these studies was to link the isotopic variability recorded in precipitation to climate parameters and air mass circulation and the transfer of this isotopic signal through the global and complex altitudinal hydrosystem from glaciers to tropical valleys. Regional precipitation studies of the southern external border of Himalaya (Jeelani and Deshpande, 2017) from Kashmir (western Himalaya) to Assam (eastern Himalaya), or of the whole Tibetan Plateau (Li and Garzione, 2017), showed that the isotopic variation observed in precipitation across the Himalayas conforms to the regional repartition of the two main moisture sources: the westerly fluxes and Asian monsoon. Local studies of precipitation isotopes were carried out in central Nepal, Kathmandu, and the north of Kathmandu (Wen et al., 2012) as well as in the Khumbu Valley at the Pyramid Laboratory (Balestrini et al., 2014, 2016).

The current article aims to present, analyze and discuss, on the one hand, the geochemical behavior of the water flows used by the inhabitants of Pangboche for their activities, during the year 2011, exploring the conductivity, pH, major ions, and trace elements dissolved in the water; and, on the other hand, the water-stable isotopes in the precipitation and river flows of the Khumbu area, during the period from November 2014 to May 2017. The article aims to link these data to the water origins and seasonal variability in the context of global change.

STUDY AREA AND METHODS

Study Area

The climate of the study area is dominated from June to September by monsoon dynamics (Wang, 2006; Bookhagen and Burbank, 2010; Immerzeel et al., 2010; Turner and Annamalai, 2012), but winter and pre-monsoon precipitations can occur from December to April due to the Western Disturbances, which are part of the westerlies entry, originating from the Mediterranean region (Pisharoty and Desai, 1956; Madhura et al., 2015).

Above 5000 m in general, and lower during the winter, satellite imagery shows that the snow cover can be wide; however, the difficulty of monitoring snowfall in high mountains (Sevruk, 1989; Tahir et al., 2011) does not allow us to quantify precisely the volume of snowfall in the study area. Recent studies have explored the spatial distribution of precipitation in this area (Savéan et al., 2015; Gonga-Saholiariliva et al., 2016; Eeckman et al., 2017; Mimeau et al., 2019). They roughly show, beside a large local heterogeneity mainly due to the steep relief, the valley orientation and the slope aspect, a positive gradient with the

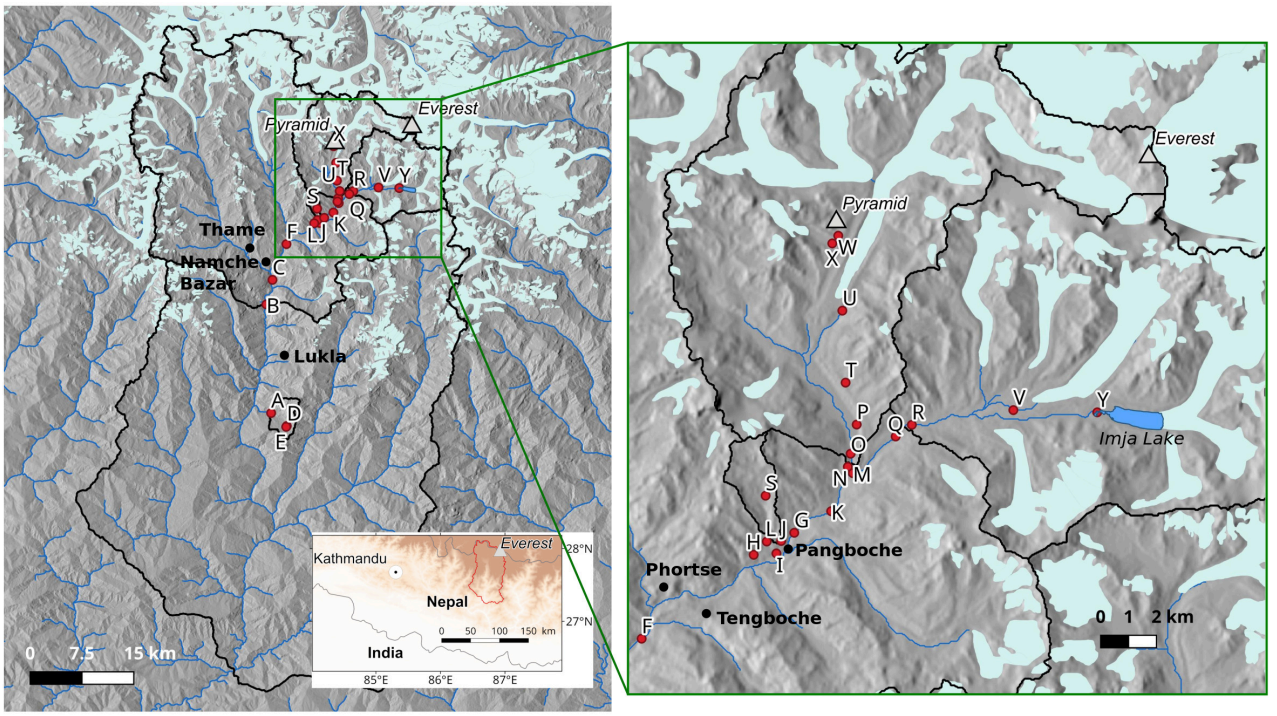

FIGURE 1 | Bottom left: location of the Dudh Koshi River basin (red line). Left: Dudh Koshi River basin and sub-basins, southern Mount Everest. Right: details of the Upper Khumbu and Imja area. The red dots represent the sampling points. The labels refer to **Table 1**. Sources: for relief, digital elevation model based on Spot-HRS images with a 40-m resolution (Gardelle et al., 2013); for glacier extension, Randolf Glacier Inventory (RGI Consortium 2017).

altitude until a peak of annual precipitation between 2500 and 3200 m and a negative one above.

The geology of the southern area of Mount Everest has been detailed by Bortolami (1998) and Searle et al. (2003). It is dominated by Precambrian-Early Paleozoic sillimanite gneisses in the high faces, which alternate in some places with intrusive Miocene leucogranites. The highest zone (Everest, Lhotse), above 6500 m, presents Ordovician shale series and limestone layers. Except for those slopes covered by glaciers or rock glaciers, the valley slopes and valley bottoms are mainly composed of fluvio-glacial deposits and debris, with the presence of moraines of different levels and ages. According to Bortolami (1998), the composition of the rocks leads to a low weathering and a low impact on the chemical composition of the flows. The same author notes that the aquifers located in the debris material have a high porosity. Their thicknesses are largely unknown. By contrast, the fissured rocks, which constitute the bed rock, are generally impermeable. A few other studies are devoted to groundwater storage in the Himalayas. Although their findings are not very helpful with regard to the geological characteristics (Dongol et al., 2005; Jeelani, 2008) or the scale of the approach used (Andermann et al., 2012), these studies highlight a notable contribution of snow and glacier melt to groundwater. Andermann et al. (2012) assess the storing capacity of the whole Dudh Koshi basin (3700 km^2) to be approximately 300 mm, i.e., less than 20% of the average annual discharge, which represents a low impact of the groundwater in our study area, considering that most of the reservoirs are very likely concentrated in the bottom material of the middle and low elevations. Other authors, including Nepal et al. (2014), Savéan et al. (2015), and Eeckman et al. (2019), consider in their modeling approaches that the volume stored over a long period in groundwater reservoirs is negligible.

Water Resources for Local Population

The Khumbu zone (**Figure 1**) encompasses an area of approximately 1100 km^2 along the border between Nepal and the Tibet Autonomous Region of China. It is included in the Nepalese administrative division of the Solu-Khumbu district. The area is divided into three major distinct valleys—Imja Valley, Dudh Koshi Valley, and Bhote Khosi Valley—forming a U-shape, a testimonial to the glacial erosion and draining of the main rivers in the region. The Dudh Koshi first meets the Imja Khola on the eastern side of the region, and it then meets the Bhote Koshi before running out of Khumbu toward the south into a deep gorge. Khumbu settlements span elevations from 2805 m (Jorsalle) to 5170 m (Gorak Shep). The villages are located extensively on the rare alluvial terraces, hanging valleys, and amphitheater slumps and comprise mostly south- and north-facing slopes. Khumbu corresponds to the former Village Development Committees (VDCs, before administrative restructuring in 2017) of Khumjung and Namche hosting approximately 3500 residents belonging mostly to the

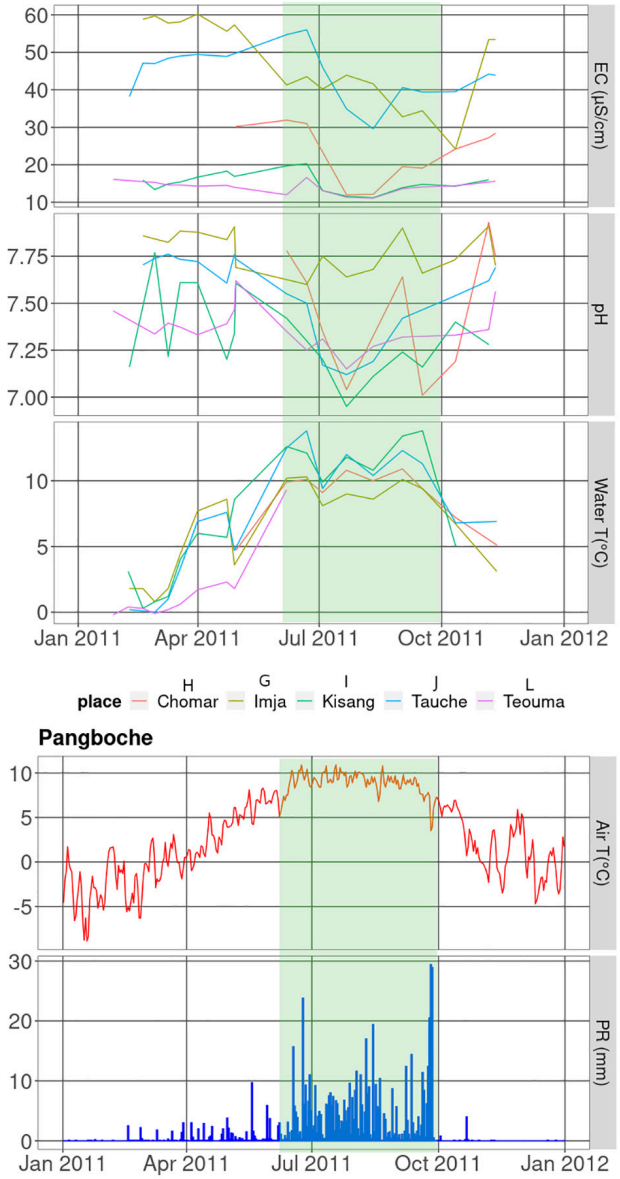

FIGURE 2 | Year 2011. Up: electrical conductivity (EC), pH and water temperature (T) at the five sampling points around Pangboche (~4000 m). Down: daily temperature (T) and precipitation (PR) at Pangboche weather station. The monsoon season (JJAS) is highlighted in green.

Sherpa ethnic group with a growing number of non-Sherpa residents (Rais, Tamangs, Magar, and Bahun-Chhetri). With the establishment of the Sagarmatha National Park (SNP) in 1976 and its designation as a UNESCO World Heritage Site in 1979, the economy of the region has shifted to a more tourism-centered form (Spoon, 2011). The number of visitors to the SNP increased to 45,000 in 2017 (Jacquemet, 2018) leading to an important trekking and expedition tourism hub, including the popular trekking route to Mount Everest Base Camp.

All these territorial and economic mutations have led to profound changes in water resources, increasing needs previously limited to domestic (drinking water, cooking, personal hygiene), agricultural (irrigation of barley), and religious purposes (water-driven prayer wheels, water spirit shrine) (Aubriot et al., 2019). Water is taken directly from springs or small streams flowing through the settlements or channeled by pipes to houses, since large rivers are not the primary source of water for villagers (McDowell et al., 2012). In Pangboche village, changes appeared some 20 years ago with the installation of running water supplying guest houses, a bottled-water manufacturing plant in 2003, and a micro-hydroelectric plant in 2004 (Puschiasis, 2015). Water has become a "commodity" (André-Lamat, 2017) with a proliferation of uses for tourism (shower, flushing toilets, bottled water) and for electrification. Khumbu inhabitants have become highly dependent on reliable water supply systems to respond to the new types of usages, which is key to local development. Nevertheless, there is a lack of a proper management system at a regional level to reduce the pressure on water resources.

Methods of Sampling and Analysis

Labels A to Y refer to the sampling points shown in **Figure 1** and described in **Table 1**. They are ordered by altitude from bottom to top.

Conductivity, Major, and Trace Elements

Temperature, pH, and electrical conductivity (T_{ref} = 25°C) were measured in the field, using a portable pH meter and conductivity meter (WTW 3210i®). Water samples (125 mL) were filtered in the field with a PP syringe and Durapore® membrane (0.22 µm) and stored in acid-washed HDPE bottles. Aliquots for major cations and trace elements were acidified with ultrapure HNO_3 (1‰ v/v). Samples were stored at 4°C before reaching Montpellier for analysis.

Five sites in the surroundings of Pangboche village were selected for the water sampling (G, H, I, J, L):

- The G point on the Imja River represents the reference site for the main river after the confluence of the Khumbu branch and the Imja branch. These catchments include, on the one hand, the large glaciers of the south side of the Everest Range and, on the other hand, the Imja moraine lake, which concentrates the melting runoff from the majority of the glaciers of the upper Imja Valley.
- The Tauche point (J) on the east stream of the southern slope of the Tauche Peak (6542 m). This watercourse collects the melt flow from the very small glacier located on the peak summit.
- The Teouma (L) and Kisang (I) points on the central stream flow do not receive water of glacial origin. Because this watercourse flows through the village of Pangboche, the first point was chosen upstream and the second downstream from the village in order to analyze how the water quality of the stream is influenced by the village.
- The Chomar (H) source on the west side of Pangboche was also sampled, because its water was drawn and bottled

TABLE 1 | Main characteristics of the sampling points (ordered by altitude).

Name (+)	Label (++)	Coordinates			Data type (*)	Sample (**)	Glaciers (***)
		Longitude	Latitude	Altitude (m)			
Kharikhola	A	86°43′16″	27°36′22″	1981	R	IS	N
Phakding	B	86°42′47″	27°44′53″	2620	R	IS	Y
Jorsalle	C	86°43′19″	27°46′48″	2850	R	IS	Y
Pangom river	D	86°44′38″	27°35′24″	2880	R	IS	N
Pangom village	E	86°44′35″	27°35′17″	2890	P	IS	–
Phuki Tenga	F	86°44′35″	27°49′37″	3200	R	IS	Y
Pangboche-Imja	G	86°47′53″	27°51′40″	3917	R	MT IS	Y
Pangboche-Chomar	H	86°46′59″	27°51′14″	3930	R & bottle	MT	N
Pangboche-Kisang	I	86°47′31″	27°51′18″	3971	R	MT	N
Pangboche-Tauche	J	86°47′35″	27°51′32″	4005	R	MT	S
Shomare	K	86°48′40″	27°52′5″	4021	R	IS	N
Pangboche-Teouma	L	86°47′17″	27°51′32″	4148	R	MT IS	N
Imja confluence	M	86°49′08″	27°52′52″	4172	R	CP	Y
Khumbu confluence	N	86°49′05″	27°52′59″	4172	R	CP	Y
Pheriche hydro	O	86°49′08″	27°53′13″	4216	R	IS	Y
Pheriche village	P	86°49′16″	27°53′46″	4260	P R	MT IS	Y
Dingboche village	Q	86°50′06″	27°53′35″	4370	R	IS	Y
Dingboche hydro	R	86°50′28″	27°53′46″	4372	R	IS	Y
Tauche Kharka	S	86°47′17″	27°52′23″	4405	R	IS	S
Phulung Kharka	T	86°49′01″	27°54′36″	4504	R	IS	S
Tukla	U	86°48′54″	27°55′59″	4700	R	IS	Y
Chukung	V	86°52′41″	27°54′04″	4752	R	CP	Y
Lobuche river	W	86°48′50″	27°57′25″	4840	R	IS	Y
Lobuche spring	X	86°48′43″	27°57′18″	4935	R	IS	S
Imja Lake	Y	86°54′29″	27°54′00″	5001	R	MT	Y

(+) Precipitation samples are in gray; the others are river samples. (++) See location in ***Figure 1****. (*) Data type: P, precipitation; R, river. (**) Sample: MT, major/trace + conductivity/pH; IS = isotopes; CP = only conductivity/pH. (***) Glacier: N = no; Y = yes; S = not significant.*

in 2011 by a small company to be sold to tourists under the brand name of "*Namaste Sabina Tabuche Beiu.*" After 2013, the company no longer produced bottled water for unknown reasons.

The water flows were sampled 18 times between February and November 2011 following the complete annual cycle (**Figure 2**). A total of 12 samplings benefited from a complete protocol (64 samples) and 6 more samplings, in winter and autumn, from measurements of electrical conductivity and pH only.

Two complementary water samples were collected in June 2012 in Imja Lake (Y) and a rainfall reference was taken in the settlement of Pheriche (P). In addition, several measurements of electrical conductivity were carried out in different watercourses within the Imja River basin.

Chemical analyses were performed at the HydroSciences water chemistry laboratory in Montpellier (France). Total alkalinity was measured by acid titration with HCl 0.01 N (Gran method). Major ions (Cl^-, NO_3^-, SO_4^{2-}, Ca^{2+}, Mg^{2+}, Na^+, and K^+) were analyzed by ionic chromatography (Dionex ICS 1000). The precision error was $<\pm5\%$. Trace elements (Li, B, Al, Si, Ti, V, Cr, Mn, Fe, Co, Ni, Cu, Zn, As, Rb, Sr, Mo, Cd, Cs, Ba, Pb, and U) were analyzed with Q-ICPMS (X series2 Thermo Scientific®) on the AETE (*Analyse des Elements en Trace dans l'Environnement*) technical platform of Montpellier University. The precision error was $<\pm8\%$.

Stable Isotopes

Six sampling campaigns in rivers located between 1985 m (Kharikola, label A) and 5000 m (foot of glaciers, X, Y) were carried out (November to December 2014, November 2015, November 2016, March 2015, May 2016, May 2017).

In addition, during the study interval from November 2014 to December 2016, monthly rainfall was collected at Pangom (2890 m, E) using a homemade rain gage with an 80-cm^2 cross-section in a 5-L plastic tank inside an isotherm box, which was linked to the gage with a flexible pipe and hermetically sealed to avoid direct evaporation.

The rainfall and river samples were stored in amber glass bottles (25 mL) with conical plugs and transported in shaded conditions to the laboratory in Montpellier.

Water-stable isotopes were measured with an Isoprime® mass spectrometer on the LAMA platform of HydroSciences Montpellier (*LAboratoire Mutualisé d'Analyse des isotopes stables de l'eau*). The oxygen isotopic composition was measured after

equilibration of 200 μL of water with CO_2 via the dual-inlet technique, with an overall precision of ±0.06‰. Deuterium was measured by continuous-flow using a Eurovector Pyr-OH® elemental analyzer converting 0.5-μL injections of water to H_2 on Cr powder at 1070°C, with an overall precision of ±0.6‰.

Water isotopic compositions are reported as $\delta^{18}O$ and $\delta^{2}H$ on the V-SMOW scale.

RESULTS

Electrical Conductivity and pH

Figure 2 shows the dynamics of the electrical conductivity and pH during the year 2011 at the five measurement points (G, H, I, J, L) of the Pangboche area.

Regarding electrical conductivity, the absolute values are below 60 μS/cm. These very low values indicate the slight level of mineralization of the flows. Specifically, the five sites present two main behaviors: (i) Kisang and Teouma located on the same watercourse have an almost identical and constant extremely low conductivity during the year (approximately 20 μS/cm), (ii) for Tauche and Imja the values are 2–3 times higher, with a slight decrease during and shortly after the monsoon (July–October), meaning that the increasing runoff generates a dilution effect. The Chomar site fits between the two, with a decrease during the monsoon season.

The pH varies between 7 and 8, except for Pangboche-Chomar bottled drinking water (8.6) and for the rain sample (6.8). The different sites present a short-term variability from date to date. However, two main behaviors can be observed: (i) for the slope water courses (Tauche, Kisang, Teouma, and Chomar), the amplitude of the short-term variability reaches 0.5 and a relative dilution effect appears during the monsoon; (ii) the valley river (Imja) has an almost stable pH value (≈7.8) during the course of the year, but higher than the pH of the slope water courses.

Major Ions

The following ranges in concentration were shown by the major cations and anions: Ca^{2+} (1.1–11.1 mg/L), Mg^{2+} (0.1–0.7 mg/L), Na^{+} (0.4–1.8 mg/L), K^{+} (0.2–1.3 mg/L), HCO_3^{-} (5.1–32.3 mg/L), SO_4^{2-} (0.4–14.5 mg/L), NO_3^{-} (0.1–1.5 mg/L), Cl^{-} (0.1–0.6 mg/L). Silica ranges from 1.3 to 20.8 mg/L. Average concentrations of major ions are reported in **Table 2**. The Piper diagram for major cations and anions (**Figure 3** and **Table 2**) shows variations in the chemical composition of the surface waters, which is dominated by Ca^{2+} and HCO_3^{-}. The waters are mainly of Ca^{+}-Mg^{+}-HCO_3^{-} type. Waters influenced by glacier melt (Tauche and Imja sites) exhibit an enrichment in SO_4^{2-}, particularly for the Tauche site during the monsoon season. Ca^{2+} is the dominant cation contributing more than 70% to the cation budget, followed by Na^{+} (<20%) and Mg^{2+} (<10%). In Kisang waters and to a less extent in Teouma waters, before the monsoon season, Na^{+} is the dominant cation. Cl^{-} and NO_3^{-} concentrations are very low, <0.6 mg/L

TABLE 2 | Main characteristics of the geochemical samples: water temperature, pH, electrical conductivity, and major ions.

Name (+)	Label (++)	Var (*)	WT (°C)	pH	EC (μS/cm)	HCO_3^- (mg/L)	Cl^- (mg/L)	NO_3^- (mg/L)	SO_4^- (mg/L)	CA^{++} (mg/L)	Mg^{++} (mg/L)	Na^+ (mg/L)	K^+ (mg/L)	SiO_2 (mg/L)
Pang.-Teouma	L	M	7.2	7.3	13.7	6.37	0.13	0.62	1.85	1.46	0.17	0.80	0.29	4.86
		SD	3.4	0.2	1.7	0.64	0.05	0.30	0.32	0.18	0.04	0.16	0.11	0.82
Pang.-Kisang	I	M	9.7	7.3	15.4	7.46	0.30	0.46	1.85	1.56	0.19	1.11	0.36	4.93
		SD	3.6	0.2	3.2	1.58	0.23	0.26	0.26	0.18	0.04	0.49	0.12	1.17
Pang.-Tauche	J	M	9.0	7.5	42.5	12.27	0.12	0.82	9.41	5.99	0.57	0.96	0.39	4.46
		SD	3.9	0.2	7.8	4.35	0.03	0.23	2.17	1.44	0.09	0.14	0.05	0.63
Pang.-Imja	G	M	7.5	7.7	45.0	20.16	0.20	0.53	6.73	7.50	0.37	1.02	0.85	10.56
		SD	3.0	0.1	9.1	4.49	0.12	0.54	1.24	1.45	0.06	0.43	0.13	6.12
Pang.-Chomar	H	M	8.7	7.4	22.4	15.31	0.12	0.34	0.68	3.68	0.23	0.97	0.28	5.93
		SD	2.3	0.3	7.8	5.21	0.03	0.22	0.20	1.13	0.06	0.37	0.07	1.93
Pang.-Chomar bottled water	H			8.6	29.3	15.75	0.44	1.38	0.54	4.87	0.16	0.43	0.19	8.19
Imja Lake	Y			7.0	30.0	9.86	0.37	1.52	6.28	3.90	0.24	0.71	0.73	1.61
Pheriche hydro	O			7.4	62.6	27.70	1.02	0.24	0.47	8.60	0.22	1.10	1.31	2.04
Pheriche village	P			6.2		14.16	0.29	0.79	8.38	2.77	0.17	0.57	1.53	0.07

(+) precipitation sample is in gray; the others are river samples. (++) see location in ***Figure 1****. (*) M, mean; SD, standard deviation. WT, water temperature; EC, electrical conductivity.*

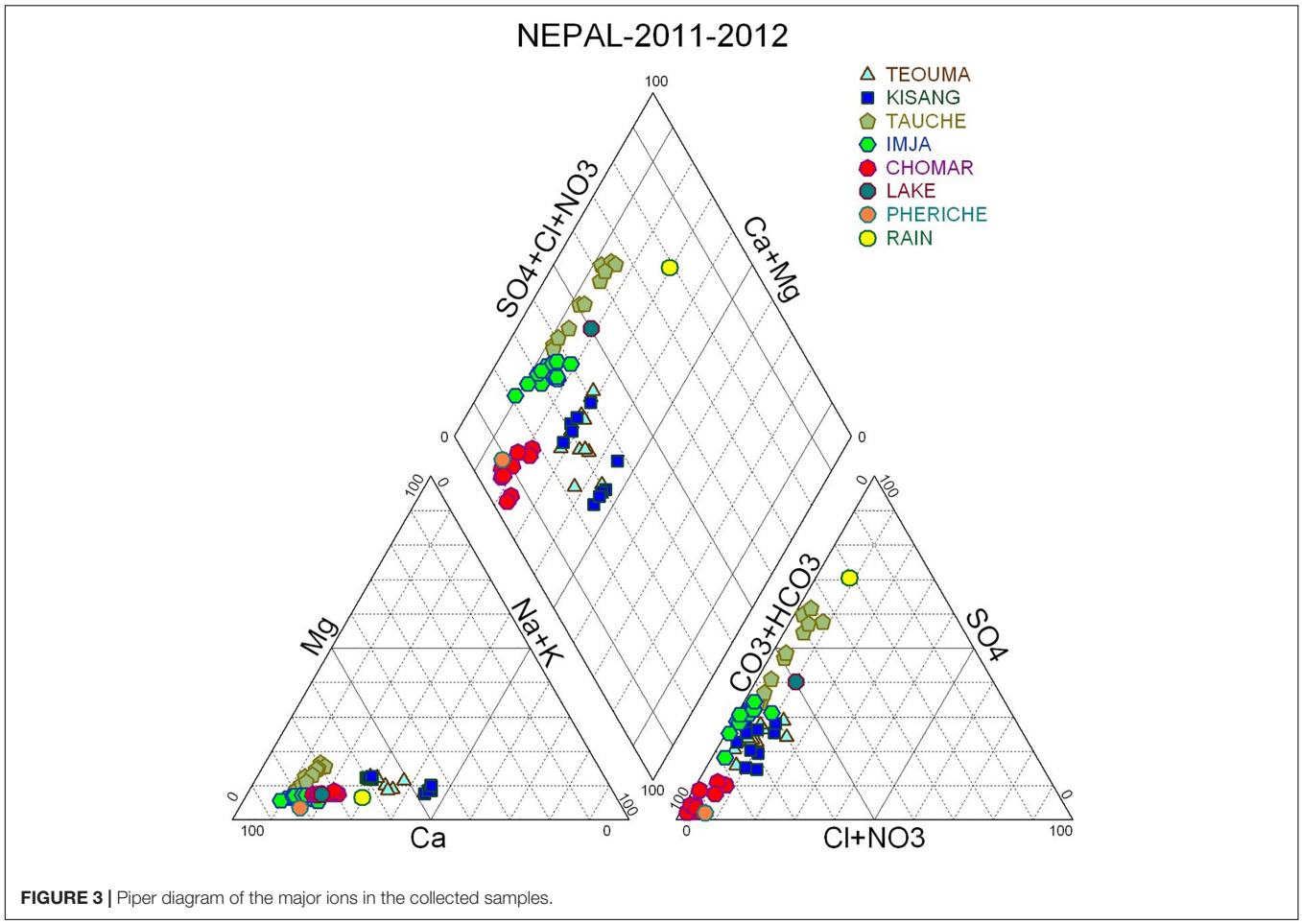

FIGURE 3 | Piper diagram of the major ions in the collected samples.

and <1.5 mg/L, respectively. The HCO_3^- contribution to the anion budget ranges between 60 and 90%, except for Tauche water during the monsoon season, which evolves to a Ca^+-Mg^+-SO_4^{2-} type. The origin of sulfates is found in sulfide oxidation via glacier runoff, as suggested by Hodson et al. (2002), because no anhydrite or gypsum have been identified in the region. The plot of $Ca^+ + Mg^+ + Na^+$ versus $HCO_3^- + SO_4^{2-}$ from all the waters shows that most of the samples lie close to the 1:1 line, indicating the dissolution of calcite, dolomite, silicates, and sulfides (**Figure 4**) as suggested by Crespo et al. (2017).

For all major elements, including SiO_2, the temporal evolution of the concentrations displays a dilution effect during the monsoon season, except for the Imja site where an increase in the concentration of all the major elements occurs during the same season, especially in August 2011, which corresponds to the maximum glacier melt. This enrichment demonstrates that the glaciated catchment undergoes more intense chemical weathering taking place beneath the glacier than catchments that do not have a glacier because the CO_2 dissolved in the proglacial zone with the aerated flow conditions characteristic of the meltwater environments may promote chemical weathering by maintaining the acid potential of the water (Reynolds and Johnson, 1972) in Singh and Hasnain (1998).

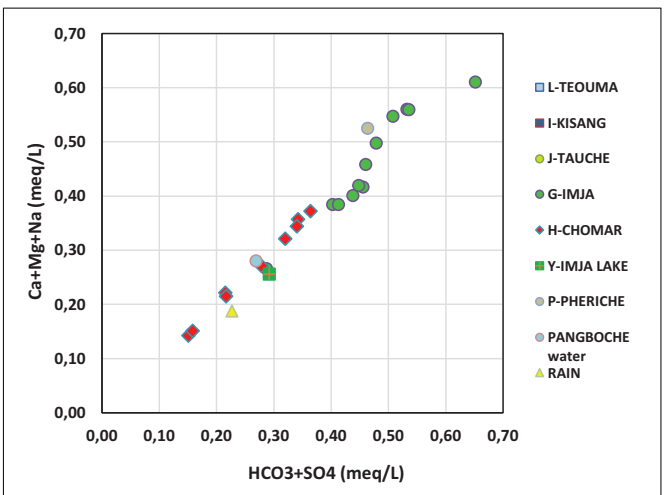

FIGURE 4 | Ca + Mg + Na versus HCO_3 + SO_4 (meq/L).

Trace Elements

Average concentrations for measured trace elements are presented in **Table 3**. Dissolved trace elements such as Li, B, Ni, Zn, Cu, Rb, Sr, Ba, and U show a dilution effect during the

monsoon season at the Teouma, Kisang, Tauche, and Chomar sites whereas the Imja site in the same season exhibits, except for boron, a high concentration increase, by a factor of 10–100, as shown, for example, for rubidium (**Figure 5**). The origin of this increase can be found in the glacier melt enriched in subglacial material leached by the heavy rain during the monsoon. This phenomenon underlines the integrating power of the Imja Khola River. On the other hand, Al, Ti, Fe, and Mn to a lesser extent increase in all the sites during the monsoon season. In comparison with the Upper Mustang rivers in the western region of Nepal Himalaya (Ghezzi et al., 2017), the concentrations are elevated, from 5 to 6600 μg/L for Al, from 0.5 to 485 μg/L for Ti, from 5 to 7130 μg/L for Fe, and from 2 to 200 μg/L for Mn. These elements are mobilized by the surface runoff during the monsoon season and their common origin is to be found in the weathered bedrock.

In regards of the WHO drinking water guidelines, no major or trace elements exceed the recommended values, even if the concentrations for some major or trace elements of the Imja River are elevated.

Stable Isotopes

Three complete years (2014–2016) of meteorological data (P, T) are available at the Pangom station (2885 m, label D) (Chevallier et al., 2017), and a monthly sampling of rainfall for water isotope analysis was carried out between November 2014 and December 2016. The comparison of all the results is only qualitative owing to the small temporal record at the Pangom weather station.

The mean annual temperature measured at Pangom in 2015 was 6.7°C (7.6°C in 2014 and 8.0°C in 2016) with lower temperatures in the dry season (minimum in December: −1.1°C) and higher temperatures during the monsoon season (**Figure 6**) (maximum in June: 12°C). In the higher part of the Khumbu valley at the Pyramid Laboratory station, monthly temperatures follow the same pattern ranging between −12 and 4°C for the 2012–2014 interval (Balestrini et al., 2016).

Precipitations

Annual rainfall in Pangom was 3046 mm in 2015 (3683 mm in 2014 and 3947 mm in 2016). The South Asia monsoon (JJAS) accounts for more than 80% of the precipitation amount (**Figure 6**) (84.7–86.1% from 2014 to 2016) with no specific rainier month in this season (JAS between 888 and 1075 mm).

During the sampling interval (November 2014 to December 2016, with a gap in May 2016), a large isotopic variation is observed (**Figure 6**): 3.25 to −15.26‰ V-SMOW for $\delta^{18}O$ and 43.3 to −109.5‰ V-SMOW for $\delta^{2}H$. **Figure 6** shows the isotopic composition of all precipitations giving a local water line following the equation:

$$\delta^2H = 8.57\,\delta^{18}O + 20.5 \quad (R^2 = 0.997;\ n = 25)$$

The slope is slightly higher than the slope of the global meteoric water line (GMWL, $\delta^2H = 8.13\ \delta^{18}O + 10.13$) defined by Rozanski et al. (1993) and also shows an intercept $d = 20.5$ higher, close to the meteoric line of the precipitation in the southern Tibetan plateau (Yao et al., 2013):

$$\delta^2H = 8.89\,\delta^{18}O + 23.0 \quad (R^2 = 0.980;\ n = 374).$$

At the Pyramid Laboratory station at the weekly scale between June 2012 and December 2013, Balestrini et al. (2016) found:

$$\delta^2H = 8.17\,\delta^{18}O + 16.6$$

In Pangom, if one distinguishes between the seasons, the equations are:

ONDJFMAM (extra-monsoon)

$$\delta^2H = 8.46\,\delta^{18}O + 20.6 \quad (R^2 = 0.997;\ n = 17)$$

JJAS (monsoon),

$$\delta^2H = 8.52\,\delta^{18}O + 18.4 \quad (R^2 = 0.999;\ n = 8).$$

The more enriched monthly values above −1‰ in $\delta^{18}O$ ($n = 5$) do not show an evaporation mark; a high deuterium excess is observed (between 17.4 and 21.6‰) for low to medium rainfall amount (21 to 142 mm). These values belong to the extra-monsoon season and are linked to notable continental recycling mainly from non-fractional processes such as transpiration or soil evaporation. In the regional study by Jeelani and Deshpande (2017), stations in Nepal and Assam also showed a high d-excess (>20‰) associated with a high $\delta^{18}O > -1$‰ value, suggesting a dominant influence of transpiration, increasing the $\delta^{18}O$ of vapor over the forest floor (Lai and Ehleringer, 2010).

The isotopic values recorded during the 2 years, including monsoon and extra-monsoon seasons, display different patterns, globally more depleted in the monsoon season (2015, −10.05‰; 2016, −8.48‰, weighted mean for $\delta^{18}O$) and more enriched in the extra-monsoon season (2015, −4.48‰; 2016, −0.81‰, weighted mean for $\delta^{18}O$). The much more enriched values in the extra-monsoon season in 2016 could be an effect on isotope composition and deuterium excess in the beginning of the monsoon season with a possibly late isotope re-equilibration of the air mass, perhaps due to higher mixing with the recycled continental vapor. Indeed, in June and July 2016, isotope values were more enriched than in June and July 2015, also with a greater d-excess. Then, it is only in August 2016, in the middle of the monsoon season, that isotope values and d-excess seem to be consistent with isotope values in the monsoon season, and this continues until the beginning of the extra-monsoon season (October 2016) with a dephasing of 2 months.

The relationship between isotope values and temperature (temperature effect) shows an inverse correlation with a low coefficient ($R = -0.336$; $n = 25$) as well as with rainfall (amount effect) with $R = -0.392$, which are not significant using a t-distribution with n-2 degrees of freedom at a significance level $a = 0.05$; the critical values associated with $df = 23$ are ±0.396 (Bravais-Pearson table). The monsoon season corresponds to a more depleted rainfall (Dansgaard, 1964). In fact, the main effect on isotope variability in our site is the origin of air masses, as shown in previous regional studies cited in this article or in the local Khumbu Valley at the Pyramid Laboratory (Balestrini et al., 2016).

TABLE 3 | Average concentrations of trace elements.

Name (+)	Label (++)	n (*)	Var (**)	Li	B	Al	Ti	Cr	Mn	Fe	Ni	Cu	Zn	Rb	Sr	Cs	Ba	Pb	U
											µg/L								
Pang.- Teouma	L	12	M	0.3	0.6	36.6	1.4	0.2	0.6	20.4	0.9	0.3	1.6	1.3	3.4	0.2	1.1	0.0	0.8
			SD	0.1	0.2	23.0	1.4	0.1	0.7	19.0	1.3	0.1	1.9	0.3	0.5	0.1	0.5	0.0	0.3
Pang.- Kisang	I	12	M	0.4	0.8	68.0	3.1	0.2	1.1	50.6	1.0	0.4	2.6	1.5	3.7	0.2	1.3	0.1	0.8
			SD	0.1	0.2	33.0	2.7	0.1	0.7	36.7	1.6	0.1	1.6	0.2	0.5	0.1	0.3	0.1	0.2
Pang.- Tauche	J	12	M	0.8	1.2	34.9	2.4	0.1	0.5	29.2	1.2	0.3	1.5	1.6	8.9	0.6	0.8	0.0	5.8
			SD	0.1	0.2	23.6	2.0	0.2	0.3	23.8	1.4	0.1	1.4	0.2	2.0	0.1	0.2	0.0	2.4
Pang.- Imja	G	12	M	18.9	4.2	2365.6	205.8	4.3	56.9	3019.4	4.3	4.2	11.2	18.5	15.8	4.7	17.1	2.4	11.0
			SD	13.3	1.5	2325.6	173.6	3.8	61.8	2616.1	2.6	4.6	9.1	15.7	3.3	4.3	17.2	2.4	3.8
Pang.- Chomar	H	12	M	0.4	0.6	35.9	1.6	0.5	0.6	23.2	0.5	0.3	2.0	1.3	6.7	0.3	0.7	0.0	1.1
			SD	0.1	0.1	20.4	1.5	0.7	0.5	17.8	0.7	0.1	1.1	0.3	2.3	0.1	0.2	0.0	0.2
Imja Lake	Y	1		4.8	1.9	9.7	na	0.0	1.2	7.4	0.1	0.1	1.8	1.3	3.9	0.1	0.5	0.0	0.1
Pheriche hydro	O	1		9.4	2.7	8.6	na	0.0	6.3	3.1	0.1	0.1	3.1	2.6	29.0	0.3	0.7	0.0	0.2
Pang.-Chomar bottled water	G	1		0.5	*LOD*	11.2	na	0.0	0.1	1.2	0.0	0.0	19.6	0.1	6.4	0.0	0.7	0.0	0.8
Pheriche village	P	1		0.1	0.8	5.5	na	0.1	1.5	1.5	0.10	0.2	5.9	2.0	5.30	0.0	1.6	0.1	0.0

(+) Precipitation sample in gray; the others are river samples. (++) see location in ***Figure 1****. (*) Number of samples. (**) M, mean; SD, standard deviation; LOD, limit of detection; na, not available.*

The year 2015, which is complete, gives a weighted annual value $[\Sigma(P_i\ \delta_i)/\Sigma P_i]$ of −9.24‰ V-SMOW for $\delta^{18}O$ and −60.1‰ V-SMOW for $\delta^{2}H$ (2016: 95.9‰ of rainfall, −8.20‰ and −50.6‰), which is in good agreement with the altitude effect in the region, regarding the results obtained in Kathmandu (1320 m, −8.7‰) and Nyalang (3811 m, −11.3‰) (Wen et al., 2012; Balestrini et al., 2016); at the Pyramid Laboratory station (5050 m), the isotope content during the monsoon season in 2012 and 2013 does not show a large variation (−17.74 to −17.81‰ in $\delta^{18}O$). The gradient is −0.23‰/100 m, in good agreement with the range of the isotope altitudinal gradient in Himalaya (−0.15, −0.33‰) (Wen et al., 2012).

The d-excess is a good indicator for evaluating the contribution of different water vapor sources (Clark and Fritz, 1997). In Himalaya, low d-excess values characterize moisture coming from the Indian Ocean and the Bay of Bengal, and high values continental moisture carried by the Western Disturbance (Jeelani and Deshpande, 2017). At Pangom in 2015 and 2016, d-excess values during the monsoon season were between 11.3 and 18.7‰ (n = 8, mean = 13.6‰), while in the two extra-monsoon seasons (2015 and 2016) d-excess values were between 14.3 and 23.9‰ (n = 14, mean = 19.1‰).

At the Pyramid Laboratory, we have the same pattern for isotope content and d-excess during the monsoon (depleted values up to −30‰ for $\delta^{18}O$ and d-excess <15‰) and the extra-monsoon seasons (more enriched values and high d-excess until 26‰). The difference observed with the local meteoric line (LML) in d-excess is due to the different repartition of measurements in the monsoon season (n = 38) and the extra-monsoon season (n = 8).

We note in the total observed interval a good correlation between oxygen-18 and d-excess values (R^2 = 0.62; n = 25), which reaches R^2 = 0.72 if the more enriched point is removed (April 2016); this may indicate a slight alteration in isotope air mass signal by the evaporation process.

To conclude, in Pangom as in other Himalayan sites, the change in air circulation patterns, marine vapor from the Indian Ocean and the Bay of Bengal, on the one hand, and continental vapor from the Western Disturbances, on the other, modify the isotope composition and d-excess of precipitation.

Rivers

For the river isotope sampling, in the general spatial pattern, depleted values are observed in the headwaters of the streams and enriched values at lower elevations of the catchments. The water isotope variability of stream water shows a lower variability with respect to local precipitation at Pangom, in spite of altitudinal sampling (1981–4935 m) and six campaigns between November 2014 and May 2017 (local sampling between one and six campaigns) that ranged from −10.10 to −18.39‰ for $\delta^{18}O$ and from −64.5 to −135.8‰ for $\delta^{2}H$ (**Figure 7** and **Table 4**). The sampling was carried out at the beginning of the extra-monsoon season, with possibly the influence of the end of the monsoon season, and at the end of the extra-monsoon season. However, the variability registered is mainly very low,

lower than 0.6‰ for $\delta^{18}O$ for 89% of local stations. Two stations with at least five samplings (D – Pangom and J – Tauche) show a large difference; both stations in March 2015 have a high depleted value (−16.65 and −16.53‰ in $\delta^{18}O$, respectively); not considering this result, Pangom has a mean value of −10.47‰ with a range interval of 0.45 (n = 4) and Tauche has a mean value of −15.31‰ with a range interval of 1.22 (n = 5). Both sampling points are located in non-glaciated catchment for Pangom and small glaciated catchment (less than 1% of the basin area) for Tauche. The river in this extra-monsoon season with few precipitations (at Pangom in 2015, precipitation amounts are 19 mm in January, 19 mm in February and 66 mm in March) is supplied mainly by superficial aquifer whose main characteristic is an isotopic composition relatively constant over the year at a local altitudinal point (Jeelani et al., 2018). The main hypothesis to explain this important change is the presence of snow cover at higher altitude with more depleted isotopic content during this season, which was melting and supplied by direct runoff from the river.

Although there were no measurements during the monsoon season in this study, the works of Balestrini et al. (2014) in the high part of the Khumbu Valley (>4200 m) have shown a higher variability (2‰) close to glacier and morainic lake inflow and low variability (0.39‰ in $\delta^{18}O$) at Pheriche (label P in **Figure 1**) during monthly sampling between July and October 2008. The authors suggest that the area extension of the hydrological basin buffers the isotopic signal. Another fact is the difficulty to link directly the isotope content of monthly precipitation and isotopic content of river water at the same time.

The isotopic composition of the stream water in the whole study interval is close to the local precipitation regression line (**Figure 7**) following the equation:

$$\delta^2H = 8.23\,\delta^{18}O + 15.0 \quad (R^2 = 0.987;\ n = 58)$$

For each season the slope and the d-excess value can differ greatly, but the number of samples is small (except for May 2017, which is close to the global river equation) and these variations are not representative of a particular process:

November 2014	$\delta^2H = 8.11\,\delta^{18}O + 4.1$	(R^2 = 0.972; n = 5)
March 2015	$\delta^2H = 7.56\,\delta^{18}O + 22.2$	(R^2 = 0.999; n = 9)
November 2015	$\delta^2H = 6.71\,\delta^{18}O + 9.3$	(R^2 = 0.934; n = 11)
May 2016	$\delta^2H = 8.24\,\delta^{18}O + 16.3$	(R^2 = 0.994; n = 10)
November 2016	$\delta^2H = 8.08\,\delta^{18}O + 13.3$	(R^2 = 0.992; n = 9)
May 2017	$\delta^2H = 8.47\,\delta^{18}O + 19.1$	(R^2 = 0.997; n = 17)

The mean d-excess value at each sampling point is between 5.6 and 14.4‰. For the whole dataset, d-excess values vary between 3.1 and 15.6‰ with 19% of samples lower than 10‰, which are altered by an evaporation process. The samples with d-excess between 10 and 14‰ do not show a special trend, likely linked to glacier melt and aquifer discharge where the main accumulation and recharge are during monsoon season when the d-excess value of the monthly precipitation is between 11 and 14‰. For d-excess values higher than 14‰, there is possibly a partial contribution of rainfall or melted snow during the extra-monsoon season where d-excess values of monthly precipitation can reach 24‰ during the 2014–2016 interval.

Contrary to the results of another study in southern Himalaya by Wen et al. (2012), who found a very good correlation between the isotope content in the Boqu River and altitude (n = 39, R^2 = 0.90, September 2011) between 1845 and 5060 m, the relationship between the altitude of the sampling sites and isotope content is not well correlated (R^2 = 0.399; n = 18) very likely due to the heterogeneity of the catchments and their glacier cover varying between 0 and 70%. The river in catchments with glacier cover at all altitudes is mainly controlled by the ice melting and by higher depleted value with respect to no glacier catchments. This is the case of the Phakding samples, located at a low altitude (2620 m), which show an isotope content in $\delta^{18}O$ of −15.89‰, with a 20.9% glacier cover (Everest catchment). By comparison, the weighted mean annual rainfall in Pangom (2890 m) yields −9.24‰, in better accordance with the isotope values collected in the Pangom River (watershed without glacier) and reflecting the isotope composition of rainfall in the whole study area (−11.71‰).

By contrast, rivers in catchments without any or with small glacier cover (Kharikola, Pangom, Tauche, Chomar, Teouma), spring (Lobuche spring), or surface flow not connected to glacier melt such as wet saturated pastures (*kharka* in Nepali; e.g., Phulung Kharka) show (**Figure 8**) a better correlation with altitude (R^2 = 0.809; n = 8). Focusing only on the river sampling points that depending on glacier melt, the correlation with altitude is significantly improved (R^2 = 0.525; n = 10). Indirectly, the lower the altitude, the more the glacier component in the river decreases and the more the aquifer component increases.

The isotopic altitude gradient for river sampling in no or in a lightly glaciated catchments shows for $\delta^{18}O$ a value of −0.20‰/100m; this is in the range (−0.11/− 0.36‰/100 m) of other studies referenced by Wen et al. (2012) and Ren et al. (2017) in Himalaya and is close to results found by Florea et al. (2017), in the same zone, i.e., −0.28‰/100 m. By comparison with the study of Florea et al. (2017), in the Dudh Koshi River with a sampling set located between Gorak Shek (5180 m), upstream of Lobuche, and downstream of Phakding (2550 m) in May 2011, values in $\delta^{18}O$ are between −17.9 and −9.7‰. The relationship between $\delta^{18}O$ and δ^2H demonstrates a lower slope and d-excess value than our global study, with the equation:

$$\delta^2H = 7.8\,\delta^{18}O + 4.0 \quad (R^2 = 0.94;\ n = 32).$$

Individually, tributary streams and direct sampling in the Dudh Koshi River show a d-excess ranging between 4.4 and 12.7‰ (72% of samples lower than 10‰), which is globally lower than the d-excess measured in this study. The slope is lower than 8, but overall the low d-excess values imply that an evaporation process during the study interval (Florea et al., 2017) may be due to the sampling time (end of extra-monsoon

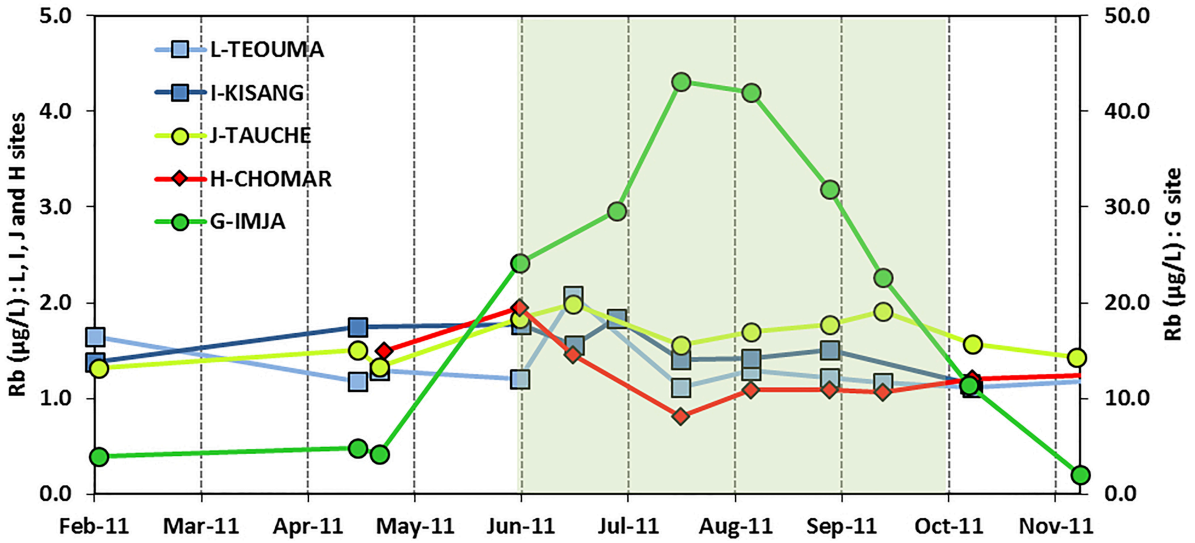

FIGURE 5 | Temporal variation of Rb concentration. The monsoon season is highlighted in green.

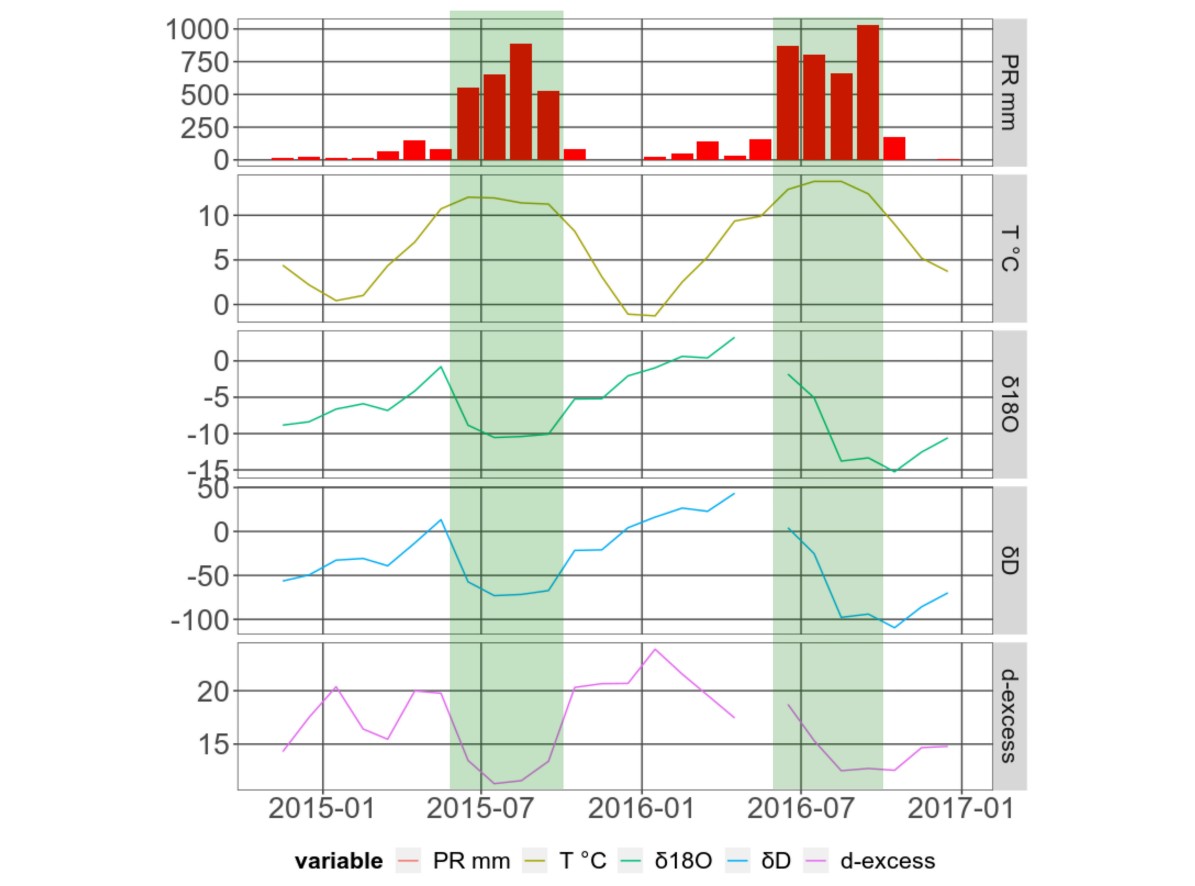

FIGURE 6 | Monthly precipitation data in Pangom (E): precipitation (PR), air temperature (T), and stable isotopes ($\delta^{18}O$, δD, d-excess, ‰ VSMOW). The monsoon seasons (JJAS) are highlighted in green.

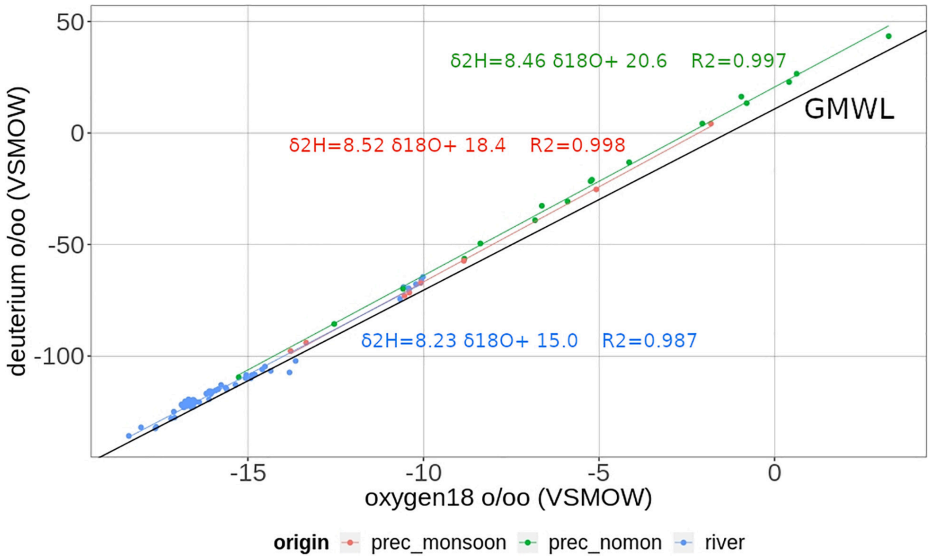

FIGURE 7 | $\delta^{18}O$ versus $\delta^{2}H$ for precipitation samples in Pangom (monsoon and extra-monsoon seasons in red and green, respectively) and for river samples in blue, compared with the Global Meteoric Water Line (GMWL).

season), with warmer conditions than during the sampling times of this study.

DISCUSSION

Water Origins

Not surprisingly, the isotope properties of the precipitation highlight the double climatic influence from the arrival of the westerlies in winter and from the Asian monsoon in summer.

The isotope response to ground ice melt has been investigated since the mid-1970s (Stuiver et al., 1976; Fujino and Kato, 1978) who relies on isotope fractionation that occurs during phase changes (i.e., freezing, condensation, adsorption) and the resulting difference in the slope of the regression of δD on $\delta^{18}O$ with a slope between 3 and 7 (Jouzel and Souchez, 1982; Lacelle, 2011). Ala-aho et al. (2018) show in western Siberia the possible discrimination of water origin between precipitation, river, lakes and thawing permafrost. The slope of the regression of δD on $\delta^{18}O$ was lower than the precipitation (7.6) with soils/permafrost (4.64) < lakes (5.54) < rivers (6.08) and a strong variability of median isotope content in precipitation (−15.6‰ in $\delta^{18}O$), rivers (−15.3‰), soils/permafrost (−13.0‰) and lakes (−11.1‰) > rivers (−15.1‰). In our study case the river points do not show an obvious influence of thawing permafrost during the sampling period which correspond before or after monsoon when temperatures are lower, may-be during monsoon period of higher temperature, an important thawing permafrost could be detected in some rivers.

Locally, the results of the current study confirm that few chemical patterns can be used to distinguish the waterflow origins during the different seasons. Rb, as Li, Cu, Sr, Ba, and SiO_2, originating from the minerals of the bedrock, characterizes substantially the water originating from glacier melt, as shown in **Figure 5**, especially during the monsoon season. Nevertheless, the isotopic results appear to be less useful for that task, even if differences are observed: the isotopic climate signal in the water courses is very likely mixed with the signal emitted by the storage in groundwater temporary reservoirs, which limits a clear interpretation. Factually, it depends on the sampling location and of the ratio of glacierized area. In the high altitudes (>4000 m) the river reflects the isotope content mainly of the ice and snow melt because the climatic conditions do not allow an important weathering of the rocks and a strong development of an aquifer structure; the consequence is a reduced groundwater capacity, and a fast groundwater circulation reflecting isotope content of ice and snow. At lower altitude, the weathering is higher and the aquifer can develop itself with a higher storage capacity involving local recharge by rainfall; the isotope content is enriched with respect to ice and snow melt (altitude effect): the lower the altitude, the richer is the isotope content of total flow. It is a consequence of the higher base flow in the dry season and of the higher contribution of the surface runoff in the monsoon season, this last being enriched in isotope with respect to ice and snow melt more depleted.

However, the meltwater marking (glacier as snow cover melt) by the isotopes can be more visible than by the chemical signature in downstream sampling sites, because it is less dissolved, with the inconvenience of a smoothed seasonal effect. The result at the Phakding (20.9% glacier covered) and Pangom (no glacier) stations, detailed in the previous section, is, therefore, significant.

The pH remains in a relatively narrow range in the different sampling points and does not seem useful for characterizing the water paths or the seasons, while electrical conductivity shows slightly higher values for flows originating from glaciers and lower values in the monsoon runoffs of streams not fed by glacier melt (**Figure 2**).

TABLE 4 | Main characteristics of the stable isotope river samples.

Name	Label (+)	Altitude (m)	Sampling seasons (*)						Isotope data				
			N14	MH15	N15	MY16	N16	MY17	Mean ^{18}O	Mean D	Maximum difference ^{18}O	maximum difference D	Mean d-excess
Kharikhola	A	1981				X	X	X	−10,16	−66,9	0,40	5,4	14,4
Phakding	B	2620		X	X	X	X	X	−15.89	−114.87	0.47	2.9	12.2
Jorsalle	C	2850		X	X 2		X	X	−16.05	−116.3	0.34	2.1	12.1
Pangom river	D	2880	X	X		X		X	−11.71	−80.5	5.98	53.6	13.2
Phunki Tenga	F	3200		X	X	X	X	X 2	−16.54	−120.5	0.20	0.1	11.8
Pangboche-Imja	G	3917			X	X	X	X	−16.67	−120.7	0.22	2.5	12.6
Pangboche-Tauche	J	4005	X	X	X	X	X	X	−15.51	−113.7	1.65	10.9	10.3
Shomare	K	4021	X		X				−14.08	−107.2	0.53	0.7	5.6
Pangboche-Teouma	L	4148			X	X	X		−14.6	−107.8	1.70	10.8	8.9
Pheriche hydro	O	4216			X	X	X	X	−16.7	−121.7	0.39	2.29	11.9
Pheriche village	P	4260	X						−16.55	−122.8			9.6
Dingboche village	Q	4370	X		X	X		X	−16.83	−121.7	0.57	5.2	12.9
Dingboche hydro	R	4372	X 2						−17.63	−132.2	0.03	0.7	8.8
Tauche Kharka	S	4405				X			−14.51	−104.7			11.4
Phulung Kharka	T	4504	X 2						−17.13	−127.9	0.10	0.47	9.2
Tukla	U	4700	X		X				−18.21	−133.93	0.35	3.84	11.8
Lobuche river	W	4840	X 2						−16.71	−123.03	0.21	0.1	10.7
Lobuche spring	X	4935			X				−15.06	−109.9			10.5

*(+) See location in **Figure 1**. (*) Axx: A = M (monsoon) or (extra-monsoon); xx is the year (e.g., 14 = 2014). N14, November 2014; MH15, March 2015; N15, November 2015; My16, May 2016, N16, November 2016; My17, May 2017.*

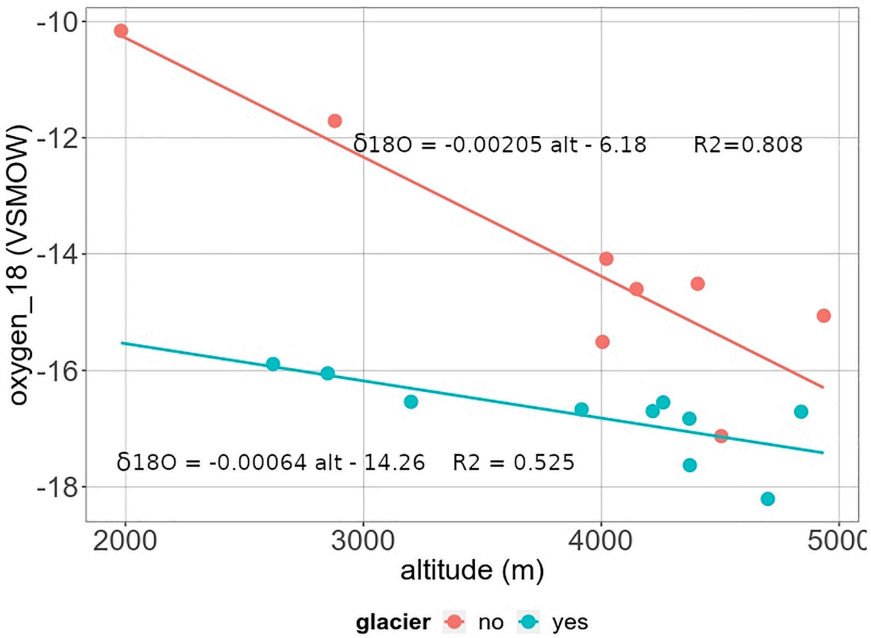

FIGURE 8 | Isotope altitude gradient from sampling in no glacier watershed (isotope value determined by local rainfall and aquifer isotope value), and sampling in partial glacier watershed (isotope value determined by mixing between melt from high altitude and local rainfall and aquifer isotope value).

TABLE 5 | Additional observations of electrical conductivity, performed on June 19, 21, and 22, 2012.

Name	Label (+)	Electrical conductivity (μS/cm)
Pangboche-Imja	G	53.0
Khumbu confluence	N	67.6
Pheriche hydro	O	62,6
Imja confluence	M	35.4
Dingboche hydro	R	32.9
Chukung	V	41.5
Imja Lake (*)	Y	29.7
		30.7
		29.6

*(+) See location in **Figure 1**. (*) Three different sampling points in the outlet narrows.*

FIGURE 9 | Confluence of the Khumbu River (down left) and the Imja River branch (upper right). The image has been saturated for a better depiction of the difference in turbidity between both branches. Photo by P. Chevallier, June 19, 2012.

In addition to the previous considerations, complementary observations on electrical conductivity were made in the main rivers of this area and in the Imja Lake during a 3-day interval in the second half of June 2012, in the early monsoon season. They are summarized in **Table 5**, which shows that the flows arising from the Imja Lake are approximately twofold less mineralized than those of the Khumbu upper valley. Both basins have similar areas and ratios of glaciated surfaces. Because the flows are from the same geological and glaciological origin, the conductivity difference observed can only be explained by the presence of the lake. The higher value observed in the lateral Imja River, which does not flow from the lake, confirms this hypothesis. This phenomenon could be attributed to the sedimentation only within the lake of the solid load generated by the glacier abrasion, due to quieter hydraulic conditions. This hypothesis is reinforced by the visual observations at the confluence between the Imja and the Khumbu rivers, which showed that the turbulence of the runoff was higher in the Khumbu branch than in the Imja branch (**Figure 9**).

Water Uses

Before commenting, it must be stressed that in the framework of this study no analysis was performed regarding the

bacterial and organic quality of the water used by the inhabitants and by the visitors. The reason is that, at the time of the study, the only laboratory for analyzing samples, poorly equipped and without dedicated manpower, was located in the Khumjung Hospital, close to the village of Namche Bazar, several hours' walking distance from the sampling points. This is unfortunate, because the sources of bacterial and organic pollution are numerous, especially high-altitude pastures, perfunctory toilet installations, uncontrolled waste disposal, etc. (Manfredi et al., 2010). These sources of pollution are increasing with the rapid development of tourist activities. Furthermore, inhabitants in Pangboche expressed more concerns about the future of the water quality than about water quantity since no proper sewage system exists and they are witnessing a dissemination of plastic waste in streams.

The quality of the natural water can be chemically considered good with a very low mineralization degree. It appears that the reticence to consider the water of the large valley river is mainly justified by the danger in accessing and harvesting it and also by its white color, due to the fine particles mentioned in the previous section. This particular property gave its name to the Dudh Koshi River, which means *Milk River* in Nepali. Nevertheless, these statements cannot conclude on the drinkability of the river water, since, as written above, organic and microbiological analysis have not been done in the current study framework.

The sampling points L (Pangboche-Teouma) and I (Pangboche-Kisang) were chosen for their location, upstream and downstream of the village, respectively, in order to examine an eventual degradation due to the human activities. No notable differences can be observed in terms of the major ions (**Table 2**). Nevertheless, in **Figure 4**, the trace elements collected throughout the year in Teouma (upstream) appear grouped, when a dispersion is noted for those collected downstream in Kisang. This dispersion is very likely due to the limited pollution of the water used in the village. Shortly after Kisang, the slope torrent is intercepted by the large Dudh Koshi River, where the low chemical pollution is dissolved.

Finally, the issue of bottled water consumption by tourists is of some importance to the local economy, because it is a non-negligible income for the communities (Puschiasis, 2015; Jacquemet, 2018). Several small companies have been established in the region to exploit this niche. One of them collected water at the Pangboche-Chomar point (labeled H in **Figure 1**) and, after a basic filtration process, bottled it. The bottled water was also analyzed with the same procedure as the other samples, except that it was transported to France after several months in the original PET bottle and not in a standard analysis recipient (see section "Conductivity, Major, and Trace Elements"). As shown in **Figure 4**, no difference is observed between the bottle and the other samples from the Chomar site. In **Table 2**, a few differences are notable, especially regarding pH, Cl^-, NO_3^-, and Na^+. They can be explained by the very long storage in a bad-quality recipient, but this is the reality for most of the water bottles available in the study zone. Nevertheless, in terms of chemical quality, the bottled water and the river water are similar. It seems that for some reason the water company did not pursue the exploitation of the Chomar site, which no longer functioned after 2013. However, water bottles from other places, particularly those collected in the surroundings of Namche Bazar, were sold in the Pangboche shops and lodges.

CONCLUSION

Between many studies, the recent IPCC special report on the cryosphere future (Pörtner et al., 2019) confirms the loss of cryospheric mass and the rapid permafrost thaw. It is also verified in the Central Himalaya, which presents threats on physical entities (water resources, flood, landslide, avalanche) and on ecosystems (forest, tundra). The Khumbu inhabitants are strongly preoccupied by this situation, which directly impacts their livelihood. In addition, they face difficulties in terms of inequalities in the social water management system, failing to regulate proper access of water in villages (Puschiasis, 2015; Faulon and Sacareau, 2020). More than climatic variations, changes in water use over the past decades are due to a growing need for tourism and for domestic purposes. Regarding the future of accessible water resources, this does not seem to be threatened in terms of quantity, even if seasonal pressures should lead to a better water management, especially during the high season of tourism activities (Aubriot et al., 2019). However, water quality could evolve in a worrisome direction.

Apart from the bacteriological and organic issue, which is not considered here, the points addressed could change as follows:

- The isotopic signature of precipitation and rivers is a good indicator of climate change and flow paths. It should be periodically analyzed. On the one hand, it could follow changes observed in the seasonal precipitation patterns in the study region (Shea et al., 2015). On the other hand, it facilitates the recognition of the transitory storage of surface water (glacier, snow cover, or underground reservoirs).
- In this study the chemical properties of the water used for domestic activities do not seem to be hazardous to human and animal health at present. However, with changes in precipitation and river regimes, in land use and land cover due to economic income, in cropping strategies, in the very low level of waste and toilet water management, the current fragile balance could be seriously jeopardized. The project of road construction in the valley, for instance, validated until Surkhe, close to Lukla ("The Rising Nepal: Everest Region Closer with Bridge over Sunkoshi". January 16, 2020. http://therisingnepal.org.np/news/1084. Accessed on August 10, 2020), will lead to the importation of chemical products and molecules that have been thus far unknown.

DATA AVAILABILITY STATEMENT

The raw data supporting the conclusions of this article will be made available by the authors, without undue reservation.

ETHICS STATEMENT

Ethical review and approval was not required for the study on human participants in accordance with the local legislation and institutional requirements. Written informed consent for participation was not required for this study in accordance with the national legislation and the institutional requirements.

AUTHOR CONTRIBUTIONS

PC coordinated the whole study, including the field collection, wrote the introduction, discussion, and conclusion sections, and assembled the different parts of the manuscript. J-LS contributed to the geochemistry analysis of the major ions and trace elements and J-DT of the stable isotopes. OP lived in Pangboche during the whole year in 2011 at an elevation of 4000 m, collecting the water samples and she wrote the parts regarding water use by the local inhabitants. All authors contributed to the article and approved the submitted version.

FUNDING

The global research action, the sample analysis, and the Ph.D. grant, followed by a post-doctoral grant, of OP were supported by *Agence Nationale de la Recherche – France* (references: ANR-09-CEP-005-04/PAPRIKA and ANR-13-SENV-005-03/PRESHINE). Some monitoring equipment was acquired through the *Glacioclim* SNO (French National Observation Service).

ACKNOWLEDGMENTS

The analyses of major ions and trace elements were done by Sandra Van Exter and J-LS, and the analysis of stable isotopes by Nicolas Patris at the *Laboratoire HydroSciences Montpellier (CNRS, IRD, University of Montpellier)*. Dawa Nuru Sherpa translated the dialogs with Pangboche's inhabitants and facilitated the measurements. Ang Jangmu Sherpa collected and stored the precipitation samples in Pangom. Yves Arnaud, Olivia Aubriot, Anneke De Rouw, François Delclaux, Judith Eeckman, Michel Esteves, Frédéric Hernandez, Devesh Koirala, Luc Neppel, Rémi Muller, Marie Savéan, Joëlle Smadja, and Patrick Wagnon participated in the field operations, as well as extraordinary, indispensable and friendly local porters. Yves Arnaud and Isabelle Sacareau were, respectively, the coordinators of the Paprika and Preshine projects, which benefited from a partnership with the following institutions: Nepalese Academy of Science and Technology (Kathmandu, Nepal), EvK2-CNR Association (Bergamo, Italy), International Center of Integrated Mountain Development (Kathmandu, Nepal), Tribhuvan University (Kathmandu, Nepal), and Department of Hydrology and Meteorology (Kathmandu, Nepal). Finally, the authors thank the two reviewers who allow to substantially improve the definitive version of the manuscript.

REFERENCES

Ala-aho, P., Soulsby, C., Pokrovsky, O. S., Kirpotin, S. N., Karlsson, J., Serikova, S., et al. (2018). Using stable isotopes to assess surface water source dynamics and hydrological connectivity in a high-latitude wetland and permafrost influenced landscape. *J. Hydrol.* 556, 279–293. doi: 10.1016/j.jhydrol.2017.11.024

Andermann, C., Longuevergne, L., Bonnet, S., Crave, A., Davy, P., and Gloaguen, R. (2012). Impact of transient groundwater storage on the discharge of himalayan rivers. *Nat. Geosci.* 5, 127–132. doi: 10.1038/ngeo1356

André-Lamat, V. (2017). *De l'eau Source à l'eau Ressource: Production d'un Capital Environnemental Ou d'un Commun. L'exemple de l'eau Domestique Au Pharak (Népal). Développement Durable et Territoires*. Available online at: https://halshs.archives-ouvertes.fr/halshs-01959313 (accessed December 18, 2018).

Aubriot, O., Faulon, M., Sacareau, I., Puschiasis, O., Jacquemet, E., Smadja, J., et al. (2019). Reconfiguration of the water–energy–food nexus in the everest tourist region of Solukhumbu, Nepal. *Mountain Res. Dev.* 39, R47–R59. doi: 10.1659/MRD-JOURNAL-D-17-00080.1

Balestrini, R., Delconte, C. A., Sacchi, E., Wilson, A. N., Williams, M. W., Cristofanelli, P., et al. (2016). Wet deposition at the base of Mt Everest: seasonal evolution of the chemistry and isotopic composition. *Atmos. Environ.* 146, 100–112. doi: 10.1016/j.atmosenv.2016.08.056

Balestrini, R., Polesello, S., and Sacchi, E. (2014). Chemistry and isotopic composition of precipitation and surface waters in Khumbu Valley (Nepal Himalaya): N dynamics of high elevation basins. *Sci. Total Environ.* 485–486, 681–692. doi: 10.1016/j.scitotenv.2014.03.096

Bonasoni, P., Laj, P., Marinoni, A., Sprenger, M., Angelini, F., Arduini, J., et al. (2010). Atmospheric brown clouds in the himalayas: first two years of continuous observations at the Nepal climate observatory-pyramid (5079 m). *Atmos. Chem. Phys.* 10, 7515–7531. doi: 10.5194/acp-10-7515-2010

Bookhagen, B., and Burbank, D. W. (2010). Toward a complete Himalayan hydrological budget: spatiotemporal distribution of snowmelt and rainfall and their impact on river discharge. *J. Geophys. Res. Earth Surf.* 115:F03019. doi: 10.1029/2009jf001426

Bortolami, G. (1998). "Geology of the Khumbu region, Mt Everest, Nepal," in *Limnology of High Altitude Lakes in the Mt Everest Region, Nepal. Memorie Dell' Istituto Italiano Di Idrobiologia*, Vol. 57, eds A. Lami and G. Giussani (Verbania: Instito per lo studio degli ecosistemi), 41–49.

Chevallier, P., Delclaux, F., Wagnon, P., Neppel, L., Arnaud, Y., Esteves, M., et al. (2017). *Paprika – Preshine Hydrology Data Sets in the Everest Region (Nepal). 2010-18. Data base. 2017*. Montpellier, France: Laboratoire HydroSciences. doi: 10.23708/000521

Clark, I., and Fritz, P. (1997). *Environmental Isotopes in Hydrogeology*. Boca Raton, FL: Lewis Publisher.

Crespo, S., Aranibar, J., Gomez, L., Schwikowski, M., Bruetsch, S., Cara, L., et al. (2017). Ionic and stable isotope chemistry as indicators of water sources to the Upper Mendoza River basin, Central Andes of Argentina. *Hydrol. Sci. J.* 62, 588–605. doi: 10.1080/02626667.2016.1252840

Dansgaard, W. (1964). Stable isotopes in precipitation. *Tellus* 16, 436–468. doi: 10.1111/j.2153-3490.1964.tb00181.x

Dongol, B. S., Merz, J., Schaffner, M., Nakarmi, G., Shah, P. B., Shrestha, S. K., et al. (2005). Shallow groundwater in a middle mountain catchment of Nepal: quantity and quality issues. *Environ. Geol.* 49, 219–229. doi: 10.1007/s00254-005-0064-5

Eeckman, J., Chevallier, P., Boone, A., Neppel, L., De Rouw, A., Delclaux, F., et al. (2017). Providing a non-deterministic representation of spatial variability of precipitation in the everest region. *Hydrol. Earth Syst. Sci.* 21, 4879–4893. doi: 10.5194/hess-21-4879-2017

Eeckman, J., Nepal, S., Chevallier, P., Camensuli, G., Delclaux, F., Boone, A., et al. (2019). Comparing the ISBA and J2000 approaches for surface flows modelling at the local scale in the everest region. *J. Hydrol.* 569, 705–719. doi: 10.1016/j.jhydrol.2018.12.022

Faulon, M., and Sacareau, I. (2020). Tourisme gestion sociale de l'eau et changement climatique dans un territoire de haute altitude: le massif de l'Everest au Népal. *J. Alpine* 108–111. doi: 10.4000/rga.6759

Florea, L., Bird, B., Lau, J. K., Wang, L., Lei, Y., Yao, T., et al. (2017). Stable isotopes of river water and groundwater along altitudinal gradients in the high Himalayas and the eastern Nyainqentanghla mountains. *J. Hydrol. Regional Stud.* 14, 37–48. doi: 10.1016/j.ejrh.2017.10.003

Fujino, K., and Kato, K. (1978). "Determination ofoxygen isotopic concentration in the ground ice of a tundra area," in *Joint Studies on Physical and Biological Environments in the Permafrost, Alaska and North Canada, July to August 1977*, ed. S. Kinosita (Sapporo: The Institute of Low Temperature Science, Hokkaido University), 77–83.

Gardelle, J., Berthier, E., Arnaud, Y., and Kaab, A. (2013). Region-wide glacier mass balances over the Pamir-Karakoram-Himalaya during 1999–2011. *Cryosphere* 7, 1263–1286. doi: 10.5194/tc-7-1263-2013

Garzione, C. N., Quade, J., De Celles, P. G., and English, N. B. (2000). Predicting paleoelevation of Tibet and the Himalaya from Δ18O vs altitude gradients in meteoric water across the Nepal Himalaya. *Earth Planet Sci. Lett.* 183, 215–229. doi: 10.1016/s0012-821x(00)00252-1

Ghezzi, L., Petrini, R., Montomoli, C., Carosi, R., Paudyal, K., and Cidu, R. (2017). Findings on water quality in Upper Mustang (Nepal) from a preliminary geochemical and geological survey. *Environ. Earth Sci.* 76:651. doi: 10.1007/s12665-017-6991-0

Gonga-Saholiariliva, N., Neppel, L., Chevallier, P., François, D., and Savéan, M. (2016). geostatistical estimation of daily monsoon precipitation at fine spatial scale: koshi river basin. *J. Hydrol. Eng.* 21:05016017. doi: 10.1061/(ASCE)HE.1943-5584.0001388

Guo, X., Tian, L., Wen, R., Yu, W., and Qu, D. (2017). Controls of precipitation Δ18O on the northwestern tibetan plateau: a case study at ngari station. *Atmos. Res.* 189, 141–151. doi: 10.1016/j.atmosres.2017.02.004

He, S., and Richards, K. (2016). Stable isotopes in monsoon precipitation and water vapour in Nagqu, tibet, and their implications for monsoon moisture. *J. Hydrol.* 540, 615–622. doi: 10.1016/j.jhydrol.2016.06.046

Hodson, A., Porter, P., Lowe, A., and Mumford, P. (2002). Chemical denudation and silicate weathering in himalayan glacier basins: batura glacier, Pakistan. *J. Hydrol.* 262, 193–208. doi: 10.1016/S0022-1694(02)00036-7

Immerzeel, W. W., van Beek, L. P. H., and Bierkens, M. F. P. (2010). Climate change will affect the asian water towers. *Science* 328, 1382–1385. doi: 10.1126/science.1183188

Jacobi, H.-W., Lim, S., Ménégoz, M., Ginot, P., Laj, P., Bonasoni, P., et al. (2015). Black carbon in snow in the upper Himalayan Khumbu Valley, Nepal: observations and modeling of the impact on snow albedo, melting, and radiative forcing. *Cryosphere* 9, 1685–1699. doi: 10.5194/tc-9-1685-2015

Jacquemet, E. (2018). *The Sherpa Community in the 'Yak Donald's' Era: Locational Struggles for Access to Resources in Mount Everest Touristic Region (Nepal)*. Ph.D. thesis, Université Michel de Montaigne – Bordeaux, Pessac.

Jeelani, G. (2008). Aquifer response to regional climate variability in a part of kashmir Himalaya in India. *Hydrogeol. J.* 16, 1625–1633. doi: 10.1007/s10040-008-0335-9

Jeelani, G., Bhat, N. A., Shivanna, K., and Bhat, M. Y. (2011). Geochemical characterization of surface water and spring water in SE kashmir valley, western himalaya: implications to water-rock interaction. *J. Earth Syst. Sci.* 120, 921–932. doi: 10.1007/s12040-011-0107-0

Jeelani, G., and Deshpande, R. D. (2017). Isotope fingerprinting of precipitation associated with western disturbances and Indian summer monsoons across the himalayas. *J. Earth Syst. Sci.* 126:108. doi: 10.1007/s12040-017-0894-z

Jeelani, G., Deshpande, R. D., Shah, R. A., and Hassan, W. (2017). Influence of southwest monsoons in the Kashmir valley, Western himalayas. *Isotopes Environ. Health Stud.* 53, 400–412. doi: 10.1080/10256016.2016.1273224

Jeelani, G., Saravana Kumar, U., and Kumar, B. (2013). Variation of Δ18O and ΔD in precipitation AND Stream waters across the Kashmir Himalaya (India) to distinguish and estimate the seasonal sources of stream flow. *J. Hydrol.* 481, 157–165. doi: 10.1016/j.jhydrol.2012.12.035

Jeelani, G., Shah, R. A., and Deshpande, R. D. (2018). Application of water Isotopes to Identify the sources of groundwater recharge in a karstified landscape of western himalaya. *J. Clim. Change* 4, 37–47. doi: 10.3233/jcc-180005

Jouzel, J., and Souchez, R. A. (1982). Melting andrefreezing at the glacier sole and the isotopic composition of the ice. *J. Glaciol.* 28, 35–42. doi: 10.3189/s0022143000011771

Kaspari, S. D., Schwikowski, M., Gysel, M., Flanner, M. G., Kang, S., Hou, S., et al. (2011). Recent Increase in black carbon concentrations from a mt. Everest ice core spanning 1860-2000 AD. *Geophys. Res. Lett.* 38:L04703. doi: 10.1029/2010gl046096

Kumar, A., Tiwari, S. K., Verma, A., and Gupta, A. K. (2018). Tracing isotopic signatures (ΔD and Δ18O) in precipitation and glacier melt over chorabari glacier–hydroclimatic inferences for the upper ganga basin (UGB), Garhwal Himalaya. *J. Hydrol. Regional Stud.* 15, 68–89. doi: 10.1016/j.ejrh.2017.11.009

Lacelle, D. (2011). On the d18O, dD and D-excess relations in meteoric precipitation and during equilibrium freezing: theoretical approach and field examples. *Permafrost Periglacial Process.* 22, 13–25. doi: 10.1002/ppp.712

Lai, C. T., and Ehleringer, J. R. (2010). Deuterium excess reveals diurnal sources of water vapor in forest air. *Oecologia* 165, 213–223. doi: 10.1007/s00442-010-1721-2

Li, L., and Garzione, C. N. (2017). Spatial distribution and controlling factors of stable isotopes in meteoric waters on the tibetan plateau: implications for paleoelevation reconstruction. *Earth Planet. Sci. Lett.* 460, 302–314. doi: 10.1016/j.epsl.2016.11.046

Madhura, R. K., Krishnan, R., Revadekar, J. V., Mujumdar, M., and Goswami, B. N. (2015). Changes in western disturbances over the western himalayas in a warming environment. *Clim. Dyn.* 44, 1157–1168. doi: 10.1007/s00382-014-2166-9

Manfredi, E. C., Flury, B., Viviano, G., Thakuri, S., Nath Khanal, S., Kumar Jha, P., et al. (2010). Solid waste and water quality management models for sagarmatha national park and buffer zone, Nepal. Implementation of a participatory modeling framework. *Mountain Res. Dev.* 30, 127–142. doi: 10.1659/MRD-JOURNAL-D-10-00028.1

McDowell, G., Ford, J. D., Lehner, B., Berrang-Ford, L., and Sherpa, A. (2012). Climate-related hydrological change and human vulnerability in remote mountain regions: a case study from khumbu, Nepal. *Regional Environ. Change* 13, 299–310. doi: 10.1007/s10113-012-0333-2

Mimeau, L., Esteves, M., Jacobi, H.-W., and Zin, I. (2019). Evaluation of gridded and in situ precipitation datasets on modeled glacio-hydrologic response of a small glacierized himalayan catchment. *J. Hydrometeorol.* 20, 1103–1121. doi: 10.1175/JHM-D-18-0157.1

Nepal, S., Krause, P., Flügel, W.-A., Fink, M., and Fischer, C. (2014). Understanding the hydrological system dynamics of a glaciated alpine catchment in the himalayan region using the J2000 hydrological model. *Hydrol. Process.* 28, 1329–1344. doi: 10.1002/hyp.9627

Pisharoty, P. R., and Desai, B. N. (1956). Western disturbances and Indian weather. *Indian J. Meteorol. Geophys.* 8, 333–338.

Pörtner, H.-O., Roberts, D. C., Masson-Delmotte, V., Zhai, P., Tignor, M., Poloczanska, E., et al. (2019). *IPCC Special Report on the Ocean and Cryosphere in a Changing Climate*. Geneva: IPCC.

Puschiasis, O. (2015). *Des Enjeux planétaires aux Perceptions Locales du Changement Climatique: Pratiques et discours au fil de l'eau chez les Sherpa de la vallée du Khumbu (Everest, Népal)*. Doctorat, Nanterre Université Paris Ouest Nanterre La Défense, Nanterre.

Puschiasis, O. (2019). Un vent de Changements Souffle sur l'Everest. Multiples Facettes de la Perception de la Météorologie et du climat chez les Sherpa. Available online at: http://www.ethnographiques.org/2019/Puschiasis (accessed August 10, 2020).

Ren, W., Yao, T., Xie, S., and He, Y. (2017). Controls on the stable isotopes in precipitation and surface waters across the southeastern tibetan plateau. *J. Hydrol.* 545, 276–287. doi: 10.1016/j.jhydrol.2016.12.034

Reynolds, R. C., and Johnson, N. M. (1972). Chemical weathering in temperate glacial environment of the Northern cascade mountains. *Geochim. Cosmochim. Acta* 36, 537–554. doi: 10.1016/0016-7037(72)90074-9

Rozanski, K., Araguas-Araguas, L., and Gonfiantini, R. (1993). "Isotopic patterns in modern global precipitation," in *Climate Change in Continental Isotopic Records, 1–36. Geophysical Monograph 78*, eds P. K. Swart, K. C. Lohmann, J. Mckenzie, and S. Savin (Washington, DC: American Geophysical Union).

Savéan, M., Delclaux, F., Chevallier, P., Wagnon, P., Gonga-Saholiariliva, N., Sharma, R., et al. (2015). Water budget on the dudh koshi river (Nepal):

uncertainties on precipitation. *J. Hydrol.* 531, 850–862. doi: 10.1016/j.jhydrol.2015.10.040

Searle, M. P., Simpson, R. L., Law, R. D., Parrish, R. R., and Waters, D. J. (2003). The structural geometry, metamorphic and magmatic evolution of the everest massif, high Himalaya of Nepal-south tibet. *J. Geol. Soc.* 160, 345–366. doi: 10.1144/0016-764902-126

Sevruk, B. (1989). "Reliability of precipitation measurements," in *Not in File*, ed. B. Sevruck (St Moriz: Swiss Federal Institute of Technology, Zurich), 13–19.

Shea, J. M., Wagnon, P., Immerzeel, W. W., Biron, R., Brun, F., and Pellicciotti, F. (2015). A comparative high-altitude meteorological analysis from three catchments in the Nepalese himalaya. *Int. J. Water Resour. Dev.* 31, 174–200. doi: 10.1080/07900627.2015.1020417

Shen, H., and Poulsen, C. J. (2019). Precipitation $\delta^{18}O$ on the himalaya–tibet orogeny and its relationship to surface elevation. *Clim. Past* 15, 169–187. doi: 10.5194/cp-15-169-2019

Singh, A. T., Rahaman, W., Sharma, P., Laluraj, C. M., Patel, L. K., Pratap, B., et al. (2019). Moisture sources for precipitation and hydrograph components of the sutri dhaka glacier basin, western himalayas. *Water* 11:2242. doi: 10.3390/w11112242

Singh, K. A., and Hasnain, S. I. (1998). Major ion chemistry and weathering control in a high altitude basin: alaknanda river, garhwal himalaya, India. *Hydrol. Sci. J.* 43, 825–843. doi: 10.1080/02626669809492181

Spoon, J. (2011). The heterogeneity of khumbu sherpa ecological knowledge and understanding in sagarmatha (Mount Everest) national park and buffer zone, Nepal. *Hum. Ecol.* 39, 657–672. doi: 10.1007/s10745-011-9424-9

Stuiver, M., Yang, I. C., and Denton, G. H. (1976). Permafrost oxygen isotope ratios and chronology of three cores from Antarctica. *Nature* 261, 547–550. doi: 10.1038/261547a0

Tahir, A. A., Chevallier, P., Arnaud, Y., Neppel, L., and Ahmad, B. (2011). Modeling snowmeltrunoff under climate scenarios in the Hunza River basin, Karakoram Range, Northern Pakistan. *J. Hydrol.* 409, 104–117. doi: 10.1016/j.jhydrol.2011.08.035

Turner, A. G., and Annamalai, H. (2012). Climate change and the south asian summer monsoon. *Nat. Clim. Change* 2, 587–595. doi: 10.1038/nclimate1495

Verma, A., Kumar, A., Gupta, A. K., Tiwari, S. K., Bhambri, R., and Naithani, S. (2018). Hydroclimatic significance of stable isotopes in precipitation from glaciers of garhwal himalaya, upper ganga basin (UGB), India. *Hydrol. Process.* 32, 1874–1893. doi: 10.1002/hyp.13128

Wang, B. (2006). *The Asian Monsoon. Springer-Praxis Books in Environmental Sciences*. Berlin: Springer.

Wen, R., Tian, L., Weng, Y., Liu, Z., and Zhao, Z. (2012). The altitude effect of Δ18O in precipitation and river water in the southern himalayas. *Chin. Sci. Bull.* 57, 1693–1698. doi: 10.1007/s11434-012-4992-7

Wester, P., Mishra, A., Mukherji, A., and Shrestha, A. B. (eds). (2019). *The Hindu Kush Himalaya Assessment. Mountains, Climate Change, Sustainability and People. ICIMOD*. Kathmandu: Springer Nature. doi: 10.1007/978-3-319-92288-1

Yao, T., Masson−Delmotte, V., Gao, J., Yu, W., Yang, X., Risi, C., et al. (2013). A review of climatic controls on Δ18O in precipitation over the tibetan plateau: observations and simulations. *Rev. Geophys.* 51, 525–548. doi: 10.1002/rog.20023

Conflict of Interest: The authors declare that the research was conducted in the absence of any commercial or financial relationships that could be construed as a potential conflict of interest.

frontiers in Earth Science

ORIGINAL RESEARCH
published: 11 September 2020
doi: 10.3389/feart.2020.559175

Assessing Multi-Temporal Snow-Volume Trends in High Mountain Asia From 1987 to 2016 Using High-Resolution Passive Microwave Data

Taylor Smith and Bodo Bookhagen*

Institute of Geosciences, Universität Potsdam, Potsdam, Germany

High Mountain Asia (HMA) is dependent upon both the amount and timing of snow and glacier meltwater. Previous model studies and coarse resolution (0.25° × 0.25°, ~25 km × 25 km) passive microwave assessments of trends in the volume and timing of snowfall, snowmelt, and glacier melt in HMA have identified key spatial and seasonal heterogeneities in the response of snow to changes in regional climate. Here we use recently developed, continuous, internally consistent, and high-resolution passive microwave data (3.125 km × 3.125 km, 1987–2016) from the special sensor microwave imager instrument family to refine and extend previous estimates of changes in the snow regime of HMA. We find an overall decline in snow volume across HMA; however, there exist spatially contiguous regions of increasing snow volume—particularly during the winter season in the Pamir, Karakoram, Hindu Kush, and Kunlun Shan. Detailed analysis of changes in snow-volume trends through time reveal a large step change from negative trends during the period 1987–1997, to much more positive trends across large regions of HMA during the periods 1997–2007 and 2007–2016. We also find that changes in high percentile monthly snow-water volume exhibit steeper trends than changes in low percentile snow-water volume, which suggests a reduction in the frequency of high snow-water volumes in much of HMA. Regions with positive snow-water storage trends generally correspond to regions of positive glacier mass balances.

Keywords: snow, glacier, climate change, passive microwave, special sensor microwave imager, special sensor microwave imager/sounder

OPEN ACCESS

Edited by:
Mohamed Rasmy,
National Graduate Institute for Policy Studies, Japan

Reviewed by:
Maheswor Shrestha,
Water and Energy Commission Secretariat, Nepal
Renguang Wu,
Institute of Atmospheric Physics (CAS), China
Jeff Dozier,
University of California, Santa Barbara, United States

****Correspondence:***
Taylor Smith
tasmith@uni-potsdam.de

Specialty section:
This article was submitted to Cryospheric Sciences, a section of the journal Frontiers in Earth Science

Received: *06 May 2020*
Accepted: *18 August 2020*
Published: *11 September 2020*

Citation:
Smith T and Bookhagen B (2020) Assessing Multi-Temporal Snow-Volume Trends in High Mountain Asia From 1987 to 2016 Using High-Resolution Passive Microwave Data. Front. Earth Sci. 8:559175. doi: 10.3389/feart.2020.559175

1. INTRODUCTION

Rivers draining from High Mountain Asia (HMA) are relied upon by more than a billion people for agriculture, hydropower, and household use (Immerzeel et al., 2010; Bolch et al., 2012; Vaughan et al., 2013). In much of HMA, snow and glacier meltwaters provide key seasonal water buffers that help maintain water availability year-round (Barnett et al., 2005; Bookhagen and Burbank, 2010; Immerzeel et al., 2010; Berghuijs et al., 2014; Lutz et al., 2014; Huss et al., 2017). A large body of research has identified significant changes in HMA's cryosphere in recent decades, and in particular, the retreat of many regional glaciers (e.g., Hewitt, 2005; Déry and Brown, 2007; Scherler et al., 2011; Bolch et al., 2012; Gardelle et al., 2012; Kääb et al., 2012; Sorg et al., 2012; Kapnick et al., 2014; Wulf

et al., 2016; Sakai and Fujita, 2017; Smith et al., 2017; Smith and Bookhagen, 2018; Lievens et al., 2019; Rounce et al., 2019; Treichler et al., 2019; Shean et al., 2020); however, there exist large spatial heterogeneities in glacier trends (Hewitt, 2005; Gardelle et al., 2012; Kääb et al., 2012; Yao et al., 2012; Sakai and Fujita, 2017; Treichler et al., 2019). Previous work has also identified spatial and seasonal patterns in snow depth and the timing of snowmelt in HMA, which are mostly coherent with changes in glacier mass balances (Smith et al., 2017; Smith and Bookhagen, 2018; Wang et al., 2018; Treichler et al., 2019; Notarnicola, 2020; Shean et al., 2020). In-depth analyses of changes in HMA's cryosphere are often limited by lack of *in-situ* data and rugged terrain which hinders high-resolution data collection (Bookhagen and Burbank, 2010); estimates of climate trends from *in-situ*, satellite, and modeled data often result in heterogeneous and complex spatial patterns (Smith and Bookhagen, 2018).

Passive microwave data have long provided the best global dataset for studying snow depth and snow-water storage (Chang et al., 1982). However, they are limited by spatial resolution—data are typically available as 0.25° × 0.25° (~25 km × 25 km) grid cells which hinders many analyses. Recently, the National Snow and Ice Data Center has re-gridded and re-processed the special sensor microwave imager (SSMI, 1987–2009) and special sensor microwave imager/sounder (SSMI/S, 2003–2016) to a 3.125 km × 3.125 km (~10 km^2) spatial resolution (Brodzik et al., 2016). In this study, we leverage this high-resolution, cross-calibrated, multi-satellite dataset to consider 1.02 million passive microwave grid cells over 29 complete October-September water years across HMA (25–45°N, 60–110°E, 1987–2016; **Figure 1**). The enhanced resolution of this dataset allows us to more closely examine spatio-temporal trends in snow-water storage which have previously been shown to have strong impacts on climate and glacier dynamics in the region (Zhao and Moore, 2004; Fujita and Nuimura, 2011; Kapnick et al., 2014; Smith and Bookhagen, 2018).

2. DATA AND METHODS

2.1. Study Area and Data Sources

Our study covers the region from 25 to 45°N and from 65 to 105°E, running across some of the most densely populated regions of the world. Several key watersheds, such as the Indus, Syr Darya, Amu Darya, Yangtze, Salween, and Ganges/Brahmaputra drain from HMA (**Figure 1A**, blue outlines).

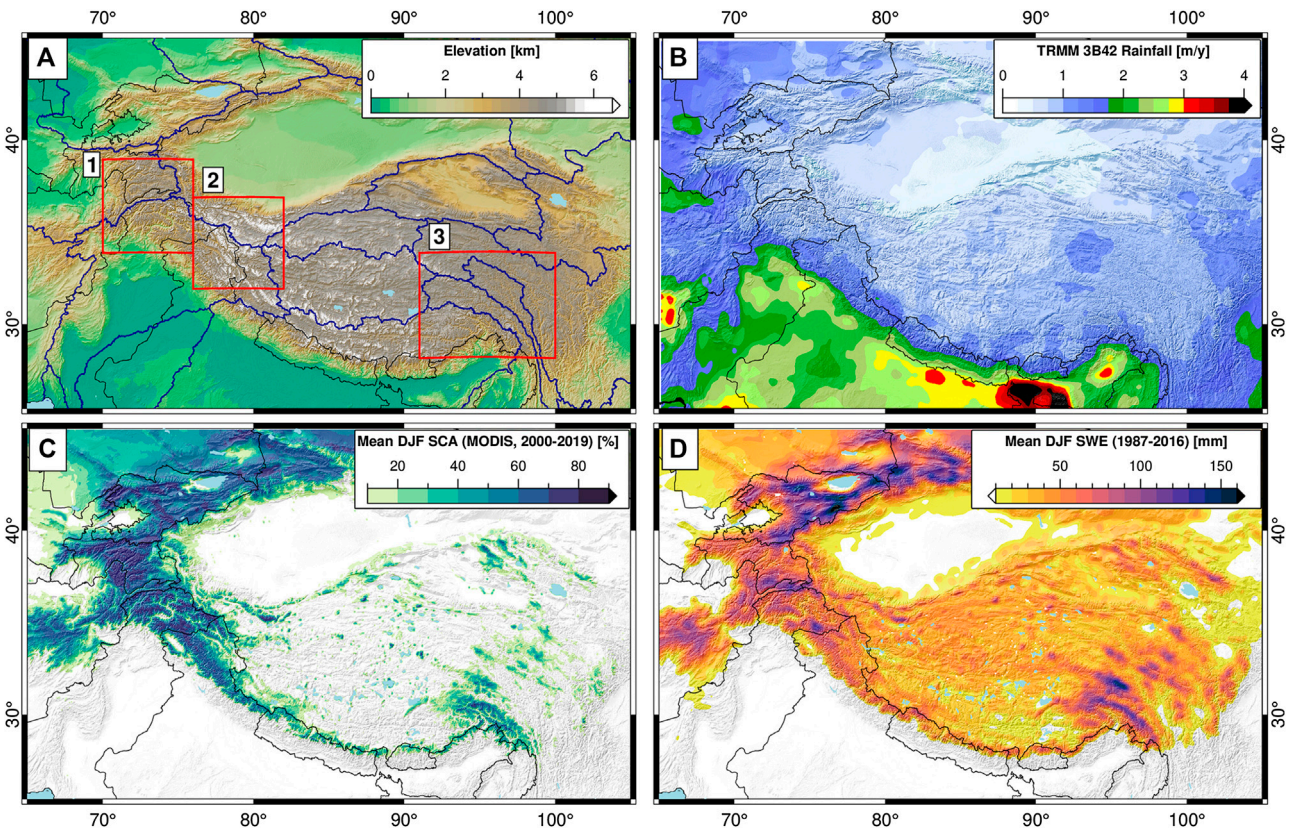

FIGURE 1 | Study area **(A)** topography **(B)** average annual Tropical Rainfall Measurement Mission precipitation sum [0.25°, 1998–2018 (Huffman et al., 2007)], **(C)** average December-January-February (DJF) snow-covered area percentage from MODIS MOD10A [500 m, 2000–2019 (Hall and Riggs, 2016)], and **(D)** average DJF snow-water equivalent (SWE) volume from 3.125 km resolution special sensor microwave imager and special sensor microwave imager/sounder (1987–2016). Deep snow is generally confined to high-elevation regions. Blue outlines on **(A)** show major watersheds from HydroBASINS (Lehner and Grill, 2013), black lines show international borders. Labeled boxes indicate sub-areas shown in **Figures 4** and **8**.

Precipitation in HMA is driven by three main weather systems—the Indian Summer Monsoon, the East Asian Summer Monsoon, and the Winter Westerly Disturbances (Bookhagen and Burbank, 2010; Cannon et al., 2016b). These major weather systems interact to bring a heterogeneous mix of snow and rain to different regions of HMA. Recent changes in the timing and intensity of precipitation from these major weather systems have been observed (e.g., Kitoh et al., 2013; Menon et al., 2013; Vaughan et al., 2013; Cannon et al., 2015; Singh et al., 2014; Cannon et al., 2016b; Malik et al., 2016; Norris et al., 2020), and have been shown to impact the timing and volume of snow-water storage and snowmelt (Kapnick et al., 2014; Smith et al., 2017; Smith and Bookhagen, 2018).

2.2. Satellite Data Preparation

Snow has been extensively studied with passive microwave data—albeit at low spatial resolutions (e.g., 0.25° × 0.25°) (Chang et al., 1987; Kelly et al., 2003; Smith and Bookhagen, 2016; Smith and Bookhagen, 2018). Recent image processing advances have allowed researchers to take advantage of the elliptical nature of passive microwave footprints to re-process the data onto a much finer spatial grid than previous approaches had allowed. In this study, we use the EASE-grid 2.0 high-resolution passive microwave product (1987–2016) (Early and Long, 2001; Brodzik et al., 2012; Brodzik et al., 2016; Long and Brodzik, 2016), which provides the 19 and 37 GHz passive microwave frequencies at spatial resolutions of 6.25 and 3.125 km, respectively. This dataset has been carefully cross-calibrated between the various SSMI and SSMI/S satellite platforms to provide consistent and homogenized data through the entire time series (Brodzik et al., 2016).

To produce consistent snow-water equivalent (SWE) estimates over the entire study region, we further re-grid the 19 GHz passive microwave data to a 3.125 km spatial resolution. We then remove areas near lakes and areas with shallow or infrequent snow-cover, as these areas are not suitable for long-

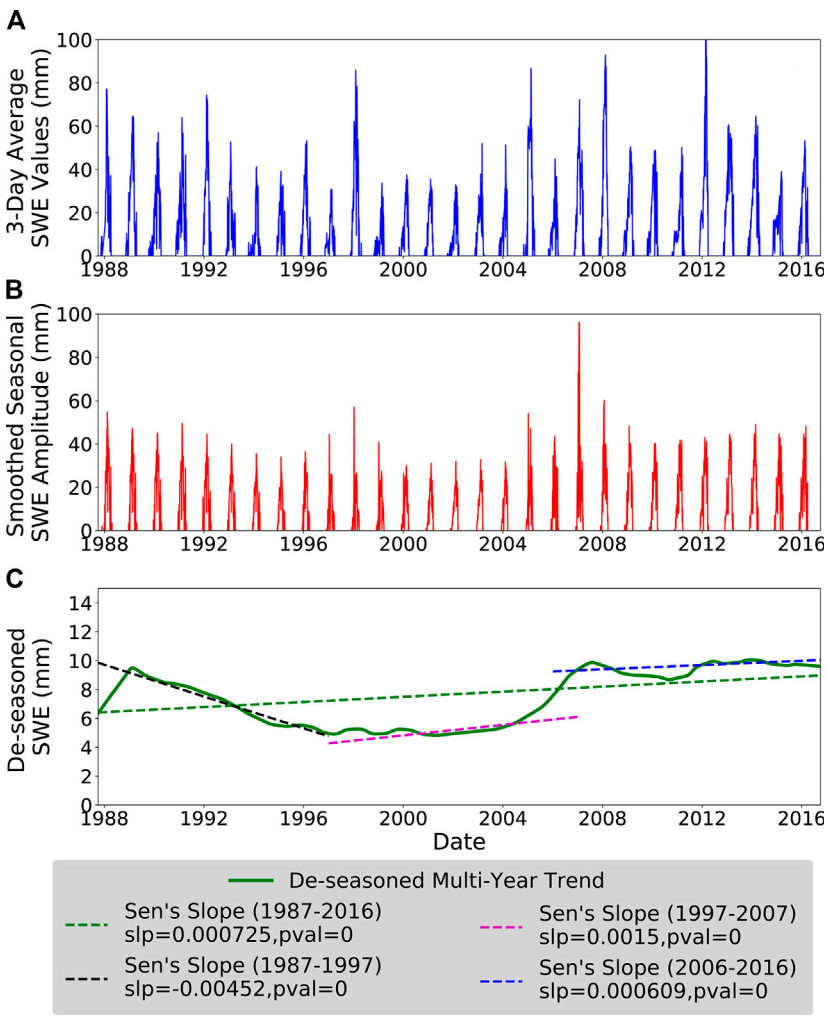

FIGURE 2 | Sample location (approx. 72.06°E, 38.64°N) illustrating the **(A)** snow-water equivalent (SWE) time series, **(B)** seasonal signal to be removed, and **(C)** the long-term de-seasoned data. Dashed lines on **(C)** show fitted lines using Sen's slope estimator over the whole dataset (green), the first decade (black), the second decade (purple), and the third decade (blue). There are strong oscillations in the fitted SWE trend based on the start and end dates chosen.

term SWE trend analysis. Finally, following the methodology of Smith and Bookhagen (2018), we use the computationally efficient algorithm proposed by Chang et al. (1987) to convert the passive microwave data to snow depth:

$$SD = 1.59 \times (Tb_{19V} - Tb_{36V}) \quad (1)$$

We then convert those snow depth estimates to SWE using a constant snow density of 0.24 g/cm^3, which has been shown to be a reasonable global average (Sturm et al., 2010; Takala et al., 2011). In short, the Chang et al. (1987) algorithm uses the difference between the 19 and 37 GHz passive microwave channels to estimate snow depth based on a comparison with extensive snow survey data collected throughout the Canadian and Russian Arctic (Chang et al., 1982; Chang et al., 1987). This algorithm is widely used to estimate SWE over diverse terrain, and has served as the basis for further updates to passive microwave SWE retrieval algorithms which take advantage of additional passive microwave channels not carried on SSMI/S to better constrain the impacts of vegetation cover on SWE estimates (Chang et al., 1991; Chang et al., 1996; Foster et al., 2005; Derksen, 2008; Kelly, 2009; Langlois et al., 2011; Smith and Bookhagen, 2016). In our low-vegetation study area, we rely on the Chang et al. (1987) algorithm to take advantage of the full SSMI/S time series.

2.3. Trend Analysis

For parts of the passive microwave time series, there are multiple overlapping satellite overpasses. For consistency, we aggregate all night-time overpasses (October 1987–September 2016) into an average daily SWE estimate over HMA (number of grid cells = 1,027,847) using the median of all available night-time measurements per day. As the various SSMI satellite platforms have been carefully cross-calibrated (Brodzik et al., 2016), this step serves simply to homogenize the temporal sampling of the dataset over the entire time period. For computational efficiency, we then further resample each individual daily SWE time series to a temporal frequency of three days before computing trends; in our tests this does not significantly modify computed long-term trends.

Before trend analysis, we first remove the seasonal component of each individual time series via Seasonal Trend Decomposition by Loess (Cleveland et al., 1990), using a decomposition window of 365 days (**Figure 2**). This method yields a seasonal signal, long-term signal, and residual short-term signal from a given time series by removing oscillations at the chosen decomposition time frequency. We then test the resulting de-seasoned time series for significant increasing or decreasing trends using the Mann-Kendall test (Mann, 1945; Kendall, 1948). If there exists a significant trend, we use Sen's slope method to capture the overall trend at that grid cell (Sen, 1968). We thus use a conservative approach by testing for significance both with the Mann-Kendall test and *via* Sen's slope method. We only present results from statistically significant ($p < 0.05$) trends in this study.

3. RESULTS

3.1. Long-Term Snow-Water Equivalent Trends

Aggregate trends over the entirety of HMA are slightly negative (sum: −55.5 mm/yr, average: −0.01%) over 3,618 km^2× 10^3 km^2, including only trends with $p < 0.05$ and areas at least 500 m above sea level). While the aggregate trends appear to be small, we emphasize that trends are measured over 9.75 km^2 grid cells, and represent a snow-water storage loss of 5.41 m^3 × 10^5 m^3 of water per year (**Figure 3**).

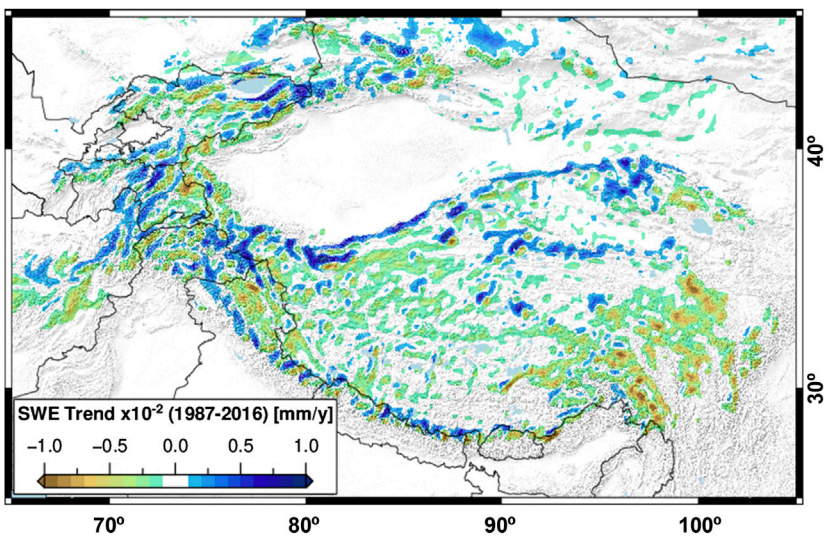

FIGURE 3 | Annual snow-water equivalent (SWE) trends (1987–2016) for High Mountain Asia (HMA). There is no spatially coherent SWE trend throughout HMA, but rather several 100 km^2 × 100 km^2 or larger regions with similar characteristics (Fujita and Nuimura, 2011; Smith and Bookhagen, 2018; Wang et al., 2018). Large-scale negative SWE trends are observed in the Tien Shan and Pamir Mountains in western HMA, and at the eastern margin of the Tibetan plateau. The Kunlun Shan, Karakoram, and western Himalaya are characterized by positive SWEs trends.

It is clear that SWE trends are spatially diverse—positive SWE trends are concentrated in the Karakoram, Pamir, Kunlun Shan, and the high Himalaya (**Figures 3** and **4A–D**). The most negative trends are concentrated in the south-eastern Tibetan Plateau (**Figures 4E,F**), at the headwaters of the Yangtze, Salween, and Mekong rivers. There also exist many small-scale features; for example, there are clear alternating positive-negative SWE trend patterns along the front of the Himalaya. While there are multiple possible causes for such small-scale variability, the extreme topography and the microclimates it creates can drastically

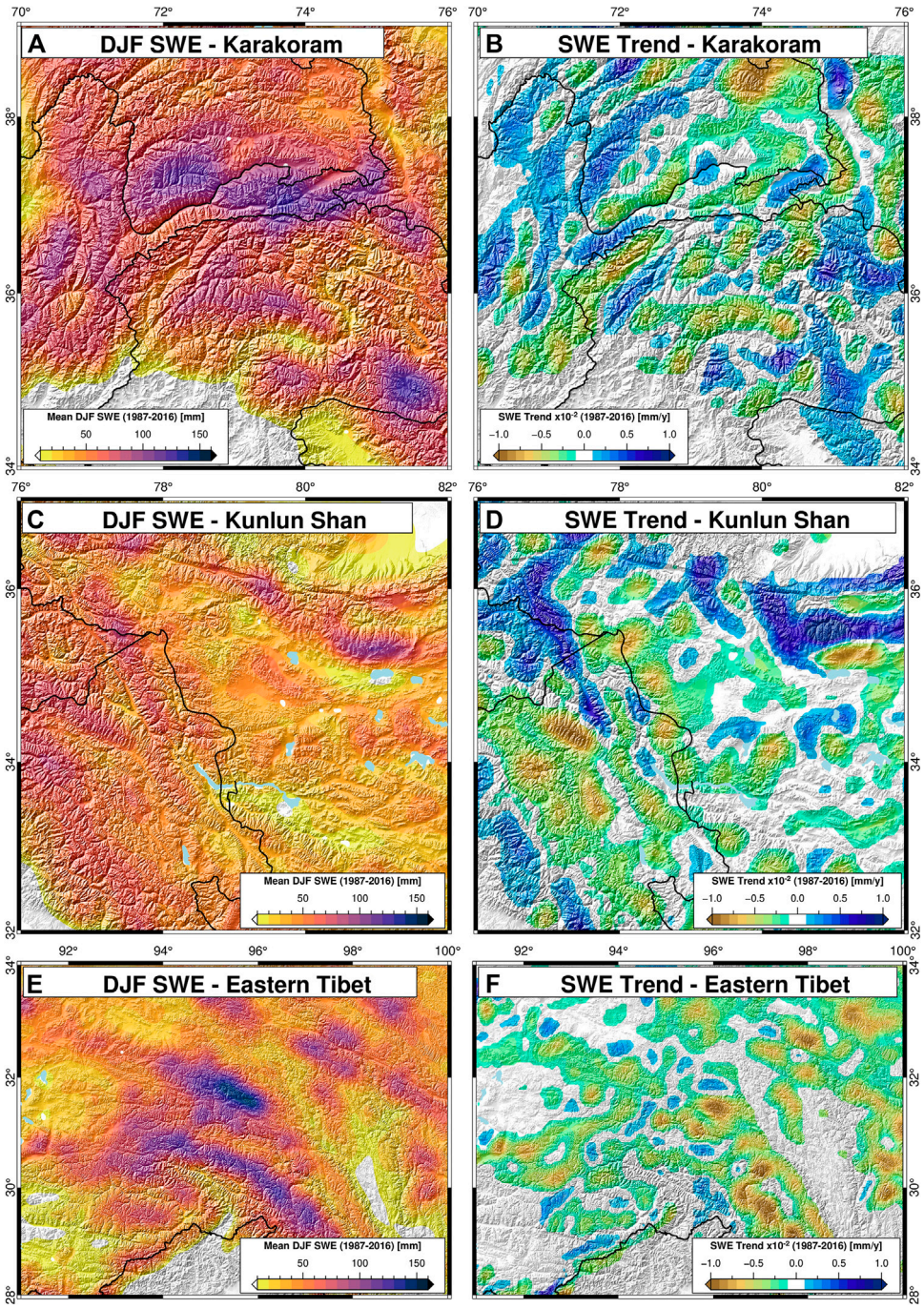

FIGURE 4 | Regional zoom maps (see **Figure 1** for locations). Average December-January-February (DJF) snow-water equivalent (SWE) (left column) and annual SWE trends (1987–2016, right column) for the **(A,B)** Karakoram-Pamir, **(C,D)** Kunlun Shan, and **(E,F)** Eastern Tibetan regions. Regional SWE trends show clear differences in magnitudes and directions: high SWE areas in the **(A)** Karakoram and Pamir Mountains have a wide range of trends, but overall more negative trends in high SWE areas. The **(B)** Kunlun Shan has lower average SWE, but stronger positive trends. **(E)** Eastern Tibet has high SWE with overall strongly negative SWE trends.

alter snow-loading and snow-water storage on nearby slopes—particularly when there are large differences in the sun exposure and overall aspect of neighboring slopes (**Supplemental Figures S1–S5**).

3.2. Seasonal Snow-Water Equivalent Trends

When the SWE data are further divided into seasonal components, clear differences in trend direction and magnitude appear (**Figure 5**). Strong positive winter (December-January-February) trends are visible in most of the highest peaks of HMA—running along the Himalaya, into the Pamir-Karakoram-Kunlun Shan region, as well as through the Tien Shan. These positive trends are visible through the spring (March-April-May) and fall (September-October-November) seasons as well; the only region, however, to maintain positive trends through the full year and in each seasonal slice is the Karakoram-Kunlun Shan region, which has been noted for glacier stability and growth in recent years (Hewitt, 2005; Kääb et al., 2012; Kapnick et al., 2014; Treichler et al., 2019; Shean et al., 2020). These positive trends are offset by large negative SWE trends in lower-elevation regions of HMA and along the eastern edge of the Tibetan Plateau which has seen rapidly decreasing SWE—particularly in the December-January-February and September-October-November periods (**Figure 5**).

3.3. Magnitude Variations in Snow-Water Equivalent Trends

To further explore the dynamics of SWE trends in HMA, we have performed a second set of regressions using monthly SWE percentiles (**Figure 6**). In short, we calculate the 10th, 25th, 50th, 75th, and 90th percentile SWE value at each pixel over each month using daily-averaged SWE data (October 1987–September 2016), remove the long-term monthly mean value for each given month to reduce the impacts of seasonality, and perform regressions through each SWE percentile separately. This yields a set of SWE trend results based on only the lowest (e.g., 10th percentile) or highest (e.g., 90th percentile) SWE value for each month.

When the SWE trend magnitudes at each percentile are compared, differences between high- and low-percentile trends are apparent (**Figure 6**). In almost all cases, the trends in high-percentile SWE are steeper than those in low-percentile SWE. In positive SWE-trend regions, this indicates that high SWE amounts are becoming relatively more frequent. For example, along the border of India and Pakistan, positive SWE-trend regions (see

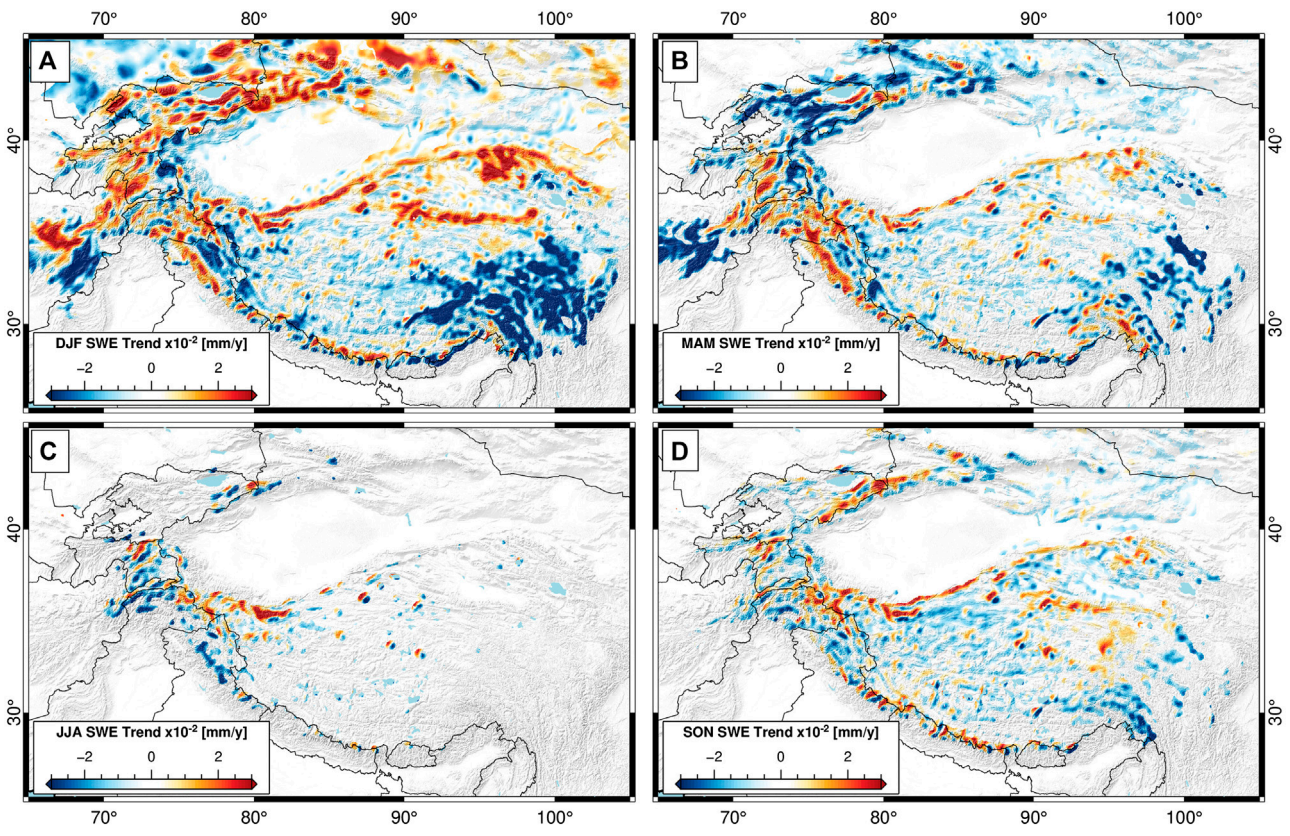

FIGURE 5 | Seasonal components of snow-water equivalent (SWE) trend (1987–2016). **(A)** December-January-February (DJF), **(B)** March-April-May (MAM), **(C)** June-July-August (JJA), and **(D)** September-October-November (SON) trends all have distinct spatial patterns. Note that the magnitude scaling of the seasonal trends is three times as large as that of the annual trends (see **Figure 3**). The Karakoram-Kunlun Shan is the only region to maintain large-scale positive SWE trends in the summer months.

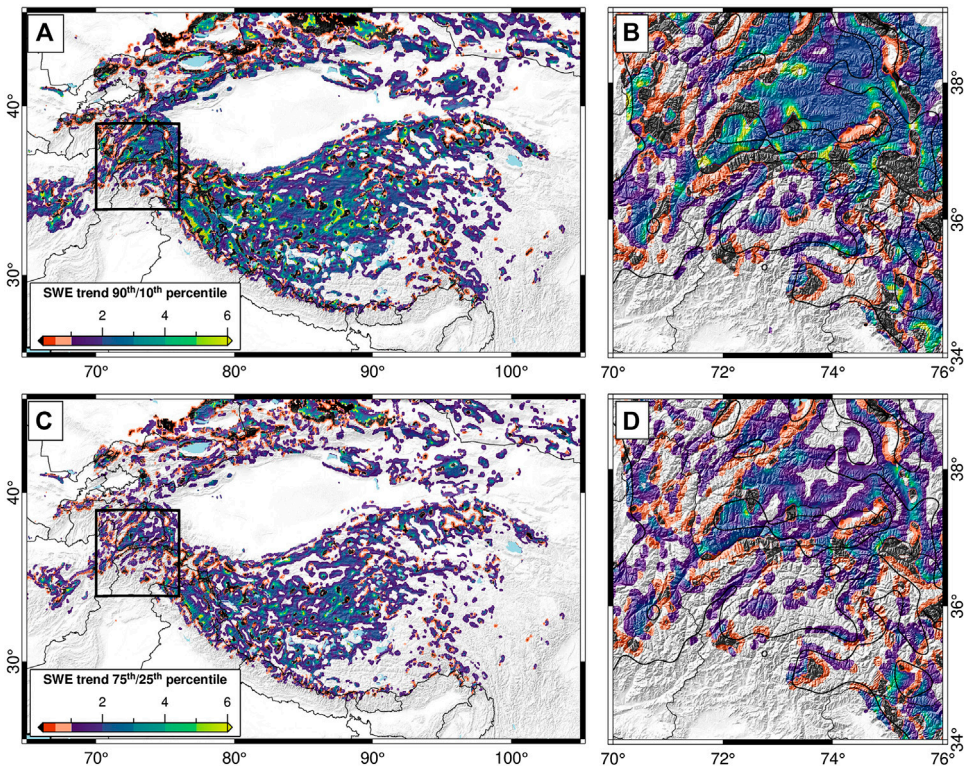

FIGURE 6 | Ratios of trends in **(A,B)** 90th/10th percentile snow-water equivalent (SWE) and **(C,D)** 75th/25th percentile SWE. Panels **(B,D)** show zoom in box over the Karakoram, with 100 mm average December-January-February SWE contour line in thick black. Positive (e.g., blue to green) values indicate that the trend in 90th (75th) percentile SWE values is larger than the trend in 10th (25th) percentile SWE values, and that both trends have the same direction. Orange and red areas have higher 10th (25th) percentile trends than 90th (75th). Black areas indicate a reversal of trend between the 90th/10th (75th/25th) percentiles. The vast majority of High Mountain Asia—in both positive and negative SWE trend areas (see **Figure 3**)—has steeper trends in high-percentile SWE than in low-percentile SWE.

Figure 3) have a more than six-fold higher trends in 90th percentile monthly SWE than in 10th percentile SWE, indicating a drastic increase in monthly high-SWE day frequency or magnitude. This could be due to the increased strength of the Winter Westerlies, which has been previously reported (Cannon et al., 2016b). In contrast, positive SWE-trend areas in the Pamir have higher 10th percentile magnitudes than 90th, indicating a that positive SWE trends are driven by increases in low-magnitude SWE rather than in high-magnitude SWE.

In the majority of HMA, however, SWE trends are negative (**Figure 3**). Thus, the high 90th/10th (75th/25th) percentile trend ratios indicate that declines in SWE have been steeper in the higher end of the monthly SWE distribution, and that high-SWE values are becoming less common overall. This agrees well with previous research, which points to overall increasing temperatures in HMA, particularly on the Tibetan Plateau (e.g., Wang et al., 2018).

4. DISCUSSION

4.1. Comparison With Previous Work

Previous work by Smith and Bookhagen (2018) used data at 0.25° × 0.25° spatial resolution from only the SSMI-series of satellites (1987–2009) to establish trends in SWE over HMA. The higher spatial resolution data used in this study yields only slight differences in SWE trend when the same period (e.g., 1987–2009) is considered. However, there are clear differences in the trends presented by Smith and Bookhagen (2018) and those shown in **Figure 3**, which are due to the difference in analysis time window. To test the sensitivity of SWE trends to the analysis window, we first break our dataset into three decade-long slices, as seen in **Figure 7**.

It is clear that SWE trends are highly variable in time. The long-term reversal from negative to positive SWE trends seen in **Figure 7**, however, is supported by analysis of other related climate variables. Previous work has noted changes in regional precipitation and temperature patterns (e.g., Archer and Fowler, 2004; Yao et al., 2012; Palazzi et al., 2013; Lutz et al., 2014; Cannon et al., 2016a, Cannon et al., 2016b; Zhang et al., 2017; Wang et al., 2018; Treichler et al., 2019; Norris et al., 2020) and increases in high-elevation snowcover (Kapnick et al., 2014; Tahir et al., 2015) in recent years. Furthermore, Treichler et al. (2019) showed that increasing lake levels on the Tibetan Plateau are strongly correlated with regions of increased precipitation; modeled precipitation data suggest stepwise increases in mean annual precipitation on the Tibetan Plateau between the ~1980s–1990s and 2000s–onwards (e.g., Kääb et al., 2018).

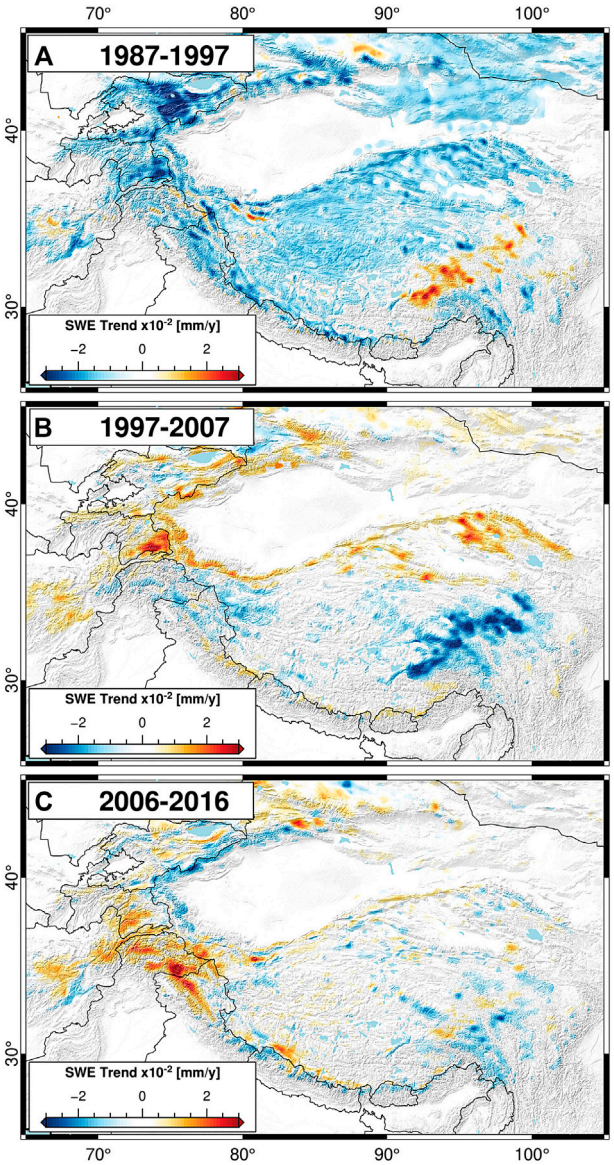

FIGURE 7 | Annual snow-water equivalent (SWE) trends from **(A)** 1987–1997, **(B)** 1997–2007, and **(C)** 2006–2016. There are stark differences in the spatial distribution of SWE trends depending on the decade chosen. In particular, the trends in the early part of the time series (1987–1997) are significantly more negative than SWE trends over the past two decades. Note that the magnitude scaling of the decadal trends is three times as large as that of the long-term annual trends (1987–2016, see **Figure 3**).

Recent analysis also indicates that the timing of the snowmelt season has changed over the past decades (Smith et al., 2017). While the long-term trends (1987–2016) were found to be generally negative (e.g., earlier and more rapid snowmelt), recent trends (e.g., 2004–2016) were found to be much more positive (later and slower onset of snowmelt) (Smith et al., 2017). It is therefore possible that there has been a reversal of the long-term losses in SWE storage in HMA; however, it is not clear if this is a temporary or long-term shift in the snow dynamics of HMA.

4.2. Sliding Window and Spatio-Temporal Trend Analysis

The timing and magnitude of SWE trend variability can be further explored by performing the same trend analysis on a set of time windows and start dates. We use time windows of 5, 10, 15, 20, 25, and 29 years, along with each possible combination of start years (e.g., 1987–2011) to examine changes in SWE trends through time (**Figure 8**).

Long-term (>25 years) SWE trends are generally negative; these trends also correspond to a particularly negative period of short-term trends starting in the late 1980s (**Figure 8**). More recent trends (e.g., 15–20 years) are generally positive starting in the early 1990s. One possible explanation for this phenomena is the previously proposed large-scale changes in regional precipitation over the past decades (e.g., Kääb et al., 2018). However, the impacts of changes in temperature cannot be ruled out—increasing regional temperatures can have highly variable positive and negative impacts on snow-water storage, for example, by enhancing atmospheric water content, snow density, and snowmelt rates.

There also exist strong regional variations in windowed trends (**Figures 8B–D**), driven by differences in climatic conditions, major weather systems, snow accumulation and ablation regimes, and dust and aerosol melt forcing between regions (Fujita, 2008; Kaspari et al., 2014; Sarangi et al., 2019). Generally positive SWE trends in the Kunlun Shan region are contrasted by mixed trends in the Karakoram, and majority negative trends in Eastern Tibet (**Figures 3** and **4**).

4.3. Relationship to Regional Glacier Changes

Many recent studies have investigated changes in HMA's glaciers using a range of satellite (Bolch et al., 2012; Kääb et al., 2012; Loomis et al., 2019; Treichler et al., 2019; Shean et al., 2020) and modeling (Kapnick et al., 2014; Rounce et al., 2019) approaches to derive spatial patterns in glacier gains and losses. Using the Randolph Glacier Inventory (Arendt et al., 2015), we can measure the areal extent of glaciers within each passive microwave pixel, and—where glaciers are large enough—derive SWE trends over only glaciated areas, defined here as areas with at least 10% glacier coverage (**Figure 9**).

In general, SWE trends over glaciated terrain are negative, outside of parts of the Tien Shan, Karakoram, and Kunlun Shan. Areas with positive SWE trends agree well with regions of positive glacier mass balance, as presented by Shean et al. (2020) and Treichler et al. (2019). While there are many factors that influence glacier dynamics, it is likely that changes in snowfall are one of the key drivers of glacier mass gain and loss over HMA (Fujita, 2008; Fujita and Nuimura, 2011; Kapnick et al., 2014).

4.4. Data Caveats

It is important to mention caveats to the trend analysis presented in this study. The largest caveat is that passive microwave SWE estimates are often uncertain—especially over large and complex regions such as HMA (Kelly, 2009; Takala et al., 2011; Smith and Bookhagen, 2016). We also cannot rule out the impacts of both

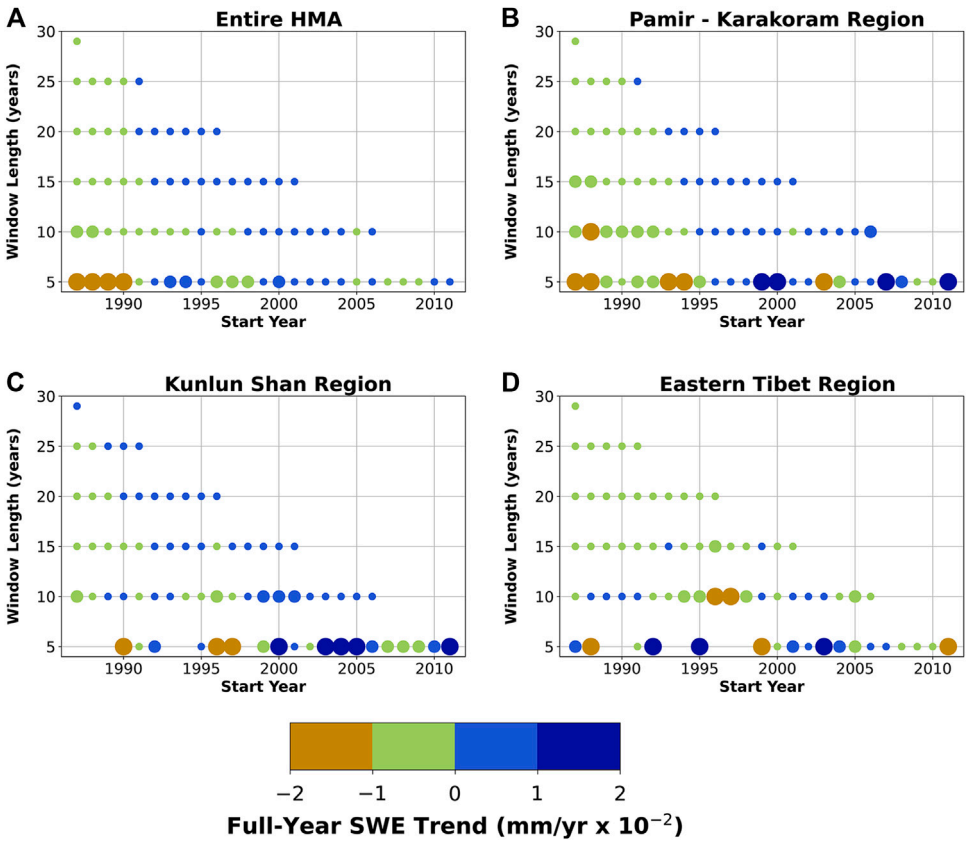

FIGURE 8 | Impact of window length on measured annual snow-water equivalent (SWE) trends. Trends calculated over **(A)** the entire study area, **(B)** the Pamir-Karakoram, **(C)** Kunlun Shan, and **(D)** Eastern Tibetan regions (see **Figures 1** and **4**). Each dot represents averaged trends over a single window size (5–29 years) and start year (1987–2011) combination. Only statistically significant trends ($p < 0.05$) are included in this analysis. Larger dots indicate positive or negative trends larger than 1×10^{-2} mm/yr, very small dots indicate trends below 0.5×10^{-2} mm/yr. SWE trend direction is highly variable over short (e.g., 5 years) time spans, but grows more stable over longer time frames. Trends starting in the 1980s are generally more negative; there is a distinct change in the early 1990s where SWE trends become generally positive.

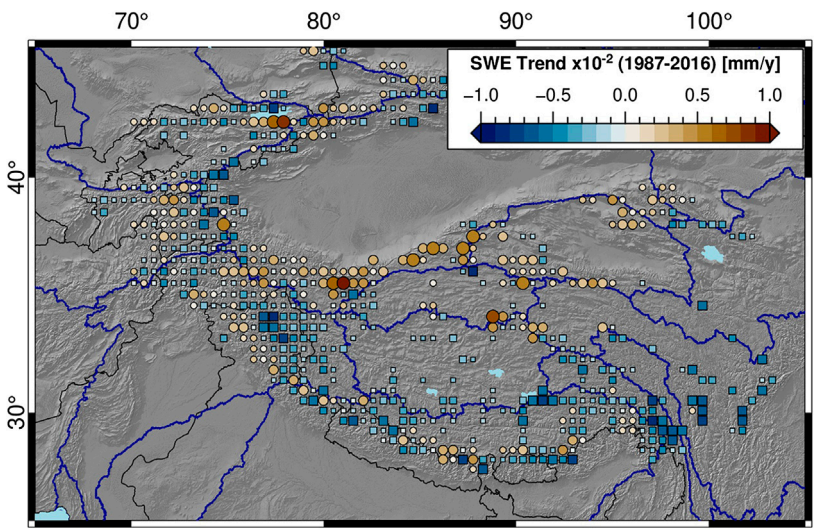

FIGURE 9 | Snow-water equivalent (SWE) trends and glacier areas aggregated into 50 km × 50 km boxes. Positive (negative) trends are symbolized as circles (squares), and sized logarithmically by total glacier area within each 50 km × 50 km aggregation window, from 1 to 1,500 km^2. Blue outlines show major watersheds (Lehner and Grill, 2013). There are clear positive SWE trends over the heavily glaciated Karakoram-Kunlun Shan region, which are contrasted by negative SWE trends throughout much of the rest of High Mountain Asia.

natural seasonality and regional temperature changes on snow densities, which could also modify passive microwave SWE estimates over the course of our time series, and thus are part of the trends that we present as changes in SWE in this study (Judson and Doesken, 2000; Chen et al., 2011; Dai et al., 2012). The impact of seasonal oscillations in snow density is somewhat mitigated by removing the seasonal cycle from our data before trend fitting, as some of the seasonality in SWE estimates will be driven by changes in snow density. However, without a more in-depth understanding of snow-density evolution in HMA, we cannot fully constrain this part of our analysis.

Passive microwave signal saturation could bias the presented SWE trends in deep-snow areas, as previous work has suggested that passive microwave SWE estimates saturate around 200 mm of SWE (Takala et al., 2011; Vander Jagt et al., 2013; Dozier et al., 2016). In examining our dataset, we find that the vast majority of HMA is not severely impacted by passive microwave signal saturation (**Figure 10**); however, it is likely that passive microwave signal saturation still biases some of our trend results. In our percentile regressions, we find that SWE trends generally maintain a consistent direction between high- and low-percentiles, indicating that saturation biases don't drastically influence SWE trend direction (**Figure 6**).

The third caveat is that trends are somewhat biased by the first and last values of the time series—this could also play a role in the trend reversals seen between previous studies of SWE trends in HMA (e.g., Smith and Bookhagen, 2018; Wang et al., 2018) and this study (**Figures 3** and **7**). We attempt to minimize this effect by using Sen's slope estimator, which is less sensitive to the first and last values of the time series (Sen, 1968). We further attempt to mitigate the impact of the time window over which the trend is calculated by using multiple overlapping time windows and window lengths (**Figure 8**). Finally, we compare our results to a percentile-regression approach and find that while the magnitudes of the trends vary between percentiles and between the de-seasoned trend and percentile approaches, the trend directions found are consistent. However, snowfall can have high inter-annual variability, and we do not preclude the possibility that variations in the timing of large snowfall events between years, or shifts in the timing of snowfall and snowmelt (Smith et al., 2017) could impact estimated annual and seasonal SWE trends.

Lastly, it is important to emphasize that the trends presented here are relative to the SWE time series as estimated, and are not calibrated by *in-situ* measurements. While the SWE algorithms used here have been extensively validated throughout the world and have been shown to be generally reliable in low-vegetation areas (Chang et al., 1982; Chang et al., 1987; Chang et al., 1991; Chang et al., 1996; Armstrong and Brodzik, 2002; Foster et al., 2005; Derksen, 2008; Kelly, 2009; Langlois et al., 2011; Dai et al., 2015; Smith and Bookhagen, 2016), the complex topography and inaccessibility of HMA poses unique challenges for *in-situ* data collection. Unfortunately, calibration data of sufficient spatial and temporal resolution to properly assess our SWE estimates and trend results is not currently available in our study region. Future work could consider other approaches to constraining the estimated SWE trends, for example, by using watershed-level snowmelt runoff measurements across HMA.

5. CONCLUSIONS

The increased fidelity and spatio-temporal resolution of newly re-processed passive microwave data allows for important updates to analyses of trends in snow-water storage over HMA. While overall trends are negative, there exist large spatial and seasonal heterogeneities in snow-water storage trends. High variability in year-to-year snowfall means that trends are strongly influenced by the start and end years of any trend analysis. By using multiple overlapping time windows, we show that while long-term snow-water storage trends are majority negative, recent (e.g., past 20 years) trends are more positive. Furthermore, by using a percentile regression approach, we show that trends in high-percentile monthly SWE are generally steeper than those in low-percentile, indicating that there have been spatially diverse changes in the magnitude distributions of SWE across HMA.

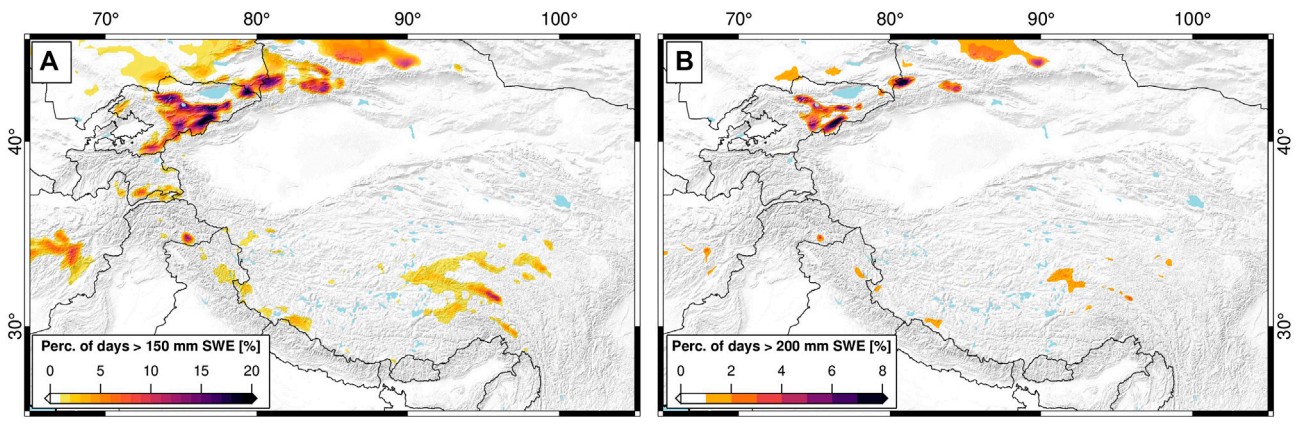

FIGURE 10 | Percentage of days with snow-water equivalent (SWE) above **(A)** 150 mm and **(B)** 200 mm (1987–2016). While some areas—particularly in the Tien Shan—are impacted by SWE signal saturation, the majority of the study area should not see large signal saturation effects. Many regions where there are saturation effects also do not yield statistically significant SWE trends, and are thus not considered in our discussion of SWE trends (see **Figure 3**).

Snow-water storage trends over glaciated regions generally align with previous estimates of glacier mass balance—those glaciers that are growing are highly correlated with regions of positive snow-water storage trends. However, snow-water storage trends are distinct between regions and watersheds, and can vary greatly over small distances. As the combined meltwaters from both snow and glaciers are essential to year-round water provision in the densely populated regions surrounding HMA, any changes in water storage must be considered in local and regional water planning. The high resolution and long time series data presented here allows for new and improved estimates of changes in snow-water storage that can be used to inform regional and local analyses of future water availability and watershed-level management plans.

DATA AVAILABILITY STATEMENT

The passive microwave and snow-cover datasets used in this study are available from the NSIDC (Brodzik et al., 2016; Hall and Riggs, 2016). Our derived SWE trends are available on Zenodo: https://zenodo.org/record/3898517 (Smith and Bookhagen, 2020).

AUTHOR CONTRIBUTIONS

TS and BB designed the study, TS prepared and analyzed all data, and BB contributed to the development of the methodology. Both authors wrote the manuscript led by TS.

FUNDING

The State of Brandenburg (Germany) through the Ministry of Science and Education and the NEXUS project supported TS for part of this study (grant to BB).

ACKNOWLEDGMENTS

We also acknowledge support from the BMBF ORYCS project.

SUPPLEMENTARY MATERIAL

The Supplementary Material for this article can be found online at: https://www.frontiersin.org/articles/10.3389/feart.2020.559175/full#supplementary-material

REFERENCES

Archer, D. R., and Fowler, H. J. (2004). Spatial and temporal variations in precipitation in the upper Indus basin, global teleconnections and hydrological implications. *Hydrol. Earth Syst. Sci.* 8 (1), 47–61. doi:10.5194/hess-8-47-2004

Arendt, A., Bolch, T., Cogley, J., Gardner, A., Hagen, J., Hock, R., et al. (2015). "Randolph glacier inventory: a dataset of global glacier outlines," in *Global land ice measurements from space*. Boulder, CO: Digital Media.

Armstrong, R. L., and Brodzik, M. J. (2002). Hemispheric-scale comparison and evaluation of passive-microwave snow algorithms. *Ann. Glaciol.* 34 (1), 38–44. doi:10.3189/172756402781817428

Barnett, T. P., Adam, J. C., and Lettenmaier, D. P. (2005). Potential impacts of a warming climate on water availability in snow-dominated regions. *Nature* 438 (7066), 303–309. doi:10.1038/nature04141

Berghuijs, W. R., Woods, R. A., and Hrachowitz, M. (2014). A precipitation shift from snow towards rain leads to a decrease in streamflow. *Nat. Clim. Change* 4 (7), 583–586. doi:10.1038/nclimate2246

Bolch, T., Kulkarni, A., Kääb, A., Huggel, C., Paul, F., Cogley, J. G., et al. (2012). The state and fate of himalayan glaciers. *Science* 336 (6079), 310–314. doi:10.1126/science.1215828

Bookhagen, B., and Burbank, D. W. (2010). Toward a complete Himalayan hydrological budget: spatiotemporal distribution of snowmelt and rainfall and their impact on river discharge. *J. Geophys. Res. Earth Surf.* 115 (F3), F03019. doi:10.1029/2009JF001426

Brodzik, M., Long, D., Hardman, M., Paget, A., and Armstrong, R. (2016). *Measures calibrated enhanced-resolution passive microwave daily EASE-grid 2.0 brightness temperature ESDR*. Boulder, CO: National Snow and Ice Data Center.

Brodzik, M. J., Billingsley, B., Haran, T., Raup, B., and Savoie, M. H. (2012). EASE-grid 2.0: incremental but significant improvements for earth-gridded data sets. *Int. J. Geoinf.* 1 (1), 32–45. doi:10.3390/ijgi1010032

Cannon, F., Carvalho, L. M. V., Jones, C., and Bookhagen, B. (2015). Multi-annual variations in winter westerly disturbance activity affecting the Himalaya. *Clim. Dyn.* 44, 441–455. doi:10.1007/s00382-014-2248-8

Cannon, F., Carvalho, L., Jones, C., Hoell, A., Norris, J., Kiladis, G., et al. (2016a). The influence of tropical forcing on extreme winter precipitation in the western Himalaya. *Clim. Dynam.* 48, 1213–1232. doi:10.1007/s00382-016-3137-0

Cannon, F., Carvalho, L. M., Jones, C., and Norris, J. (2016b). Winter westerly disturbance dynamics and precipitation in the western Himalaya and Karakoram: a wave-tracking approach. *Theor. Appl. Climatol.* 125, 27–44. doi:10.1007/s00704-015-1489-8

Chang, A. T. C., Foster, J. L., and Hall, D. K. (1987). Nimbus-7 SMMR derived global snow cover parameters. *Ann. Glaciol.* 9 (9), 39–44. doi:10.3189/s0260305500200736

Chang, A. T. C., Foster, J. L., and Hall, D. K. (1996). Effects of forest on the snow parameters derived from microwave measurements during the boreas winter field campaign. *Hydrol. Process.* 10 (12), 1565–1574. doi:10.1002/(sici)1099-1085(199612)10:12<1565::aid-hyp501>3.0.co;2-5

Chang, A. T. C., Foster, J. L., Hall, D. K, Rango, A, and Hartline, B. K. (1982). Snow water equivalent estimation by microwave radiometry. *Cold Reg. Sci. Technol.* 5 (3), 259–267. doi:10.1016/0165-232x(82)90019-2

Chang, A. T. C., Foster, J. L., and Rango, A. (1991). Utilization of surface cover composition to improve the microwave determination of snow water equivalent in a mountain basin. *Int. J. Remote Sens.* 12 (11), 2311–2319. doi:10.1080/01431169108955260

Chen, X., Wei, W., and Liu, M. (2011). Change in fresh snow density in Tianshan mountains, China. *Chin. Geogr. Sci.* 21 (1), 36–47. doi:10.1007/s11769-010-0434-0

Cleveland, R. B., Cleveland, W. S., McRae, J. E., and Terpenning, I. (1990). STL: a seasonal-trend decomposition procedure based on loess. *J. Off. Stat.* 6 (1), 3–73.

Dai, L., Che, T., and Ding, Y. (2015). Inter-calibrating SMMR, SSM/I and SSMI/S data to improve the consistency of snow-depth products in China. *Rem. Sens.* 7 (6), 7212–7230. doi:10.3390/rs70607212

Dai, L., Che, T., Wang, J., and Zhang, P. (2012). Snow depth and snow water equivalent estimation from AMSR-E data based on a priori snow characteristics in Xinjiang, China. *Remote Sens. Environ.* 127, 14–29. doi:10.1016/j.rse.2011.08.029

Derksen, C. (2008). The contribution of AMSR-E 18.7 and 10.7 GHz measurements to improved boreal forest snow water equivalent retrievals. *Remote Sens. Environ.* 112 (5), 2701–2710. doi:10.1016/j.rse.2008.01.001

Déry, S. J., and Brown, R. D. (2007). Recent northern hemisphere snow cover extent trends and implications for the snow-albedo feedback. *Geophys. Res. Lett.* 34 (22), L22504. doi:10.1029/2007gl031474

Dozier, J., Bair, E. H., and Davis, R. E. (2016). Estimating the spatial distribution of snow water equivalent in the world's mountains. *WIREs Water* 3 (3), 461–474. doi:10.1002/wat2.1140

Early, D. S., and Long, D. G. (2001). Image reconstruction and enhanced resolution imaging from irregular samples. *IEEE Trans. Geosci. Remote. Sens.* 39 (2), 291–302. doi:10.1109/36.905237

Foster, J. L., Sun, C., Walker, J. P., Kelly, R., Chang, A., Dong, J., et al. (2005). Quantifying the uncertainty in passive microwave snow water equivalent observations. *Remote Sens. Environ.* 94 (2), 187–203. doi:10.1016/j.rse.2004.09.012

Fujita, K. (2008). Effect of precipitation seasonality on climatic sensitivity of glacier mass balance. *Earth Planet. Sci. Lett.* 276 (1), 14–19. doi:10.1016/j.epsl.2008.08.028

Fujita, K., and Nuimura, T. (2011). Spatially heterogeneous wastage of Himalayan glaciers. *Proc. Natl. Acad. Sci. U.S.A.* 108 (34), 14011–14014. doi:10.1073/pnas.1106242108

Gardelle, J., Berthier, E., and Arnaud, Y. (2012). Slight mass gain of Karakoram glaciers in the early twenty-first century. *Nat. Geosci.* 5 (5), 322–325. doi:10.1038/ngeo1450

Hall, D. K., and Riggs, G. A. (2016). MODIS/terra snow cover daily L3 global 500m SIN grid, version 6. Data Set ID: MOD10A1.

Hewitt, K. (2005). The Karakoram anomaly? Glacier expansion and the 'elevation effect,' Karakoram Himalaya. *Mt. Res. Dev.* 25 (4), 332–340. doi:10.1659/0276-4741(2005)025[0332:tkagea]2.0.co;2

Huffman, G. J., Bolvin, D. T., Nelkin, E. J., Wolff, D. B., Adler, R. F., Gu, G., et al. (2007). The TRMM multisatellite precipitation analysis (TMPA): quasi-global, multiyear, combined-sensor precipitation estimates at fine scales. *J. Hydrometeorol.* 8 (1), 38–55. doi:10.1175/jhm560.1

Huss, M., Bookhagen, B., Huggel, C., Jacobsen, D., Bradley, R., Clague, J., et al. (2017). Towards mountains without permanent snow and ice. *Earth's Future* 5, 418–435. doi:10.1002/2016EF000514.

Immerzeel, W. W., van Beek, L. P. H., and Bierkens, M. F. P. (2010). Climate change will affect the Asian water towers. *Science* 328 (5984), 1382–1385. doi:10.1126/science.1183188

Judson, A., and Doesken, N. (2000). Density of freshly fallen snow in the central Rocky Mountains. *Bull. Am. Meteorol. Soc.* 81 (7), 1577–1588. doi:10.1175/1520-0477(2000)081<1577:doffsi>2.3.co;2

Kääb, A., Berthier, E., Nuth, C., Gardelle, J., and Arnaud, Y. (2012). Contrasting patterns of early twenty-first-century glacier mass change in the Himalayas. *Nature* 488 (7412), 495–498. doi:10.1038/nature11324

Kääb, A., Leinss, S., Gilbert, A., Bühler, Y., Gascoin, S., Evans, S. G., et al. (2018). Massive collapse of two glaciers in western Tibet in 2016 after surge-like instability. *Nat. Geosci.* 11 (2), 114–120. doi:10.1038/s41561-017-0039-7

Kapnick, S. B., Delworth, T. L., Ashfaq, M., Malyshev, S., and Milly, P. C. D. (2014). Snowfall less sensitive to warming in Karakoram than in Himalayas due to a unique seasonal cycle. *Nat. Geosci.* 7 (11), 834–840. doi:10.1038/ngeo2269

Kaspari, S., Painter, T. H., Gysel, M., Skiles, S. M., and Schwikowski, M. (2014). Seasonal and elevational variations of black carbon and dust in snow and ice in the Solu-Khumbu, Nepal and estimated radiative forcings. *Atmos. Chem. Phys.* 14 (15), 8089–8103. doi:10.5194/acp-14-8089-2014

Kelly, R. (2009). The AMSR-E snow depth algorithm: description and initial results. *J. Remote Sens. Soc. Jpn.* 29 (1), 307–317. doi:10.11440/rssj.29.307

Kelly, R. E., Chang, A. T., Tsang, L., and Foster, J. L. (2003). A prototype AMSR-E global snow area and snow depth algorithm. *IEEE Trans. Geosci. Remote Sens.* 41 (2), 230–242. doi:10.1109/tgrs.2003.809118

Kendall, M. G. (1948). *Rank correlation methods. Griffin.*

Kitoh, A., Endo, H., Krishna Kumar, K., Cavalcanti, I. F. A., Goswami, P., and Zhou, T. (2013). Monsoons in a changing world: a regional perspective in a global context. *J. Geophys. Res. Atmos.* 118 (8), 3053–3065. doi:10.1002/jgrd.50258

Langlois, A., Royer, A., Dupont, F., Roy, A., Goïta, K., and Picard, G. (2011). Improved corrections of forest effects on passive microwave satellite remote sensing of snow over boreal and subarctic regions. *IEEE Trans. Geosci. Remote. Sens.* 49 (10), 3824–3837. doi:10.1109/tgrs.2011.2138145

Lehner, B., and Grill, G. (2013). Global river hydrography and network routing: baseline data and new approaches to study the world's large river systems. *Hydrol. Process.* 27 (15), 2171–2186. doi:10.1002/hyp.9740

Lievens, H., Demuzere, M., Marshall, H.-P., Reichle, R. H., Brucker, L., Brangers, I., et al. (2019). Snow depth variability in the northern hemisphere mountains observed from space. *Nat. Commun.* 10 (1), 1–12. doi:10.1038/s41467-019-12566-y

Long, D. G., and Brodzik, M. J. (2016). Optimum image formation for spaceborne microwave radiometer products. *IEEE Trans. Geosci. Remote Sens.* 54 (5), 2763–2779. doi:10.1109/tgrs.2015.2505677

Loomis, B. D., Richey, A. S., Arendt, A. A., Appana, R., Deweese, Y., Forman, B. A., et al. (2019). Water storage trends in High Mountain Asia. *Front. Earth Sci.* 7, 235. doi:10.3389/feart.2019.00235

Lutz, A. F., Immerzeel, W. W., Shrestha, A. B., and Bierkens, M. F. P. (2014). Consistent increase in High Asia's runoff due to increasing glacier melt and precipitation. *Nat. Clim. Change* 4 (7), 587–592. doi:10.1038/nclimate2237

Malik, N., Bookhagen, B., and Mucha, P. J. (2016). Spatiotemporal patterns and trends of Indian monsoonal rainfall extremes. *Geophys. Res. Lett.* 43 (4), 1710–1717. doi:10.1002/2016gl067841

Mann, H. B. (1945). Nonparametric tests against trend. *Econometrica* 13, 245–259. doi:10.2307/1907187

Menon, A., Levermann, A., and Schewe, J. (2013). Enhanced future variability during India's rainy season. *Geophys. Res. Lett.* 40 (12), 3242–3247. doi:10.1002/grl.50583

Norris, J., Carvalho, L. M., Jones, C., and Cannon, F. (2020). Warming and drying over the central Himalaya caused by an amplification of local mountain circulation. *NPJ Clim. Atmos. Sci.* 3 (1), 1–11. doi:10.1038/s41612-019-0105-5

Notarnicola, C. (2020). Hotspots of snow cover changes in global mountain regions over 2000–2018. *Remote Sens. Environ.* 243 (111), 781. doi:10.1016/j.rse.2020.111781

Palazzi, E., Von Hardenberg, J., and Provenzale, A. (2013). Precipitation in the Hindu-Kush Karakoram Himalaya: observations and future scenarios. *J. Geophys. Res. Atmos.* 118 (1), 85–100. doi:10.1029/2012jd018697

Rounce, D. R., Hock, R., and Shean, D. (2019). Glacier mass change in High Mountain Asia through 2100 using the open-source python glacier evolution model (PyGEM). *Front. Earth Sci.* 7, 331. doi:10.3389/feart.2019.00331

Sakai, A., and Fujita, K. (2017). Contrasting glacier responses to recent climate change in High-Mountain Asia. *Sci. Rep.* 7 (1), 1–8. doi:10.1038/s41598-017-14256-5

Sarangi, C. N., Qian, Y., Rittger, K., Bormann, K. J., Liu, Y., Wang, H., et al. (2019). Impact of light-absorbing particles on snow albedo darkening and associated radiative forcing over High-Mountain Asia: high-resolution WRF-chem modeling and new satellite observations. *Atmos. Chem. Phys.* 19 (10), 7105–7128. doi:10.5194/acp-19-7105-2019

Scherler, D., Bookhagen, B., and Strecker, M. R. (2011). Spatially variable response of Himalayan glaciers to climate change affected by debris cover. *Nat. Geosci.* 4 (3), 156–159. doi:10.1038/ngeo1068

Sen, P. K. (1968). Estimates of the regression coefficient based on Kendall's Tau. *J. Am. Stat. Assoc.* 63 (324), 1379–1389. doi:10.1080/01621459.1968.10480934

Shean, D., Bhushan, S., Montesano, P., Rounce, D., Arendt, A., and Osmanoglu, B. (2020). A systematic, regional assessment of High Mountain Asia glacier mass balance. *Front. Earth Sci.* 7, 363. doi:10.3389/feart.2019.00363

Singh, D., Tsiang, M., Rajaratnam, B., and Diffenbaugh, N. S. (2014). Observed changes in extreme wet and dry spells during the south Asian summer monsoon season. *Nat. Clim. Change* 4 (6), 456–461. doi:10.1038/nclimate2208

Smith, T., and Bookhagen, B. (2016). Assessing uncertainty and sensor biases in passive microwave data across High Mountain Asia. *Remote Sens. Environ.* 181, 174–185. doi:10.1016/j.rse.2016.03.037

Smith, T., and Bookhagen, B. (2018). Changes in seasonal snow water equivalent distribution in High Mountain Asia (1987 to 2009). *Sci. Adv.* 4 (1), 550. doi:10.1126/sciadv.1701550

Smith, T., and Bookhagen, B. (2020). Data from: Snow variables for High Mountain Asia. doi:10.5281/zenodo.3898517

Smith, T., Bookhagen, B., and Rheinwalt, A. (2017). Spatiotemporal patterns of High Mountain Asia's snowmelt season identified with an automated snowmelt detection algorithm, 1987–2016. *Cryosphere* 11 (5), 2329–2343. doi:10.5194/tc-11-2329-2017

Sorg, A., Bolch, T., Stoffel, M., Solomina, O., and Beniston, M. (2012). Climate change impacts on glaciers and runoff in Tien Shan (Central Asia). *Nat. Clim. Change* 2 (10), 725–731. doi:10.1038/nclimate1592

Sturm, M., Taras, B., Liston, G. E., Derksen, C., Jonas, T., and Lea, J. (2010). Estimating snow water equivalent using snow depth data and climate classes. *J. Hydrometeorol.* 11 (6), 1380–1394. doi:10.1175/2010jhm1202.1

Tahir, A. A., Chevallier, P., Arnaud, Y., Ashraf, M., and Bhatti, M. T. (2015). Snow cover trend and hydrological characteristics of the Astore River basin (western

Himalayas) and its comparison to the Hunza basin (Karakoram region). *Sci. Total Environ.* 505, 748–761.doi:10.1016/j.scitotenv.2014.10.065

Takala, M., Luojus, K., Pulliainen, J., Derksen, C., Lemmetyinen, J., Kärnä, J. P., et al. (2011). Estimating northern hemisphere snow water equivalent for climate research through assimilation of space-borne radiometer data and ground-based measurements. *Remote Sens. Environ.* 115 (12), 3517–3529. doi:10.1016/j.rse.2011.08.014

Treichler, D., Kääb, A., Salzmann, N., and Xu, C. Y. (2019). Recent glacier and lake changes in High Mountain Asia and their relation to precipitation changes. *Cryosphere* 13 (11), 2977–3005. doi:10.5194/tc-13-2977-2019

Vander Jagt, B. J., Margulis, S. A., Kim, E. J., Molotch, N. P., and Molotch, N. P. (2013). The effect of spatial variability on the sensitivity of passive microwave measurements to snow water equivalent. *Remote Sens. Environ.* 136, 163–179. doi:10.1016/j.rse.2013.05.002

Vaughan, D. G., Comiso, J. C., Allison, I., Carrasco, J., Kaser, G., Kwok, R., et al. (2013). "Observations: cryosphere," in *Climate change 2013: the physical science basis. Contribution of Working Group I to the Fifth Assessment Report of the Intergovernmental Panel on Climate Change.* Editors T. F. Stocker, D. Qin, G.-K. Plattner, M. Tignor, S. K. Allen, J. Boschung, A. Nauels, Y. Xia, V. Bex and P.M. Midgley (Cambridge, United Kingdom and New York, NY, USA: Cambridge University Press). Contribution of working group I to the fifth assessment report of the IPCC.

Wang, Z., Wu, R., and Huang, G. (2018). Low-frequency snow changes over the Tibetan plateau. *Int. J. Climatol.* 38 (2), 949–963. doi:10.1002/joc.5221

Wulf, H., Bookhagen, B., and Scherler, D. (2016). Differentiating between rain, snow, and glacier contributions to river discharge in the western Himalaya using remote-sensing data and distributed hydrological modeling. *Adv. Water Resour.* 88, 152–169. doi:10.1016/j.advwatres.2015.12.004

Yao, T., Thompson, L., Yang, W., Yu, W., Gao, Y., Guo, X., et al. (2012). Different glacier status with atmospheric circulations in Tibetan plateau and surroundings. *Nat. Clim. Change* 2 (9), 663–667. doi:10.1038/nclimate1580

Zhang, C., Tang, Q., and Chen, D. (2017). Recent changes in the moisture source of precipitation over the Tibetan plateau. *J. Clim.* 30 (5), 1807–1819. doi:10.1175/jcli-d-15-0842.1

Zhao, H., and Moore, G. (2004). On the relationship between Tibetan snow cover, the Tibetan plateau monsoon and the Indian summer monsoon. *Geophys. Res. Lett.* 31 (14), L14204. doi:10.1029/2004gl020040

Conflict of Interest: The authors declare that the research was conducted in the absence of any commercial or financial relationships that could be construed as a potential conflict of interest.

frontiers in Earth Science

REVIEW
published: 04 December 2020
doi: 10.3389/feart.2020.560403

Progress and Challenges in Studying Regional Permafrost in the Tibetan Plateau Using Satellite Remote Sensing and Models

Huiru Jiang[1,2], Guanheng Zheng[3], Yonghong Yi[4,5], Deliang Chen[1], Wenjiang Zhang[2], Kun Yang[6] and Charles E. Miller[4]*

[1]Regional Climate Group, Department of Earth Sciences, University of Gothenburg, Gothenburg, Sweden, [2]State Key Laboratory of Hydraulics and Mountain River, Sichuan University, Chengdu, China, [3]State Key Laboratory of Hydroscience and Engineering, Department of Hydraulic Engineering, Tsinghua University, Beijing, China, [4]Jet Propulsion Laboratory, California Institute of Technology, Pasadena, CA, United States, [5]Joint Institute for Regional Earth System Science and Engineering, University of California, Los Angeles, CA, United States, [6]Department of Earth System Science, Tsinghua University, Beijing, China

OPEN ACCESS

Edited by:
Tobias Conradt, Potsdam Institute for Climate Impact Research (PIK), Germany

Reviewed by:
Dongliang Luo, Chinese Academy of Sciences (CAS), China
Guo Donglin, Institute of Atmospheric Physics (CAS), China
Rinat Manasypov, Tomsk State University, Russia
Susan Hubbard, Lawrence Berkeley National Laboratory, United States

***Correspondence:**
Yonghong Yi
yonghong.yi@jpl.nasa.gov

Specialty section:
This article was submitted to Cryospheric Sciences, a section of the journal Frontiers in Earth Science

Received: *08 May 2020*
Accepted: *28 October 2020*
Published: *04 December 2020*

Citation:
Jiang H, Zheng G, Yi Y, Chen D, Zhang W, Yang K and Miller CE (2020) Progress and Challenges in Studying Regional Permafrost in the Tibetan Plateau Using Satellite Remote Sensing and Models. Front. Earth Sci. 8:560403. doi: 10.3389/feart.2020.560403

Recent climate change has induced widespread soil thawing and permafrost degradation in the Tibetan Plateau. Significant advances have been made in better characterizing Tibetan Plateau soil freeze/thaw dynamics, and their interaction with local-scale ecohydrological processes. However, factors such as sparse networks of *in-situ* sites and short observational period still limit our understanding of the Tibetan Plateau permafrost. Satellite-based optical and infrared remote sensing can provide information on land surface conditions at high spatial resolution, allowing for better representation of spatial heterogeneity in the Tibetan Plateau and further infer the related permafrost states. Being able to operate at "all-weather" conditions, microwave remote sensing has been widely used to retrieve surface soil moisture, freeze/thaw state, and surface deformation, that are critical to understand the Tibetan Plateau permafrost state and changes. However, coarse resolution (>10 km) of current passive microwave sensors can add large uncertainties to the above retrievals in the Tibetan Plateau area with high topographic relief. In addition, current microwave remote sensing methods are limited to detections in the upper soil layer within a few centimetres. On the other hand, algorithms that can link surface properties and soil freeze/thaw indices to permafrost properties at regional scale still need improvements. For example, most methods using InSAR (interferometric synthetic aperture radar) derived surface deformation to estimate active layer thickness either ignore the effects of vertical variability of soil water content and soil properties, or use site-specific soil moisture profiles. This can introduce non-negligible errors when upscaled to the broader Tibetan Plateau area. Integrating satellite remote sensing retrievals with process models will allow for more accurate representation of Tibetan Plateau permafrost conditions. However, such applications are still limiting due to a number of factors, including large uncertainties in current satellite products in the Tibetan Plateau area, and mismatch between model input data needs and information provided by current satellite sensors. Novel approaches to combine diverse datasets with models through model initialization, parameterization and data assimilation are needed to address the

above challenges. Finally, we call for expansion of local-scale observational network, to obtain more information on deep soil temperature and moisture, soil organic carbon content, and ground ice content.

Keywords: process models, satellite remote sensing, freeze/thaw, permafrost, Tibetan plateau

INTRODUCTION

The Tibetan Plateau has an average elevation of 4,000 m and encompasses an area of approximately 2.5×10^6 km^2 (**Figure 1**). It is the home to ~100,000 km^2 of glaciers (Yao et al., 2012) and possesses the largest alpine permafrost area in the world (Ran et al., 2018; Cheng et al., 2019). The Tibetan Plateau is also the headwater of many major Asian rivers including the Yangtze, Yellow, Mekong, Indus, and Ganges (Immerzeel et al., 2010). Due to its vast domain and high elevation, the Tibetan Plateau is extremely sensitive to climate change and has a profound influence on the regional climate (Duan and Wu, 2005).

Long-term *in-situ* surface meteorology measurements show that the Tibetan Plateau has been experiencing a significant warming trend since 1960s, with an average rate of 0.3–0.4°C per decade, which exceeds the global average during the same period (Chen et al., 2015a). Previous studies further indicated such warming trend is elevation-dependent. Specifically, the warming rate increases with elevation for lower altitude regions (<~4,500–5,000 m) and this phenomenon is more obvious during autumn and winter (Yan and Liu, 2014), while this warming trend is absent or lower at higher elevations (>~5,000 m) based on satellite-based temperature datasets (Guo et al., 2019; Pepin et al., 2019). Other changes include slight increases in precipitation, wind speed weakening, solar radiation declining and mixed trends of relative humidity (Yang et al., 2014; Bibi et al., 2018). These changes can have significant impact on regional water and energy balance, and cause non-negligible changes in the cryosphere, including glacier retreat, soil warming and permafrost degradation.

Frozen ground occupies the most area of the Tibetan Plateau (**Figure 1**), with approximately 40% coverage of permafrost and 55% coverage of seasonally frozen ground (Zou et al., 2017). Since the 1970s, several *in-situ* observation networks have been established to monitor the thermal state of Tibetan Plateau frozen ground (Yang et al., 2010). These *in-situ* soil temperature records have demonstrated substantial changes occurred in Tibetan Plateau frozen ground including permafrost degradation over the past few decades. For example, the *in-situ* observations in the Beiluhe region indicated that the active layer thickness has increased at a rate of ~4.26 cm yr^{-1} from 2002 to 2012 while the permafrost

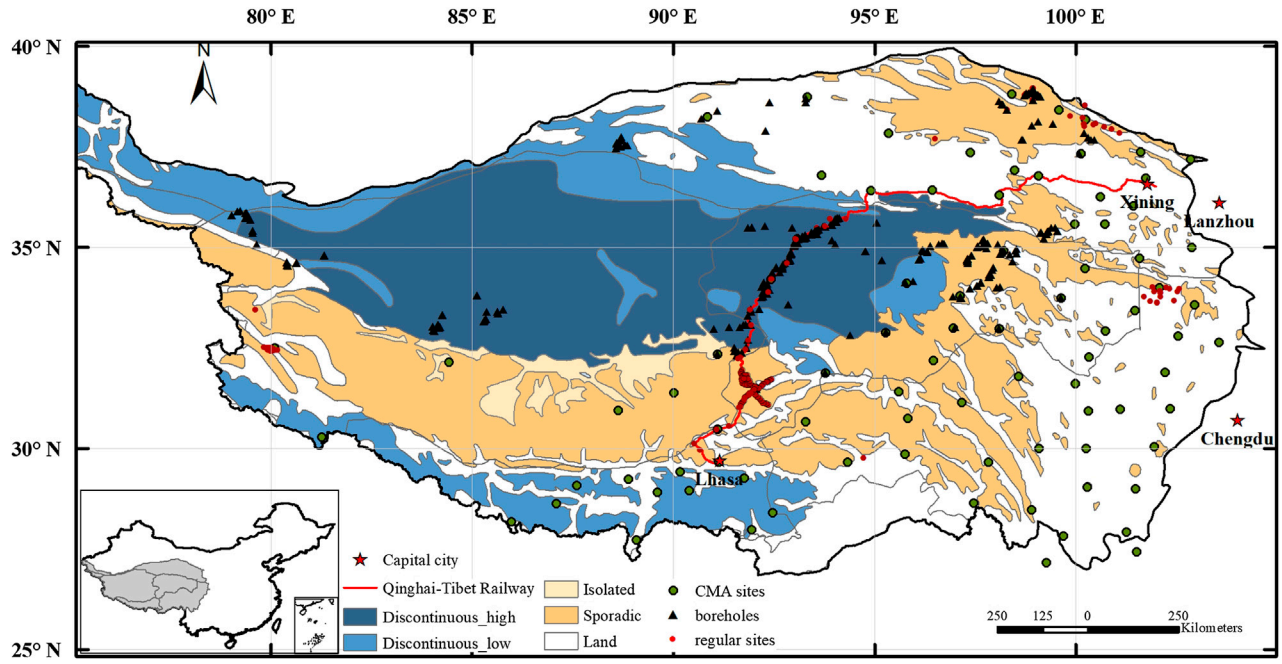

FIGURE 1 | The distribution of permafrost and *in-situ* observations over the Tibetan Plateau region. The permafrost classification is based on the international permafrost association permafrost map (Brown et al., 1997), and the "high" and "low" in the legend refer to the ice content of permafrost. Green dots represent meteorological stations from China Meteorological Administration, black triangles refer to the borehole sites with deeper soil temperature measurements from previous studies (Wu and Zhang, 2008; Luo et al., 2012; Cao et al., 2019), and red dots are regular observation sites with soil temperature observations within a depth of a few meters (data source including Yang et al., 2013a; Cao et al., 2019; Zheng et al., 2020).

temperatures at 10 m depth have increased by ~0.14°C during the same period (Wu et al., 2015). In the inner Tibetan plateau, maximum frozen depth decreased at a rate of 0.71 cm yr^{-1} during the period 1967–1997 (Zhao et al., 2004), and reduction in the maximum frozen depth has accelerated since 2000 (Peng et al., 2017). Previous study also revealed that a distinct talik layer separating the permafrost from overlying active layer has already formed along the Qinghai-Tibet Highway (Jin et al., 2008).

Previous studies based on the *in-situ* observations provided detailed assessments of *permafrost thermal state at local scales*. However, extrapolating site-level observations across the Tibetan Plateau is likely to entail large uncertainties, due to the sparse *in-situ* stations, shallow observation depth at most sites, inconsistency in the measurement methods and data gaps. Most *in-situ* observations and boreholes (up to 10 m) were established along the Qinghai-Tibet Railway/Highway to meet the engineering demand (Wu and Zhang, 2008; Jin et al., 2011; Wu et al., 2020), while most of the meteorological stations from China Meteorological Administration are located in the seasonally frozen ground of the central or eastern Tibetan Plateau (**Figure 1**).There are limited *in-situ* observations in the western Tibetan Plateau, with only a few boreholes located in A-erh-chin Mountain, Gaize and west Kunlun (Zou et al., 2017). The limited number of *in-situ* sites poses great challenges for a comprehensive, regional-scale assessment of the Tibetan Plateau permafrost thermal state. For example, there are large discrepancies among the current Tibetan Plateau permafrost coverage maps (Zou et al., 2017; Wu et al., 2018; Zheng et al., 2020), and it is difficult to accurately evaluate these maps due to the different compilation approaches and insufficient *in-situ* observations (Cao et al., 2019).

Satellite or airborne remote sensing can provide information on environmental conditions and freeze/thaw state related to underlying permafrost properties with improved sensitivity to subsurface soil properties (Jorgenson and Grosse, 2016), which can provide critical constraints on assessing regional permafrost vulnerability. With a wide range of satellite and airborne observations available from existing and upcoming missions, remote sensing data are increasingly becoming an essential element for regional permafrost monitoring (NRC, 2014). However, current satellite remote sensing systems cannot provide information on deeper (>~10 cm) soils; therefore, an integration of remote sensing data with process-based models are needed to obtain information on permafrost properties and dynamics. This review summarizes recent progress and challenges using multi-source satellite remote sensing data and process-based models to improve regional permafrost monitoring across Tibetan Plateau. Airborne remote sensing also plays an important role in regional permafrost studies (Miller et al., 2019). For example, the airborne electromagnetic method has shown a great potential in mapping Alaskan permafrost (Minsley et al., 2012; Rey et al., 2019). However, there is very limited airborne experiment in the Tibetan Plateau; therefore, we only briefly discuss its application in regional permafrost studies, which mainly occur in other permafrost areas (*Discussion*).

The paper is structured as follows: we first discuss the unique characteristics of Tibetan Plateau permafrost environment (*Environmental Controls on Tibetan Plateau Permafrost Distribution and Soil Freeze/Thaw Dynamics*), and then summarize the recent advances in regional Tibetan Plateau permafrost studies using various remote sensing technologies, and through combination of remote sensing with modeling approaches (*Regional Monitoring Approaches and Associated Challenges*). We also discuss the unique challenges in Tibetan Plateau permafrost monitoring, the potential of geophysical measurements and other methods to characterize subsurface variability and spatial heterogeneity in permafrost areas (*Discussion*). We conclude by addressing research priorities and future studies needed to accurately simulate the evolution of Tibetan Plateau permafrost and eco-hydrology (*Research Priorities and Recommendations*).

Environmental Controls on Tibetan Plateau Permafrost Distribution and Soil Freeze/Thaw Dynamics

The Tibetan Plateau is characterized by relatively thin and warm permafrost with low ice content, potentially more vulnerable to ongoing and future warming due to the unique environmental conditions, arid climate, high elevation and steep geothermal gradient (Wang and French, 1995; Yang et al., 2010; Zhao et al., 2010; Cheng et al., 2019; Zhao et al., 2020). Therefore, an improved understanding of permafrost sensitivity to environmental conditions in the Tibetan Plateau region is essential for effectively monitoring potential changes and vulnerability of Tibetan Plateau permafrost (**Figure 2**).

Permafrost distribution in the Tibetan Plateau is controlled by the high elevation and complex topography, and has characteristics different from permafrost in other regions (Wang and French, 1995). Topographic factors such as elevation affect regional climate through the effects on precipitation, temperature lapse rates and solar radiation loading (Gruber et al., 2017). Therefore, topography can affect soil freeze/thaw dynamics by altering the land surface temperature and the surface energy budget. Field investigations show that the lower limit of permafrost in the Yellow River region is ~4,400 a.s.l., while seasonally frozen ground occurs at lower elevations such as major river valleys (Luo et al., 2012). Other topographic factors, such as aspect and slope, also influence permafrost distribution. Due to different solar radiation loading on different slope and aspect, the lower limit of Tibetan Plateau permafrost on the north slope is usually lower than that on the south slope with more sunny conditions (Cheng and Wu, 2007). *In-situ* data from the central Tibetan Plateau show that the average frost depth was much deeper on north facing slopes than on south facing slopes, and varied considerably with elevation on both slopes (Ma et al., 2015).

Soil conditions also have a significant influence on permafrost thermal state. Soil texture is one of the major factors determining soil thermal conductivity, heat capacity, and hydraulic conductivity (Chen et al., 2012; Yi et al., 2018a). For example, gravel soils have a larger thermal conductivity and can result in a

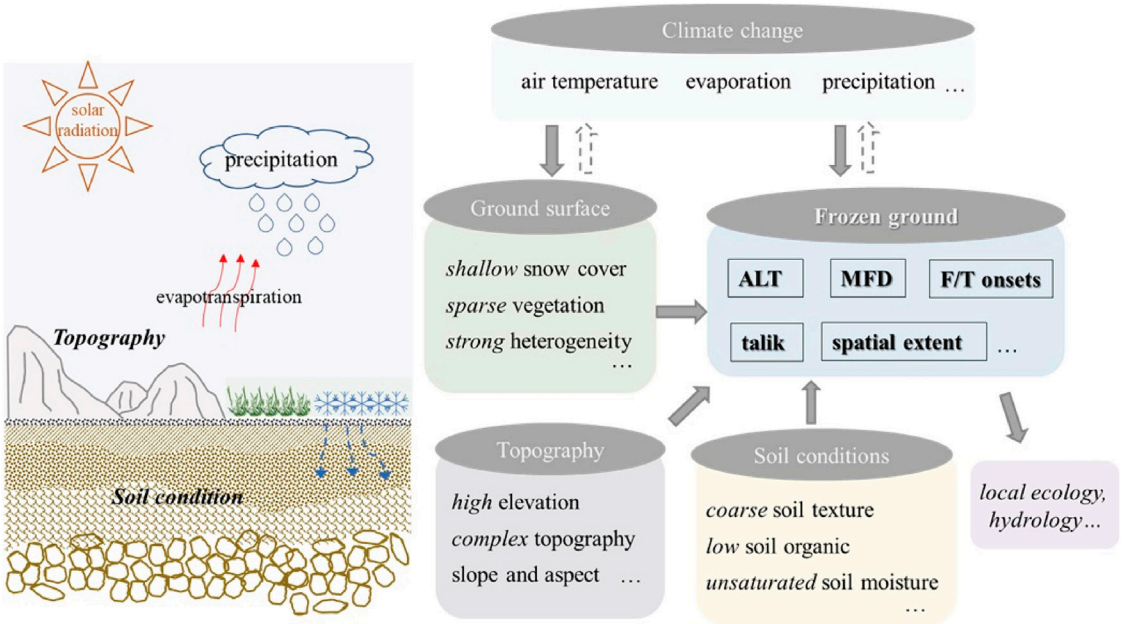

FIGURE 2 | Interaction among different environmental factors and soil freeze/thaw (F/T) dynamics in the Tibetan Plateau region. Solid and dash arrows indicate the influences and feedbacks respectively. ALT and MFD represent active layer thickness (defined for permafrost area) and maximum frozen depth (defined for seasonally frozen ground) respectively.

rapid response of soil temperatures to climate change. The existence of gravels also tends to reduce the soil water holding capacity and enhance hydraulic conductivity and drainage (Pan et al., 2017). As the consequence of slow soil-forming processes and strong erosion, gravel soils are widespread in the Tibetan Plateau and has distinct physical properties from agricultural soils (Arocena et al., 2012; Yi et al., 2018a). In addition, given that bedrock has quite different hydrological and thermal properties from upper soil layers, soil depth (or the depth to bedrock) also has significant influence on soil freeze/thaw dynamics especially for deep soils. Soil moisture content also affects the soil freeze/thaw processes through soil water phase change and changing physical properties such as soil thermal and hydraulic conductivity (Scherler et al., 2010). Higher soil moisture content is generally associated with a longer zero-curtain period, and thus delay soil freeze/thaw onsets (Luo et al., 2014; Jiang et al., 2018). Tibetan Plateau soils are usually unsaturated and soil moisture shows a strong heterogeneity both vertically and spatially (Yang et al., 2013a), and how it affects the Tibetan Plateau soil freeze/thaw dynamics and permafrost changes remains under investigated (Yang et al., 2010). Moreover, although soil organic content in the Tibetan Plateau is relatively low compared with the northern high-latitude region, it can strongly influence soil thermal conditions due to its correlation with soil properties such as high soil porosity and high soil moisture content (Chen et al., 2012; Zhou et al., 2013).

In addition, surface conditions, such as vegetation cover and snow cover, act as important environmental controls on soil freeze/thaw dynamics and permafrost distribution. Vegetation cover affects the partition among the sensible, latent and soil heat fluxes, and therefore plays an important role in surface water and energy balances (Li et al., 2015a). Although most Tibetan Plateau permafrost region is dominated by alpine meadows or grasslands with sparse vegetation, Wang et al. (2012a) still found that decrease of alpine meadow and alpine swamps in the Tibetan Plateau were related to the increasing sensitivity of soil to climate changes and the greater shifts in soil temperature and water dynamics. Furthermore, different types of vegetation cover may exert different impacts on soil thawing (Wang et al., 2012b). Winter snow cover also has an important effect on soil freeze/thaw dynamics and permafrost temperature (Zhang, 2005; Yi et al., 2015). Snow cover plays an important role in determining how soil responds to surface warming due to its strong insulation effects and impact on surface energy balance associated with changes in surface albedo and snow water phase change (Zhang, 2005). Different from the overall thicker snow cover in the northern high latitude region, snow in the Tibetan Plateau often melts quickly due to strong solar radiation, and snow cover is generally shallow and ephemeral, with overall low albedo of fresh snow and limited insulation effects (Wang et al., 2020; Zheng et al., 2020). Therefore, snow cover in the Tibetan Plateau may have a cooling effect on underlying soil temperature due to the dissipated latent heat resulted from frequent snow melting or sublimation (Zhu et al., 2017). Moreover, snow meltwater that infiltrates into the soil could result in additional soil temperature fluctuations due to soil heat transport through convection and soil water phase change (Scherler et al., 2010; Luo et al., 2014).

REGIONAL MONITORING APPROACHES AND ASSOCIATED CHALLENGES

Remote Sensing of Tibetan Plateau Permafrost

Current Progress

The sparse distribution of *in-situ* observation sites over the Tibetan Plateau (**Figure 1**) highlights the potential of satellite remote sensing to significantly improve regional permafrost monitoring across Tibetan Plateau. Remote sensing technology, including optical, near- and thermal-infrared, passive and active microwave remote sensing, has been used to directly or indirectly monitor the near-surface soil freeze/thaw and permafrost state in the Tibetan Plateau. The wavelength ranges from 0.4–0.7, 0.7–3.0, and 3.0–100 μm for optical, near- and thermal-infrared remote sensing, respectively; microwave remote sensing covers the spectrum from 1 mm to ~1 m in wavelength and has a much deeper penetration depth (Ulaby et al., 1982). Optical and near-infrared remote sensing are often used to detect the vegetation canopy and land surface properties, while microwave sensors can provide information on land surface moisture and temperature variations due to strong sensitivity to changes in land surface dielectric properties and emissivity. The applications of remote sensing in permafrost can be largely grouped into two categories: 1) identifying and mapping surface features and objects typical for permafrost areas; and 2) retrieving physical variables directly or indirectly relevant to subsurface thermal conditions (Tedesco, 2014). The first category was dominated by the application of high spatial-resolution optical and near-infrared images, while the second category covers a wider range of remote sensing systems from optical to microwave sensors as discussed below.

Permafrost Monitoring Using Optical and Infrared Remote Sensing

Optical and near-infrared remote sensing with high spatial resolutions (<100 m) has been widely used to identify geological structures and landscapes associated with permafrost, e.g., hummock, thermokarst lakes, freeze/thaw boils, and surface classification, which can be used to infer the presence of underlying permafrost (Panda et al., 2010; Wang et al., 2014; Niu et al., 2018; Ran et al., 2018; Huang et al., 2020). Data from some high-resolution satellites such as Landsat-8 and GaoFen-1, 2, can be used to extract the landscape features and structures (Niu et al., 2018). This is especially useful for permafrost research in mountain regions characterized by heterogeneous surface condition like Tibetan Plateau. On the other hand, optical and near-infrared remote sensing can also provide information on land surface variables that can be used as auxiliary data to empirical or process-based models to infer the permafrost thermal state (Wang et al., 2014; Dai et al., 2018; Ran et al., 2018). For example, regional snow cover extent, surface albedo and vegetation cover products, which are available from optical sensors such as MODIS (250-m resolution), Landsat (30-m resolution), and Sentinel-2 (20-m resolution), have been used as model ancillary inputs to simulate the permafrost thermal state due to significant influences of vegetation and snow cover on surface energy and water balance (Niu et al., 2018; Zheng et al., 2019b). In addition, many thermal infrared satellite systems (e.g.,, Terra, Aqua, and geostationary platforms like GOES and METEOSAT) could monitor the land surface temperature at spatial resolutions of 1–50 km, which is more directly linked to the subsurface ground thermal state (Holmes et al., 2009). Optical and thermal infrared remote sensing can provide information at high spatial resolution; however, it should be noted that factors such as frequent clouds and mixing pixels will introduce large uncertainties to these land surface products, and affect their application in permafrost studies (Kou et al., 2017).

Optical and thermal infrared imaging methods provide valuable regional datasets; however, permafrost is essentially a subsurface phenomenon and these methods are limited to imaging the land surface. Permafrost monitoring requires knowledge of soil temperature and heat transfer at deep layers; therefore, statistical or empirical models have been developed to utilize surface parameters derived from optical and infrared remote sensing to map permafrost extent and distribution (Zou et al., 2017; Aalto et al., 2018; Obu et al., 2019). Statistical models, e.g., decision tree or logistic regression models, have been applied to Tibetan Plateau permafrost mapping through building relationship between permafrost indices and multiple environmental factors including satellite-based land surface temperature and snow cover extent products. More recent studies are also developed using deep learning methods to create Tibetan Plateau permafrost maps (Wang et al., 2019a; Huang et al., 2020). Empirical models such as the TTOP (temperature at the top of permafrost) model and Kudryavtsev model that are derived from simplified heat transfer equations and require fewer inputs have been also widely used in Tibetan Plateau permafrost mapping (Zhao et al., 2017a; Zou et al., 2017).

Permafrost Monitoring Using Microwave Remote Sensing

Microwave remote sensing shows strong sensitivity to soil dielectric changes induced by landscape and particularly soil freeze/thaw state, and can operate under all-weather conditions (Ulaby et al., 2014); therefore, it has been widely used to map surface soil freeze/thaw status and permafrost changes in both high latitude and high elevation regions (e.g.,, Li et al., 2012a; Li et al., 2013; Park et al., 2016).

Brightness temperature (Tb) measured by passive microwave remote sensing is associated with changes in surface emissivity and temperature conditions, both of which are closely associated with soil freeze/thaw status. Depending on the frequency and its penetration ability, relatively higher frequency (e.g., Ka-band, ~27–40 GHz) is commonly used to detect the freeze/thaw state of landscape surface elements, while lower frequencies such as L-band (~1–2 GHz) and P-band (~250–500 MHz) provide enhanced sensitivity to soil surface and profile freeze/thaw conditions (Du et al., 2015; Naderpour and Schwank, 2018). The Tb at Ka-band shows less sensitivity to freeze/thaw induced changes in surface emissivity, and is more correlated with land surface temperature especially for the vertical polarization (Holmes et al., 2009). A negative spectral gradient between 18 and 37 GHz was also found for the frozen soils due to volume

scatter darkening within the frozen soil (Zuerndorfer and England, 1992). Therefore, a combination of low Tb37V (37 GHz Tb at vertical polarization) and negative 18–37 GHz spectral gradient values has been widely used in frozen soil classification (Zhao et al., 2011; Han et al., 2015). Surface conditions such as dry snow may confound the soil freeze/thaw classification, and a number of groups have explored combining different indices to identify different surface conditions. For example, Jin et al. (2009) developed a decision tree algorithm to classify surface soil freeze/thaw state, through incorporating Tb37V, polarization Tb difference at 19 GHz, and a scattering index to distinguish scattering and non-scattering surfaces. Zhao et al. (2011) developed a discriminant algorithm that employs the Tb37V and the quasi-emissivity of Tb18.7H based on model simulations and Fisher linear discrimination analysis of different surface ground conditions. More recent studies also explored the values of L-band Tb in soil freeze/thaw classifications due to its deeper penetration depth (~50 and ~5 cm for the frozen and thaw soils, respectively) (Rautiainen et al., 2016; Zheng et al., 2019a).

Despite with high revisit frequency (less than a few days), current passive microwave sensors have the spatial resolutions on the order of 10–50 km, which can add large uncertainties to freeze/thaw classifications in an area with high topographic relief like the Tibetan Plateau (Li et al., 2013). Alternatively, space-borne synthetic aperture radar (SAR) sensors provide measurements of radar backscatter at much finer scales (~10–100 m) but have a much longer temporal revisit (>10 days). SAR signals share similar frequency-dependent responses to vegetation canopy and surface soil dielectric changes as microwave emission techniques, and radar backscatter at different frequencies (eg C-band, ~4–8 GHz; Ku-band, ~12–18 GHz) can be potentially used to characterize surface freeze/thaw and soil moisture status in the Tibetan Plateau (Van der Velde and Su, 2009; Han et al., 2011). The integration of active and passive microwave remote sensing provides a promising way to monitor surface and soil freeze/thaw and soil moisture states of Tibetan Plateau permafrost, leveraging the strengths of each method (Dente et al., 2014). A few studies also explored the value of combining passive microwave remote sensing and MODIS land surface temperature for high-resolution freeze/thaw mapping in the Tibetan Plateau (Zhao et al., 2017b; Kou et al., 2017).

More recently, interferometric synthetic aperture radar (InSAR) has shown great potential for regional mapping of active layer thickness. InSAR works by detecting surface deformation resulting from soil freezing induced uplift and thawing induced subsidence through measuring the phase shifts between repeat pass SAR images acquired at different times (Liu et al., 2012; Li et al., 2015b; Daout et al., 2017; Jia et al., 2017; Wang et al., 2018). It should be noted that this technique requires repeat passes to be obtained with less than 5 m deviation to enable accurate interferograms and phase shifts to be produced. Different techniques have been developed to generate interferograms and reconstruct the long-term series and seasonal trends in the surface deformation, which are linked with the long-term permafrost thaw and seasonal active layer thawing rate, respectively. Empirical approaches have been used to convert the surface deformation to active layer thickness assuming a uniform soil saturation profile (e.g.,, Liu et al., 2012; Jia et al., 2017). A more recent study accounts for *the soil saturation differences* among different land cover types in the Tibetan Plateau (Wang et al., 2018), which results in different response curves of surface deformation to thaw depth. Li et al. (2015b) developed a new approach that uses the time lag between the periodic features of InSAR-observed surface deformation and land surface temperature to estimate the time interval between maximum surface air temperature and maximum seasonal thaw depth.

Challenges

Currently, there are no direct remote sensing methods to detect deeper soil freeze/thaw and thermal conditions. Most satellite detection of soil freeze/thaw is generally limited to upper soil layer within a few centimeters of the surface. A potential approach to overcome this limitation is to introduce lower frequency sensors such as P-band SAR for soil profile characterization (Chen et al., 2019) and incorporate multi-frequency microwave observations such as joint L- and P-band SAR for enhanced delineations of soil profile freeze/thaw characteristics (Du et al., 2015). On the other hand, algorithms that can link surface properties and soil freeze/thaw indices to permafrost properties still need improvements. For example, most methods using InSAR derived surface deformation to estimate active layer thickness either ignore the effects of vertical variability of soil water content and soil properties (Liu et al., 2012; Li et al., 2015b; Jia et al., 2017), or use site-specific soil moisture profiles (Wang et al., 2018). This can introduce non-negligible errors when upscaled to the broader Tibetan Plateau, which is characterized by strong heterogeneous soil conditions, deep active layer and more variable soil moisture profiles. A drier surface layer can result in a delayed thawing subsidence period, comparing with the Arctic permafrost region (Daout et al., 2017). In addition, prior knowledge of ground ice content is important to interpret the long-term trend of surface deformation, but such information is still lacking at regional scale in the Tibetan Plateau.

Current satellite sensors still cannot provide measurements with sufficient spatial and temporal resolution to meet requirements for regional soil freeze/thaw and permafrost monitoring in the Tibetan Plateau. Satellite passive microwave remote sensing measurements are available at 10–50 km resolutions, which may not accurately represent the surface and subsurface conditions for each resolution element, especially in the heterogeneous mountain regions (Li et al., 2014). In addition, ambiguity often exists in the remote sensing retrievals using a single frequency due to its sensitivity to multiple land surface properties. More comprehensive evaluations on the accuracy of current satellite measurements or retrievals should be conducted through integrating point-scale in-situ measurements, multi-resolution satellite observations and forward radiative transfer model simulations (Dai et al., 2017). Moreover, it is highly desirable to understand the scaling effects of freeze/thaw state and bridge the multi-sensor retrievals especially for landscape freeze/thaw monitoring over complex terrain and diverse land cover types (Li et al., 2014; Du et al.,

2015). On the other hand, the Tibetan Plateau is characterized by large diurnal temperature range and rapid freeze/thaw changes, with long freeze/thaw transition periods (up to a few months) (Jin and Li, 2009). Therefore, remote sensing data with finer temporal resolution are needed for better monitoring the diurnal freeze/thaw cycles in the Tibetan Plateau permafrost area.

Process-Based Modeling of Tibetan Plateau Permafrost

As mentioned above, current satellite remote sensing is largely restricted to the measurements of near-surface soils and their properties, while *subsurface* properties are more relevant to permafrost conditions. Many studies have combined satellite remote sensing data with empirical or statistical models to estimate the presence of permafrost as discussed above. However, these models usually oversimplify or overlook key processes controlling soil freeze/thaw and permafrost dynamics (Zheng et al., 2019b). Additionally, simple models also generally assume that the frozen subsurface is in equilibrium with the current climate, which may not capture the transient changes in frozen ground (Zhao et al., 2017a). Process-based models can better represent the underlying processes with the potential to provide more reliable estimates of regional permafrost distribution and changes.

Current Progress

Frozen soil parameterizations in early process models was implemented using analytic or approximate solution of Stefan problem due to computational limitations (Li and Koike, 2003). With increased computational power, numerical models with high precision have been widely used in Tibetan Plateau. Most numerical models simulate the soil temperature in one dimension by employing a finite-difference or finite-element form of heat transfer equation, while many of them also consider other processes such as soil water migration, and link soil freeze/thaw process with hydrological process (Riseborough et al., 2008). A range of models have been used to model Tibetan Plateau permafrost distribution and changes, including soil process model GIPL2.0, land surface model CoupModel, CLM, and some hydrological models incorporating soil freeze/thaw scheme into water transfer process like VIC and GBEHM (Geomorphology-Based Eco-Hydrological Model) (Guo and Wang, 2013; Lan et al., 2015; Qin et al., 2017; Zheng et al., 2019b).

Earlier permafrost models like GIPL 2.0 (Qin et al., 2017) do not simulate surface energy balance, and usually directly set land/ground surface temperature as the upper boundary condition for soil heat transfer. These models are able to simulate soil temperature for deep layers which could be used to identify the presence of permafrost, while other processes like surface energy balance, snow melting are generally not included (Qin et al., 2017; Sun et al., 2019). These models have relatively lower requirements on climatic forcing data and usually use land/ground surface temperature and external soil moisture data as inputs. Despite the simplified heat-water transfer processes, it can reduce the uncertainties that may be introduced by external inputs such as highly uncertain precipitation data in the Tibetan Plateau. Nevertheless, current soil moisture products available from global satellite remote sensing and land model data assimilation system also show large uncertainties in the Tibetan Plateau region (Yang et al., 2013a; Zhao et al., 2014; Chen et al., 2017). In addition, although using ground surface temperature as upper boundary conditions can reduce the need of calculating surface energy balance budget, those data may not be widely available at the regional scale. The remotely sensed land surface temperature can be used as a substitute, but the difference between ground surface temperature and land surface temperature can be large due to the buffering effects of surface vegetation or snow cover (Luo et al., 2018; Luo et al, 2020).

A number of regional and global land hydrological models are also adapted for permafrost simulation in the Tibetan Plateau region (**Table 1**). Some hydrological models link the soil freeze/thaw scheme with hydrological-related process. For example, GBEHM model is developed from a hillslope-based hydrology model (GBHM) (Yang et al., 2015; Zheng et al., 2019b). Land models describe the complex land system, and therefore often include many processes related to soil freeze/thaw, such as surface energy balance processes, snow melting and infiltration process, soil water migration, and variability in soil thermal properties due to soil organic content changes etc. In addition to traditional numerical solution used in most models, there are also some variations in the model concepts and solution in recent models. For example, there is a new solution of 1-D heat transfer based on enthalpy in a land surface model HydroSiB2, showing good performance in soil freeze/thaw modeling in the Tibetan Plateau (Bao et al., 2016; Wang et al., 2017). These models have been applied to either site scale or regional scale in the Tibetan Plateau, with differences in the forcing data and representations of essential physical processes.

The parametrizations or representations of hydrological and thermal processes are different among different land hydrological models, such as the soil column depth and lower boundary conditions (**Table 1**), resulting in varying model performance. For example, SHAW model assumes that the soil thermal conductivity is a weighting average of various components in the soil, while CoupModel calculate the soil thermal conductivity based on three soil freeze/thaw state (i.e., unfrozen, frozen and partially frozen). Yang et al. (2013b) compared the simulation results from CoupModel and SHAW model at northern Tibetan Plateau sites, and found that soil heat transfer scheme used in CoupModel showed a better performance than SHAW model. Usually, these models require meteorological forcing including air temperature, wind speed, precipitation and radiation to solve the surface energy and water balance. It is generally difficult to directly use satellite data (such as land surface temperature) to drive these land models, which imposes additional difficulties for high-resolution ($\sim \leq 1$ km) simulations as high-resolution surface meteorology datasets are not readily available in the Tibetan Plateau. Moreover, most land surface models are originally developed for surficial soil layers with a focus on the energy and mass exchange between the surface and the atmosphere, and therefore generally have simplified representation of the soil properties and thermal processes in deep soil layers (Sun et al., 2019).

TABLE 1 | Comparisons of models used for Tibetan Plateau permafrost simulation. All models include soil heat transfer process, which is not included here.

	Time step	Forcing data	Soil water transfer	Surface energy balance	Snow	Soil organic	Soil column depth	Lower boundary condition	Reference
SHAW	1 h/daily	Tair, prec, W, SW, Q	✓	✓	✓	–	User defined	User defined model-estimated Tg	Liu et al. (2013)
CoupModel	10 min/1 h/daily	Tair, prec, W, SW, Q. . .	✓	✓	✓	✓	User defined	User defined model-estimated Tg	Zhou et al. (2013)
GBEHM	Daily	Tair, prec, CF, Q, pres, land surface temperature	✓	✓	–	–	User defined	Assigned geothermal flux	Yang et al. (2015)
GIPL2.0	Daily	Tg0[a]	No	No	No	No	User defined	Assigned geothermal flux	Qin et al. (2017)
CLM	3 h/daily	Tair, prec, W, SW, LW, Q, pres	✓	✓	✓	✓	45.1 m	$g = 0$	Guo and Wang (2013)
Noah	30 min/3 h	Tair, prec, W, SW, LW, Q, pres	✓	✓	✓	✓	40 m	Estimated Tg at 40 m	Wu et al. (2018)
VIC	1 h/3 h/daily	Tair, prec, W, SW, LW, Q, pres	✓	✓	✓	✓	50 m	$g = 0$	Lan et al. (2015)

Note: Tair, air temperature; Prec, precipitation; W, near surface wind speed; SW, downward shortwave radiation; LW, downward longwave radiation; Q, specific humidity; Pres, air pressure; CF, cloud fraction; Tg, soil temperature; g, soil thermal gradient.

[a]*The required parameter is not listed in the table.*

Challenges

Large uncertainties exist in the reanalysis data, surface meteorology, surface and soil datasets in the Tibetan Plateau region, which are required for model inputs and parameterization, limiting a comprehensive evaluation of model processes and structure across the region (Dai et al., 2019). Ground-based meteorological data are particularly sparse in the Tibetan Plateau, with current stations mainly located in the central plateau and along the Qinghai-Tibet Railway/Highways, and complex topography adds additional challenges to upscaling local meteorological data to regional scale. For example, Zheng et al. (2019b) showed that the uncertainties associated with the extrapolation or interpolation of meteorological data were comparable to the uncertainties of model parameterizations. Previous studies also found that similar uncertainties were associated with model simulated frozen ground using different atmospheric forcing data comparing with model simulations using different parameterizations (Wang et al., 2016a; Guo et al., 2017). On the other hand, meteorological forcing data generated from global climate models has a coarse spatial resolution and cannot represent the local or small-scale climate variability (Su et al., 2013; Westermann et al., 2015). The unique topography and strong heterogeneous surface conditions in the Tibetan Plateau make it particular challenging to downscale coarse-resolution meteorology datasets (Yue et al., 2016). A recently released China meteorological forcing data incorporating meteorological stations, satellite data and re-analysis data has somewhat improved quality in the Tibetan Plateau and has been widely used; however, its uncertainty remains higher in the Tibetan Plateau than other regions of China (He et al., 2020). In addition, regional-scale soil datasets in the Tibetan Plateau, including soil properties (such as soil texture and soil organic carbon content), soil depth and ground ice content are extremely limited, which are important for model parameterization due to their significant impacts on soil heat and water transfer (Chen et al., 2015b; Cao et al., 2019).

Process representation in current models also needs improvement. A large gradient can exist in the surface air-ground temperature in the Tibetan Plateau region due to arid climate and high solar radiation (Wang and French, 1995). Without accounting for this temperature gradient, large biases can exist in the model simulated soil temperatures. Soil properties in global land models are generally derived from agriculture soil samples, while the physical properties of gravel soils in Tibetan Plateau are less considered (Yi et al., 2018a). Although most models have coupled soil heat transfer with soil water movement, the soil moisture profile is not generally well represented, partly due the complex interactions between topography, soil organic carbon content, vegetation distribution and their coupled effects on the dynamics of soil moisture (Wang et al., 2012a). Some key factors affecting the soil heat transfer unique to the mountain areas are also not adequately represented in current models (Zhou et al., 2013). For example, lateral water flow is generally ignored in most models, which may be of particular importance in the mountain areas (Zheng et al., 2019b). Simulating ground ice content in the

Tibetan Plateau permafrost is also a challenge. Accurate representation of ground ice content especially near the permafrost table will have a large impact on projecting future permafrost dynamics due to potentially large latent heat release and thermokarst activity as a result of thawing ground ice (Chen et al., 2015b; Liljedahl et al., 2016). On the other hand, model performance is highly affected by boundary and initial conditions, which vary greatly among models. Zero heat flux at lower boundary is widely adopted in most land models, while the geothermal gradient in the Tibetan Plateau show high spatial variability (Wu et al., 2010). Assigning a zero or constant geothermal flux might lead to large biases in model simulated deep soil temperature and permafrost depth especially at longer time scale (Xiao et al., 2013). More data on deep-soil layer like borehole observations are needed to improve deep soil parameterization and representation of lower boundary conditions in the permafrost models.

Integrate Remote Sensing Data With Process-Based Models to Improve Tibetan Plateau Permafrost Monitoring

Remote sensing can provide spatially continuous landscape and climatic forcing data across large scale, which is especially useful for regional modeling in a heterogeneous terrain like the Tibetan Plateau. Here we summarize recent efforts that use multi-source remote sensing datasets to improve regional modeling of Tibetan Plateau permafrost or closely related environmental parameters, through model initialization, parameterization and data assimilation.

Climatic factors (such as air temperature and precipitation) in the Tibetan Plateau area show *evident elevation dependence*. In many process-based simulations, the SRTM (Shuttle Radar Topographic Mission) DEM (Digital Elevation Model) is used as a basis to extrapolate the *in-situ* meteorology observations to regional scale and generate model forcing data (e.g., Guo and Wang, 2013; Gao et al., 2018). However, in addition to elevation, other factors such as vegetation, soil wetness, slope, and aspect, also play *important roles* on the regional climate variability, and large uncertainties may exist in the spatial extrapolation using sparse ground observations (Wang et al., 2019b; Zheng et al., 2019b). Previous studies found that MODIS land surface temperature is able to capture the spatial pattern of near-surface air temperature and is especially useful in reducing the spatial interpolation errors in data-scarce regions (Zhu et al., 2013; Shamir and Georgakakos, 2014). In the northeast Tibetan Plateau, Wang et al. (2016b) used the lapse rate derived from MODIS land surface temperature product during the spatial interpolation of air temperature, and found the model simulated snow processes was improved comparing with simulations using the interpolated air temperature data. Regarding precipitation, previous studies found that the precipitation-elevation relationship contrasts between the northern and southern Tibetan Plateau, and the satellite-based precipitation data can approximately capture such patterns (Tang et al., 2018; Wang et al., 2019b). Nevertheless, very few studies have investigated the impacts of such satellite-based improvements in spatial extrapolation of climatic forcing on frozen soil simulations.

In addition to producing regional climatic forcing data, satellite remote sensing data has been also directly used as model parameters, such as vegetation coverage, slope and aspect, to improve regional simulations of Tibetan Plateau frozen ground. For example, based on the SRTM DEM, Zhang et al. (2018) quantified the topographic effects of solar radiation on permafrost distribution in the northeast Tibetan Plateau and the simulated permafrost coverage increased by 8% when accounting for the impact of topographic shadows on surface energy budget. Li et al. (2019) found that introducing MODIS-based vegetation coverage data into the CoLM can reduce the warming biases in land surface temperature and surface soil temperature by ~10°C in sparse vegetated areas in the Tibetan Plateau. Jin and Li (2009) assimilated the satellite microwave-based brightness temperature into SHAW model at the Amdo station in the central Tibetan Plateau, and found that the errors of simulated upper (0–2.58 m) soil temperature during wintertime reduced by 0.76°C. Through assimilating *in-situ* soil moisture data, Zhou et al. (2008) found the accuracy of frozen depth simulation has improved.

A process-based model fully driven by satellite observations would bridge the data gap in data-scarce region such as the Tibetan Plateau with the potential to improve regional permafrost simulation. As discussed above, most process-based models heavily rely on surface meteorological forcing data (Zheng et al., 2019b; Guo et al., 2017), while satellite observations are not fully consistent with the requirements of these models. For example, satellite remote sensing is not able to observe the near-surface wind speed, which, however, is an essential factor in solving the surface energy balance. In a recent study, Zheng et al. (2019b) used a maximum entropy production-based parameterization of surface energy balance to replace the originally turbulent theory-based scheme in GBEHM to make it fully driven by satellite data and capable of capturing the water-heat coupled processes within soil layers. The model was applied to simulate the frozen soil distribution and recent changes across the entire Tibetan Plateau (Zheng et al., 2020). The satellite-based model simulations showed overall higher accuracy, comparing with previous Tibetan Plateau permafrost maps generated using ground-based measurements (**Figure 3**, adapted from Zheng et al., 2020). In addition to the physics-based scheme, machine learning and artificial intelligence have also obtained reliable performance in solving the surface energy budget (Adnan et al., 2017; Zhao et al., 2019) as well as in regional permafrost mapping (Pastick et al., 2015; Aalto et al., 2018). A hybrid approach that combines machine learning-based surface energy balance and process-based heat-water coupled processes seems to be a potentially useful tool for regional mapping of Tibetan Plateau permafrost, while such studies are still lacking.

Although currently there are very limited studies using satellite data to directly improve model performance in simulating Tibetan Plateau permafrost through data assimilation, many efforts have been devoted to improving the simulation of variables closely related to the permafrost thermal state, such

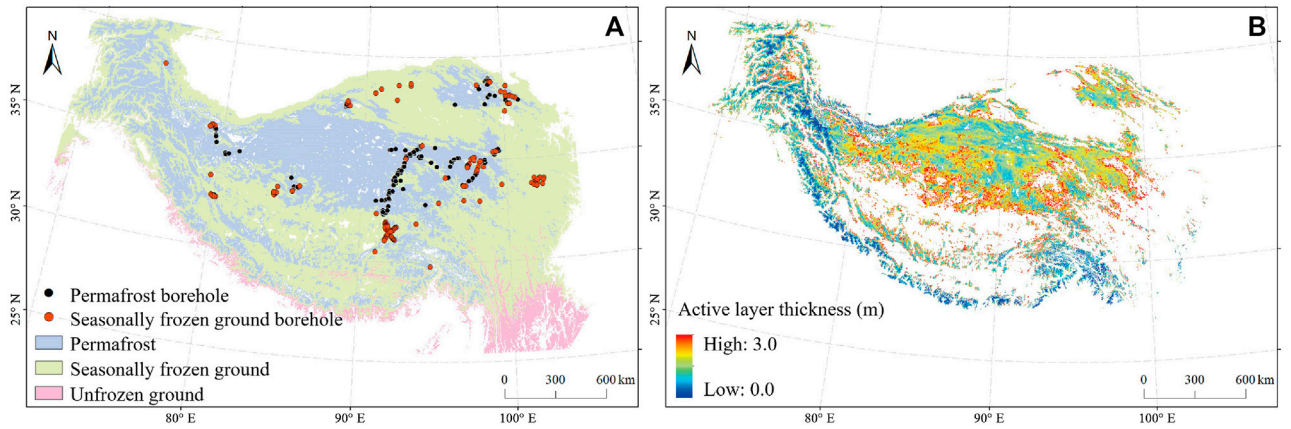

FIGURE 3 | Mean spatial patterns of permafrost distribution **(A)** and active layer thickness **(B)** over the Tibetan Plateau during the period of 2002–2016, simulated using a remote sensing driven hydrology model (Zheng et al., 2019b; Zheng et al., 2020). The satellite-based permafrost map indicates that permafrost and seasonally frozen ground account for ~37% and ~56% of the Tibetan Plateau respectively, with an overall accuracy of 79.3–90.7% in identifying permafrost boreholes and 76.5–86.4% in identifying seasonally frozen ground boreholes. The accuracy is generally higher than permafrost maps generated using ground-stations, which demonstrates the advantage of satellite remote sensing-based methods in simulating frozen soils in data-scarce regions.

as soil moisture (Zhao et al., 2014; Yang et al., 2020), snow cover and snow depth (Zhang et al., 2014; Wang et al., 2020), and other key environmental variables including air temperature and net radiation (Li et al., 2012b; Lin et al., 2016). Through assimilating the satellite-based microwave brightness temperature at 6.9 and 18.7 GHz, Yang et al. (2007a) found the accuracy of simulated surface energy budget was improved. Lin et al. (2016) found that assimilating MODIS snow cover would be especially important in reducing uncertainties in air temperature predictions in the Tibetan Plateau. Those results could potentially improve the model simulated soil thermal regime and thus permafrost distribution. Despite its potential advantages in improving frozen soil simulation, the application of data assimilation is greatly limited due to large uncertainties in current satellite products and retrieval algorithms in the Tibetan Plateau (Chen et al., 2017). In addition, satellite-based soil moisture and snow cover retrievals from passive microwave remote sensing data have generally coarse spatial resolution, and appropriate downscaling scheme is needed to characterize the spatial heterogeneities within the coarse-grid in the mountain areas (Zhao et al., 2014).

DISCUSSION

Unique Challenges in Tibetan Plateau Permafrost Monitoring

Unique environmental conditions in the Tibetan Plateau result in permafrost characteristics different from that in the northern high latitudes or other alpine environments as discussed above. The topography in the Tibetan Plateau is complex and characterized by strong heterogeneity at small spatial scales, exerting strong control on local permafrost distribution (Luo et al., 2012), while most satellite data or models have relatively coarse resolutions (>1 km) and cannot well represent such local-scale variability (Yang et al., 2010). Moreover, the complex topography in the Tibetan Plateau can result in strong spatial heterogeneity in local-scale snow cover and land surface temperature conditions, which adds additional uncertainties to satellite-based freeze/thaw detection (Zhao et al., 2017b; Dai et al., 2018). For example, snow accumulated in shady areas can result in strong scattering, impacting the accuracy of coarse-resolution passive microwave remote sensing retrievals (Dai et al., 2017). Accurately accounting for the impact of topography on Tibetan Plateau soil freeze/thaw dynamics and permafrost distribution requires improved remote sensing algorithms and models.

Other surface or subsurface conditions affecting the Tibetan Plateau permafrost are also different from those in the high-latitude regions. The Arctic is mostly underlain by continuous permafrost (Brown et al., 1997), characterized by overall high soil carbon content, thicker snow cover and more saturated soil condition (Hinzman et al., 2013). Previous study showed the uncertainty in spatial and vertical soil organic distribution is the main factor affecting the model simulated active layer thickness in Alaska, followed by the impacts of soil moisture (Yi et al., 2018b). The timing and amount of snow cover also play an important role in affecting pan-Arctic soil temperatures, especially in deeper soils, due to its strong insulation effects (Yi et al., 2015; Jones et al., 2016). However, the frozen ground in the Tibetan Plateau is generally characterized by unsaturated soils, low organic carbon content, shallow snow cover, and shorter snow duration (Li et al., 2008; Kang et al., 2010). Large uncertainties exist in Tibetan Plateau remote sensing and model soil moisture products due to strong spatial and vertical variability in soil moisture. The uncertainties limit their usefulness in regional permafrost monitoring (Han et al., 2015; Bi et al., 2016). For example, most InSAR-based active layer retrieval algorithms assume a saturated soil profile within the active layer, while Tibetan Plateau permafrost generally shows a much deeper and drier active layer compared with that in the

Arctic region (Jia et al., 2017). Other Tibetan Plateau environmental factors also need to be carefully considered in model parameterization. For example, the insulation effects of soil organic carbon in the Tibetan Plateau is likely limited due to its lower content; however, soil carbon content can significantly affect Tibetan Plateau soil freeze/thaw dynamics through altering the soil hydraulic properties and soil moisture distribution (Zhou et al., 2013; Jiang et al., 2020). Shallow snow cover may have a cooling effect on subsurface soil temperature through reducing the absorption of solar radiation (Wang et al., 2020). In addition, the coarse-fragment soil with a larger thermal conductivity is widespread in the Tibetan Plateau, unlike the prevailing peat soils in the Arctic. This should be considered in the model parameterization when simulating the Tibetan Plateau permafrost (Arocena et al., 2012; Pan et al., 2017; Yi et al., 2018a).

Potential of Geophysical Measurements in Regional Permafrost Studies

Current satellite remote sensing cannot directly detect deep soils and the permafrost, while geophysical techniques have been proven to be useful for subsurface soil characterization and permafrost detection in a minimally invasive manner. Examples of geophysical approaches include thermistors and dielectric sensors, ground penetrating radar, and electromagnetic methods (Dafflon et al., 2016). Among these techniques, electromagnetic methods are becoming increasingly popular, which calculates the ground conductivity or resistivity through measuring the changes in the eddy currents and induced magnetic fields in the subsurface (Hauck et al., 2001). Based on the distinct difference of resistivity between frozen and unfrozen materials, the electromagnetic method can detect permafrost existence with a relatively high spatial resolution. It has the advantage of being sensitive to the liquid soil water content, and providing information on the structure and content of the deep soil layer, which is lacking but usually required by models (Minsley et al., 2012; Mikucki et al., 2015). In addition to the surface geophysical measurements, airborne electromagnetic methods have been widely used in the polar regions to detect the permafrost over diverse landscapes at the regional scale (Minsley et al., 2012; Rey et al., 2019). Airborne electromagnetic methods have less terrain-induced noise than ground measurements, and may be particular useful for permafrost mapping in mountain regions (Hauck et al., 2001; Su et al., 2020), while such applications are still lacking in the Tibetan region.

The geophysical measurements in combination with other datasets have shown great potential to improve model representation of subsurface properties in permafrost region. For example, Dafflon et al. (2016) combined electromagnetic method and other types of observations, and successfully mapped subsurface variability in polygon shaped Arctic tundra area and document the key controls on the spatial distribution of soil properties. Léger et al. (2019) used the soil temperature data from a spatially distributed temperature profiling system and electrical resistivity data to identify correspondences between surface and subsurface property distribution in discontinuous permafrost regions. The results from these studies provide the basis for model parameterization and initialization, while other studies have directly used such observations to improve process representation in the permafrost models (Tran et al., 2017, Tran et al., 2018). Due to strong influences of organic carbon content on soil hydrological-thermal parameters, Tran et al. (2017) performed joint inversion of multiple datasets including soil temperature, moisture and electrical resistivity data to estimate the soil organic carbon profile along a transect in Barrow, Alaska, through linking the petrophysical and geophysical models with the CLM model. Combining the CLM model and electrical resistivity data, a follow-on study further investigated the soil thaw depth and its controlling factor at a high spatiotemporal resolution over a long period (Tran et al., 2018). However, it should be noted that additional errors may be introduced into the model estimates due to uncertainties in electrical resistivity inversion method and retrievals.

Improving Model Representation of Spatial Heterogeneity

An important feature of permafrost affected landscapes is the large spatial heterogeneity in soil active layer conditions, which are generally poorly represented in global land models (Muster et al., 2012; Mishra et al., 2017). Information on active layer soil conditions at landscape scales is needed to better represent the spatial heterogeneity and scaling functions in global models and reconcile coarser model simulations with more extreme local heterogeneity in active layer and permafrost conditions. Many studies have combined *in-situ* measurements, satellite remote sensing and models to address this problem. However, most studies focus on the high-latitude permafrost landscapes while Tibetan Plateau permafrost studies represent a relatively new research topic. Therefore, we summarize relevant studies in the high-latitudes, and hope to provide some insights for similar applications to the Tibetan Plateau region.

Local to landscape scale variations in active layer conditions can be effectively monitored using *in-situ* ground measurements (Brown et al., 2000; Romanovsky et al., 2010) or ground-based remote sensing including ground penetrating radar and electrical resistivity measurements (Hubbard et al., 2013; Schaefer et al., 2015). While these methods provide detailed assessments of active layer properties, they are generally applied over limited local areas ($<1\ km^2$) and are unsuitable for mapping and monitoring over large regions. Regionally refined active layer products upscaled from carefully designed *in-situ* network measurements using remote sensing based geospatial data layers offer the potential to improve the representation of permafrost active layer properties in global land models. Earlier studies used empirical models driven by *in-situ* ground observations to map permafrost and active layer properties over larger areas (e.g., Anisimov et al., 2002; Panda et al., 2010). More recent studies used machine learning data-fusion approaches and remote sensing data, including optical-infrared and LIDAR data, to extend ground-based or airborne measurements to produce regional active layer and permafrost maps (Hubbard et al., 2013;

Pastick et al., 2015). Similar as active layer thickness, a variety of methods including geospatial analysis and machine-learning data-driven approaches have been applied to upscale *in-situ* soil organic carbon content and soil moisture measurements to provide grid-cell mean estimates at a large footprint for direct comparison with satellite or model-based products (e.g., Mishra and Riley, 2015; Clewley et al., 2017).

The above spatial analysis and datasets provide critically needed information on permafrost distribution for global model parameterization and validation (Mishra et al., 2017). Previous studies have demonstrated the importance of considering sub-grid scale variability in land cover and surface properties in large-scale global models to accurately simulate water, energy and carbon exchange in permafrost landscapes (Liston, 2004; Gouttevin et al., 2012). However, how to represent those local effects to facilitate upscaling of model simulated water, energy and carbon fluxes remains a challenge (Muster et al., 2012). Potential improvements may include statistical representation of spatial distribution and temporal changes in the surface variables related to permafrost properties. For example, Zhang et al. (2014) used statistical functions derived from field measurements to characterize the spatial variability of surface ground and soil conditions and incorporated this information into a process model to simulate the frequency of permafrost occurrence at very high spatial (<1 km) resolution. Much better accuracy in model simulated ground temperatures in Norway was achieved when using a gamma distribution to represent sub-grid variability in snow distribution than using grid-cell average snow depth (Gisnås et al., 2016). Yi et al. (2018b) also found the model better represented the statistical distribution of active layer thickness when using a logistic distribution consistent with the spatial distribution of surface wetness derived from the P-band radar data to represent sub-grid variability of organic layer thickness. In addition, the zonation approach can combine diverse datasets over different scales and identify the large-scale zones that have distinct properties, which can be used to characterize the spatial heterogeneity in complex permafrost environments. For example, Wainwright et al. (2015) employed a nested polygon geomorphic zonation approach to characterize the distributions of environmental properties in Arctic tundra and assess their impact on ecosystem carbon fluxes. The combination of zonation approach and emerging technologies such as machine learning approach can generate spatially-explicit datasets from a diverse range of observations supporting the model needs of parameterization and initialization, and may have great potential in permafrost research (Hubbard et al., 2018; Hubbard et al., 2020).

RESEARCH PRIORITIES AND RECOMMENDATIONS

We have reviewed the state of knowledge for Tibetan Plateau permafrost, soil freeze/thaw state, and summarized recent progress in using satellite remote sensing data and models to monitor Tibetan Plateau permafrost. This exercise has revealed important gaps in capabilities for monitoring and modeling the current state of Tibetan Plateau permafrost as well as projecting its future trajectory. Here we recommend the following research priorities to address these gaps.

Satellite-based optical and infrared remote sensing provide high spatial resolution land surface conditions. These techniques have great potential for producing Tibetan Plateau classification maps and determining correlations between these classifications and permafrost distributions, especially in regional-scale applications. Particularly, high-resolution imagery (<10 m scale) can be used to capture the high degree of spatial heterogeneity in the Tibetan Plateau and further infer the related permafrost states, such as using high-resolution imaging of swamps, wetlands and small watersheds to monitor changes in the hydrologic state that may be coupled with local permafrost degradation.

Microwave remote sensing has shown great potential in surface freeze/thaw and permafrost monitoring due to its strong sensitivity to soil water content and phase changes, its ability to penetrate clouds, and providing all-weather monitoring of the land surface. However, current microwave remote sensing methods are limited to detections in the upper soil layer within a few centimeters of the surface. Deeper soil remote sensing requires lower frequency surveys (such as P-band SAR) and multi-frequency observations (such as joint L- and P-band SAR) to enable soil vertical profile retrievals. These sensors and corresponding algorithms should be developed. InSAR have been widely used to map regional subsidence and active layer thickness in the Tibetan Plateau, but more systematic subsidence mapping is still needed, with particular emphasis on the permafrost transition zone that is vulnerable to abrupt thaw and degradation. Improved approaches and regional data such as accurate DEM and soil moisture information are also needed to support InSAR active layer retrieval.

The apparent scarcity of local-scale observations greatly limits our process understanding in the Tibetan Plateau permafrost area. Therefore, we also call for the expansion of the *in-situ* sampling network, particularly in the western Tibetan Plateau, along the transition zones between discontinuous and sporadic permafrost zones, and along elevation gradients (**Figure 1**). Additional information on deep soil temperature, ground ice content, more consistent soil moisture and dielectric profiles, improved mapping of soil texture and soil organic content are required for improving remote sensing algorithms and regional models. Geophysical measurements especially airborne electromagnetic method can obtain information on deep ground structure and unfrozen water content, and provide more spatially extensive measurements than point-scale observations, and should be considered when expanding the local-scale observational network in the Tibetan Plateau.

Integrating local-scale observations, remote sensing data with process-based models will be an effective way to monitor regional permafrost and project its future state. However, a number of factors limit such applications in Tibetan Plateau permafrost research, including but not limiting to large uncertainties in current satellite products for the Tibetan Plateau area, mismatch between model input data needs and information provided by current satellite sensors, insufficient accounting for spatial heterogeneity impact on permafrost distribution.

Better approaches to combine diverse datasets at different spatial and temporal scales with models are needed to address the above challenges, and should be developed. In addition, current model scheme and parameterization also require improvements to better reproduce the unique soil freeze/thaw characteristics in the Tibetan Plateau region.

AUTHOR CONTRIBUTIONS

YY initiated the study. HJ, GZ, and YY wrote the paper. Other co-authors contributed to the discussion and provided feedback.

FUNDING

YY acknowledges support by the NASA Terrestrial Ecology program under the Arctic Boreal Vulnerability Experiment (ABoVE, NNH18ZDA001N-TE). It was also supported by the Strategic Priority Research Program of Chinese Academy of Sciences (Grant No. XDA20060401), National Natural Science Foundation of China (41771112), and the Swedish Research Council (VR 2014–5320). A portion of this research was carried out at the Jet Propulsion Laboratory, California Institute of Technology, under contract with NASA.

REFERENCES

Aalto, J., Karjalainen, O., Hjort, J., and Luoto, M. (2018). Statistical forecasting of current and future circum-Arctic ground temperatures and active layer thickness. *Geophys. Res. Lett.* 45, 4889–4898. doi:10.1029/2018gl078007

Adnan, M., Ahsan, M., Rehman, A., and Nazir, M. (2017). Estimating evapotranspiration using machine learning techniques. *Int. J. Adv. Comput. Sci. Appl.* 8, 108–113. doi:10.14569/ijacsa.2017.080915

Anisimov, O. A., Shiklomanov, N. I., and Nelson, F. E. (2002). Variability of seasonal thaw depth in permafrost regions: a stochastic modeling approach. *Ecol. Model.* 153, 217–227. doi:10.1016/s0304-3800(02)00016-9

Arocena, J., Hall, K., and Zhu, L. P. S. J. O. S. S. (2012). Soil formation in high elevation and permafrost areas in the Qinghai plateau (China). *Spanish J. Soil Sci.* 2, 34–49. doi:10.3232/SJSS.2012.V2.N2.02

Bao, H., Koike, T., Yang, K., Wang, L., Shrestha, M., and Lawford, P. (2016). Development of an enthalpy-based frozen soil model and its validation in a cold region in China. *J. Geophys. Res. Atmos.* 121, 5259–5280. doi:10.1002/2015jd024451

Bi, H., Ma, J., Zheng, W., and Zeng, J. (2016). Comparison of soil moisture in GLDAS model simulations and *in situ* observations over the Tibetan Plateau. *J. Geophys. Res. Atmos.* 121, 2658–2678. doi:10.1002/2015jd024131

Bibi, S., Wang, L., Li, X., Zhou, J., Chen, D., and Yao, T. (2018). Climatic and associated cryospheric, biospheric, and hydrological changes on the Tibetan Plateau: a review. *Int. J. Climatol.* 38, e1–e17. doi:10.1002/joc.5411

Brown, J., Ferrians, O. J., Heginbottom, J. A., and Melnikov, E. S. (1997). *Circum arctic map of permafrost and ground ice conditions*. Middleton, WI: Center for Integrated Data Analytics Wisconsin Science Center.

Brown, J., Hinkel, K. M., and Nelson, F. E. (2000). The circumpolar active layer monitoring (calm) program: research designs and initial results. *Polar Geogr.* 24, 166–258. doi:10.1080/10889370009377698

Cao, B., Zhang, T., Wu, Q., Sheng, Y., Zhao, L., and Zou, D. (2019). Brief communication: evaluation and inter-comparisons of Qinghai-Tibet Plateau permafrost maps based on a new inventory of field evidence. *Cryosphere* 13, 511–519. doi:10.5194/tc-13-511-2019

Chen, D., Xu, B., Yao, T., Guo, Z., Cui, P., Chen, F., et al. (2015a). Assessment of past, present and future environmental changes on the Tibetan Plateau. *Chin. Sci. Bull.* 60, 3025–3035. doi:10.1360/n972015-00849

Chen, H., Nan, Z., Zhao, L., Ding, Y., Chen, J., and Pang, Q. (2015b). Noah modelling of the permafrost distribution and characteristics in the west Kunlun area, qinghai-tibet plateau, China. *Permafr. Periglac. Process.* 26, 160–174. doi:10.1002/ppp.1841

Chen, R. H., Tabatabaeenejad, A., and Moghaddam, M. (2019). Retrieval of permafrost active layer properties using time-series P-band radar observations. *IEEE Trans. Geosci. Rem. Sens.* 57, 6037–6054. doi:10.1109/tgrs.2019.2903935

Chen, Y., Yang, K., Qin, J., Cui, Q., Lu, H., La, Z., et al. (2017). Evaluation of SMAP, SMOS, and AMSR2 soil moisture retrievals against observations from two networks on the Tibetan Plateau. *J. Geophys. Res. Atmos.* 122, 5780–5792. doi:10.1002/2016jd026388

Chen, Y., Yang, K., Tang, W., Qin, J., and Zhao, L. (2012). Parameterizing soil organic carbon's impacts on soil porosity and thermal parameters for Eastern Tibet grasslands. *Sci. China Earth Sci.* 55, 1001–1011. doi:10.1007/s11430-012-4433-0

Cheng, G., and Wu, T. (2007). Responses of permafrost to climate change and their environmental significance, Qinghai-Tibet Plateau. *J. Geophys. Res.* 112. doi:10.1029/2006jf000631

Cheng, G., Zhao, L., Li, R., Wu, X., Sheng, Y., Hu, G., et al. (2019). Characteristic, changes and impacts of permafrost on Qinghai-Tibet Plateau. *Chin. Sci. Bull.* 64, 2783–2795. (in Chinese). doi:10.136./tb-2019-0191

Clewley, D., Whitcomb, J. B., Akbar, R., Silva, A. R., Berg, A., Adams, J. R., et al. (2017). A method for upscaling in situ soil moisture measurements to satellite footprint scale using random forests. *IEEE J. Sel. Top. Appl. Earth Observations Remote Sensing* 10, 2663–2673. doi:10.1109/jstars.2017.2690220

Dafflon, B., Hubbard, S., Ulrich, C., Peterson, J., Wu, Y., Wainwright, H., et al. (2016). Geophysical estimation of shallow permafrost distribution and properties in an ice-wedge polygon-dominated Arctic tundra region. *Geophysics* 81, WA247–WA263. doi:10.1190/geo2015-0175.1

Dai, L., Che, T., Ding, Y., and Hao, X. (2017). Evaluation of snow cover and snow depth on the Qinghai-Tibetan Plateau derived from passive microwave remote sensing. *Cryosphere* 11, 1933–1948. doi:10.5194/tc-11-1933-2017

Dai, L., Che, T., Xie, H., and Wu, X. (2018). Estimation of snow depth over the Qinghai-Tibetan plateau based on AMSR-E and MODIS data. *Rem. Sens.* 10. doi:10.3390/rs10121989

Dai, Y., Xin, Q., Wei, N., Zhang, Y., Shangguan, W., Yuan, H., et al. (2019). A global high-resolution data set of soil hydraulic and thermal properties for land surface modeling. *J. Adv. Model. Earth Syst.* 11, 2996–3023. doi:10.1029/2019ms001784

Daout, S., Doin, M. P., Peltzer, G., Socquet, A., and Lasserre, C. (2017). Large-scale InSAR monitoring of permafrost freeze-thaw cycles on the Tibetan Plateau. *Geophys. Res. Lett.* 44, 901–909. doi:10.1002/2016gl070781

Dente, L., Ferrazzoli, P., Su, Z., Van Der Velde, R., and Guerriero, L. (2014). Combined use of active and passive microwave satellite data to constrain a discrete scattering model. *Rem. Sens. Environ.* 155, 222–238. doi:10.1016/j.rse.2014.08.031

Drusch, D. M., Walvoord, M., Minsley, B., Rover, J., and Singha, K. (2019). Investigating lake-area dynamics across a permafrost-thaw spectrum using airborne electromagnetic surveys and remote sensing time-series data in Yukon Flats, Alaska. *Environ. Res. Lett.* 14, 025001. doi:10.1088/1748-9326/aaf06f

Du, J., Kimball, J., and Moghaddam, M. (2015). Theoretical modeling and analysis of L- and P-band radar backscatter sensitivity to soil active layer dielectric variations. *Rem. Sens.* 7, 9450–9472. doi:10.3390/rs70709450

Duan, A. M., and Wu, G. X. (2005). Role of the Tibetan Plateau thermal forcing in the summer climate patterns over subtropical Asia. *Clim. Dynam.* 24, 793–807. doi:10.1007/s00382-004-0488-8

Gao, B., Yang, D., Qin, Y., Wang, Y., Li, H., Zhang, Y., et al. (2018). Change in frozen soils and its effect on regional hydrology, upper Heihe basin, northeastern Qinghai-Tibetan Plateau. *Cryosphere* 12. doi:10.5194/tc-12-657-2018

Gisnås, K., Westermann, S., Schuler, T. V., Melvold, K., and Etzelmüller, B. (2016). Small-scale variation of snow in a regional permafrost model. *Cryosphere* 10, 1201–1215. doi:10.5194/tc-10-1201-2016

Gouttevin, I., Krinner, G., Ciais, P., Polcher, J., and Legout, C. (2012). Multi-scale validation of a new soil freezing scheme for a land-surface model with physically-based hydrology. *Cryosphere* 6, 407–430. doi:10.5194/tc-6-407-2012

Gruber, S., Fleiner, R., Guegan, E., Panday, P., Schmid, M.-O., Stumm, D., et al. (2017). Review article: inferring permafrost and permafrost thaw in the mountains of the Hindu Kush Himalaya region. *Cryosphere* 11, 81–99. doi:10.5194/tc-11-81-2017

Guo, D., Sun, J., Yang, K., Pepin, N., and Xu, Y. (2019). Revisiting recent elevation-dependent warming on the Tibetan plateau using satellite-based data sets. *J. Geophys. Res. Atmos.* 124, 8511–8521. doi:10.1029/2019jd030666

Guo, D., and Wang, H. (2013). Simulation of permafrost and seasonally frozen ground conditions on the Tibetan Plateau, 1981–2010. *J. Geophys. Res. Atmos.* 118, 5216–5230. doi:10.1002/jgrd.50457

Guo, D., Wang, H., and Wang, A. (2017). Sensitivity of historical simulation of the permafrost to different atmospheric forcing data sets from 1979 to 2009. *J. Geophys. Res. Atmos.* 122 (12), 269–212. doi:10.1002/2017jd027477

Han, L., Tsunekawa, A., and Tsubo, M. (2011). Radar remote sensing of springtime near-surface soil thaw events at mid-latitudes. *Int. J. Rem. Sens.* 32, 8555–8574. doi:10.1080/01431161.2010.542203

Han, M., Yang, K., Qin, J., Jin, R., Ma, Y., Wen, J., et al. (2015). An algorithm based on the standard deviation of passive microwave brightness temperatures for monitoring soil surface freeze/thaw state on the Tibetan plateau. *IEEE Trans. Geosci. Rem. Sens.* 53, 2775–2783. doi:10.1109/tgrs.2014.2364823

Hauck, C., Guglielmin, M., Isaksen, K., and Vonder Mühll, D. (2001). Applicability of frequency-domain and time-domain electromagnetic methods for mountain permafrost studies. *Permafr. Periglac. Process.* 12, 39–52. doi:10.1002/ppp.383

He, J., Yang, K., Tang, W., Lu, H., Qin, J., Chen, Y., et al. (2020). The first high-resolution meteorological forcing dataset for land process studies over China. *Scientific Data* 7, 1–11. doi:10.1038/s41597-020-0369-y

Hinzman, L. D., Deal, C. J., Mcguire, A. D., Mernild, S. H., Polyakov, I. V., and Walsh, J. E. (2013). Trajectory of the Arctic as an integrated system. *Ecol. Appl.* 23, 1837–1868. doi:10.1890/11-1498.1

Holmes, T. R. H., De Jeu, R. a. M., Owe, M., and Dolman, A. J. (2009). Land surface temperature from Ka band (37 GHz) passive microwave observations. *J. Geophys. Res. Atmos.* 114. doi:10.1029/2008jd010257

Huang, L., Luo, J., Lin, Z., Niu, F., and Liu, L. (2020). Using deep learning to map retrogressive thaw slumps in the Beiluhe region (Tibetan Plateau) from CubeSat images. *Rem. Sens. Environ.* 237, 111534. doi:10.1016/j.rse.2019.111534

Hubbard, S. S., Gangodagamage, C., Dafflon, B., Wainwright, H., Peterson, J., Gusmeroli, A., et al. (2013). Quantifying and relating land-surface and subsurface variability in permafrost environments using LiDAR and surface geophysical datasets. *Hydrogeol. J.* 21, 149–169. doi:10.1007/s10040-012-0939-y

Hubbard, S. S., Varadharajan, C., Wu, Y., Wainwright, H., and Dwivedi, D. (2020). Emerging technologies and radical collaboration to advance predictive understanding of watershed hydrobiogeochemistry. *Hydrol. Process.* 34, 3175–3182. doi:10.1002/hyp.13807

Hubbard, S. S., Williams, K. H., Agarwal, D., Banfield, J., Beller, H., Bouskill, N., et al. (2018). The east river, Colorado, watershed: a mountainous community testbed for improving predictive understanding of multiscale hydrological-biogeochemical dynamics. *Vadose Zone J.* 17, 180061. doi:10.2136/vzj2018.03.0061

Immerzeel, W. W., Van Beek, L. P. H., and Bierkens, M. F. P. (2010). Climate change will affect the Asian water towers. *Science* 328, 1382–1385. doi:10.1126/science.1183188

Jia, Y., Kim, J.-W., Shum, C., Lu, Z., Ding, X., Zhang, L., et al. (2017). Characterization of active layer thickening rate over the northern qinghai-Tibetan plateau permafrost region using ALOS interferometric synthetic aperture radar data, 2007–2009. *Rem. Sens.* 9, 84. doi:10.3390/rs9010084

Jiang, H., Yi, Y., Zhang, W., Yang, K., and Chen, D. (2020). Sensitivity of soil freeze/thaw dynamics to environmental conditions at different spatial scales in the central Tibetan Plateau. *Sci. Total Environ.* 734, 139261. doi:10.1016/j.scitotenv.2020.139261

Jiang, H., Zhang, W., Yi, Y., Yang, K., Li, G., and Wang, G. (2018). The impacts of soil freeze/thaw dynamics on soil water transfer and spring phenology in the Tibetan Plateau. *Arctic Antarct. Alpine Res.* 50, e1439155. doi:10.1080/15230430.2018.1439155

Jin, H.-j., Yu, Q.-h., Wang, S.-l., and Lü, L.-z. (2008). Changes in permafrost environments along the Qinghai-Tibet engineering corridor induced by anthropogenic activities and climate warming. *Cold Reg. Sci. Technol.* 53, 317–333. doi:10.1016/j.coldregions.2007.07.005

Jin, H., Luo, D., Wang, S., Lü, L., and Wu, J. (2011). Spatiotemporal variability of permafrost degradation on the Qinghai-Tibet Plateau. *Sci. Cold Arid Regions* 3, 281–305. doi:10.3724/sp.j.1226.2011.00281

Jin, R., Li, X., and Che, T. (2009). A decision tree algorithm for surface soil freeze/thaw classification over China using SSM/I brightness temperature. *Rem. Sens. Environ.* 113, 2651–2660. doi:10.1016/j.rse.2009.08.003

Jin, R., and Li, X. (2009). Improving the estimation of hydrothermal state variables in the active layer of frozen ground by assimilating *in situ* observations and SSM/I data. *Sci. China Earth Sci.* 52, 1732. doi:10.1007/s11430-009-0174-0

Jones, B. M., Baughman, C. A., Romanovsky, V. E., Parsekian, A. D., Babcock, E. L., Stephani, E., et al. (2016). Presence of rapidly degrading permafrost plateaus in south-central Alaska. *Cryosphere* 10, 2673–2692. doi:10.5194/tc-10-2673-2016

Jorgenson, M. T., and Grosse, G. (2016). Remote sensing of landscape change in permafrost regions. *Permafr. Periglac. Process.* 27, 324–338. doi:10.1002/ppp.1914

Kang, S., Xu, Y., You, Q., Flügel, W.-A., Pepin, N., and Yao, T. (2010). Review of climate and cryospheric change in the Tibetan Plateau. *Environ. Res. Lett.* 5, 015101. doi:10.1088/1748-9326/5/1/015101

Kou, X., Jiang, L., Yan, S., Zhao, T., Lu, H., and Cui, H. (2017). Detection of land surface freeze-thaw status on the Tibetan Plateau using passive microwave and thermal infrared remote sensing data. *Rem. Sens. Environ.* 199, 291–301. doi:10.1016/j.rse.2017.06.035

Lan, C., Zhang, Y., Bohn, T. J., Zhao, L., Li, J., Liu, Q., et al. (2015). Frozen soil degradation and its effects on surface hydrology in the northern Tibetan Plateau. *J. Geophys. Res. Atmos.* 120, 8276–8298. doi:10.1002/2015jd023193

Léger, E., Dafflon, B., Robert, Y., Ulrich, C., Peterson, J. E., Biraud, S. C., et al. (2019). A distributed temperature profiling method for assessing spatial variability in ground temperatures in a discontinuous permafrost region of Alaska. *Cryosphere* 13, 2853–2867. doi:10.5194/tc-13-2853-2019

Li, C., Lu, H., Leung, L. R., Yang, K., Li, H., Wang, W., et al. (2019). Improving land surface temperature simulation in CoLM over the Tibetan plateau through fractional vegetation cover derived from a remotely sensed clumping index and model-simulated leaf area index. *J. Geophys. Res. Atmos.* 124, 2620–2642. doi:10.1029/2018jd028640

Li, X., Cheng, G., Jin, H., Kang, E., Che, T., Jin, R., et al. (2008). Cryospheric change in China. *Global Planet. Change* 62, 210–218. doi:10.1016/j.gloplacha.2008.02.001

Li, X., Jin, R., Pan, X., Zhang, T., and Guo, J. (2012a). Changes in the near-surface soil freeze-thaw cycle on the Qinghai-Tibetan Plateau. *Int. J. Appl. Earth Obs. Geoinf.* 17, 33–42. doi:10.1016/j.jag.2011.12.002

Li, X., and Koike, T. (2003). Frozen soil parameterization in SiB2 and its validation with GAME-Tibet observations. *Cold Reg. Sci. Technol.* 36, 165–182. doi:10.1016/s0165-232x(03)00009-0

Li, X., Zhang, L., Weihermüller, L., Jiang, L., and Vereecken, H. (2013). Measurement and simulation of topographic effects on passive microwave remote sensing over mountain areas: a case study from the Tibetan Plateau. *IEEE Trans. Geosci. Remote Sens.* 52, 1489–1501. doi:10.1109/tgrs.2013.2251887

Li, Y., Sun, R., and Liu, S. (2015a). Vegetation physiological parameter setting in the Simple Biosphere model 2 (SiB2) for alpine meadows in the upper reaches of Heihe river. *Sci. China Earth Sci.* 58, 755–769. doi:10.1007/s11430-014-4909-1

Li, Z., Tang, P., Zhou, J., Tian, B., Chen, Q., and Fu, S. (2014). Permafrost environment monitoring on the Qinghai-Tibet Plateau using time series ASAR images. *Int J Digit Earth* 8, 840–860. doi:10.1080/17538947.2014.923943

Li, Z., Zhao, L., and Fu, Z. (2012b). Estimating net radiation flux in the Tibetan Plateau by assimilating MODIS LST products with an ensemble Kalman filter and particle filter. *Int. J. Appl. Earth Obs. Geoinf.* 19, 1–11. doi:10.1016/j.jag.2012.04.003

Li, Z., Zhao, R., Hu, J., Wen, L., Feng, G., Zhang, Z., et al. (2015b). InSAR analysis of surface deformation over permafrost to estimate active layer thickness based on one-dimensional heat transfer model of soils. *Sci. Rep.* 5, 15542. doi:10.1038/srep15542

Liljedahl, A. K., Boike, J., Daanen, R. P., Fedorov, A. N., Frost, G. V., Grosse, G., et al. (2016). Pan-Arctic ice-wedge degradation in warming permafrost and its influence on tundra hydrology. *Nat. Geosci.* 9, 312. doi:10.1038/ngeo2674

Lin, P., Wei, J., Yang, Z. L., Zhang, Y., and Zhang, K. (2016). Snow data assimilation-constrained land initialization improves seasonal temperature prediction. *Geophys. Res. Lett.* 43 (11), 423–411. doi:10.1002/2016gl070966

Liston, G. E. (2004). Representing subgrid snow cover heterogeneities in regional and global models. *J. Clim.* 17, 1381–1397. doi:10.1175/1520-0442(2004)017<1381:rsschi>2.0.co;2

Liu, L., Schaefer, K., Zhang, T., and Wahr, J. (2012). Estimating 1992–2000 average active layer thickness on the Alaskan North Slope from remotely sensed surface subsidence. *J. Geophys. Res.* 117. doi:10.1029/2011jf002041

Liu, Y., Zhao, L., and Li, R. (2013). Simulation of the soil water-thermal features within the active layerin Tanggula region, Tibetan plateau, by using SHAW model. *J. Glaciol. Geocryol.* 35, 280–290.

Luo, D., Jin, H., Lin, L., He, R.-X., Yang, S.-Z., and Chang, X.-L. (2012). New progress on permafrost temperature and thickness in the source area of the Huanghe River. *Sci. Geogr. Sin.* 32, 898–904. doi:10.13249/j.cnki.sgs.2012.07.898

Luo, D., Jin, H., Lü, L., and Wu, Q. (2014). Spatiotemporal characteristics of freezing and thawing of the active layer in the source areas of the Yellow River (SAYR). *Chin. Sci. Bull.* 59, 3034–3045. doi:10.1007/s11434-014-0189-6

Luo, D., Jin, H., Marchenko, S. S., and Romanovsky, V. E. (2018). Difference between near-surface air, land surface and ground surface temperatures and their influences on the frozen ground on the Qinghai-Tibet Plateau. *Geoderma* 312, 74–85. doi:10.1016/j.geoderma.2017.09.037

Luo, D., Liu, L., Jin, H., Wang, X., and Chen, F. (2020). Characteristics of ground surface temperature at chalaping in the source area of the Yellow River, northeastern Tibetan plateau. *Agric. For. Meteorol.* 281, 107819. doi:10.1016/j.agrformet.2019.107819

Ma, Y., Zhang, Y., Zubrzycki, S., Guo, Y., and Farhan, S. B. (2015). Hillslope-scale variability in seasonal frost depth and soil water content investigated by GPR on the southern margin of the sporadic permafrost zone on the Tibetan plateau. *Permafr. Periglac. Process.* 26, 321–334. doi:10.1002/ppp.1844

Mikucki, J. A., Auken, E., Tulaczyk, S., Virginia, R. A., Schamper, C., Sorensen, K. I., et al. (2015). Deep groundwater and potential subsurface habitats beneath an Antarctic dry valley. *Nat. Commun.* 6, 6831. doi:10.1038/ncomms7831

Miller, C. E., Griffith, P. C., Goetz, S. J., Hoy, E. E., Pinto, N., Mccubbin, I. B., et al. (2019). An overview of ABoVE airborne campaign data acquisitions and science opportunities. *Environ. Res. Lett.* 14, 080201. doi:10.1088/1748-9326/ab0d44

Minsley, B. J., Abraham, J. D., Smith, B. D., Cannia, J. C., Voss, C. I., Jorgenson, M. T., et al. (2012). Airborne electromagnetic imaging of discontinuous permafrost. *Geophys. Res. Lett.* 39. doi:10.1029/2011gl050079

Mishra, U., Drewniak, B., Jastrow, J. D., Matamala, R. M., and Vitharana, U. W. A. (2017). Spatial representation of organic carbon and active-layer thickness of high latitude soils in CMIP5 earth system models. *Geoderma* 300, 55–63. doi:10.1016/j.geoderma.2016.04.017

Mishra, U., and Riley, W. J. (2015). Scaling impacts on environmental controls and spatial heterogeneity of soil organic carbon stocks. *Biogeosci. Discuss.* 12, 1721–1751. doi:10.5194/bgd-12-1721-2015

Muster, S., Langer, M., Heim, B., Westermann, S., and Boike, J. (2012). Subpixel heterogeneity of ice-wedge polygonal tundra: a multi-scale analysis of land cover and evapotranspiration in the Lena River Delta, Siberia. *Tellus B* 64, 17301. doi:10.3402/tellusb.v64i0.17301

Naderpour, R., and Schwank, M. (2018). Snow wetness retrieved from L-band radiometry. *Rem. Sens.* 10, 359. doi:10.3390/rs10030359

National Research Council (2014). *Opportunities to use remote sensing in understanding permafrost and related ecological characteristics: report of a workshop*. Washington, DC: The National Academies Press.

Niu, F., Yin, G., Luo, J., Lin, Z., and Liu, M. (2018). Permafrost distribution along the qinghai-tibet engineering corridor, China using high-resolution statistical mapping and modeling integrated with remote sensing and GIS. *Rem. Sens.* 10 (2), 215. doi:10.3390/rs10020215

Obu, J., Westermann, S., Bartsch, A., Berdnikov, N., Christiansen, H. H., Dashtseren, A., et al. (2019). Northern Hemisphere permafrost map based on TTOP modelling for 2000–2016 at 1 km^2 scale. *Earth Sci. Rev.* 193, 299–316. doi:10.1016/j.earscirev.2019.04.023

Pan, Y., Lyu, S., Li, S., Gao, Y., Meng, X., Ao, Y., et al. (2017). Simulating the role of gravel in freeze-thaw process on the Qinghai-Tibet Plateau. *Theor. Appl. Climatol.* 127, 1011–1022. doi:10.1007/s00704-015-1684-7

Panda, S. K., Prakash, A., Solie, D. N., Romanovsky, V. E., and Jorgenson, M. T. (2010). Remote sensing and field-based mapping of permafrost distribution along the Alaska Highway corridor, interior Alaska. *Permafr. Periglac. Process.* 21, 271–281. doi:10.1002/ppp.686

Park, H., Kim, Y., and Kimball, J. S. (2016). Widespread permafrost vulnerability and soil active layer increases over the high northern latitudes inferred from satellite remote sensing and process model assessments. *Rem. Sens. Environ.* 175, 349–358. doi:10.1016/j.rse.2015.12.046

Pastick, N. J., Jorgenson, M. T., Wylie, B. K., Nield, S. J., Johnson, K. D., and Finley, A. O. (2015). Distribution of near-surface permafrost in Alaska: estimates of present and future conditions. *Rem. Sens. Environ.* 168, 301–315. doi:10.1016/j.rse.2015.07.019

Peng, X., Zhang, T., Frauenfeld, O. W., Wang, K., Cao, B., Zhong, X., et al. (2017). Response of seasonal soil freeze depth to climate change across China. *Cryosphere* 11, 1059–1073. doi:10.5194/tc-11-1059-2017

Pepin, N., Deng, H., Zhang, H., Zhang, F., Kang, S., and Yao, T. (2019). An examination of temperature trends at high elevations across the Tibetan plateau: the use of MODIS LST to understand patterns of elevation-dependent warming. *J. Geophys. Res. Atmos.* 124, 5738–5756. doi:10.1029/2018jd029798

Qin, Y., Wu, T., Zhao, L., Wu, X., Li, R., Xie, C., et al. (2017). Numerical modeling of the active layer thickness and permafrost thermal state across Qinghai-Tibetan plateau. *J. Geophys. Res. Atmos.* 122 (11), 604–611. doi:10.1002/2017jd026858

Ran, Y., Li, X., and Cheng, G. (2018). Climate warming over the past half century has led to thermal degradation of permafrost on the Qinghai-Tibet Plateau. *Cryosphere* 12, 595–608. doi:10.5194/tc-12-595-2018

Rautiainen, K., Parkkinen, T., Lemmetyinen, J., Schwank, M., Wiesmann, A., Ikonen, J., et al. SMOS prototype algorithm for detecting autumn soil freezing. *Rem. Sens. Environ.* 180, 346–360. doi:10.1016/j.rse.2016.01.012

Rey, D. M., Walvoord, M., Minsley, B., Rover, J., and Singha, K. (2019). Investigating lake-area dynamics across a permafrost-thaw spectrum using airborne electromagnetic surveys and remote sensing time-series data in Yukon Flats, Alaska. *Environ. Res. Lett.* 14, 025001. doi:10.1088/1748-9326/aaf06f

Riseborough, D., Shiklomanov, N., Etzelmüller, B., Gruber, S., and Marchenko, S. (2008). Recent advances in permafrost modelling. *Permafr. Periglac. Process.* 19, 137–156. doi:10.1002/ppp.615

Romanovsky, V. E., Drozdov, D. S., Oberman, N. G., Malkova, G. V., Kholodov, A. L., Marchenko, S. S., et al. (2010). Thermal state of permafrost in Russia. *Permafr. Periglac. Process.* 21, 136–155. doi:10.1002/ppp.683

Schaefer, K., Liu, L., Parsekian, A., Jafarov, E., Chen, A., Zhang, T., et al. (2015). Remotely sensed active layer thickness (ReSALT) at Barrow, Alaska using interferometric synthetic aperture radar. *Rem. Sens.* 7, 3735–3759. doi:10.3390/rs70403735

Scherler, M., Hauck, C., Hoelzle, M., Stähli, M., and Völksch, I. (2010). Meltwater infiltration into the frozen active layer at an alpine permafrost site. *Permafr. Periglac. Process.* 21, 325–334. doi:10.1002/ppp.694

Shamir, E., and Georgakakos, K. P. (2014). MODIS land surface temperature as an index of surface air temperature for operational snowpack estimation. *Rem. Sens. Environ.* 152, 83–98. doi:10.1016/j.rse.2014.06.001

Su, B., Rao, R., Li, Z., Song, L., and Yue, J. (2020). Detecting permafrost in plateau and mountainous areas by airborne transient electromagnetic sensing. *Electronics* 9 (8), 1229. doi:10.3390/electronics9081229

Su, F., Duan, X., Chen, D., Hao, Z., and Cuo, L. (2013). Evaluation of the global climate models in the CMIP5 over the Tibetan Plateau. *J. Clim.* 26, 3187–3208. doi:10.1175/jcli-d-12-00321.1

Sun, Z., Zhao, L., Hu, G., Qiao, Y., Du, E., Zou, D., et al. (2019). Modeling permafrost changes on the Qinghai-Tibetan plateau from 1966 to 2100: a case study from two boreholes along the Qinghai-Tibet engineering corridor. *Permafr. Periglac. Process.* 31, 156–171. doi:10.1002/ppp.2022

Tang, G., Long, D., Hong, Y., Gao, J., and Wan, W. (2018). Documentation of multifactorial relationships between precipitation and topography of the Tibetan Plateau using spaceborne precipitation radars. *Rem. Sens. Environ.* 208, 82–96. doi:10.1016/j.rse.2018.02.007

Tedesco, M. (2014). *Remote sensing of the cryosphere*. New York, NY: John Wiley & Sons.

Tran, A. P., Dafflon, B., Bisht, G., and Hubbard, S. S. (2018). Spatial and temporal variations of thaw layer thickness and its controlling factors identified using time-lapse electrical resistivity tomography and hydro-thermal modeling. *J. Hydrol.* 561, 751–763. doi:10.1016/j.jhydrol.2018.04.028

Tran, A. P., Dafflon, B., and Hubbard, S. S. (2017). Coupled land surface-subsurface hydrogeophysical inverse modeling to estimate soil organic carbon content and explore associated hydrological and thermal dynamics in the Arctic tundra. *Cryosphere* 11, 2089–2109. doi:10.5194/tc-11-2089-2017

Ulaby, F. T., Long, D. G., Blackwell, W. J., Elachi, C., Fung, A. K., Ruf, C., et al. (2014). *Microwave radar and radiometric remote sensing*. Ann Arbor, MI: University of Michigan Press.

Ulaby, F. T., Moore, R. K., and Fung, A. K. (1982). *Microwave remote sensing: active and passive*. Reading, MA: Addison-Wesley.1064.

Van Der Velde, R., and Su, Z. (2009). Dynamics in land-surface conditions on the Tibetan plateau observed by advanced synthetic aperture radar (ASAR). *Hydrol. Sci. J.* 54, 1079–1093. doi:10.1623/hysj.54.6.1079

Wainwright, H. M., Dafflon, B., Smith, L. J., Hahn, M. S., Curtis, J. B., Wu, Y., et al. (2015). Identifying multiscale zonation and assessing the relative importance of polygon geomorphology on carbon fluxes in an Arctic tundra ecosystem. *J. Geophys. Res. Biogeosci.* 120, 788–808. doi:10.1002/2014jg002799

Wang, A., Zeng, X., and Guo, D. (2016a). Estimates of global surface hydrology and heat fluxes from the community land model (CLM4.5) with four atmospheric forcing datasets. *J. Hydrometeorol.* 17, 2493–2510. doi:10.1175/jhm-d-16-0041.1

Wang, B., and French, H. M. (1995). Permafrost on the Tibet plateau, China. *Quat. Sci. Rev.* 14, 255–274. doi:10.1016/0277-3791(95)00006-b

Wang, C., Zhang, Z., Zhang, H., Zhang, B., Tang, Y., and Wu, Q. (2018). Active layer thickness retrieval of qinghai-tibet permafrost using the TerraSAR-X InSAR technique. *IEEE J. Sel. Top. Appl. Earth Observations Remote Sensing* 11, 4403–4413. doi:10.1109/jstars.2018.2873219

Wang, G., Liu, G., Li, C., and Yang, Y. (2012a). The variability of soil thermal and hydrological dynamics with vegetation cover in a permafrost region. *Agric. For. Meteorol.* 162–163, 44–57. doi:10.1016/j.agrformet.2012.04.006

Wang, G., Liu, G., and Li, G. (2012b). Effects of changes in alpine grassland vegetation cover on hillslope hydrological processes in a permafrost watershed. *J. Hydrol.* 444-445, 22–33. doi:10.1016/j.jhydrol.2012.03.033

Wang, J., Li, H., Hao, X., Huang, X., Hou, J., Che, T., et al. (2014). Remote sensing for snow hydrology in China: challenges and perspectives. *J. Appl. Remote Sens.* 8 (1), 084687. doi:10.1117/1.jrs.8.084687

Wang, L., Sun, L., Shrestha, M., Li, X., Liu, W., Zhou, J., et al. (2016b). Improving snow process modeling with satellite-based estimation of near-surface-air-temperature lapse rate. *J. Geophys. Res. Atmos.* 121 (20), 12005–12030. doi:10.1002/2016jd025506

Wang, L., Zhou, J., Qi, J., Sun, L., Yang, K., Tian, L., et al. (2017). Development of a land surface model with coupled snow and frozen soil physics. *Water Resour. Res.* 53, 5085–5103. doi:10.1002/2017wr020451

Wang, T., Yang, D., Fang, B., Yang, W., Qin, Y., and Wang, Y. (2019a). Data-driven mapping of the spatial distribution and potential changes of frozen ground over the Tibetan Plateau. *Sci. Total Environ.* 649, 515–525. doi:10.1016/j.scitotenv.2018.08.369

Wang, W., Yang, K., Zhao, L., Zheng, Z., Lu, H., Mamtimin, A., et al. (2020). Characterizing surface albedo of shallow fresh snow and its importance for snow ablation on the interior of the Tibetan Plateau. *J. Hydrometeorol.* 21 (4), 815–827. doi:10.1175/jhm-d-19-0193.1

Wang, Y., Chen, J., and Yang, D. (2019b). Bayesian assimilation of multiscale precipitation data and sparse ground gauge observations in mountainous areas. *J. Hydrometeorol.* 20, 1473–1494. doi:10.1175/jhm-d-18-0218.1

Westermann, S., Elberling, B., Højlund Pedersen, S., Stendel, M., Hansen, B. U., and Liston, G. E. (2015). Future permafrost conditions along environmental gradients in Zackenberg, Greenland. *Cryosphere* 9, 719–735. doi:10.5194/tc-9-719-2015

Wu, Q., Hou, Y., Yun, H., and Liu, Y. (2015). Changes in active-layer thickness and near-surface permafrost between 2002 and 2012 in alpine ecosystems, Qinghai-Xizang (Tibet) Plateau, China. *Global Planet. Change* 124, 149–155. doi:10.1016/j.gloplacha.2014.09.002

Wu, Q., Sheng, Y., Yu, Q., Chen, J., and Ma, W. (2020). Engineering in the rugged permafrost terrain on the roof of the world under a warming climate. *Permafr. Periglac. Process.* 31 (3), 417–428. doi:10.1002/ppp.2059

Wu, Q., Zhang, T., and Liu, Y. (2010). Permafrost temperatures and thickness on the qinghai-tibet plateau. *Global Planet. Change* 72, 32–38. doi:10.1016/j.gloplacha.2010.03.001

Wu, Q., and Zhang, T. (2008). Recent permafrost warming on the Qinghai-Tibetan plateau. *J. Geophys. Res.* 113. doi:10.1029/2007jd009539

Wu, X., Nan, Z., Zhao, S., Zhao, L., and Cheng, G. (2018). Spatial modeling of permafrost distribution and properties on the Qinghai-Tibet Plateau. *Permafr. Periglac. Process.* 29, 86–99. doi:10.1002/ppp.1971

Xiao, Y., Zhao, L., Dai, Y., Li, R., Pang, Q., and Yao, J. (2013). Representing permafrost properties in CoLM for the Qinghai-Xizang (Tibetan) plateau. *Cold Reg. Sci. Technol.* 87, 68–77. doi:10.1016/j.coldregions.2012.12.004

Yan, L., and Liu, X. (2014). Has climatic warming over the Tibetan Plateau paused or continued in recent years. *J. Earth Ocean Atmos. Sci.* 1, 13–28.

Yang, D., Gao, B., Jiao, Y., Lei, H., Zhang, Y., Yang, H., et al. (2015). A distributed scheme developed for eco-hydrological modeling in the upper Heihe River. *Sci. China Earth Sci.* 58, 36–45. doi:10.1007/s11430-014-5029-7

Yang, K., Chen, Y., He, J., Zhao, L., Lu, H., Qin, J., et al. (2020). Development of a daily soil moisture product for the period of 2002–2011 in Mainland China. *Sci. China Earth Sci.*, 63, 1113–1125. doi:10.1007/s11430-019-9588-5

Yang, K., Qin, J., Zhao, L., Chen, Y., Tang, W., Han, M., et al. (2013a). A multiscale soil moisture and freeze-thaw monitoring network on the third Pole. *Bull. Am. Meteorol. Soc.* 94, 1907–1916. doi:10.1175/bams-d-12-00203.1

Yang, K., Watanabe, T., Koike, T., Li, X., Fujii, H., Tamagawa, K., Ma, Y., and Ishikawa, H. (2007a). Auto-calibration system developed to assimilate AMSR-E data into a land surface model for estimating soil moisture and the surface energy budget. *J. Meteorol. Soc. Jpn. Ser.* II 85, 229–242.

Yang, K., Wu, H., Qin, J., Lin, C., Tang, W., and Chen, Y. (2014). Recent climate changes over the Tibetan Plateau and their impacts on energy and water cycle: a review. *Global Planet. Change* 112, 79–91. doi:10.1016/j.gloplacha.2013.12.001

Yang, M., Nelson, F. E., Shiklomanov, N. I., Guo, D., and Wan, G. (2010). Permafrost degradation and its environmental effects on the Tibetan Plateau: a review of recent research. *Earth Sci. Rev.* 103, 31–44. doi:10.1016/j.earscirev.2010.07.002

Yang, Y., Chen, R.-S., Ye, B.-S., Song, Y.-X., Liu, J.-F., Han, C.-T., et al. (2013b). Heat and water transfer processes on the typical underlying surfaces of frozen soil in cold regions (I): model comparison. *J. Glaciol. Geocryol.* 35, 1545–1554. [in Chinese with English abstract]. doi:10.7522/j.issn.1000-0240.2013.0171

Yao, T., Thompson, L., Yang, W., Yu, W., Gao, Y., Guo, X., et al. (2012). Different glacier status with atmospheric circulations in Tibetan Plateau and surroundings. *Nat. Clim. Change* 2 (9), 663–667. doi:10.1038/nclimate1580.

Yi, S., He, Y., Guo, X., Chen, J., Wu, Q., Qin, Y., et al. (2018a). The physical properties of coarse-fragment soils and their effects on permafrost dynamics: a case study on the central Qinghai-Tibetan Plateau. *Cryosphere* 12, 3067–3083. doi:10.5194/tc-12-3067-2018

Yi, Y., Kimball, J. S., Chen, R. H., Moghaddam, M., Reichle, R. H., Mishra, U., et al. (2018b). Characterizing permafrost active layer dynamics and sensitivity to landscape spatial heterogeneity in Alaska. *Cryosphere* 12, 145–161. doi:10.5194/tc-12-145-2018

Yi, Y., Kimball, J. S., Rawlins, M. A., Moghaddam, M., and Euskirchen, E. S. (2015). The role of snow cover affecting boreal-arctic soil freeze-thaw and carbon dynamics. *Biogeosciences* 12, 5811–5829. doi:10.5194/bg-12-5811-2015

Yue, T., Zhao, N., Fan, Z., Li, J., Chen, C., Lu, Y., et al. (2016). CMIP5 downscaling and its uncertainty in China. *Global Planet. Change* 146, 30–37. doi:10.1016/j.gloplacha.2016.09.003

Zhang, T. (2005). Influence of the seasonal snow cover on the ground thermal regime: an overview. *Rev. Geophys.* 43. doi:10.1029/2004rg000157

Zhang, Y.-F., Hoar, T. J., Yang, Z.-L., Anderson, J. L., Toure, A. M., and Rodell, M. (2014). Assimilation of MODIS snow cover through the data assimilation research testbed and the community land model version 4. *J. Geophys. Res. Atmos.* 119, 7091–7103. doi:10.1002/2013jd021329

Zhang, Y. L., Li, X., Cheng, G. D., Jin, H. J., Yang, D. W., Flerchinger, G. N., et al. (2018). Influences of topographic shadows on the thermal and hydrological processes in a cold region mountainous watershed in northwest China. *J. Adv. Model. Earth Syst.* 10, 1439–1457. doi:10.1029/2017ms001264

Zhao, L., Ping, C.-L., Yang, D., Cheng, G., Ding, Y., and Liu, S. (2004). Changes of climate and seasonally frozen ground over the past 30 years in Qinghai-Xizang (Tibetan) Plateau, China. *Global Planet. Change* 43, 19–31. doi:10.1016/j.gloplacha.2004.02.003

Zhao, L., Wu, Q., Marchenko, S. S., Sharkhuu, N., and Lewkowicz, A. G. (2010). Thermal state of permafrost and active layer in central asia during the international polar year. *Permafr. Periglac. Process.* 21, 198–207. doi:10.1002/ppp.688

Zhao, L., Yang, K., Qin, J., Chen, Y., Tang, W., Lu, H., et al. (2014). The scale-dependence of SMOS soil moisture accuracy and its improvement through land data assimilation in the central Tibetan Plateau. *Rem. Sens. Environ.* 152, 345–355. doi:10.1016/j.rse.2014.07.005

Zhao, L., Zou, D., Hu, G., Du, E., Pang, Q., Xiao, Y., et al. (2020). Changing climate and the permafrost environment on the qinghai–tibet (xizang) plateau. *Permafr. Periglac. Process.* 31 (3), 396–405. doi:10.1002/ppp.2056

Zhao, S.-P., Nan, Z.-T., Huang, Y.-B., and Zhao, L. (2017a). The application and evaluation of simple permafrost distribution models on the qinghai-tibet plateau. *Permafr. Periglac. Process.* 28, 391–404. doi:10.1002/ppp.1939

Zhao, T., Shi, J., Hu, T., Zhao, L., Zou, D., Wang, T., et al. (2017b). Estimation of high-resolution near-surface freeze/thaw state by the integration of microwave and thermal infrared remote sensing data on the Tibetan Plateau. *Earth and Space Science* 4, 472–484. doi:10.1002/2017ea000277

Zhao, T., Zhang, L., Jiang, L., Zhao, S., Chai, L., and Jin, R. (2011). A new soil freeze/thaw discriminant algorithm using AMSR-E passive microwave imagery. *Hydrol. Process.* 25, 1704–1716. doi:10.1002/hyp.7930

Zhao, W. L., Gentine, P., Reichstein, M., Zhang, Y., Zhou, S., Wen, Y., et al. (2019). Physics-constrained machine learning of evapotranspiration. *Geophys. Res. Lett.* 46 (24), 14496–14507. doi:10.1029/2019GL085291

Zheng, D., Li, X., Wang, X., Wang, Z., Wen, J., Van Der Velde, R., et al. (2019a). Sampling depth of L-band radiometer measurements of soil moisture and freeze-thaw dynamics on the Tibetan Plateau. *Rem. Sens. Environ.* 226, 16–25. doi:10.1016/j.rse.2019.03.029

Zheng, G., Yang, Y., Yang, D., Dafflon, B., Lei, H., and Yang, H. (2019b). Satellite-based simulation of soil freezing/thawing processes in the northeast Tibetan Plateau. *Rem. Sens. Environ.* 231, 111269. doi:10.1016/j.rse.2019.111269

Zheng, G., Yang, Y., Yang, D., Dafflon, B., Yi, Y., Zhang, S., et al. (2020). Remote sensing spatiotemporal patterns of frozen soil and the environmental controls over the Tibetan Plateau during 2002–2016. *Rem. Sens. Environ.* 247, 111927. doi:10.1016/j.rse.2020.111927

Zhou, J., Kinzelbach, W., Cheng, G., Zhang, W., He, X., and Ye, B. (2013). Monitoring and modeling the influence of snow pack and organic soil on a permafrost active layer, Qinghai-Tibetan Plateau of China. *Cold Reg. Sci. Technol.* 90-91, 38–52. doi:10.1016/j.coldregions.2013.03.003

Zhou, J., Wang, G., Li, X., Yang, Y., and Pan, X. (2008). Data assimilation algorithm apply to energy-water balance analysis of the high cold ecosystem at Qinghai-Tibet plain, Northwest China. *Adv. Earth Sci.* 23, 965–973.

Zhu, F., Cuo, L., Zhang, Y., Luo, J.-J., Lettenmaier, D. P., Lin, Y., et al. (2017). Spatiotemporal variations of annual shallow soil temperature on the Tibetan Plateau during 1983–2013. *Clim. Dynam.* 51, 2209–2227. doi:10.1007/s00382-017-4008-z

Zhu, W., Lű, A., and Jia, S. (2013). Estimation of daily maximum and minimum air temperature using MODIS land surface temperature products. *Rem. Sens. Environ.* 130, 62–73. doi:10.1016/j.rse.2012.10.034

Zou, D., Zhao, L., Sheng, Y., Chen, J., Hu, G., Wu, T., et al. (2017). A new map of permafrost distribution on the Tibetan Plateau. *Cryosphere* 11, 2527–2542. doi:10.5194/tc-11-2527-2017

Zuerndorfer, B., and England, A. W. (1992). Radiobrightness decision criteria for freeze/thaw boundaries. *IEEE Trans. Geosci. Rem. Sens.* 30, 89–102. doi:10.1109/36.124219

Conflict of Interest: The authors declare that the research was conducted in the absence of any commercial or financial relationships that could be construed as a potential conflict of interest.

frontiers in Earth Science

REVIEW
published: 04 December 2020
doi: 10.3389/feart.2020.574707

Hydrological Basis and Discipline System of Cryohydrology: From a Perspective of Cryospheric Science

Yongjian Ding[1,2,3,4], Shiqiang Zhang[5,6]*, Rensheng Chen[3], Tianding Han[1], Haidong Han[2,3], Jinkui Wu[3], Xiangying Li[5,6], Qiudong Zhao[1,2,3], Donghui Shangguan[1,2], Yong Yang[3], Junfeng Liu[3], Shengxia Wang[3], Jia Qin[3] and Yaping Chang[3]*

[1]State Key Laboratory of Cryospheric Science, Northwest Institute of Eco-Environment and Resources, Chinese Academy of Sciences, Lanzhou, China, [2]China-Pakistan Joint Research Center on Earth Science, Chengdu, China, [3]Key Laboratory of Ecohydrology of Inland River Basin, Chinese Academy of Sciences, Lanzhou, China, [4]University of Chinese Academy Sciences, Beijing, China, [5]Shaanxi Key Laboratory of Earth Surface System and Environmental Carrying Capacity, Northwest University, Xi'an, China, [6]College of Urban and Environmental Sciences, Northwest University, Xi'an, China

OPEN ACCESS

Edited by:
Chunqiao Song,
Nanjing Institute of Geography and Limnology (CAS), China

Reviewed by:
Chunyu Dong,
Sun Yat-sen University, China
Fangfang Yao,
University of Colorado Boulder, United States
Rijan Bhakta Kayastha,
Kathmandu University, Nepal

***Correspondence:**
Yongjian Ding
dyj@lzb.ac.cn
Shiqiang Zhang
zhangsq@nwu.edu.cn

Specialty section:
This article was submitted to Cryospheric Sciences, a section of the journal Frontiers in Earth Science

Received: 21 June 2020
Accepted: 28 October 2020
Published: 04 December 2020

Citation:
Ding Y, Zhang S, Chen R, Han T, Han H, Wu J, Li X, Zhao Q, Shangguan D, Yang Y, Liu J, Wang S, Qin J and Chang Y (2020) Hydrological Basis and Discipline System of Cryohydrology: From a Perspective of Cryospheric Science. Front. Earth Sci. 8:574707. doi: 10.3389/feart.2020.574707

Initially, cryohydrology was referred to as hydrology involving low temperatures, for example, the hydrological study of snow, ice, frozen ground, and cold water. This discipline broadened with the development of cryospheric science and now involves hydrological processes of various cryosphere elements systematically coupled with river basin hydrological processes. However, limited studies have introduced the characteristics and discipline connotations of cryohydrology from a perspective of cryospheric science. Here, we reviewed the evolution of the connotations of cryohydrology and analyzed its hydrological basis and discipline system. Three major conclusions were drawn. (1) Cryohydrology was developed based on traditional hydrology for a single element of the cryosphere and focuses on the hydrological functions of the cryosphere and its impact on the water cycle and water supply to other spheres. (2) The hydrological basis of cryohydrology can be summarized as water conservation, runoff recharge, and hydrological regulation. In detail, the water conservation function is primarily expressed as "source of freshwater" and "cold and wet islands," the runoff recharge function is concerned with water supply, and the regulation function is effective at intra- and inter-annual scales. (3) The core research issues of cryohydrology are research methods, hydrological processes, watershed functions, and regional impact. The important characteristics of cryohydrology are frequent water phase transitions and high variability across spatial and temporal scales. Cryohydrology aims to deepen the understanding of the theoretical and cognitive levels of its mechanisms and processes, accurately quantify the hydrological functions of the basin, and promote understanding of the ecological and environmental impacts of the cryosphere.

Keywords: cryohydrology, hydrological function, discipline system, cryospheric science, cold region hydrology

INTRODUCTION

The cryosphere refers to the negative temperature zone of the surface of the Earth, which mostly exists in the form of solid water (Steffen et al., 2012). The elements of the cryosphere primarily include glaciers, ice sheets, frozen ground, snow cover, sea ice, river ice, and lake ice (IPCC, 2013). The interaction between the cryosphere and the hydrosphere is an important hydrological process affecting the Earth's climate (Slaymaker and Kelly, 2009; French and Slaymaker, 2012; National Academy of Sciences, 2012; Yao et al., 2012; Qin et al., 2018), which in turn affects the global sea level and global water-cycle processes (Ding et al., 2017). Therefore, the cryosphere is unique and plays a critical role in global water cycles (Qin et al., 2018).

Under the intensified impact of climate change, in the past decade, the hydrological impacts of the cryosphere have been increasing from the Arctic (Li et al., 2010) to the Tibetan Plateau (Immerzeel et al., 2010; Yao et al., 2019), from the Andes (Masiokas et al., 2010) to the Alps (Bavay et al., 2013; Pellicciotti et al., 2014), from the endorheic river basins (Wang et al., 2009; Zhao et al., 2015) to Siberia (Liljedahl et al., 2016; Kalyuzhnyi and Lavrov, 2017), and from high-latitude oceans to the global sea level (IPCC, 2013). Therefore, the hydrological processes of the cryosphere have become a popular topic within water science for climate change, focusing on global sea level change and the concept of "water towers," for several large rivers and their downstream basins (e.g., Georg et al., 2010; Immerzeel et al., 2010, 2019; Sorg et al., 2012; Biemans et al., 2019; Ye and Lau, 2019).

From the perspective of disciplinary systems, previous studies on cryosphere water issues focused on the hydrological processes of an individual element of the cryosphere, such as glacial hydrology (Yang, 1991; Singh, 2001; Irvine-Fynn et al., 2011), permafrost hydrology (Woo, 2012), and snow hydrology (Singh, 2001; DeWalle and Rango, 2008; Ye and Lau, 2019). For example, research on glacial hydrology primarily involves glacier melt, runoff generation, and the role of glacial runoff in the watershed (Ding et al., 2017; Immerzeel et al., 2019; Tang et al., 2019). With the increasing impact of global warming on the cryosphere, the hydrological processes of different cryosphere elements and their impacts often occur simultaneously in the same watershed or region (Ding et al., 2017). Water issues related to the cryosphere can no longer be resolved from the process and impact of a single cryosphere element. It is necessary to examine the water problems of the cryosphere from the integrated perspective of cryospheric science, which can be called cryospheric hydrology, or cryohydrology.

Initially, cryohyrdrology was referred to as hydrology at low temperatures, for example the hydrological study of snow, ice, frozen ground, and cold water (Woo, 2019). However, the discipline connotation of cryohydrology needs to be broadened from the perspective of cryospheric science. To accurately understand the hydrological effects of different cryosphere elements and the overall hydrological process of the basin under the influence of climate change, it is necessary to consider the hydrological processes of various cryosphere elements systematically and couple them with river basin hydrological processes. This is critical for properly responding to climate change and satisfying the social and economic needs of cryosphere water issues. The integrated view of different hydrological processes of the cryosphere is the core idea behind the term cryohydrology.

Although the term cryohydrology has been mentioned or used in some studies (Phillips et al., 2013; Singh, 2017; Woo, 2019), few studies have named it as an independent discipline system integrating the common and different hydrological characteristics of cryosphere elements. In this study, by condensing the core academic thoughts behind cryohydrology, we attempt to comprehensively construct its research framework from the succession of the discipline, the common hydrological characteristics of the cryosphere, to the research content, and the discipline's constituents. This study will help understand the integrated hydrological functions of the different elements of the cryosphere at the regional or global scale. The paper is organized as follows: *Introduction* introduced the background and the aim of the research; *Developing the Cryohydrology Discipline* describes the development of the cryohydrology discipline including the origin of the cryohydrology concept, and its relationship and difference with cold region hydrology; *Hydrological Basis of Cryohydrology* analyzes the hydrological basis of cryohydrology including water conservation, runoff recharge, and hydrological regulation; *Discipline System of Cryohydrology* depicts the discipline system of cryohydrology; and *Summary and Perspective* presents summary and perspective.

DEVELOPING THE CRYOHYDROLOGY DISCIPLINE

Origin of the Cryohydrology Concept

Cryospheric hydrology studies have focused on a single element of the cryosphere for a long time. For example, snowmelt runoff modelling started in the 1960s based on papers by Martinec (1960), Martinec (1965). Before that, also in the USA, snow hydrological investigations had already been carried out (US Army Snow Hydrology, 1956). The earliest attempts at quantifying the glacial meltwater proportion of watershed yield were achieved by leveraging glacier mass balance, climate, and discharge data (Collier, 1958; Henoch 1971), while a glacier physics investigation was done on the Penny Ice Cap, Baffin Island (Ward, 1955). The surface hydrology of permafrost was summarized by Dingman (1971) and Church (1974), while *in situ* observations and cursory measurements were made in permafrost areas in the early half of the twentieth century by the Cold Regions Research and Engineering Laboratory (CRREL), USA (Sellmann, 1967). With these early research works on glaciers, frozen ground, snow cover, or other elements, corresponding studies on glacier hydrological processes and snow hydrology were performed, and a discipline system based on the methodology of different elements of the cryosphere was gradually formed, including glacier hydrology (Yang, 1991), snow hydrology (DeWalle and Rango, 2008), and permafrost hydrology (Woo, 2012). They either belonged to a branch of glaciology or became a special part of hydrology.

In these studies, water issues related to cryosphere elements were often attributed to cold region hydrology (Yang et al., 2000) or permafrost hydrology (Woo, 2012). However, the term cold region hydrology was used in a broad sense and lacks scientific definition. Sometimes, cold region hydrology is limited to the hydrology of the permafrost region (Yang et al., 2000; Woo, 2012). Generally, it refers to hydrology in cold regions, including the hydrological phenomena of glaciers, frozen ground, and snow cover, as well as river and lake ice (Woo, 2008; Ding et al., 2017). Studies on multi-element hydrological phenomena of the cryosphere are sometimes also expressed as permafrost hydrology, particularly by Canadian scholars (Woo, 2012). Whether called permafrost hydrology or cold region hydrology, the research subjects concentrate on the hydrological issues of a certain cryosphere element. The discipline system inherits the respective disciplinary characteristics of each single cryosphere element and focuses on the intersection of individual cryosphere elements. In terms of research content and disciplinary structure, they are the same as the subject on a single element of the cryosphere, such as glacier hydrology and snow hydrology. The combined effect of different elements of the cryosphere at basinal, regional, and global scales were rarely addressed.

With the recent development of cryospheric science and the increasing socioeconomic demand for water resources from the cryosphere for global sustainability, research within the cryohydrology discipline urgently requires a transition from the traditional single element perspective to a multi-element, integrated, comprehensive view. Therefore, integrating cryosphere water issues into one research framework and building its disciplinary system from a perspective of cryospheric science is inevitable. In this discipline system, the hydro-thermal processes related to glaciers, frozen ground, snow cover, and lake ice, and the hydrological function of the cryosphere elements need to be considered within the same framework.

Therefore, cryohydrology can be seen as both a traditional and an emerging discipline. Traditionally, the theory and methodology of mass balance, ablation, hydrothermal processes, and generation and convergence mechanisms of single cryosphere elements are the theoretical basis of cryohydrology. However, owing to the increasing impact of global warming on the cryosphere, the hydrological processes and influences of cryosphere elements are receiving broader attention. Water issues related to the cryosphere can no longer be understood separately from the traditional hydrology of a single cryosphere element. It is necessary to move to a cryospheric science perspective, thereby promoting the formation of the cryohydrology discipline.

Relationship Between Cryohydrology and Cryospheric Science

Cryospheric science studies the formation and evolution of the cryosphere, as well as the interactions between the cryosphere and other spheres of the environment, particularly the impacts of the cryosphere on the rest of the environment and adaptation mechanisms (Qin et al., 2017; Qin et al., 2018). Cryospheric science includes: i) the mechanisms of formation, development and evolution of cryosphere elements, and their interactions; ii) the interaction between each element and the whole cryosphere, and other earth spheres including atmosphere, hydrosphere, lithosphere, and biosphere, among which the intersection of cryosphere and hydrosphere focus on the water cycle and water availability (**Figure 1A**); and iii) the impact and risk of cryospheric change on other earth spheres, including the relationship between the cryosphere and social sustainable development, particularly adaptation and countermeasures to address cryospheric changes at global and regional scales (Qin et al., 2018). Cryohydrology is accompanied by the simultaneous development of cryospheric science, and several of its research fields are closely related to the elements of cryospheric Science. From the perspective of hydrology, the hydrological effect, water cycle, and water resources of the cryosphere elements are the focus of cryohydrology.

The research tree of cryohydrology is highly similar to that of cryospheric science, and the research contents of cryohydrology make up a part of cryospheric science. In the cryospheric science discipline system, cryohydrology is located together with the impacts of water availability, sea level, and thermohaline circulation at the applied basic research level (**Figure 1B**). The formation mechanism and changes in cryosphere elements at the basic research level are the scientific basis for cryohydrology. The service, adaptation, and sustainability of water availability, and sea level change at the applied research level are the outputs of cryohydrology (**Figure 1B**).

Scope of Cryohydrology and Cold Region Hydrology

Among the cryosphere elements, except for some unstable snow cover (snow days less than two months) and short-term frozen ground (freezing periods less than fifteen days), most elements are stable and generally persist long-term. There is no commonly accepted definition for cold regions. They generally refer to high-latitude or high-altitude regions. Therefore, hydrological research in these regions has generally been called cold region hydrology (Yang et al., 2000).

The cold region can be regarded as the core area affected by the cryosphere, but does not represent its full extent, which is significantly larger. Theoretically, cryohydrology research involves all hydrological phenomena and laws in all extents, including the core area and impact area of the cryosphere, but cold region hydrology primarily involves water issues in the core areas of the cryosphere. Both cryohydrology and cold region hydrology concentrate on cryosphere elements with active hydrological functions and their impacts, thus from this perspective cold region hydrology and cryohydrology are the same.

The major difference between cold region hydrology and cryohydrology is that cold region hydrology focuses more on the special hydrological process of different cryosphere elements, including parts of or all the research methods, processes/mechanisms, basinal functions, and global/regional impacts (**Figure 2**). But cryohydrology focuses more on the common

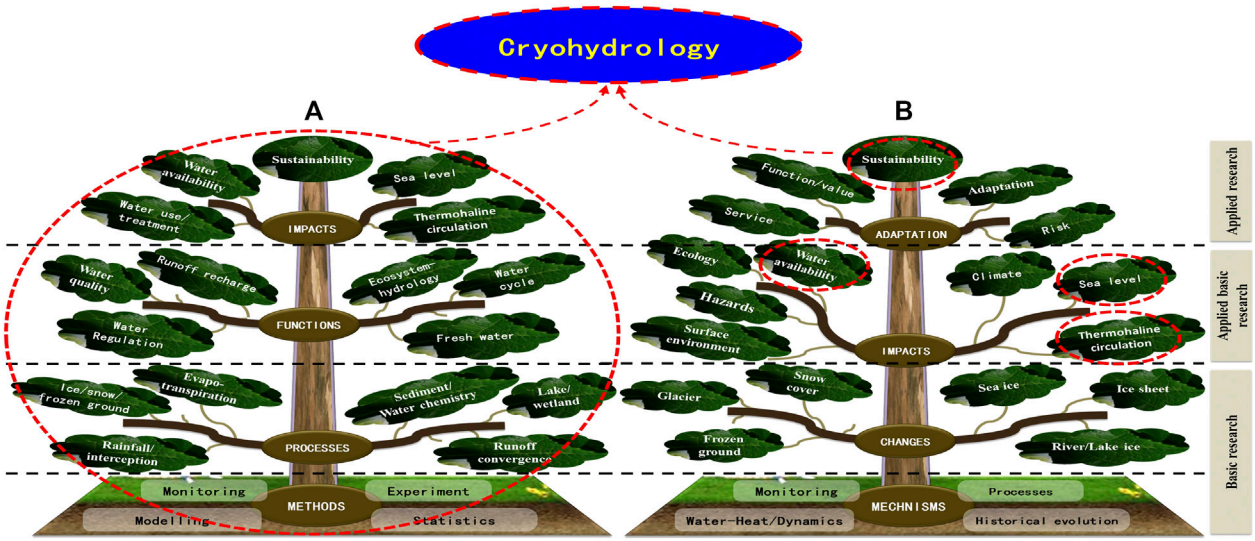

FIGURE 1 | Research content tree of hydrology **(A)** and **(B)** cryospheric science (after Qin et al., 2018) as well as and the relationship between hydrology, cryohydrology, and cryospheric science. Note that cryohydrology focuses on the water cycle and water availability, and the intersection between cryospheric science and hydrology.

characteristics of different cryosphere elements, such as the research methods of all cryosphere elements including ice shelf/iceberg, sea ice, snow cover, frozen ground, glacier/ice sheet, and the combined impact of all the elements at the basinal/global scale (**Figure 2**). For example, the study of the importance and vulnerability of the world's water towers (Immerzeel et al., 2019) concerns not only their water-supplying role in the cryosphere's core area, but also the downstream dependence of the ecosystem and society in the cryosphere's impact areas. This is typical of a cryohydrology study, but not a typical study of cold region hydrology.

Therefore, cold region hydrology studies focus on single cryosphere elements from a vertical perspective of method, process, and impact, while cryohydrology plays with the common cryosphere hydrological law of associated cryosphere elements as much as possible. For example, in cold region hydrology, glacier, permafrost, snow, river/lake ice, and sea ice are all affected by water formation (generation and convergence processes), change (increased and decreased ice volume), and impact (the function of runoff and water resources in basins, regions, and the world) (**Figure 2**). However, in the cryohydrology discipline system, the hydrothermal processes and hydrological functions in basins related to glaciers, frozen ground, snow, and river ice are studied within one framework (**Figure 2**). In addition, the cold region has area attributes, and its scope and boundaries are blurred, thus, the scientific concept of cold region hydrology is not as explicit as cryohydrology.

HYDROLOGICAL BASIS OF CRYOHYDROLOGY

The hydrological functions of different cryosphere elements and their integrated basinwide impacts are the basis of cryohydrology. They are primarily manifested as water conservation, runoff recharge, and water resource regulation.

Water Conservation

The water conservation function of cryohydrology includes two main aspects: the source of freshwater, and the cold and wet island effect. Owing to the intrinsic nature of high altitudes or high latitudes, the cryosphere is the birthplace of several of the largest rivers in the world. Several rivers originate from the high altitudes and mountains of North America, the South American Andes, Northern Europe, Siberia, the Alps, and Central Asia. Water from the cryosphere has a significant impact on the sustainable use of water resources in these areas and their downstream basins and were thus called the "water towers" (Immerzeel et al., 2019). The Qinghai-Tibet Plateau, which is also called the Asia's water tower, is the source of the Yangtze River, Yellow River, Tarim River, Nu River, Lancang River, Yili River, Irtysh River, Yarlung Zangbo River, Indus River, Ganges River, etc. (Ding et al., 2017; Yao et al., 2019). The total snow melt contribution across the full basins above 2000 m is between 65 and 72% for the Syr Darya, Amu Darya, Indus, and the Brahmaputra, and 43% for the Ganges (Armstrong et al., 2019). Freshwater sources in cryohydrology are different from rainfall runoff sources. A frozen water source converts solid water to liquid water, and releases past water storage. The cryosphere is a natural reservoir that contains frozen stock which accumulates water during the cold season and releases water during the warm season when water demand is high. The reduction of water storage volume requires long-term climate fluctuations. Therefore, the freshwater sources function of cryohydrology to some extent provides permanent and inexhaustible water sources. The renewal cycle of different elements of cryohydrology is varied. Glacier renewal cycles take hundreds to thousands of years, while ice sheet and permafrost cycles take an even longer

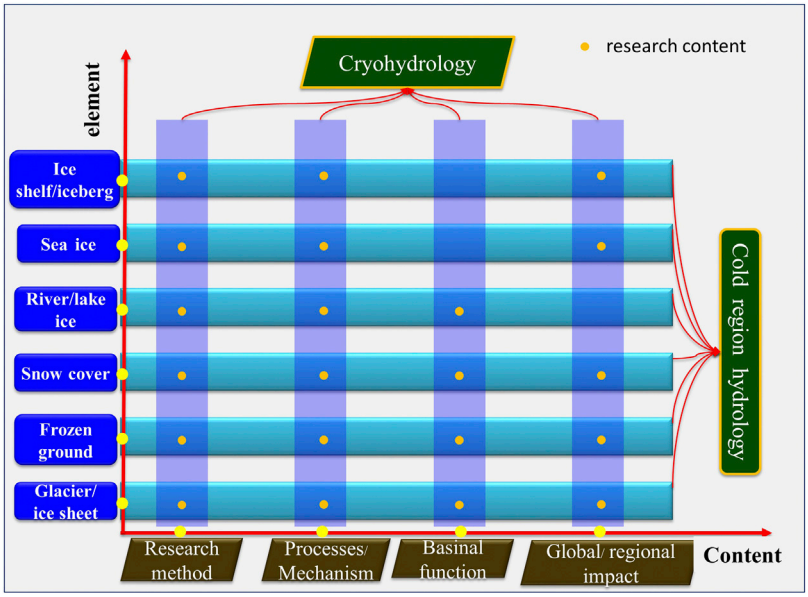

FIGURE 2 | Scope of cryohydrology and cold region hydrology. Note that cryohydrology focuses on the common hydrological law of different elements of the cryosphere, while cold region hydrology focuses on the content of the research method, processes/mechanism, basinal function, and global/regional impact of the single element of the cryosphere.

period of time. Therefore, while the cryosphere constantly receives material supplies, its melting water also consumes past accumulations. The release of historical accumulated water depends on the mass gain or loss status of the elements of the cryosphere. Under the influence of continuous warming, the cryosphere is in negative mass balance, which indicates that it has less water storage. The freshwater source function thus becomes more important under a warming world, particularly when river runoff is projected to decrease.

Another aspect of water conservation is the cold and wet island effect, which has not been fully addressed. As a widely distributed cold sphere (cold island), the cryosphere changes the temperature and humidity field and circulation patterns of the region. It can effectively trap and condense water vapor to form more local precipitation, thereby forming a local cold and humid micro environment of climate (wet island) and strengthening the horizontal turbulence and intensifying the internal turbulence field, which effectively conserves water sources (Ding and Zhang, 2018; Chen et al., 2019). In the meantime, the local convection of endorheic river basins is strengthened, and the recycled moisture over downstream deserts like the Gobi was possibly transported to the alpine region through atmospheric water vapor cycling. This increases the precipitation in alpine regions and strengthens the wet island effect of the high mountain area (Chen et al., 2019).

For example, the upper reach of Hei and Shule river basins in China's Qilian Mountains are primarily composed of glaciers, alpine cold desert, alpine meadow, and alpine steppe permafrost regions. The runoff from the Hei river was simulated by a distributed heat-water coupled (DWHC) model (Chen et al., 2008), while the runoff from the Shule river was simulated by a variable infiltration capacity (VIC-CAS) model that coupled a glacier scheme with a VIC-3L model (Zhao et al., 2015; Zhang and Sheng, 2019). Modeling results suggest that the glacier-alpine cold desert-alpine meadow and steppe of the two basins contribute more than 85% of the total runoff for the entire basin. The isotope trace method also proved that 80.2% of the annual total mountainous runoff was generated at the alpine permafrost-snow-ice zone at an altitude of above 3600 m a. s. l. (Wang et al.,2009). The annual precipitation over a glacier is nearly twice that over forests and shrubland, both in the Hei and the Shule river basins, which is consistent with the reported results that precipitation in the cryosphere and plain regions of the endorheic basin in arid regions of China can differ by 5–10 times (Yang, 1991; Ding, 1992; Chen et al., 2018). These phenomena are difficult to explain by large-scale circulation, it can only be explained by the cold and humid island effect of cryohydrology. However, the cold and wet island effect of cryohydrology still needs further quantitative study from the inter-discipline of climatology and hydrology.

Runoff Recharge

A well-known hydrological function of cryohydrology is runoff recharge. As a solid water reservoir, the cryosphere is an important freshwater resource. The resource attributes are expressed in terms of total storage volume and annual melting recharge. Reservoirs store ice present in the cryosphere and participate in river runoff and ocean circulation by melting from their frozen state. The annual river recharge by the cryosphere is an important component of land surface runoff.

Approximately 68.7% of global freshwater resources are stored in the cryosphere, with glaciers and ice sheets most dominant. The ice storage in both the Antarctic and Greenland ice sheets, and mountain glaciers are approximately 56.6, 7.3, and 0.4% of global freshwater, respectively. The annual maximum water equivalent of snow in the northern hemisphere is approximately 3×10^3 km^3 (IPCC, 2013), and one recent research suggested that the seasonal snowpack pool is between 2.6 and 3.5×10^3 km^3(Abbott et al., 2019). Based on the Second Chinese Glacier Inventory (SCGI), China has 48,571 glaciers with a total area of 51,770 km^2, accounting for approximately 7.1% of the world's glacier area (except for Antarctica and Greenland ice sheets), with ice reserves of 4,500 km^3 (Liu et al., 2015). The ground ice in the permafrost of China's Tibetan Plateau has been estimated as 9,530 km^3 (Zhao et al., 2010). According to the latest survey data, the ground ice content in the Tibetan Plateau has been updated to 12,700 km^3 (Zhao et al., 2019), which is 2.8 times the ice storage in glaciers. Snow cover in China is primarily concentrated in Xinjiang, the Qinghai–Tibet Plateau, and in northeast China. The annual maximum snow water equivalent of the three snow covered areas is approximately 960×10^8 m^3, or approximately 10% of the average annual runoff of the Yangtze River (Li et al., 2008).

On a global scale, different cryosphere elements influence the hydrological processes and water cycle on land surfaces and in the ocean in various ways. Arctic sea ice and snow meltwater greatly exceed water in the precipitation-evaporation processes of the Antarctic and Arctic oceans beyond 60° latitude. They significantly affect the strength of deep-water convection and thereby ocean thermohaline circulation. The contributions to sea level rise of thermal expansion by ocean warming of the cryosphere are nearly stable since industrialization began, if we ignore the impact of changes in land water storage. The projected contribution to global average sea level rise from the cryosphere will exceed that of thermal expansion (Ding and Zhang, 2015). At a regional scale, the cryosphere affects the seasonal distribution of river discharge under changed climate. For example, in the snowmelt-dominated Kelan River basin in the Altai mountains in China, the seasonal distribution of river discharge has changed in the last few decades. The permafrost degradation has significantly affected runoff regulation of the ratio of winter runoff to annual runoff. The ratio of maximum monthly runoff (Qmax) and minimum monthly runoff (Qmin) had changed both in the Arctic and in China. The glacier runoff in several regions has changed. For example, the estimated glacier runoff in China by a modified monthly degree day model (Zhang et al., 2012) has increased during the past 50 years.

The average annual glacial meltwater runoff in China was estimated to be 630×10^8 m^3 yr^{-1}, from 1962 to 2006 (Ding et al., 2017), which is approximately 2.2% of the total river runoff in China and is more than the average annual runoff of the Yellow River flowing into the sea. It is equivalent to 10.5% of the total river runoff ($5{,}760 \times 10^8$ m^3 yr^{-1}) of Gansu, Qinghai, Xinjiang, and Tibet in Western China. Several rivers are supplied by 15–25% of the runoff from snowmelt in Northern China (Hu, 2013). The contribution of snowmelt runoff recharge to river discharge in northern Xinjiang, particularly the Altai mountains, reaches 60–70% in comparison to 40%, 20–25%, 15–20% of the basins in the Tianshan and the Qilian Mountains, and the Tibetan Plateau, respectively.

This indicates that changes in the cryosphere will inevitably affect the global water cycle, basinal or regional hydrological processes, and water resource utilization.

Water Resource Regulation

Compared to the water conservation and runoff recharge functions, the hydrological regulation of cryohydrology is more important. Elements of the cryosphere such as glaciers, snow, and frozen ground regulate the basin wide runoff process in different ways on seasonal, interannual, and interdecadal scales, influencing the use of water resources downstream. Glaciers have a function in both seasonal and interdecadal runoff regulation. The freeze-thaw process impacts the seasonal runoff generation and convergence processes of the basin, while the changes in ground ice can affect the runoff and water resources for a very long period. Snow cover primarily affects the seasonal runoff distribution. At the basinal scale, the regulatory effect of cryohydrology is primarily reflected in its combined effect with rainfall runoff in mountainous areas, its regulating role in river basin runoff by reducing drought, as well as flood mitigation effects in different seasons and years (Ye et al., 2012; Ding and Zhang, 2018).

The interdecadal and seasonal regulation of glaciers on runoff is primarily reflected in solid reservoirs. The glaciers determine the amount of meltwater based on the water (rainfall) and heat (ablation) conditions of the basin to regulate the basin runoff process at the seasonal scale. In this manner, the river runoff in basins with glaciers remains relatively stable, which has a significant role in regulating the variation in runoff (Ye et al., 2012). This is beneficial for the use of water resources in the downstream oases of arid areas. Studies in the Cascade Mountains in the United States, the European Alps, and the arid regions of China suggest that the coefficient of variation of summer runoff in glacial-covered watersheds is significantly lower than in other areas (Chen and Ohmura, 1990; Ye et al., 1999; Casassa et al., 2009; Moore et al., 2009; Viviroli et al., 2011).

This regulatory capacity is related to glacier coverage in the watershed. When the glacial coverage of a given watershed exceeds 5% (Casassa et al., 2009; Ye et al., 2012), the regulation of glacial meltwater runoff on river runoff is significant. It primarily reduces the variation in annual runoff and decreases the annual runoff variation coefficients of the basin. Similar studies (Collins, 2006; Stahl and Moore, 2006) also demonstrate that intra-annual runoff changes in the basin decrease with increasing glacier coverage in basins with only 2–3% glacial coverage. When glacial coverage reaches 30–40%, runoff tends to be stable, but when it is higher than 40%, the variation in river runoff tends to increase (Bayard et al., 2005).

Snow cover primarily affects the seasonal distribution of river runoff. Snow has a seasonal regulation and storage function, which can temporarily accumulate a certain amount of water. The curves of the snowmelt runoff process are gentler than those of the rainfall runoff process, thereby altering the rainfall runoff

process of the basin and achieving the effect of regulating runoff. In addition, in cryospheric basins, when precipitation is abundant, solid precipitation formed at high altitudes slows the peak runoff in the form of snow, then melts after precipitation, which regulates runoff to some extent. In the alpine areas of the basin, there is more snowfall in summer with short-term accumulation, which generally affects the generation and convergence processes of river runoff.

The regulatory effect of frozen ground primarily appears as the influence of the freezing and thawing processes on runoff. These processes change the generation and confluence processes of the basin at the interannual scale, while variations in ground ice can affect the runoff and water resources of the basin for a longer period. The runoff generated from precipitation and snowmelt tends to be larger under the influence of the barrier of the frozen ground, leading to the generation of high runoff even when the precipitation is low. In summer, seasonally frozen ground melts. An active layer of permafrost also gradually melts and the lower limit of the active layer descends to a deeper location. The profile of soil moisture increases with depth, extending to deeper soil in active layers. The underground water table over permafrost declines, while the total water storage capacity of soil increases. The melting permafrost and seasonally frozen ground promotes the water storage capacity of the basin, increases evapotranspiration, and regulates runoff by cutting flood peaks. Existing studies (e.g., Bayard et al., 2005; Gibsona et al., 2011; Kalyuzhnyi and Lavrov, 2012; Liljedahl et al., 2016; Melissa and Scott, 2019; Yang et al., 2019; Huissteden van, 2020) have suggested that under climate change, permafrost will degrade by deepening the thickness of the active layer, which will increase soil water storage space, and thereby increase the amount of water from summer precipitation stored in the active layer of permafrost, leading to a prolonged convergence time of runoff. In the Arctic region, the thick ground ice in the permafrost melts and recharges to river runoff or to lakes, with climate warming. This may lead to an increase in winter (dry season) runoff in permafrost regions, a decrease in summer runoff, and a slower interannual runoff process. The intensity of change is related to the permafrost coverage of the basin.

DISCIPLINE SYSTEM OF CRYOHYDROLOGY

Research Content

Cryohydrology's discipline mainline has a method-process function-impact, and its core research issues can be sorted out along this mainline (**Figure 3**).

The research methods can be summarized as field observation and experiments, laboratory experiments and analysis, remote sensing and geographic information system applications, and mathematical statistics and model simulation.

These processes and changes are the mechanisms of cryohydrology research. The process involves three major aspects: 1) the melting, runoff generation, and convergence process, 2) the runoff change process, and 3) sediment and water chemistry. The melting, runoff generation, and convergence process includes snow/ice accumulation and melting, snow/ice meltwater convergence, frozen ground freeze/melt runoff generation and convergence, river/lake/sea ice generation and migration. The runoff change process includes characteristics of different supply to cryospheric rivers, the cryospheric meltwater runoff process, and cryospheric meltwater runoff projection. Sediment and water chemistry include river sediment changes, the water chemistry process, biogeochemical processes, and the application of water chemistry.

Cryohydrology is hydrologically crucial at the basin scale. Its functions include water conservation, river runoff recharge, regulation of water resources, and alleviation of extreme hydrological events.

Cryohydrology's main impact is in its output to other spheres. The above research issues in method, processes, and function are primarily related to the hydrological characteristics of cryosphere elements. For example, a recent study (Musselman et al.,2018) suggested that rain-on-snow becomes more frequent at higher elevations where seasonal snow cover persists due to a shift from snowfall to rainfall, with correspondingly increases the flood risk by 20–200% over North America. When the meltwater flows into the catchment, it mixes with rainfall runoff. In different parts of the basin, owing to the proportion of the meltwater runoff and the impact of the coverage of frozen ground being different, the impact of the cryosphere on river runoff varies. The impact of cryohydrology includes cryospheric and fresh water within river basins, the cryosphere as part of the global water cycle, and the cryosphere as part of sea level rise.

Discipline Characteristics

The core characteristic of cryohydrology is the phase change of water. The largest difference between cryohydrology and traditional hydrology is the frequent phase transitions between the vapor-liquid-solid states of water and the associated changes in water, energy, mass, and solute during the phase transition. Owing to the large energy exchange during the water phase change, the phase transition further affects the interactions between the atmosphere, cryosphere, hydrosphere, biosphere, and even the lithosphere. The phase transition is the link between cryohydrology and other processes in cryospheric science. Their high sensitivity to climate change is a common characteristic of the cryosphere elements, and the hydrological processes of different cryosphere elements have varied response patterns, with complicated response processes. In a specific basin, different elements of the cryosphere act together on river runoff, resulting in river runoff being very sensitive to climate change. To accurately predict runoff changes in the cryospheric basin, multi-source data, multiple experimental measures, multiple models, and multiple perspectives must be used together to project the future changes of different cryosphere elements, as well as their impact on hydrological processes.

Field observations and experiments are an important characteristic of cryohydrology. The harsh natural environment makes field observation difficult, resulting in very

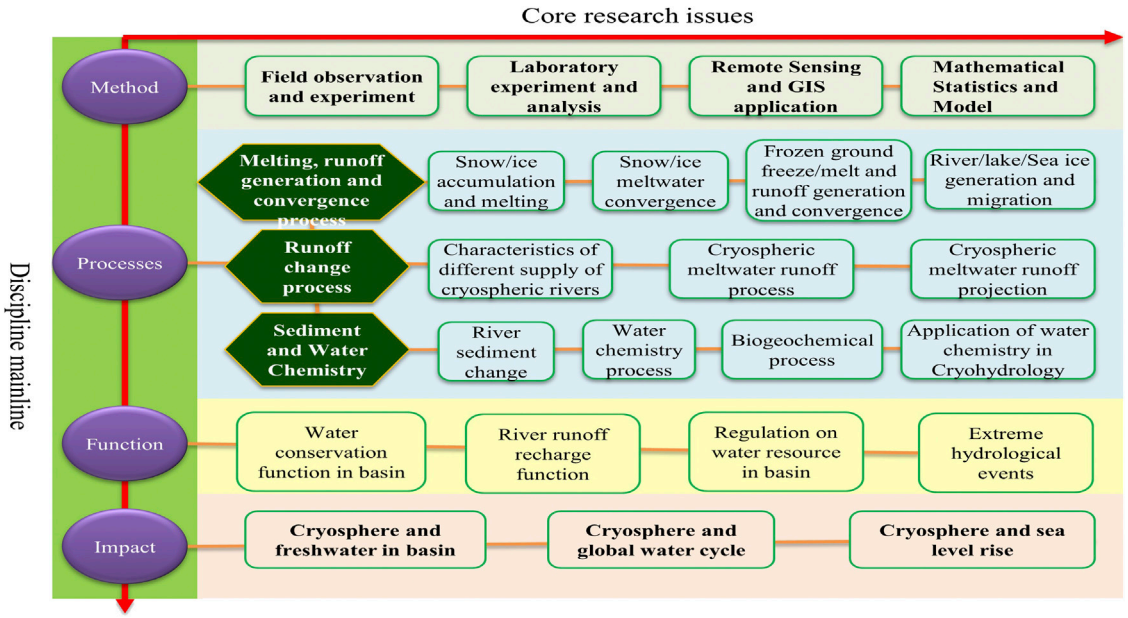

FIGURE 3 | The core research issues of cryohydrology along the discipline mainline which primarily include method (*in situ* observation, laboratory experiment, remote sensing application, and statistics/model), processes (melting, runoff generation and convergence, runoff changes, and sediment and chemistry), function (water conservation, runoff recharge, regulation, and extreme events), and impact (freshwater in basin, global water cycle, and sea level rise).

limited experimental data obtained for research. Meanwhile, cryohydrology not only requires consideration of the water cycle and water balance between different cryosphere elements at different scales, but also the energy and mass balances between them. Therefore, cryohydrology researchers need to conduct several field observations and multi-measurement experiments to satisfy the requirements of high quality *in situ* observations and experimental data.

The surplus effect is another important characteristic of the discipline. Cryohydrology not only studies the hydrological processes of the cryosphere itself, but also considers the hydrological impact on other regions outside the cryosphere. This surplus feature affects basins, regions, and even the world. The understanding of cryohydrologic processes on the formation of water resources in related regions, the hydrological functions of different components, and the potential changes of different components under future climate change scenarios are closely related to short-term, medium-term, and long-term sustainable development. One characteristic of cryohydrology is that it is the intersection of several of these disciplines. From the perspective of the mechanism, cryohydrology is a close intersection of cryospheric science, hydrology, geography, and atmospheric science. The phase transition processes of water and related water chemical processes are closely related to traditional physics and chemistry. The study of the regional and global impact of the water cycle is also closely related to social science, such as sustainable development and economics.

The last characteristic of cryohydrology is its varied temporal and broad spatial scale. Depending on the content of study, the temporal scale involved in cryohydrology ranges from hours to hundreds of years (**Figure 4**). When research issues focus on the process/mechanism, the temporal scales vary from hours to hundreds of years, with a daily or monthly scale as the general one. For example, the temporal scale of one extreme hydrological event such as a moraine-dammed lake outburst flood is generally between hours to days. When researching basinal function, the temporal scale always ranges from one to hundreds of years. For example, the intensity and frequency of extreme hydrological events probably changes under climate change, and its impact on basin also varies. When focus is on the impact of the cryosphere's freshwater cycle on the ocean, the temporal scale can reach up to a millennial scale or even longer. The spatial scales of cryohydrology range from points to global scales. The process/mechanism is generally carried out at a point/slope/field scale. The hydrological function is analyzed mostly at the basinal scale, and the impact of cryohydrology is generally illustrated at the regional/global scale (**Figure 4**). Our study found that the time scale generally increases with the expansion of the spatial scale.

Relationship Between Cryohydrology and Other Disciplines

The basis of the cryohydrology discipline comes from other related specialties. Based on the existing research foundation and scientific understanding, energy balance and water balance are the physical basis of cryohydrology and are the most basic theoretical foundation supporting its development. (**Figure 5**). In terms of the energy

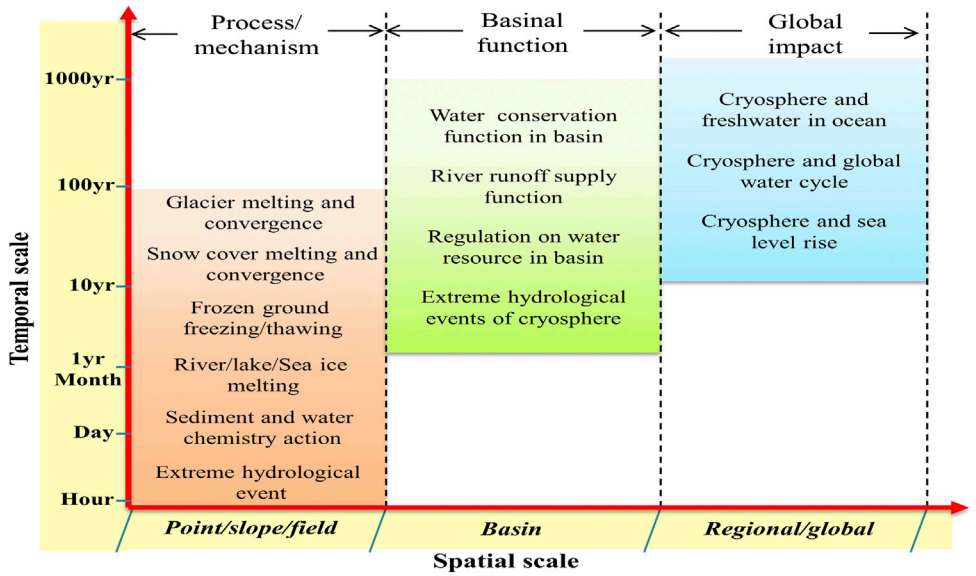

FIGURE 4 | Difference of main research contents of cryohydrology at the temporal (hour, day, month, year, and more than 1,000 years) and spatial (point/slope/field, basin, and region/global) scales.

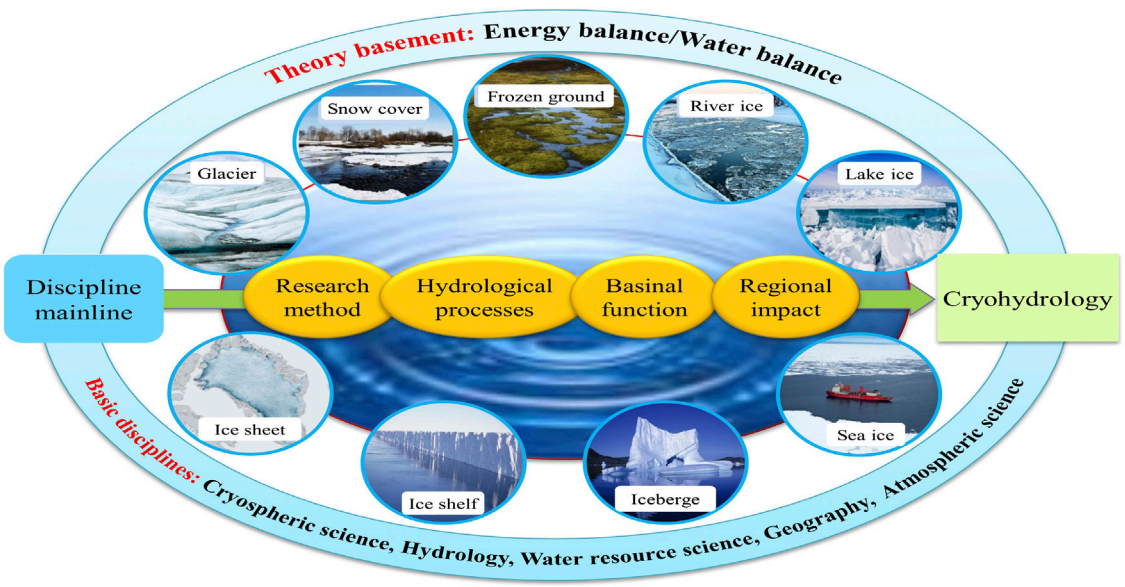

FIGURE 5 | The theory basis and basic disciplines of cryohydrology along the mainline from method, processes, and function to impact of different elements of the cryosphere.

balance theory, cryohydrology is more related to cryospheric science and atmospheric science, while water balance is more related to hydrology and water resource science. Thus, the most important basic disciplines of cryohydrology are cryospheric science and hydrology (**Figure 1**). Meanwhile, water resource science, geography, and atmospheric science are also inseparable from cryohydrology. These are all its important basic and foundational disciplines (**Figure 5**).

From this view, glaciers, snow cover, frozen ground, river ice, lake ice, sea ice, ice sheets, ice shelves, icebergs, and other elements of the cryosphere can be considered as research objects in cryohydrology; using energy balance and water balance as the theoretical basis; utilizing research method-hydrological process-watershed effect-regional impact as the mainline basis for research; and using these to conduct hydrological research on the cryosphere. The objectives of

cryohydrology are to understand the hydrological processes, clarify the hydrological functions, and understand the hydrological impacts on the society of the cryosphere.

SUMMARY AND PERSPECTIVE

This study attempts to introduce the hydrological basis and discipline system of cryohydrology from the integrated view of cryospheric science. Several conclusions were made as follows:

(1) Cryohydrology was developed based on traditional hydrology for a single element of the cryosphere and focused on the hydrological functions of the cryosphere and its impact on the water cycle and water availability of other spheres. As a discipline with significant traditional inheritance, cryohydrology needs to be further improved both in the theory of the discipline system and in the integration and systematization of the discipline.
(2) The hydrological function of cryohydrology includes water conservation, runoff recharge, and hydrological regulation. The water conservation function is primarily expressed as "freshwater source" and "cold and wet islands effect". The runoff recharge function is primarily in the supply of water, and the regulation function is primarily concerned with the intra-annual and inter-annual scales.
(3) The core research issues of cryohydrology are along the mainline of research methods, hydrological processes, watershed functions, and regional impact. The most important characteristic of cryohydrology is frequent water phase transitions at highly variate spatial and temporal scales.

Cryohydrology is not only of great significance to accurately understand and project the hydrological changes of river basins and the sustainable use of water resources. It also plays an important role in understanding the ecological and hydrological effects at the basin scale, and relevant changes in the geographic environment. However, these effects have not been fully addressed. Based on enhanced observations and experiments, the future development of cryohydrology should deepen the theoretical and cognitive levels of its mechanisms and processes. It should accurately quantify the hydrological functions on a basin scale (particularly the hydrological regulation of water resources), as well as its effects on the environment and ecosystem. It also should strengthen future research on the process and mechanism of the cryosphere's influence on the ocean.

AUTHOR CONTRIBUTIONS

YD and SZ designed the research, YD, SZ, RC, TH, HH, JW, XL, QZ, DS, YY, JL, SW, JQ, and YC performed the research and writing the draft; YD, SZ, and XL revised the draft.

ACKNOWLEDGMENTS

This work was supported by the National Natural Science Foundation of China (41730751, 41671056). A special acknowledgment should be expressed to China-Pakistan Joint Research Center on Earth Sciences that supported the implementation of this study.

REFERENCES

Abbott, B. W., Bishop, K., Zarnetske, J. P., Minaudo, C., Chapin, F. S., III, Krause, S., et al. (2019). Human domination of the global water cycle absent from depictions and perceptions. *Nat. Geosci.* 12, 533–540. 10.1038/s41561-019-0374-y

Armstrong, R. L., Rittger, K., Brodzik, M. J., Racoviteanu, A., Barrett, A. P., Singh Khalsa, S.-J., et al. (2019). Runoff from glacier ice and seasonal snow in High Asia: separating melt water sources in river flow. *Reg. Environ. Change* 19 (5), 1249–1261. doi:10.1007/s10113-018-1429-0

Bavay, M., Grünewald, T., and Lehning, M. (2013). Response of snow cover and runoff to climate change in high Alpine catchments of Eastern Switzerland. *Adv. Water Resour.* 55, 4–16. 10.1016/j.advwatres.2012.12.009

Bayard, D., Stähli, M., and Parriaux, A., FlühlerFlühler, H. (2005). The influence of seasonally frozen soil on the snowmelt runoff at two Alpine sites in southern Switzerland. *J. Hydrol.* 309 (1–4), 66–84. 10.1016/j.jhydrol.2004.11.012

Biemans, H., Siderius, C., Lutz, A. F., Nepal, S., Ahmad, B., Hassan, T., et al. (2019). Importance of snow and glacier meltwater for agriculture on the Indo-Gangetic Plain. *Natural Sustainability* 2, 594–601. 10.1038/s41893-019-0305-3

Casassa, G., López, P., Pouyaud, B., and Escobar, F. (2009). Detection of changes in glacial runoff in alpine basins: examples from North America, the Alps, central Asia and the Andes. *Hydrol. Process.* 23, 31–41. 10.1002/hyp.7194

Chen, J. and Ohmura, A. (1990). "On the influence of Alpine glaciers on runoff," in *Hydrology in mountainous regions I—hydrological measurements: the water cycle* (Wallingford, UK: IAHS Publication), 193, 117–125.

Chen, R., Han, C., Liu, J., Yang, Y., Liu, Z., Wang, L., et al. (2018). Maximum precipitation altitude on the northern flank of the Qilian Mountains, Northwest China. *Nord. Hydrol* 49 (5), 1696–1710. 10.2166/NH.2018.121

Chen, R., Lu, S., Kang, E., et al. (2008). A distributed water-heat coupled model for mountainous watershed of an inland river basin of Northwest China (I) model structure and equations. *Environ. Geol.* 53 (6), 1299–1309. 10.1007/s00254-007-0738-2

Chen, R., Zhang, S., and Yang, Y. (2019). *Impact of cryosphere change on runoff of cold regions in Western China*. Beijing: Science Press.

Church, M. (1974). "Hydrology and permafrost with reference to northern North America," in *Proc. Workshop seminar on permafrost hydrology*. Ottawa: Can. Nat. Comm.IHD, 7–20.

Collier, E. P., (1958). "Glacier variation and trends in run-off in the Canadian Cordillera," in *IAHS Publication 46, Assemble´e Ge´ne´rale de Toronto, 1957, Neiges et Glaces* (Wallingford: International Association of Hydrological Sciences), 344–357.

Collins, D. N., (2006). Climatic variation and runoff in mountain basins with differing proportions of glacier cover. *Hydrol. Res.* 37, 315–326. 10.2166/nh.2006.017

DeWalle, D. R., and Rango, A. (2008). *Principles of snow hydrology*. Cambridge: Cambridge University Press.

Ding, Y., Zhang, S., and Chen, R. (2017). *Introduction on hydrology in cold regions (in Chinese)*. Beijing: Science Press.

Ding, Y., and Zhang, S. (2018). Study on water internal recycle process and mechanism in typical mountain areas of inland basins, northwest China: progress and challenge (in Chinese with English abstract). *Adv. Earth Sci.* 33 (7), 70–78.

Ding, Y., and Zhang, S. (2015). The hydrological impact of cryosphere water cycle on global-scale water cycle (in Chinese). *Chin. Sci. Bull.* 60, 593–602. 10.1360/N972014-00899

Ding, Y., (1992). Some glacio-micrometeorological features on the north side of mount qogir(K2), karakoram mountains. *Ann. Glaciol.* 16, 67–72. 10.3189/172756406781812087

Dingman, S. L. (1971). Hydrology of the glenn creek watershed, tanana basin, central Alaska. *U.S. Army CRREL Res. Rep.* 297, 110.

French, H., and Slaymaker, O. (2012). *Changing cold environments: a Canadian perspective*. Hoboken, NJ: Wiley-Blackwell.

Georg, K., Martin, G., and Ben, M. (2010). Contribution potential of glaciers to water availability in different climate regimes. *Proc. Natl. Acad. Sci. U. S. A.* 107 (47), 20223–20227. 10.1073/pnas.1008162107

Gibsona, J. J., Yib, Y., and Birksb, S. J. (2011). Isotopic tracing of hydrologic drivers including permafrost thaw status for lakes across Northeastern Alberta, Canada: a 16-year, 50-lake assessment. *J. Hydrol.* 403 (3–4), 352–359. 10.1016/j.ejrh.2019.100643

Henoch, W. E. S. (1971). Estimate of glaciers secular (1948– 1966) volumetric change and its contribution to the discharge in the upper North Saskatchewan River Basin. *J. Hydrol.* 12, 145–160. 10.1016/0022-1694(71)90106-5

Hu, R. (2013). *Snow cover and snow hazard prevention in China*. Beijing: China Environmental Science Press.

Huissteden van, J. (2020). *Thawing permafrost*. Cham: Springer.

Immerzeel, W. W., Lutz, A. F., Andrade, M., Bahl, A., Beimans, H., Bolch, T., et al. (2020). Importance and vulnerability of the world's water towers. *Nature* 577 (7790), 364–369. doi:10.1038/s41586-019-1822-y

Immerzeel, W. W., van Beek, L. P., and Bierkens, M. F. (2010). Climate change will affect the Asian water towers. *Science* 328, 1382–1385. doi:10.1126/science.1183188

IPCC (2013). *Climate change 2013: the physical science basis*. Cambridge, CA: Cambridge University Press.

Irvine-Fynn, T. D., Hodson, A. J., Moorman, B. J., Vante, G., and Hubbard, A. L. (2011). Polythermal glacier hydrology: a review. *Rev. Geophys.* 49 (4), RG4002. 10.1029/2010RG000350

Kalyuzhnyi, I., and Lavrov, S. (2012). Basic physical processes and regularities of winter and spring river runoff formation under climate warming conditions. *Russ. Meteorol. Hydrol.* 37, 47–56. 10.3103/S1068373912010074

Kalyuzhnyi, I., and Lavrov, S. A. (2017). Mechanism of the influence of soil freezing depth on winter runoff. *Water Resource* 44, 604–613. 10.1134/S0097807817040078

Li, P., Zhang, Z., and Liu, J. (2010). Dominant climate factors influencing the Arctic runoff and association between the Arctic runoff and sea ice. *Acta Oceanol. Sin.* 29 (5), 10–20. 10.1007/s13131-010-0058-3

Li, X., Cheng, G., Jin, H., Kang, E., Che, T., Jin, R., et al. (2008). Cryospheric change in China. *Global Planet. Change* 62, 210–218. 10.1016/j.gloplacha.2008.02.001

Liljedahl, A., Boike, J., Daanen, R. P., Fedorov, A. N., Frost, G. V., Grosse, G., et al. (2016). Pan-Arctic ice-wedge degradation in warming permafrost and its influence on tundra hydrology. *Nat. Geosci.* 9, 312–318. 10.1038/ngeo2674

Liu, S., Yao, X., Guo, W., Xu, J., Shangguan, D., Wei, J., et al. (2015). The contemporary glaciers in China based on the second Chinese glacier inventory (in Chinese with English abstract). *Acta Geographic Sinica* 70 (1), 3–16. 10.11821/dlxb201501001

Martinec, J. (1965). "A representative watershed for the research of snowmelt-runoff relations," in *International Symposium on representative and experimental watersheds*. Budapest, Hungary: IAHS Publ. No. 66, 494–501.

Martinec, J. (1960). "The degree-day factor for snowmelt-runoff forecasting," in *IUGG general assembly of helsinki*. Budapest, Hungary: IAHS Publ.No. 51, Surface Waters, 468–477.

Masiokas, M. H., Villalba, R., Luckman, B. H., Christie, D. A., Betman, E., Prieto, M. R., et al. (2010). Intra-to multidecadal variations of snowpack and streamflow records in the Andes of Chile and Argentina between 30° and 37°S. *J. Hydrometeorol.* 11 (3), 822–831.

Melissa, J. L., and Scott, F. L. (2019). Effects of changing permafrost conditions on hydrological processes and fluvial fluxes. *Earth Science Rev.* 191, 212–223. 10.1016/j.earscirev.2019.02.018

Moore, R. D., Fleming, S. W., Menounos, B., Wheate, R., Fountain, A., Stahl, K., et al. (2009). Glacier change in western North America: influences on hydrology, geomorphic hazards and water quality. *Hydrol. Process.* 23, 42–61. 10.1002/hyp.7162

Musselman, K. N., Lehner, F., Ikeda, K., Clark, M. P., Prein, A. F., Liu, C., et al. (2018). Projected increases and shifts in rain-on-snow flood risk over western North America. *Nat. Clim. Change* 8 (9), 808–812. 10.1038/s41558-018-0236-4

National Academy of Sciences (2012). "Himalayan glaciers: climate change, water resources, and water security," in *Committee on himalayan glaciers, hydrology, climate change, and implications for water security, board on atmospheric studies and climate division on earth and life studies*. Washington, DC: The National Academies Press.

Pellicciotti, F., Carenzo, M., Bordoy, R., and Stoffel, M. (2014). Changes in glaciers in the Swiss Alps and impact on basin hydrology: current state of the art and future research. *Sci. Total Environ.* 493, 1152–1170. doi:10.1016/j.scitotenv.2014.04.022

Phillips, T., Rajaram, H., Colgan, W., Steffen, K., and Abdalati, W. (2013). Evaluation of cryo-hydrologic warming as an explanation for increased ice velocities in the wet snow zone, Sermeq Avannarleq, West Greenland. *J. Geophys. Res. Earth Surf.* 118, 1241–1256. 10.1002/jgrf.20079

Qin, D., Ding, Y., Xiao, C., Kang, S., Ren, J., Yang, J., et al. (2018). Cryospheric science: research framework and disciplinary system. *Nat. Sci. Rev.* 5 (2), 255–268. 10.1093/nsr/nwx108

Qin, D., Yao, T., and Ding, Y. (2017). *Introduction on cryospheric science (in Chinese)*. Beijing: Science Press.

Sellmann, P. V. (1967). Technical Report 199. *Geology of the USA CRREL permafrost tunnel, Fairbanks, Alaska*. Hanover, New Hampshire: US Army CRREL, p22.

Singh, P. (2001). *Snow and glacier hydrology*. Berlin: Springer Science & Business Media, Vol. 37.

Singh, V. P. (2017). *Handbook of applied hydrology*. 2nd Edn. McGraw-Hill Education.

Slaymaker, O., and Kelly, R. (2009). *The cryosphere and global environmental change*. Hoboken, NJ: Blackwell Publishing.

Sorg, A., Bolch, T., Stoffel, M., Solomina, O., and Beniston, M. (2012). Climate change impacts on glaciers and runoff in Tien Shan (Central Asia). *Nat. Clim. Change* 2 (10), 725–731. 10.1038/nclimate1592

Stahl, K., and Moore, R. D. (2006). Influence of watershed glacier coverage on summer streamflow in British Columbia, Canada. *Water Resour. Res.* 42, W06201. doi:10.1029/2006WR005022

Steffen, K., Yang, D., and Ryabinin, V. (2012). "ACSYS: a scientific foundation for the climate and cryosphere (CliC) project," in *Arctic climate change: the ACSYS decade and beyond. Atmospheric and oceanographic sciences library 43*. Editors P Lemke and H. W Jacobi (Dordrecht, Netherlands: Springer), 437–459.

Tang, Q., Lan, C., and Su, F. (2019). Streamflow change on the Qinghai-Tibet Plateau and its impacts (in Chinese with English abstract). *Chin. Sci. Bull.* 64, 2807–2821.

US Army Snow Hydrology (1956). *Summary report of the snow investigations*. Portland, Oregon: North Pacific Division, Corps of Engineers, 437.

Viviroli, D., Archer, D., Buytaert, W., Fowler, H. J., Greenwood, G. B., Hamlet, A. F., et al. (2011). Climate change and mountain water resources: overview and recommendations for research, management and policy. *Hydrol. Earth Syst. Sci.* 15, 471–504. doi:10.5194/hess-15-471-2011

Wang, N., Zhang, S., He, J. Q., Pu, J. C., Wu, X. B., and Jiang, X. (2009). Tracing the major source area of the mountainous runoff generation of the Heihe River in northwest China using stable isotope technique. *Chin. Sci. Bull.* 54 (16), 2751–2757. 10.1007/s11434-009-0505-8

Ward, W. H. (1955). Studies in glacier physics on the Penny ice Cap, Baffin island, 1953. Part IV: the flow of highway glacier. *J. Glaciol.* 2 (18), 592–600. doi:10.3189/002214355793702082

Woo, M. K. (2008). "Cold region atmospheric and hydrologic studies. The mackenzie GEWEX experience," in *Hydrologic process* (Springer-Verlag Berlin Heidelberg), Vol. 2.

Woo, M. K. (2019). Cryohydrology in Canada: a brief history. *Hydrol. Process.* 33 (26), 3407–3411. 10.1002/hyp.13581

Woo, M. K. (2012). *Permafrost hydrology*. Springer-Verlag Berlin Heidelberg.

Yang, Y., Wu, Q., Jin, H., Wang, Q., Huang, Y., Luo, D., et al. (2019). Delineating the hydrological processes and hydraulic connectivities under permafrost degradation on Northeastern Qinghai-Tibet Plateau, China. *J. Hydrol.* 569, 359–372. 10.1016/j.jhydrol.2018.11.068

Yang, Z. (1991). *Glacier water resources in China (in Chinese)*. Lanzhou: Gansu Science and Technology Press.

Yang, Z., Liu, X., and Zeng, Q. (2000). *Chinese cold region hydrology (in Chinese)*. Beijing: Science Press.

Yao, T., Thompson, L., Yang, W., Yu, W., Gao, Y., and Guo, X., (2012). Different glacier status with atmospheric circulations in Tibetan Plateau and surroundings. *Nat. Clim. Change* 2, 663–667. 10.1038/nclimate1580

Yao, T., Xue, Y., Chen, D., Chen, F., Thompson, L., Cui, P., et al. (2019). Recent Third Pole's rapid warming accompanies cryospheric melt and water cycle intensification and interactions between monsoon and environment: multi-disciplinary approach with observation, modeling and analysis. *Bull. Am. Meteorol. Soc.* 100 (3), 423–444. 10.1175/BAMS-D-17-0057.1

Ye, B., Ding, Y., and Jiao, K. (2012). The response of river discharge to climate warming in cold region over China. *Quat. Sci.* 32 (1), 103–110.

Ye, B., Han, T., and Ding, Y. (1999). Some changing characteristics of glacier streamflow in Northwest China (in Chinese). *J. Glaciol. Geocryol.* 21 (1), 54–58.

Ye, K., and Lau, N. (2019). Characteristics of Eurasian snowmelt and its impacts on the land surface and surface climate. *Clim. Dynam.* 52, 1115–1138. 10.1007/s00382-018-4180-9

Zhang, S., Ye, B., Liu, S., and Zhang, X. (2012). A modified monthly degree-day model for evaluating glacier runoff changes in China. Part I: model development. *Hydrol. Process.* 26 (11), 1686–1696. 10.1002/hyp.8286

Zhao, L., Ding, Y., and Liu, G. (2010). Estimates of the reserves of ground ice in permafrost regions on the Tibetan plateau. *J. Glaciol. Geocryol.* 32 (1), 1–9.

Zhao, L., and Sheng, Y. (2019). *Permafrost and changes in Tibetan plateau (in Chinese)*. Beijing: Science Press.

Zhao, Q., Ding, Y., Wang, J., Gao, H., Zhang, S., Zhao, C., et al. (2019). Projecting climate change impacts on hydrological processes on the Tibetan Plateau with model calibration against the glacier inventory data and observed streamflow. *J. Hydrol.* 573, 60–81. 10.1016/j.jhydrol.2019.03.043

Zhao, Q., Zhang, S., Ding, Y., Wang, J., Han, H., Xu, J., et al. (2015). Modeling hydrologic response to climate change and shrinking glaciers in the highly glacierized Kunma like River catchment, central Tian Shan. *J. Hydrometeorol.* 16 (6), 2383–2402. 10.1175/JHM-D-14-0231.1

Conflict of Interest: The authors declare that the research was conducted in the absence of any commercial or financial relationships that could be construed as a potential conflict of interest.

frontiers in Earth Science

REVIEW
published: 12 January 2021
doi: 10.3389/feart.2020.576838

Permafrost Hydrology of the Qinghai-Tibet Plateau: A Review of Processes and Modeling

Hongkai Gao[1,2]*, *Jingjing Wang*[2], *Yuzhong Yang*[3], *Xicai Pan*[4], *Yongjian Ding*[5,6]* and *Zheng Duan*[7]

[1]Key Laboratory of Geographic Information Science (Ministry of Education of China), East China Normal University, Shanghai, China, [2]School of Geographical Sciences, East China Normal University, Shanghai, China, [3]State Key Laboratory of Frozen Soil Engineering, Northwest Institute of Eco-Environment and Resources, Chinese Academy of Sciences, Lanzhou, China, [4]State Key Laboratory of Soil and Sustainable Agriculture, Institute of Soil Science, Chinese Academy of Sciences, Nanjing, China, [5]State Key Laboratory of Cryospheric Science, Northwest Institute of Eco-Environment and Resources, Chinese Academy of Sciences, Lanzhou, China, [6]China-Pakistan Joint Research Center on Earth Science, CAS-HEC, Islamabad, Pakistan, [7]Department of Physical Geography and Ecosystem Science, Lund University, Lund, Sweden

Permafrost extends 40% of the Qinghai-Tibet Plateau (QTP), a region which contains the headwaters of numerous major rivers in Asia. As an aquiclude, permafrost substantially controls surface runoff and its hydraulic connection with groundwater. The freeze–thaw cycle in the active layer significantly impacts soil water movement direction, velocity, storage capacity, and hydraulic conductivity. Under the accelerating warming on the QTP, permafrost degradation is drastically altering regional and even continental hydrological regimes, attracting the attention of hydrologists, climatologists, ecologists, engineers, and decision-makers. A systematic review of permafrost hydrological processes and modeling on the QTP is still lacking, however, leaving a number of knowledge gaps. In this review, we summarize the current understanding of permafrost hydrological processes and applications of some permafrost hydrological models of varying complexity at different scales on the QTP. We then discuss the current challenges and future opportunities, including observations and data, the understanding of processes, and model realism. The goal of this review is to provide a clear picture of where we are now and to describe future challenges and opportunities. We concluded that more efforts are needed to conduct long-term field measurements, employ more advanced observation technologies, and develop flexible and modular models to deepen our understanding of permafrost hydrological processes and to improve our ability to predict the future responses of permafrost hydrology to climate changes.

Keywords: permafrost, frozen soil, Qinghai-Tibet Plateau, freeze–thaw process, permafrost hydrological model

OPEN ACCESS

Edited by:
Xiuping Li,
Institute of Tibetan Plateau Research (CAS), China

Reviewed by:
Lukas Arenson,
BGC Engineering, Canada
Zhihua He,
University of Saskatchewan, Canada

***Correspondence:**
Hongkai Gao
gaohongkai2005@126.com
Yongjian Ding
dyj@lzb.ac.cn

Specialty section:
This article was submitted to Cryospheric Sciences, a section of the journal Frontiers in Earth Science

Received: *27 June 2020*
Accepted: *19 October 2020*
Published: *12 January 2021*

Citation:
Gao H, Wang J, Yang Y, Pan X, Ding Y and Duan Z (2021) Permafrost Hydrology of the Qinghai-Tibet Plateau: A Review of Processes and Modeling. Front. Earth Sci. 8:576838. doi: 10.3389/feart.2020.576838

INTRODUCTION

Permafrost, which is defined as ground that remains at or below 0°C for two or more consecutive years, covers 1.06×10^6 km^2, or approximately 40%, of the Qinghai-Tibet Plateau (QTP) (**Figure 1**; Zou et al., 2017; Zhao et al., 2020). As the source of most major Asian rivers (e.g., the Yangtze, Yellow, Indus, and Mekong; see **Figure 1**), the QTP encompasses the largest area of high-altitude permafrost

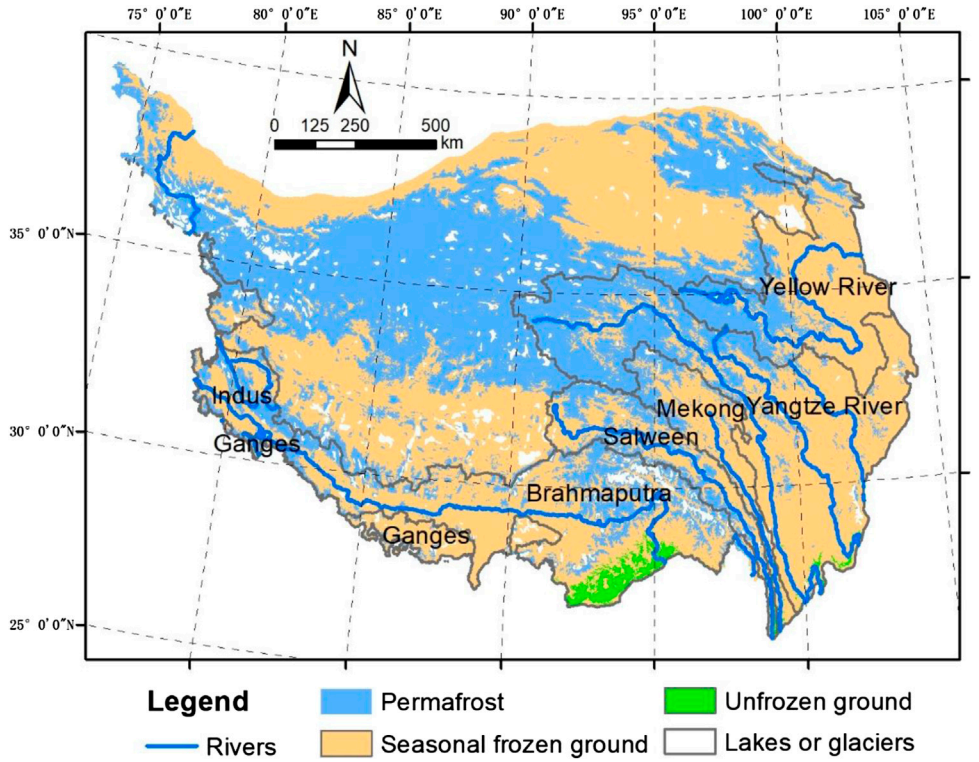

FIGURE 1 | Permafrost distribution map of the Qinghai-Tibet Plateau. The permafrost map was adapted from Zou et al. (2017), and the rivers and river basin boundary maps were obtained from the Global Runoff Data Centre (GRDC; data source: https://www.bafg.de/GRDC/EN/Home/homepage_node.html).

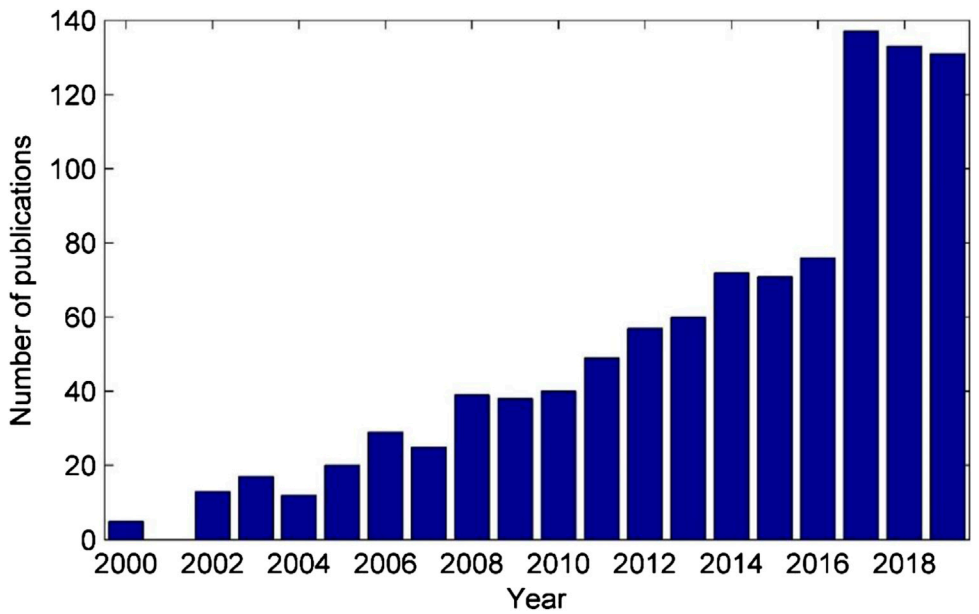

FIGURE 2 | Number of publications (2000–2019) listed in the Web of Science database for the terms "permafrost hydrology" or "frozen soil hydrology" or "permafrost water" or "frozen soil water" at "Xizang" or "Tibet" or "Qinghai" or "Heihe" or "Hei River."

and serves as the so-called water tower for nearly 1.4 billion people (Immerzeel et al., 2010). The freeze–thaw cycles of the active layer along with the aquiclude effect of the permafrost layer control the land–surface hydrology on the QTP by altering seasonal soil moisture, water storage, evaporation, and water movement through soil and vegetation (Zhang et al., 2003). The thick layer of underground ice lies near the ground surface (at depths of 1–3 m), has a thickness that ranges from 0.3 to 0.6 m (Cheng, 1983), usually occurs as lenses, and has a total volume of 1.27×10^{13} m^3 (Zhao et al., 2019). Both the vertical and lateral soil water fluxes on the QTP are strongly dependent on the soil freezing or thawing depths of the active layer, as well as the extremely low permeability of ground ice.

As the Earth's "third pole," the QTP has been getting warmer and wetter in recent decades (Chen et al., 2015; Kuang and Jiao, 2016). Air temperatures on the QTP have increased 0.3°C–0.4°C per decade over the past 5 decades, which is twice the global average warming rate (Chen et al., 2015). The most significant warming trends have occurred in the northern QTP, where continuous permafrost is present (**Figure 1**; Yang et al., 2014). Warming, associated with variations in precipitation and snow cover reduction, has resulted in the thickening of the active layer and permafrost degradation (Cheng and Wu, 2007; Zhao et al., 2019). Determining the contribution of underground ice melting to streamflow is one of the major challenges when evaluating the hydrology regime shift on the QTP under climate change (Zhao et al., 2019). Given permafrost's role as a major component of the cryosphere, its degradation is significantly altering the cold region hydrology regime (Cheng and Wu, 2007), which could result in a cascade effect on downstream water resources, a phenomenon that has already been reported in Arctic regions (Lafrenière and Lamoureux, 2019).

The interplay of the freeze–thaw process with cold region climatology, ecology, the carbon cycle, biogeochemistry, and infrastructure stability makes permafrost hydrology one of the hot topics of interdisciplinary studies, being of great interest to climatologists, ecologists, engineers, and decision-makers (Cheng et al., 2019). For example, the QTP, as the world's highest plateau and one that covers a vast area, exerts significant effects on regional-scale water fluxes and energy balance (Ma et al., 2018), and even continental-scale climate (Lu et al., 2018). The spring freeze–thaw on the QTP has a close connection with the Asian summer monsoon, as well as summer precipitation in eastern China (Wang et al., 2020). Permafrost degradation on the QTP releases carbon stored in frozen soil, likely triggering large biogeochemical changes and resulting in positive feedback to global warming (Mu et al., 2019; Wang et al., 2020). Ecosystem resilience is also threatened by permafrost degradation, the thickening of the active layer, drying of surface soil moisture, and the resultant alterations of active layer hydrology (Wang et al., 2006). Catastrophic desertification due to surface water loss occurs as a consequence of ecological degradation. In the eastern and western Tibet Plateau, desert areas have been increasing by approximately 1.8% annually (Yang et al., 2010). For permafrost infrastructure (e.g., buildings, railways, and highways), permafrost degradation results in thermokarst collapse and lake expansion, posing threats to infrastructure stability and security (Yu et al., 2008). Hence, permafrost hydrology studies on the QTP have multidisciplinary interests and broad implications for both scientific research and practical applications.

Despite the vast area of permafrost on the QTP (Cheng and Jin, 2013), our understanding of its hydrology has to some extent lagged behind that of other cold region components, that is, glacier and snow hydrology, which is a significant knowledge gap that must be filled in order to project future water resource variations under climate change (Ding et al., 2020). From a global perspective, permafrost hydrology has been intensively studied in the pan-Arctic, for example, North America and Russia, which are characterized by high-latitude climates and generally low-gradient terrain consisting of plains and wetlands (Woo et al., 2008). The QTP has a limited number of permafrost hydrology *in situ* observation areas, such as Fenghuo Mountain in the upper Yangtze River region (Wang and Zhang, 2016), the Hulugou watershed in the upper Heihe River Basin (Ma et al., 2017; Chen et al., 2018), and the Shuangchagou watershed in the source area of the Yellow River (Yang et al., 2019). The QTP permafrost has unique characteristics compared with the pan-Arctic. For instance, topographical features, including aspect and elevation, are major factors affecting permafrost distribution on the QTP. Complex mountainous terrain, as a result of neotectonic movement, leads to large spatial heterogeneities of energy and water balance. Moreover, snowfall on the QTP is not as heavy as in the pan-Arctic, since most precipitation on the QTP occurs as rainfall during the summer. Thus, although several review articles have reported the latest research progress in permafrost hydrology (Woo et al., 2008; Walvoord and Kurylyk, 2016), it is still worthwhile to review permafrost hydrology on the QTP due to its high levels of spatial heterogeneity and complexity (Cheng and Wu, 2007). From the Web of Science database, we analyzed the number of publications from 2000 to 2019 containing the terms "permafrost hydrology" or "frozen soil hydrology" or "permafrost water" or "frozen soil water" at "Xizang" or "Tibet" or "Qinghai" or "Heihe" or "Hei River" (**Figure 1**). The significant increase of publications, especially after the year 2016, demonstrates that permafrost hydrology on the QTP is a rapidly evolving discipline receiving increased attention, as documented by over 1,000 peer-reviewed articles in English.

In this study, we first reviewed the current understanding of permafrost hydrology on the QTP, including the impact of the freeze–thaw process on water movement in soil, rainfall–runoff, baseflow recession, and evaporation, as well as the impact of snow and vegetation on the freeze–thaw process. Subsequently, we reviewed permafrost hydrology modeling studies, including freeze–thaw models, catchment-scale permafrost rainfall–runoff models, model validation, and future projections. We then discussed the challenges and opportunities, including data limitation and advanced observation technology, process comprehension, and model realism testing. In the end, a general summary is provided as a conclusion.

PERMAFROST HYDROLOGY PROCESSES

Soil Water Movement

Whether in temperate or cold regions, water movement in soil is driven by water potential. The total potential at any point is the sum of the gravitational and matric (or pressure) potentials. In temperate regions, two phases of water movement in the soil porous medium need to be considered, that is, liquid water and vapor. Permafrost regions, however, exhibit more complex processes in both shallow and deep layers.

Unlike common vadose-zone soils, the existence of ice in the active layer alters the porous medium and water potential, resulting in the migration of liquid water and water vapor to the freezing front (Yu et al., 2018). At the beginning of the cold season, freezing starts at the surface and gradually moves downward. Interestingly, during this process, the soil moisture close to the freezing front moves upward, while the soil moisture close to the bottom of the supra-permafrost moves downward. An equilibrium interface (with zero-potential) may exist between the permafrost table and the freezing front. At a particular time, the bottom of the supra-permafrost begins to freeze upwards. This bidirectional freezing process and the large thermal conductivity of the frozen soil result in fast freezing (Jiao et al., 2014). In the warming season, the thawing process starts at the surface. During this process, soil moisture in the active layer moves downward, induced mostly by gravity. The thawing process usually takes four months, however, which is much slower than the freezing process (approximately 25 days) on the QTP. This is likely due to the lower amount of thermal conductivity of liquid water in topsoil, which prevents energy transfer to deep soil, thereby slowing the thawing process (Jiao et al., 2014).

In deep layers, the groundwater is controlled by the permafrost, and can be classified as three different types: supra-permafrost water, intra-permafrost water, and sub-permafrost water (Cheng and Jin, 2013). The supra-permafrost water in the seasonally thawed layer (the active layer) is sensitive to climate, and is thus significantly impacted by precipitation, temperature, snow, and vegetation (Cheng and Jin, 2013). This type of groundwater contributes most of the subsurface storm flow in warm seasons and to some degree regulates the surface runoff. Permafrost, a layer with extremely low permeability due to its low hydraulic conductivity, reduces percolation from surface water to groundwater. Thus, a shallow layer of unconfined groundwater exists in the bottom of the active layer during the thawing season; however, in the freezing season, the downward freezing acts as a water-resistant roof, resulting in a temporal layer of groundwater within the active layer. In the fast-warming permafrost regions, however, this layer might not disappear in the cold season and becomes inter-permafrost groundwater.

Sub-permafrost groundwater is defined as the water under the base of the permafrost layer (Cheng and Jin, 2013). This type of groundwater can be recharged by supra-permafrost water and surface water via non-permafrost conduits, and contributes baseflow recession or surface springs. Typically, widespread taliks—bodies or layers of unfrozen ground in permafrost regions—could form conduits when underlying permafrost disappears. Consequently, hydrogeological conditions, including groundwater flow directions, velocity, conductivity, and pathways, would be altered substantially. Particularly with climate warming, the expansion of the talik area and depth is likely increasing the hydrological connectivity between surface water (e.g., lakes and rivers) and groundwater, consequently shifting basin-scale hydrological regimes (Yang et al., 2019; O'Neill et al., 2020). Interestingly, after being "completely" frozen, unfrozen water still exists as intra-permafrost (ground ice) water, whose movement is mainly driven by temperature gradients (Cheng, 1983; Chang et al., 2015). There is a huge body of research concerning this unfrozen water because the water movement causes frost heaves, which are a significant challenge for infrastructure stability in permafrost regions (e.g., highways, railways, and pipelines). An understanding of intra-permafrost water in terms of hydrology is still generally lacking, however, indicated by the large uncertainty when estimating the release of permafrost and ground ice water to streamflow. In general, permafrost degradation can strongly influence water movement direction, velocity, storage capacity, and hydraulic conductivity.

Rainfall Runoff

Rainfall runoff is a key issue in hydrology, as it affects most permafrost regions on the QTP (Wang and Zhang, 2016). Permafrost rainfall–runoff is greatly influenced by the freeze–thaw cycle in the active, intra-permafrost, and sub-permafrost layers. The aquiclude effect of frozen soil reduces surface infiltration, increases soil moisture, and enhances surface runoff generation (Woo et al., 2008). It is well documented that permafrost increases peak flow, reduces recharge to groundwater, and amplifies streamflow seasonal variability (Ye et al., 2009).

Runoff generation in the permafrost region is controlled by multiple factors on the QTP, including soil temperature, thaw depth, precipitation frequency and amount, and antecedent soil moisture (Gao T. G. et al., 2018). The impacts of permafrost on runoff exhibit strong seasonality and are closely connected to soil temperature. It was found that the runoff coefficient is larger in spring and autumn and smaller in summer (Wang et al., 2009). This is very likely due to the seasonal variation of the thawed active layer, which has larger storage capacity and less runoff in summer and smaller storage capacity in the spring and autumn. It is interesting that permafrost hydrology only differs from that of temperate regions during the frozen season, when both precipitation and runoff are very limited on the QTP (Wang and Zhang, 2016). During the summer monsoon period, however, when dominant runoff occurs, there is no obvious difference between permafrost rainfall–runoff and that in temperate regions, given the completely thawed active layer (Wang and Zhang, 2016). The Fenghuo Mountain observatory revealed that 55–60 cm is the likely threshold thawing depth. Above this threshold depth, the thawing depth exerts a negligible impact on runoff (Wang and Zhang, 2016).

Baseflow Process

Since most rainfall–runoff processes occur beneath the surface, they generally cannot be directly measured. Hydrography itself provides a valuable and integrated signal for hydrological processes on the catchment scale. An increase of winter flow has been reported in a large number of cold regions (Liu et al., 2007). Recession flow analysis has been widely used to grasp the hydrological impacts of permafrost degradation and to derive the thawing rate of permafrost in cold regions (Lyon et al., 2009; Qin et al., 2020). Ye et al. (2009) proposed the Q_{max}/Q_{min} ratio (maximum monthly runoff divided by minimum monthly runoff) as an indicator to quantify the impact of permafrost on hydrography recession. This index has been widely used in QTP permafrost hydrology analysis, including in the headwaters of the Yellow River (Wu P. et al., 2020) and across the QTP (Liu et al., 2020; Song et al., 2020). These researchers found that there was a significant positive relationship between the Q_{max}/Q_{min} ratio and basin permafrost coverage. Most studies have found that under the influence of climate change on the QTP, Q_{max}/Q_{min} has decreased due to the decreased Q_{max} during the thawing summer season caused by the increase of infiltration and percolation, while the Q_{min} in winter has increased due to the increased groundwater recession. In other words, thawing permafrost leads to more water being routed through subsurface pathways, decreased peak flow, and increased groundwater recession. Interestingly, although an obvious basin-scale hydrological regime shift has been detected, there has been no direct evidence at the local scale reporting that the increase of taliks in permafrost have formed and enhanced the recharge to groundwater and baseflow. More intriguingly, a long-term study on the northern QTP revealed that the thawing permafrost has reduced winter runoff, for example, in the Three-River Headwaters Region and the upper Heihe River (Gao et al., 2016). The increase of deep percolation in these discontinuous permafrost regions (e.g., the upper Heihe River) could explain the decreasing trend of winter baseflow (Gao et al., 2016). In summary, hydrography recession provides a powerful indicator for understanding the impacts of permafrost on basin-scale hydrology, although the conflicting observations in different regions and scales still require further investigation.

Evaporation

Evaporation, including canopy interception, soil evaporation, water evaporation, and vegetation transpiration, is an important component in catchment water balance. Despite its importance, evaporation has not been as thoroughly explored as other hydrological processes on the QTP. The lysimeter provides accurate plot-scale evaporation data, while advanced micro-climatology observation, for example, eddy covariance, provides state-of-the-art measurements of evaporation on the field scale, and remote sensing can reveal the spatial patterns of evaporation distribution. In catchment hydrology, however, it is still common for evaporation to be derived simply from the water balance, as the residual of precipitation, runoff, and the delta of storage. The energy balance–based remote sensing approach provides an important alternative for estimating the spatial distribution and temporal variation of evaporation, although still with large uncertainty (Chen et al., 2019).

Generally, the existence of permafrost reduces the long-term average evaporation. Yang et al. (2003) discovered that freezing prevented soil moisture from evaporating on the plot scale. On the catchment scale, it was found that the runoff coefficient in permafrost regions was larger than in other regions due to the limited evaporation and larger amount of precipitation (Kang et al., 2002; Wang et al., 2009). Interestingly, when we investigated evaporation at finer temporal scales (e.g., daily), the impact of permafrost became more complex. It was found that at the beginning of the melting season, the shallow active layer leads to large supra-permafrost soil moisture, a shallow saturation zone, and a rapid increase in evaporation. This evaporation was reduced when the saturated zone moved downward due to the deepening of the active layer. A decrease of evaporation in August and September was found in the continuous permafrost region, with short-term variations coupled to precipitation events (Zhang et al., 2003; Wu et al., 2011; Wang G. X. et al., 2020). For climate change, Wang et al. (2020) proposed a new method to represent energy consumption due to ice phase changes and improved the nonlinear complementary relationship. They discovered that reductions in permafrost under a warming climate likely lead to accelerating evaporation over the QTP. Evaporation studies on the QTP remain one of the bottlenecks in hydrology and land surface research and still require more advanced measuring and modeling efforts.

Impacts of Snow and Vegetation on the Freeze–Thaw Process

Snow conditions have a significant impact on the development of soil frost. Snow cover with high albedo affects the ground thermal regime, reducing both incoming solar radiation and ground temperature. Snow as an isolation layer also prevents heat transfer between the atmosphere and soil. Thus, in winter, thick snow cover increases the soil surface temperature and reduces the depth of frozen soil. Paired-plot experiments have demonstrated that when snow cover is removed, soil freezing is deeper than in the undisturbed snow cover plot (Iwata et al., 2010; Chang et al., 2014). On the QTP, however, when the snow depth is greater than 15 cm, snow-induced thermal insulation is very limited (Zhao et al., 2018). The overall impact of snow cover on permafrost hydrology depends on the timing, duration, accumulation, and melting of snow cover (Zhou et al., 2013). There are more characteristics that influence the snow cover–permafrost relationship, such as topography, vegetation cover, and micrometeorological conditions (Zhang, 2005).

As with snow cover, vegetation helps to preserve the underlying permafrost and impacts the depth of the active layer, thereby affecting hydrology (Wang et al., 2006; Luo et al., 2018). It has been found that in well-vegetated areas, permafrost degradation was less than in locations with little vegetation (Li et al., 2015). Areas with little vegetation cover exhibited greater annual variability of soil temperature and were likely to be more sensitive to changes in air temperature. Low

TABLE 1 | A selection of hydrological models, relevant references, model characteristics, and key findings in relevant references.

Model name	References of QTP studies	Model characteristics
Stefan equation	Zhang and Wu (2012); Xie and Gough (2013)	Temperature-index freeze–thaw conceptual models providing fast solutions with less expensive computation
CoupModel	Zhou et al. (2013); Yang et al. (2013)	A numerical model for hydrological and thermal processes in the one-dimensional soil–plant–atmosphere system, including frozen soil
STEMMUS-FT	Yu et al. (2018)	A model that allows us to simulate liquid–vapor–air flow in frozen soil
Improved CoLM	Xiao et al. (2013)	Considers liquid water content in frozen soil and improves the soil liquid water content simulation of the CoLM.
DWHC/CBHM	Chen et al. (2008); Chen et al. (2018)	Water and heat transfer are coupled to simulate the impacts of frozen soil on surface hydrology
CRHM	Zhou et al. (2014)	A flexible toolkit allows us to develop tailor-made models for different cold regions
WEB-DHM	Wang et al. (2010)	Uses a temperature-based method to modify the van Genuchten equation in order to estimate the impacts of the freeze–thaw process on basin-scale hydrology
SHAW/SHAWDHM	Yang K. et al. (2013); Zhang et al. (2013)	The SHAW model was designed to simulate the soil freeze–thaw cycles and heat and water fluxes of the soil–vegetation–atmosphere transfer in cold regions
GBEHM	Gao B. et al., 2018	Energy balance and temperature-based heat transfer in frozen soil
WaSiM	Sun et al. (2020)	Hydrological processes are completely combined with soil thermodynamics
SUTRA	Evans et al. (2015)	Three-dimensional, finite element, hydrogeologic model allows us to simulate groundwater in permafrost
FEFLOW	Huang et al. (2018)	A two-dimensional model to simulate the supra-permafrost groundwater seasonal dynamics controlled by surface temperature
Soil temperature–based water saturation function	Wang et al. (2017)	A new approach to simulate the change of storage capacity after soil has frozen, which allows us to simulate the soil freeze–thaw process for basin-scale runoff generation
VIC	Cuo et al. (2015)	A physically based macroscale hydrological model that solves full water and energy balances. The frozen soil freeze–thaw process is determined by solving thermal fluxes. Runoff response is modified to reflect ice content variations in the soil

vegetation cover was also linked to higher thermal diffusivity and thermal conductivity in the soil. The maintenance of dense vegetation cover on alpine meadows was found to reduce the impact of seasonal heat cycling on the permafrost, possibly minimize the impact of climate change, and help to preserve the microenvironment of the soil (Wang G. X. et al., 2010). Additionally, the organic layer on top of the soil as well as the peat layer within the soil act as isolation layers that prevent heat transfer (Yi et al., 2007; Zhou et al., 2013).

PERMAFROST HYDROLOGICAL MODELS

There has been a revival in the development of permafrost hydrological models simulating coupled heat and water transfer (Walvoord and Kurylyk, 2016). Permafrost hydrology models are more complicated than models of temperate climate regions in terms of at least three aspects: 1) the very special solid–liquid–vapor relationship, including energy balance and phase transform, which cannot be modeled by traditional hydrology methods; 2) mountainous regions of the QTP have complex terrain and microclimates, causing significant spatial heterogeneity of almost all hydrological factors; and 3) hydrological factors in cold mountains are impacted by energy, with different phases of precipitation, radiation, and terrain shadowing. All of these factors exhibit complex daily and diurnal variations, and require detailed spatial and temporal measurements in order to sufficiently represent/capture this large variability. A key factor for water fluxes and heat transport in permafrost regions is that water undergoes a phase transition between solid ice and liquid water as the subsurface temperature fluctuates around the freezing point seasonally (Ge et al., 2011).

Freeze–Thaw Models

Physically based freeze–thaw models are based on energy and mass balance as well as heat transfer equations. Although most freeze–thaw models have governing equations that are quite similar, they differ in terms of simplification due to assumptions, numerical discretization, and diagnostic variables (Walvoord and Kurylyk, 2016). Numerous models of varying complexity have been developed to simulate freeze–thaw processes on the QTP (**Table 1**). For example, the Simultaneous Transfer of Energy Momentum and Mass in Unsaturated Soil (STEMMUS) land surface model was coupled with a freeze–thaw process, a combination known as the STEMMUS-FT, by incorporating unfrozen water content, hydraulic conductivity, and heat capacity/conductivity (Yu et al., 2018). This research has revealed that during the freeze–thaw process, not only is liquid water transferred to the freezing front but also vapor fluxes. Xiao et al. (2013) improved the Common Land Model (CoLM) by refining the permafrost algorithm and achieved an improved simulation for reproducing soil liquid water content at the Tanggula station. Yang K. et al. (2013) compared the performances of the simultaneous heat and water (SHAW) model and the coupled heat and mass transfer model (CoupModel) in simulating the transfer processes of energy and water at the Hulugou study site. They found that both models were better at simulating soil temperature than soil water content. It is worth noting that most numerical models are

computationally expensive and scale dependent due to the large spatial heterogeneity of the study field.

In addition to physically based models, temperature-index freeze–thaw conceptual models provide fast solutions with costing less computation. The Stefan equation (Xie and Gough, 2013), for example, uses the ground surface thawing (freezing) index (°C) to estimate the depth from the ground surface to the thawing (freezing) front. Zhang and Wu (2012) utilized the Stefan equation to project the change of the active layer thickness on the QTP. It is worth noting that both heat transfer models and temperature-index models are mostly 1-D vertical simulations. Meanwhile, the importance of 1-D vertical flux in catchment-scale hydrology is still not clear. Most if not all models are still too simple to describe the complex phase transition of water for the heterogeneous soil, vegetation, roots, and topographical conditions on the QTP. Thus, it is not surprising that it is still highly uncertain if involving the freeze–thaw process will increase model performance at the catchment scale, which will be discussed in *Permafrost Surface Runoff Models at the Catchment Scale*.

Permafrost Surface Runoff Models at the Catchment Scale

Most permafrost runoff modeling studies on the QTP have been based on existing catchment hydrological models coupled with different freeze–thaw modules. The freeze–thaw modules were integrated into existing physically based hydrological models by adjusting the calculations of three sets of parameters/variables: unfrozen water content, hydraulic conductivity, and heat capacity/conductivity. Chen et al. (2008), for example, designed a distributed water-heat coupled (DWHC) model and employed a simple numerical solution to the continuous water and heat equation. The DWHC model was tested in the upper Heihe River Basin. Based on the DWHC, Chen et al. (2018) further included glaciers, snow cover, and heat transfer of soil, extended their simulation to a distributed cryospheric basin hydrological model (CBHM), and used it to evaluate the effects of cryospheric changes on streamflow in the upper Heihe River Basin. Wang et al. (2010) developed a distributed hydrological model, that is, the energy budget–based distributed hydrological model (WEB-DHM), which incorporated frozen soil processes. Zhang et al. (2013) coupled the one-dimensional SHAW model with a geomorphologically based distributed hydrological model (GBHM) (Yang et al., 1998) to create the SHAWDHM model. Gao et al. (2018) extended the GBHM with cryosphere hydrological processes, developed the distributed geomorphology-based eco-hydrological model (GBEHM), and tested it in the upper Heihe River region. Zhou J. et al. (2014) employed a modular platform—the Cold Regions Hydrological Model (CRHM) (Pomeroy et al., 2007)—as a flexible toolkit to develop tailor-made models for a snowmelt-dominated high alpine basin and a soil freeze–thaw–dominated steppe basin. They found that the uncalibrated CRHM demonstrated encouraging accuracy when reproducing cold region hydrological processes, indicating its potential capability for prediction in ungauged cold basins. Sun et al. (2020) used the water balance simulation model (WaSiM) to simulate the hydrological responses to permafrost degradation in the headwaters of the Yellow River (HWYR) in High Asia and found that permafrost degradation decreased autumn runoff and increased winter/spring runoff. Cuo et al. (2015) employed the variable infiltration capacity (VIC) model with a frozen soil model to simulate soil moisture, soil temperature, soil ice content, evaporation, and runoff at 13 permafrost sites on the QTP. They discovered that precipitation plays a dominant role in surface hydrology enhancement, while frozen soil degradation is the secondary factor.

Only a few studies have been designed to couple the freeze–thaw process with existing conceptual hydrological models. Wang G. X. et al. (2017), for instance, proposed a new approach that introduced a soil temperature-based water saturation function and modified the soil water storage curve with a soil temperature threshold. By changing the water saturation function, the new model allowed us to simulate the storage capacity change after the soil had frozen, as well as the decrease of groundwater discharge caused by active layer freezing.

It is worth noting that most permafrost hydrology modeling studies on the QTP have made the a priori assumption that permafrost exerts a clear and significant effect on runoff. It is still a prevailing practice to harness a ready-to-use model, and most research efforts have been spent on forcing data preparation and parameter calibration. Intriguingly, a strong influence of permafrost on basin-scale hydrology has not always been verified in other cold regions (Shanley and Chalmers, 1999; Lindstrom et al., 2002). Conflicting conclusions obtained by modeling studies suggest that there is a need for more hypothesis-testing modeling investigations in order to accept or reject the influence of permafrost on hydrological processes at diverse scales on the QTP. Moreover, most modeling studies have been focused on 1D vertical fluxes and solving water-energy balance differential equations, while neglecting horizontal landscape heterogeneities and mountainous terrain, both of which are important factors connecting point-scale permafrost observations and basin-scale hydrograph data.

Permafrost Groundwater Models

The effects of the seasonal freeze–thaw and subsurface hydrogeological structures on groundwater recharge and discharge are critical factors in permafrost hydrology. Permafrost groundwater models provide powerful tools to quantitatively describe subsurface hydrological processes and predict future warming based on groundwater processes. Evans et al. (2015) used a three-dimensional, finite element, hydrogeological model (the saturated-unsaturated transport model, i.e., SUTRA) to evaluate the effects of climate change on groundwater movement in permafrost on the QTP. The SUTRA model simulations indicated that groundwater provides significant contributions to streams in the form of baseflow and that the majority of groundwater flow is from the shallow aquifer above the permafrost. Huang et al. (2019) used the FEFLOW hydrogeological software program to simulate supra-permafrost groundwater discharge in different land surface temperature conditions on the central QTP. They found that

topography, particularly aspect, plays an essential role in temperature, permeability, and groundwater discharge.

It is worth noting that most modeling studies have still focused on the freeze–thaw process, which has an important impact on plot-scale infiltration and groundwater recharge. Additional processes, however, for example, the thawing of underground ice, open taliks, and hydraulic connectivity, are also closely linked with permafrost runoff, but have not yet been given sufficient attention in modeling. The complex hydrogeological structures in permafrost regions pose great challenges for model development. The complexities go beyond the heterogeneous soil texture, plant roots, animal caves and wormholes, depth to rock, and permeability of bedrock, which widely exist in temperate climate regions. Permafrost hydrogeology has its own specific characteristics, for example, the complex geological characteristics of supra-permafrost, intra-permafrost, sub-permafrost, and ground ice, as well as their complex dynamics and interactions. The complex boundary conditions of the permafrost groundwater system include the water and energy budget, the impacts of snow and vegetation in the upper boundary, and the depth to rock and permeability of bedrock in the lower boundary, all of which make permafrost groundwater modeling substantially more complex than in other regions. Although a few perceptual models have been proposed to describe the permafrost-related groundwater system (Hu et al., 2019; Yang et al., 2019), physically based numerical models that can quantify these complex groundwater systems are still generally lacking.

Model Validation and Future Projection

Multivariable validation is important when testing model realism for permafrost hydrology. Variables, such as hydrograph measurements, frozen soil depth, soil temperature, snow cover, and streamflow, can all be used to validate model performance. Hydrograph information is the most widely used variable to validate catchment-scale hydrology, while soil temperature, soil water content, and frozen soil depth have generally been the variables chosen for plot-scale validation (Chen, 2008; Zhang et al., 2013; Evans et al., 2018; Yu et al., 2018; Sun et al., 2020). Zeng et al. (2016) blended satellite observations, model simulations, and *in situ* measurements to quantify soil moisture on the QTP. They discovered that there was a need to constrain the model-simulated soil moisture estimates with the *in situ* measurements prior to their further applications in scaling soil moisture satellite products. Chen et al. (2017) coupled observed snow maps to calibrate and validate a cold region hydrological model. They demonstrated the trade-off effect of snow cover area and snow water equivalent in the upper Brahmaputra River Basin. We believe that model validation with multi-source data at multiple scales is important for testing model realism.

Although it is widely recognized that permafrost degradation will result in hydrological changes on the QTP (Ge et al., 2011; Kong and Wang, 2017; Wang et al., 2018), the future relationships between permafrost degradation and the changes of streams, rivers, and lakes are still being debated. The lack of understanding concerning the mechanism behind permafrost degradation, as well as models to simulate it, remains the biggest obstacle for future projection. Take the estimation of underground ice melting as an example. The melting of ground ice increases recharge from surface water to groundwater, while the melting of ground ice itself is an important source of water that contributes to surface runoff (Yang et al., 2019). The amount of water released from ground ice is still largely uncertain in future projections, however, due to the lack of mechanism comprehension and currently available models.

CHALLENGES AND OPPORTUNITIES

Much fundamental progress has recently been made in the understanding of hydrological processes and the modeling of permafrost hydrology on the QTP (Cheng and Jin, 2013). Critical limitations in hydrologic data coverage, subsurface characterization, process-level understanding, and integrated modeling approaches still exist, however. These challenges also pose great opportunities for further exploration of permafrost hydrological processes.

Data Limitation and Advanced Observation Technology

A lack of data and inferior data quality remain two of the biggest challenges for QTP permafrost hydrology. The QTP covers a vast land area of 2.5 million km^2, but is very sparsely populated and has a limited measurement network (Yang et al., 2014). The QTP has an extremely high elevation, features a harsh climate, and lacks adequate oxygen, all of which together result in severe logistical hurdles. The formidable and even dangerous accessibility makes studying permafrost hydrology here more difficult than in other regions, resulting in poor data quality and frequent data gaps (Woo et al., 2008). Although a few local-scale long-term observations provide reliable first-hand datasets, the data issue in the permafrost region cannot be overcome in a short period of time. Tackling the data issue requires constant financial support, the dedication and enthusiasm of scientists, and the continuous investment of time and effort by researchers.

Remote sensing is a promising technique for monitoring large-scale permafrost hydrology and the land surface energy budget at various spatial and temporal resolutions in an economical way. Remote sensing techniques, including optical-thermal wavelength, passive microwave, and active microwave, have been widely implemented to fill in the data gaps on the QTP. Numerous hydrological components can be monitored by satellite remote sensing, including precipitation (Sun et al., 2018), soil moisture (Zheng et al., 2017), vegetation (Liu et al., 2017), topography and snow cover area (Che et al., 2014; Huang et al., 2017; Han et al., 2019; You et al., 2020), glacier mass balance (Brun et al., 2017), river width and water depth (Huang et al., 2018), lake variations (Wu and Zhu, 2008; Zhang et al., 2017), river flow (Huang et al., 2020), and storage variations (Xiang et al., 2016). Microwave remote sensing, for example, synthetic aperture radar, provides information on the timing, duration, and regional progression of the near-surface soil freeze–thaw status

(Zhang et al., 2009). Unlike other cryosphere components, however, many permafrost hydrological processes have subsurface features, which cannot be directly detected by remote sensing.

Geophysical detection technology allows us to measure various permafrost features at plot/field scales. For example, liquid water in frozen soil can be measured by time-domain reflectometry (TDR) and ground-penetrating radar can detect the depths of the active layer and permafrost ice layer (Wu et al., 2005; Pan et al., 2017). Gamma-ray attenuation (GRA) provides useful information for determining total water content. Combining TDR and GRA allows for the simultaneous measurement of liquid and total water content in frozen soil, and the subsequent derivation of the ice content (Zhou et al., 2014). Electromagnetic induction, electrical resistivity tomography, and seismic refraction have all shown promise for capturing the active layer thickness with good spatial coverage. These geological detection technologies have the potential to improve our understanding of permafrost degradation in climate change, evaluating the amount of melting water from permafrost, and inferring subsurface hydrological connectivity.

Water isotope and geochemical data provide important integrated and orthogonal information for catchment-scale hydrology (Liu et al., 2013). Isotope fractionation is associated with water phase transition, which provides essential auxiliary data for understanding the origin and fate of the water cycle (Kong et al., 2019). For hydrological processes, water-stable isotope data allow us to estimate the source, storage, pathway, and age of different water bodies. Wan et al. (2019) used water-stable isotope data (^{2}H, ^{18}O) to assess the thermokarst lake water balance in the headwaters of the Yellow River and proposed a perceptual model to illustrate the evolution of thermokarst lakes under permafrost degradation. Water-stable isotope studies have revealed that, as with unfrozen catchments, pre-event "old" water also plays an important role in runoff generation (Zhou et al., 2015; Ma et al., 2017), challenging the long-held belief that permafrost is an aquiclude layer. Yang et al. (2019), however, used isotope data from the headwaters of the Yellow River and drew the conclusion that rainfall ("new" water) was the most important source of streamflow and permafrost melting was another important source of streamflow. In the future, we expect to further explore isotope data in order to quantify additional processes, including evaporation, snow sublimation, snow melting, and mixing among water bodies.

Overall, remote sensing technology has advantages when exploring land surface processes and hydrology at the regional scale. Geophysical investigations definitely have the potential to identify the subsurface hydrological processes and groundwater conditions. Last, isotopic tracers exhibit great strength in illuminating runoff generation, process-based mechanism interpretation, and quantifying the study of hydrograph separation. Combining and integrating the various technologies and methods is suggested in order to further enhance our understanding of permafrost hydrological processes at diverse scales.

Improving Process Understanding and Model Realism

Field studies on the QTP continue to catalog and characterize mounting complexities and heterogeneities of permafrost hydrological processes at various scales. This is highly beneficial for accumulating first-hand data and documenting facts in order to enhance our understanding of small-scale processes. Based on field observations and experiments, many descriptive perceptual models have been proposed to describe these spatial and temporal heterogeneities. Compared with the enormous field heterogeneities, however, most modeling studies on QTP permafrost are still too parsimonious in terms of process representation, although many models utilize complex numerical solutions with expensive computations to calculate heat transfer and water movement. Most of these modeling practices could be categorized as bottom-up frameworks, meaning that the modelers assumed that small-scale physics were also appropriate at the modeling catchment scale (Sivapalan et al., 2003; McDonnell et al., 2007). Top-down modeling practices (Shanley and Chalmers, 1999; Lindstrom et al., 2002), however, found negligible influences of the freeze–thaw process on runoff at the basin scale. These seemingly counterintuitive results illustrate that permafrost likely displays a kind of self-organized pattern at the basin scale, which allows us to create simulations using surprisingly simple models. Alternatively, there are probably more dominant processes that determine permafrost hydrology than the topsoil freeze–thaw process.

Water-stable isotope data have provided valuable insights into how water and solutes are partitioned and stored, as well as their pathways, knowledge that significantly benefits model validation (Lindstrom et al., 2002; Kirchner, 2006). Ala-aho et al. (2017) extended the Spatially distributed Tracer-Aided Rainfall–Runoff (STARR) model to snow-influenced catchments and coupled the isotope fraction of snow sublimation and melting. Smith et al. (2019) adapted a tracer-aided ecohydrological model, the EcH2O-iso, for cold regions with the explicit conceptualization of dynamic soil freeze–thaw processes. These modeling frameworks have the potential to be used in QTP studies. Incorporating these new data requires us to construct more flexible and modular frameworks, which will allow us to develop tailor-made models based on specific basin characteristics, rather than using a single fixed model to fit all basins by simply calibrating parameters (Fenicia et al., 2011; Zhou et al., 2013).

Hydrology modeling is not only a science but also an art that requires modelers' creativity, inspiration, and ingenuity, as well as their experience and skill (Savenije, 2009). All models are simplifications of the real world. Hence, it is unrealistic and unnecessary to include all heterogeneous processes observed in the field in permafrost hydrology models. The appropriate level of simplification is the key for achieving model realism, which is also scale and objective dependent. In many cases, distinguishing which processes should be involved and which should be

disregarded is more important than the precision of solving numerical equations. Stepwise modeling and top-down flexible modeling frameworks allow us to develop models with a particular level of complexity in order to simulate hydrological processes, while simultaneously avoiding over-parameterization (Sivapalan et al., 2003; Gao et al., 2014a; Gao et al., 2014b). The concept of "hydrological connectivity" might be beneficial for linking local-scale observations and catchment-scale modeling, as Woo et al. (2008) suggested, and for implementation in numerous temperate basins (Gao et al., 2019).

SUMMARY

We conclude that 1) permafrost hydrology studies on the QTP are attracting broad interest, including that of hydrologists, ecologists, climatologists, and water resource managers; 2) the number of publications on QTP permafrost hydrology is mounting. Several *in situ* observation stations have been established to gather long-term measurements. Given the vast area of the QTP, however, permafrost hydrology research in this region remains far from adequate; 3) permafrost comprehensively impacts all hydrological processes on the QTP, including soil water movement, rainfall–runoff, baseflow, and evaporation; 4) permafrost hydrological modeling is a powerful tool for quantifying the spatiotemporal variations of QTP hydrological processes, and for projecting future changes. It still remains worthwhile, however, to test the importance of permafrost on basin-scale hydrology, and to incorporate landscape and topographical data in order to sufficiently represent horizontal heterogeneities; 5) data limitation will continue to exist for a long time, although *in situ* measurements, remote sensing data, isotope data, and geological detection methods are quickly improving; and 6) determining the balance point between model simplicity and catchment complexity is likely one of the most important scientific challenges yet to be solved in permafrost hydrological modeling on the QTP. Overall, the systematic and quantitative understanding of permafrost hydrology will benefit water resource management, flood mitigation, nature conservation, and adaption to climate change on the QTP and in its vast downstream regions.

AUTHOR CONTRIBUTIONS

HG, YD, and YY conceived the central idea; HG and YY wrote the initial draft of the manuscript; and all authors edited the manuscript and agreed to its submission.

FUNDING

This study was supported by the National Natural Science Foundation of China (Grant Nos. 42071081, 41801036, 4181101490, and 41771262).

ACKNOWLEDGMENTS

We thank Professor Genxu Wang for his constructive comments and discussions during the development of this manuscript. Any errors in this article are the sole responsibility of the authors. A special acknowledgement should be expressed to China-Pakistan Joint Research Center on Earth Sciences that supported the implementation of this study.

REFERENCES

Ala-Aho, P., Tetzlaff, D., Mcnamara, J. P., Laudon, H., and Soulsby, C. (2017). Using isotopes to constrain waterflux and age estimates in snow-influenced catchments using the STARR (Spatially distributed Tracer-Aided Rainfall-Runoff) model. *Hydrol. Earth Syst. Sci.* 21, 5089–5110. doi:10.5194/hess-2017-106

Brun, F., Berthier, E., Wagnon, P., Kaab, A., and Treichler, D. (2017). A spatially resolved estimate of High Mountain Asia glacier mass balances from 2000 to 2016. *Nat. Geosci.* 10, 668–673. doi:10.1038/NGEO2999

Chang, J., Wang, G. X., Gao, Y. H., and Wang, Y. B. (2014). The influence of seasonal snow on soil thermal and water dynamics under different vegetation covers in a permafrost region. *J. Mt. Sci.* 11, 727–745. doi:10.1007/s11629-013-2893-0

Chang, J., Wang, G. X., Li, C. J., and Mao, T. X. (2015). Seasonal dynamics of suprapermafrost groundwater and its response to the freeing-thawing processes of soil in the permafrost region of Qinghai-Tibet Plateau. *Sci. China Earth Sci.* 58, 727–738. doi:10.1007/s11430-014-5009-y

Che, T., Li, X., Jin, R., and Huang, C. L. (2014). Assimilating passive microwave remote sensing data into a land surface model to improve the estimation of snow depth. *Remote Sens. Environ.* 143, 54–63. doi:10.1016/j.rse.2013.12.009

Chen, D. L., Xu, B. Q., Yao, T. D., Guo, Z. T., Cui, P., Chen, F. H., et al. (2015). Assessment of past, present and future environmental changes on the Tibetan Plateau. *Chin. Sci. Bull.* 60, 3025–3035. doi:10.1360/N972014-01370

Chen, R., Lu, S., Kang, E., Ji, X., Zhang, Z., Yang, Y., et al. (2008). A distributed water-heat coupled model for mountainous watershed of an inland river basin of Northwest China (I) model structure and equations. *Env. Geol.* 53 (6), 1299–1309.

Chen, R., Wang, G., Yang, Y., Liu, J., Han, C., Song, Y., et al. (2018). Effects of cryospheric change on alpine hydrology: combining a model with observations in the upper reaches of the Hei River, China. *J. Geophys. Res. Atmos.* 123, 3414–3442. doi:10.1002/2017JD027876

Chen, X., Long, D., Hong, Y., Zeng, C., and Yan, D. H. (2017). Improved modeling of snow and glacier melting by a progressive two-stage calibration strategy with GRACE and multisource data: how snow and glacier meltwater contributes to the runoff of the Upper Brahmaputra River basin? *Water Resour. Res.* 53, 2431–2466. doi:10.1002/2016WR019656

Chen, X., Massman, W. J., and Su, Z. (2019). A column canopy-air turbulent diffusion method for different canopy structures. *J. Geophys. Res. Atmos.* 124, 488–506. doi:10.1029/2018JD028883

Cheng, G., and Wu, T. (2007). Responses of permafrost to climate change and their environmental significance, Qinghai-Tibet Plateau. *J. Geophys. Res.* 112, F02S03. doi:10.1029/2006JF000631

Cheng, G. D., Zhao, L., Li, R., Wu, X. D., Sheng, Y., Hu, G., et al. (2019). Characteristic, changes and impacts of permafrost on Qinghai-Tibet Plateau (in Chinese). *Chin. Sci. Bull.* 64, 2783–2795. doi:10.1360/TB-2019-0191

Cheng, G. D., and Jin, H. J. (2013). Groundwater in the permafrost regions on the Qinghai-Tibet Plateau and it changes. *Hydrogeol. Eng. Geol.* 40, 1–11.

Cheng, G. D. (1983). The mechanism of repeated-segregation for the formation of thick layered ground ice. *Cold Reg. Sci. Technol.* 8, 57–66.

Cuo, L., Zhang, Y. X., Bohn, T. J., Zhao, L., Li, J. L., Liu, Q. M., et al. (2015). Frozen soil degradation and its effects on surface hydrology in the northern Tibetan Plateau. *J. Geophys. Res. Atmosp.* 120, 8276–8298. doi:10.1002/2015JD023193

Ding, Y. J., Zhang, S. Q., and Chen, R. S. (2020). Cryospheric hydrology: decode the largest freshwater reservoir on Earth. *Bull. Chin. Acad. Sci.* 35, 414–424.

Evans, S. G., Ge, S., Voss, C. I., and Molotch, N. P. (2018). The role of frozen soil in groundwater discharge predictions for warming alpine watersheds. *Water Resour. Res.* 54, 1599–1615. doi:10.1002/2017WR022098

Evans, S. G., Ge, S. M., and Liang, S. H. (2015). Analysis of groundwater flow in mountainous, headwater catchments with permafrost. *Water Resour. Res.* 51, 9564–9576. doi:10.1002/2015WR017732

Fenicia, F., Kavetski, D., and Savenije, H. H. G. (2011). Elements of a flexible approach for conceptual hydrological modeling: 1. Motivation and theoretical development. *Water Resour. Res.* 47. doi:10.1029/2010WR010174

Gao, B., Yang, D. W., Qin, Y., Wang, Y. H., Li, H. Y., Zhang, Y. L., et al. (2018). Change in frozen soils and its effect on regional hydrology, upper Heihe basin, northeastern Qinghai-Tibetan Plateau. *Cryosphere.* 12, 657–673. doi:10.5194/tc-2016-289

Gao, H., Hrachowitz, M., Fenicia, F., Gharari, S., and Savenije, H. H. G. (2014a). Testing the realism of a topography-driven model (FLEX-Topo) in the nested catchments of the Upper Heihe, China. *Hydrol. Earth Syst. Sci.* 18, 1895–1915. doi:10.5194/hess-18-1895-2014

Gao, H., Hrachowitz, M., Schymanski, S. J., Fenicia, F., Sriwongsitanon, N., and Savenije, H. H. G. (2014b). Climate controls how ecosystems size the root zone storage capacity at catchment scale. *Geophys. Res. Lett.* 41, 7916–7923. doi:10.1002/2014GL061668

Gao, H. K., Birkel, C., Hrachowitz, M., Tetzlaff, D., Soulsby, C., and Savenije, H. H. G. (2019). A simple topography-driven and calibration-free runoff generation module. *Hydrol. Earth Syst. Sci.* 23, 787–809. doi:10.5194/hess-23-787-2019

Gao, T. G., Zhang, T. J., Cao, L., Kang, S. C., and Sillanpaa, M. (2016). Reduced winter runoff in a mountainous permafrost region in the northern Tibetan Plateau. *Cold Reg. Sci. Technol.* 126, 36–43. doi:10.1016/j.coldregions.2016.03.007

Gao, T. G., Zhang, T. J., Guo, H., Hu, Y. T., Shang, J. G., and Zhang, Y. L. (2018). Impacts of the active layer on runoff in an upland permafrost basin, northern Tibetan Plateau. *PLoS One.* 13. doi:10.1371/journal.pone.0192591

Gao, T., Kang, S., Chen, R., Zhang, T., and Zhang, Y. (2019). Riverine dissolved organic carbon and its optical properties in a permafrost region of the upper heihe river basin in the northern Tibetan plateau. *Sci. Total Environ.* 686, 370–381. doi:10.1016/j.scitotenv.2019.05.478

Ge, S. M., Mckenzie, J., Voss, C., and Wu, Q. B. (2011). Exchange of groundwater and surface-water mediated by permafrost response to seasonal and long term air temperature variation. *Geophys. Res. Lett.* 38. doi:10.1029/2011GL047911

Han, P. F., Long, D., Han, Z. Y., Du, M. D., Dai, L. Y., and Hao, X. H. (2019). Improved understanding of snowmelt runoff from the headwaters of China's Yangtze River using remotely sensed snow products and hydrological modeling. *Remote Sens. Environ.* 224, 44–59. doi:10.1016/j.rse.2019.01.041

Hu, Y. L., Ma, R., Wang, Y. X., Chang, Q. X., Wang, S., Ge, M. Y., et al. (2019). Using hydrogeochemical data to trace groundwater flow paths in a cold alpine catchment. *Hydrol. Process.* 33, 1942–1960. doi:10.1002/hyp.13440

Huang, K. W., Dai, J. C., Wang, G. X., Chang, J., Lu, Y. Q., Song, C. L., et al. (2019). The impact of land surface temperatures on suprapermafrost groundwater on the central Qinghai-Tibet Plateau. *Hydrol. Process.* 34, 1475–1488. doi:10.1002/hyp.13677

Huang, Q., Long, D., Du, M., Han, Z., and Pengfei, H. (2020). Daily continuous river discharge estimation for ungauged basins using a hydrologic model calibrated by satellite altimetry: implications for the SWOT mission. *Water Resour. Res.* 56, e2020WR027309. doi:10.1029/2020WR027309

Huang, Q., Long, D., Du, M. D., Zeng, C., Li, X. D., Hou, A. Z., et al. (2018). An improved approach to monitoring Brahmaputra river water levels using retracked altimetry data. *Remote Sens. Environ.* 211, 112–128. doi:10.1016/j.rse.2018.04.018

Huang, X. D., Deng, J., Wang, W., Feng, Q. S., and Liang, T. G. (2017). Impact of climate and elevation on snow cover using integrated remote sensing snow products in Tibetan Plateau. *Remote Sens. Environ.* 190, 274–288. doi:10.1016/j.rse.2016.12.028

Immerzeel, W. W., Van Beek, L. P. H., and Bierkens, M. F. P. (2010). Climate change will affect the asian water towers. *Science.* 328, 1382–1385. doi:10.1126/science.1183188

Immerzeel, W. W., Wanders, N., Lutz, A. F., Shea, J. M., and Bierkens, M. F. P. (2015). Reconciling high-altitude precipitation in the upper Indus basin with glacier mass balances and runoff. *Hydrol. Earth Syst. Sci.* 19, 4673–4687. doi:10.5194/hess-19-4673-2015

Iwata, Y., Hayashi, M., Suzuki, S., Hirota, T., and Hasegawa, S. (2010). Effects of snow cover on soil freezing, water movement, and snowmelt infiltration: a paired plot experiment. *Water Resour. Res.* 46. doi:10.1029/2009WR008070

Jiao, Y. L., Li, R., Zhao, L., Wu, T. H., Xiao, Y., Hu, G. J., et al. (2014). Processes of soil thawing-freezing and features of soil moisture migration in the permafrost active layer. *J. Glaciol. Geocryol.* 36, 237–247.

Kang, E. S., Cheng, G. D., Lan, Y. C., Chen, R. S., and Zhang, J. S. (2002). Application of a conceptual hydrological model in the runoff forecast of a mountainous watershed. *Adv. Earth Sci.* 18–26.

Kirchner, J. W. (2006). Getting the right answers for the right reasons: Linking measurements, analyses, and models to advance the science of hydrology. *Water Resour. Res.* 42, W03S04. doi:10.1029/2005WR004362

Kong, Y., and Wang, C. H. (2017). Responses and changes in the permafrost and snow water equivalent in the Northern Hemisphere under a scenario of 1.5°C warming. *Adv. Clim. Change Res.* 8, 235–244. doi:10.1016/j.accre.2017.07.002

Kong, Y., Wang, K., Pu, T., and Shi, X. (2019). Nonmonsoon precipitation dominates groundwater recharge beneath a monsoon-affected glacier in Tibetan plateau. *J. Geophys. Res. Atmos.* 124, 10913–10930. doi:10.1029/2019JD030492

Kuang, X., and Jiao, J. J. (2016). Review on climate change on the Tibetan Plateau during the last half century. *J. Geophys. Res. Atmos.* 121, 3979–4007. doi:10.1002/2015JD024728

Lafrenière, M. J., and Lamoureux, S. F. (2019). Effects of changing permafrost conditions on hydrological processes and fluvial fluxes. *Earth Sci. Rev.* 191, 212–223. doi:10.1016/j.earscirev.2019.02.018

Li, Z., Tang, P. P., Zhou, J. M., Tian, B. S., Chen, Q., and Fu, S. T. (2015). Permafrost environment monitoring on the Qinghai-Tibet Plateau using time series ASAR images. *Int. J. Digit. Earth.* 8, 840–860. doi:10.1080/17538947.2014.923943

Lindstrom, G., Bishop, K., and Lofvenius, M. O. (2002). Soil frost and runoff at Svartberget, northern Sweden - measurements and model analysis. *Hydrol. Process.* 16, 3379–3392. doi:10.1002/hyp.1106

Liu, F. J., Hunsaker, C., and Bales, R. C. (2013). Controls of streamflow generation in small catchments across the snow-rain transition in the Southern Sierra Nevada, California. *Hydrol. Process.* 27, 1959–1972. doi:10.1002/hyp.9304

Liu, J. S., Wang, S. Y., and Huang, Y. Y. (2007). Effect of climate change on runoff in a basin with mountain permafrost, northwest China. *Permafr. Periglac. Process.* 18, 369–377. doi:10.1002/ppp.602

Liu, L., Zhang, W. J., Lu, Q. F., Jiang, H. R., Tang, Y., Xiao, H. M., et al. (2020). Hydrological impacts of near-surface soil warming on the Tibetan Plateau. *Permafr. Periglac. Process.* 31, 324–336. doi:10.1002/ppp.2049

Liu, S. L., Cheng, F. Y., Dong, S. K., Zhao, H. D., Hou, X. Y., and Wu, X. (2017). Spatiotemporal dynamics of grassland aboveground biomass on the Qinghai-Tibet Plateau based on validated MODIS NDVI. *Sci. Rep.* 7, 4182. doi:10.1038/s41598-017-04038-4

Lu, M., Yang, S., Li, Z., He, B., He, S., and Wang, Z. (2018). Possible effect of the Tibetan plateau on the "upstream" climate over west Asia, North africa, south europe and the north atlantic. *Clim. Dynam.* 51, 1485–1498. doi:10.1007/s00382-017-3966-5

Luo, D., Jin, H., Jin, X., He, R., Li, X., Muskett, R. R., et al. (2018). Elevation-dependent thermal regime and dynamics of frozen ground in the Bayan Har Mountains, northeastern Qinghai-Tibet Plateau, southwest China. *Permafr. Periglac. Process.* 29, 257–270. doi:10.1002/ppp.1988

Lyon, S. W., Destouni, G., Giesler, R., Humborg, C., Morth, M., Seibert, J., et al. (2009). Estimation of permafrost thawing rates in a sub-arctic catchment using recession flow analysis. *Hydrol. Earth Syst. Sci.* 13, 595–604. doi:10.5194/hessd-6-63-2009

Ma, R., Sun, Z. Y., Hu, Y. L., Chang, Q. X., Wang, S., Xing, W. L., et al. (2017). Hydrological connectivity from glaciers to rivers in the Qinghai-Tibet Plateau: roles of suprapermafrost and subpermafrost groundwater. *Hydrol. Earth Syst. Sci.* 21, 4803–4823. doi:10.5194/hess-21-4803-2017

Ma, Y. M., Wang, Y. Y., and Han, C. B. (2018). Regionalization of land surface heat fluxes over the heterogeneous landscape: from the Tibetan Plateau to the third pole region. *Int. J. Rem. Sens.* 39, 5872–5890. doi:10.1080/01431161.2018.1508923

Mcdonnell, J. J., Sivapalan, M., Vache, K., Dunn, S., Grant, G., Haggerty, R., et al. (2007). Moving beyond heterogeneity and process complexity: a new vision for watershed hydrology. *Water Resour. Res.* 43. doi:10.1029/2006WR005467

Mu, C. C., Zhang, F., Chen, X., Ge, S. M., Mu, M., Jia, L., et al. (2019). Carbon and mercury export from the Arctic rivers and response to permafrost degradation. *Water Res.* 161, 54–60. doi:10.1016/j.watres.2019.05.082

O'neill, H. B., Roy-Leveillee, P., Lebedeva, L., and Ling, F. (2020). Recent advances (2010–2019) in the study of taliks. *Permafr. Periglac. Process.* 31, 346–357. doi:10.1002/ppp.2050

Pan, X. C., Yu, Q. H., You, Y. H., Chun, K. P., Shi, X. G., and Li, Y. P. (2017). Contribution of supra-permafrost discharge to thermokarst lake water balances on the northeastern Qinghai-Tibet Plateau. *J. Hydrol.* 555, 621–630. doi:10.1016/j.jhydrol.2017.10.046

Pomeroy, J. W., Gray, D. M., Brown, T., Hedstrom, N. R., Quinton, W. L., Granger, R. J., et al. (2007). The cold regions hydrological process representation and model: a platform for basing model structure on physical evidence. *Hydrol. Process.* 21, 2650–2667. doi:10.1002/hyp.6787

Qin, J., Ding, Y. J., and Han, T. D. (2020). Quantitative assessment of winter baseflow variations and their causes in Eurasia over the past 100 years. *Cold Reg. Sci. Technol.* 172, 102989. doi:10.1016/j.coldregions.2020.102989

Savenije, H. H. G. (2009). HESS Opinions "The art of hydrology". *Hydrol. Earth Syst. Sci.* 13, 157–161. doi:10.5194/hessd-5-3157-2008

Shanley, J. B., and Chalmers, A. (1999). The effect of frozen soil on snowmelt runoff at Sleepers River, Vermont. *Hydrol. Process.* 13, 1843–1857. doi:10.1002/(SICI)1099-1085(199909)13:12/13<1843::AID-HYP879>3.0.CO;2-G

Sivapalan, M., Bloschl, G., Zhang, L., and Vertessy, R. (2003). Downward approach to hydrological prediction. *Hydrol. Process.* 17, 2101–2111. doi:10.1002/hyp.1425

Smith, A., Tetzlaff, D., Laudon, H., Maneta, M., and Soulsby, C. (2019). Assessing the influence of soil freeze-thaw cycles on catchment water storage-flux-age interactions using a tracer-aided ecohydrological model. *Hydrol. Earth Syst. Sci.* 23, 3319–3334. doi:10.5194/hess-23-3319-2019

Song, C. L., Wang, G. X., Mao, T. X., Dai, J. C., and Yang, D. Q. (2020). Linkage between permafrost distribution and river runoff changes across the Arctic and the Tibetan Plateau. *Sci. China Earth Sci.* 63, 292–302. doi:10.1007/s11430-018-9383-6

Sun, A. L., Yu, Z. B., Zhou, J., Acharya, K., Ju, Q., Xing, R. F., et al. (2020). Quantified hydrological responses to permafrost degradation in the headwaters of the Yellow River (HWYR) in High Asia. *Sci. Total Environ.* 712, 135632. doi:10.1016/j.scitotenv.2019.135632

Sun, Q. H., Miao, C. Y., Duan, Q. Y., Ashouri, H., Sorooshian, S., and Hsu, K. L. (2018). A review of global precipitation data sets: data sources, estimation, and intercomparisons. *Rev. Geophys.* 56, 79–107. doi:10.1002/2017RG000574

Walvoord, M. A., and Kurylyk, B. L. (2016). Hydrologic impacts of thawing permafrost-A review. *Vadose Zone J.* 15. doi:10.2136/vzj2016.01.0010

Wan, C. W., Gibson, J. J., Shen, S. C., Yi, Y., Yi, P., and Yu, Z. B. (2019). Using stable isotopes paired with tritium analysis to assess thermokarst lake water balances in the Source Area of the Yellow River, northeastern Qinghai-Tibet Plateau, China. *Sci. Total Environ.* 689, 1276–1292. doi:10.1016/j.scitotenv.2019.06.427

Wang, G. X., and Zhang, Y. S. (2016). *Ecohydrology in cold regions: theory and practice.* Beijing: Science Press.

Wang, C., Yang, K., and Zhang, F. (2020). Impacts of soil freeze–thaw process and snow melting over Tibetan plateau on asian summer monsoon system: a review and perspective. *Front. Earth Sci.* 8:133. doi:10.3389/feart.2020.00133

Wang, G. X., Li, Y. S., Wu, Q. B., and Wang, Y. B. (2006). Impacts of permafrost changes on alpine ecosystem in Qinghai-Tibet Plateau. *Sci. China Earth Sci.* 49, 1156–1169. doi:10.1007/s11430-006-1156-0

Wang, G. X., Lin, S., Hu, Z. Y., Lu, Y. Q., Sun, X. Y., and Huang, K. W. (2020). Improving actual evapotranspiration estimation integrating energy consumption for ice phase change across the Tibetan plateau. *J. Geophys. Res. Atmos.* 125. doi:10.1029/2019JD031799

Wang, G. X., Liu, L. A., Liu, G. S., Hu, H. C., and Li, T. B. (2010). Impacts of grassland vegetation cover on the active-layer thermal regime, Northeast Qinghai-Tibet Plateau, China. *Permafr. Periglac. Process.* 21, 335–344. doi:10.1002/ppp.699

Wang, G. X., Mao, T. X., Chang, J., Song, C. L., and Huang, K. W. (2017). Processes of runoff generation operating during the spring and autumn seasons in a permafrost catchment on semi-arid plateaus. *J. Hydrol.* 550, 307–317. doi:10.1016/j.jhydrol.2017.05.020

Wang, N. L., Zhang, S. B., He, J. Q., Pu, J. C., Wu, X. B., and Jiang, X. (2009). Tracing the major source area of the mountainous runoff generation of the Heihe River in northwest China using stable isotope technique. *Chin. Sci. Bull.* 54, 2751–2757. doi:10.1007/s11434-009-0505-8

Wang, Y. H., Yang, H. B., Gao, B., Wang, T. H., Qin, Y., and Yang, D. W. (2018). Frozen ground degradation may reduce future runoff in the headwaters of an inland river on the northeastern Tibetan Plateau. *J. Hydrol.* 564, 1153–1164. doi:10.1016/j.jhydrol.2018.07.078

Woo, M. K., Kane, D. L., Carey, S. K., and Yang, D. Q. (2008). Progress in permafrost hydrology in the new millennium. *Permafr. Periglac. Process.* 19, 237–254.

Wu, Y. H., and Zhu, L. P. (2008). The response of lake-glacier variations to climate change in Nam Co Catchment, central Tibetan Plateau, during 1970-2000. *J. Geogr. Sci.* 18, 177–189. doi:10.1007/s11442-008-0177-3

Wu, P., Liang, S. H., Wang, X. S., Mckenzie, J. M., and Feng, Y. Q. (2020a). Climate change impacts on cold season runoff in the headwaters of the Yellow River considering frozen ground degradation. *Water.* 12, 602. doi:10.3390/w12020602

Wu, Q. B., Li, Z. J., and Shen, Y. P. (2020b). Cryosphere engineering science supporting interactivity infrastructures construction. *Bull. Chin. Acad. Sci.* 35, 443–449. doi:10.16418/j.issn.1000-3045.20200301001

Wu, S. H., Jansson, P. E., and Zhang, X. Y. (2011). Modelling temperature, moisture and surface heat balance in bare soil under seasonal frost conditions in China. *Eur. J. Soil Sci.* 62, 780–796. doi:10.1111/j.1365-2389.2011.01397.x

Wu, T. H., Li, S. X., Cheng, G. D., and Nan, Z. T. (2005). Using ground-penetrating radar to detect permafrost degradation in the northern limit of permafrost on the Tibetan Plateau. *Cold Reg. Sci. Technol.* 41, 211–219. doi:10.1016/j.coldregions.2004.10.006

Xiang, L. W., Wang, H. S., Steffen, H., Wu, P., Jia, L. L., Jiang, L. M., et al. (2016). Groundwater storage changes in the Tibetan Plateau and adjacent areas revealed from GRACE satellite gravity data. *Earth Planet Sci. Lett.* 449, 228–239. doi:10.1016/j.epsl.2016.06.002

Xiao, Y., Zhao, L., Dai, Y. J., Li, R., Pang, Q. Q., and Yao, J. M. (2013). Representing permafrost properties in CoLM for the Qinghai-Xizang (Tibetan) plateau. *Cold Reg. Sci. Technol.* 87, 68–77. doi:10.1016/j.coldregions.2012.12.004

Xie, C. W., and Gough, W. A. (2013). A simple thaw-freeze algorithm for a multi-layered soil using the stefan equation. *Permafr. Periglac. Process.* 24, 252–260. doi:10.1002/ppp.1770

Yang, D., Herath, S., and Musiake, K. (1998). Development of a geomorphology-based hydrological model for large catchments. *Ann. J. Hyd. Eng. JSCE* 42, 169–174.

Yang, K., Qin, J., Zhao, L., Chen, Y. Y., Tang, W. J., Han, M. L., Lazhu Chen, Z. Q., Lv, N., Ding, B. H., Wu, H., and Lin, C. G. (2013). A multiscale soil moisture and freeze-thaw monitoring network ON the third POLE. *Bull. Am. Meteorol. Soc.* 94, 1907–1916. doi:10.1175/BAMS-D-12-00203.1

Yang, K., Wu, H., Qin, J., Lin, C. G., Tang, W. J., and Chen, Y. Y. (2014). Recent climate changes over the Tibetan Plateau and their impacts on energy and water cycle: a review. *Global Planet. Change.* 112, 79–91. doi:10.1016/j.gloplacha.2013.12.001

Yang, M. X., Nelson, F. E., Shiklomanov, N. I., Guo, D. L., and Wan, G. N. (2010). Permafrost degradation and its environmental effects on the Tibetan Plateau: a review of recent research. *Earth Sci. Rev.* 103, 31–44. doi:10.1016/j.earscirev.2010.07.002

Yang, M. X., Yao, T. D., Gou, X. H., Koike, T., and He, Y. Q. (2003). The soil moisture distribution, thawing-freezing processes and their effects on the seasonal transition on the Qinghai-Xizang (Tibetan) plateau. *J. Asian Earth Sci.* 21, 457–465. doi:10.1016/S1367-9120(02)00069-X

Yang, Y., Chen, R. S., Ye, B. S., Song, Y. X., Liu, J. F., Han, C. T., et al. (2013). Heat and water transfer processes on the Typical underlying surfacesof frozen soil in cold regions (I): model comparison. *J. Glaciol. Geocryol.* 35, 1545–1554.

Yang, Y. Z., Wu, Q. B., Jin, H. J., Wang, Q. F., Huang, Y. D., Luo, D. L., et al. (2019). Delineating the hydrological processes and hydraulic connectivities under permafrost degradation on Northeastern Qinghai-Tibet Plateau, China. *J. Hydrol.* 569, 359–372. doi:10.1016/j.jhydrol.2018.11.068

Ye, B. S., Yang, D. Q., Zhang, Z. L., and Kane, D. L. (2009). Variation of hydrological regime with permafrost coverage over Lena Basin in Siberia. *J. Geophys. Res. Atmos.* 114. doi:10.1029/2008JD010537

Yi, S. H., Woo, M. K., and Arain, M. A. (2007). Impacts of peat and vegetation on permafrost degradation under climate warming. *Geophys. Res. Lett.* 34. doi:10.1029/2007GL030550

You, Q. L., Wu, T., Shen, L. C., Pepin, N., Zhang, L., Jiang, Z. H., et al. (2020). Review of snow cover variation over the Tibetan Plateau and its influence on the broad climate system. *Earth Sci. Rev.* 201. doi:10.1016/j.earscirev.2019.103043

Yu, L. Y., Zeng, Y. J., Wen, J., and Su, Z. B. (2018). Liquid-vapor-air flow in the frozen soil. *J. Geophys. Res. Atmos.* 123, 7393–7415. doi:10.1029/2018JD028502

Yu, Q. H., Pan, X. C., Cheng, G. D., and He, N. W. (2008). An experimental study on the cooling mechanism of a shading board in permafrost engineering. *Cold Reg. Sci. Technol.* 53, 298–304. doi:10.1016/j.coldregions.2007.07.003

Zeng, Y. J., Su, Z. B., Van Der Velde, R., Wang, L. C., Xu, K., Wang, X., et al. (2016). Blending satellite observed, model simulated, and *in situ* measured soil moisture over Tibetan plateau. *Rem. Sens.* 8, 268. doi:10.3390/rs8030268

Zhang, G. Q., Yao, T. D., Piao, S. L., Bolch, T., Xie, H. J., Chen, D. L., et al. (2017). Extensive and drastically different alpine lake changes on Asia's high plateaus during the past four decades. *Geophys. Res. Lett.* 44, 252–260. doi:10.1002/2016GL072033

Zhang, T. (2005). Influence of the seasonal snow cover on the ground thermal regime: an overview, *Rev. Geophys.* 43, RG4002. doi:10.1029/2004RG000157

Zhang, T. J., Jin, R., and Gao, F. (2009). Overview of the satellite remote sensing of frozen ground: visible-thermal infrared and radar sensor. *Adv. Earth Sci.* 24, 963–972. doi:10.1080/789610186

Zhang, Y. L., Cheng, G. D., Li, X., Han, X. J., Wang, L., Li, H. Y., et al. (2013). Coupling of a simultaneous heat and water model with a distributed hydrological model and evaluation of the combined model in a cold region watershed. *Hydrol. Process.* 27, 3762–3776. doi:10.1002/hyp.9514

Zhang, Y. S., and Guo, Y. (2011). "Water cycle changes during the past 50 years over the Tibetan Plateau: review and synthesis," in *Cold regions hydrology in a changing climate.* Editors D. Yang, P. Marsh, and A. Gelfan, 130–135.

Zhang, Y. S., Ohata, T., and Kadota, T. (2003). Land-surface hydrological processes in the permafrost region of the eastern Tibetan Plateau. *J. Hydrol.* 283, 41–56. doi:10.1016/S0022-1694(03)00240-3

Zhang, Z., and Wu, Q. (2012). Predicting changes of active layer thickness on the Qinghai-Tibet Plateau as climate change. *J. Glaciol. Geocryol.* 34 (3), 506–511

Zhao, J. Y., Chen, J., Wu, Q. B., and Hou, X. (2018). Snow cover influences the thermal regime of active layer in Urumqi River Source, Tianshan Mountains, China. *J. Mountain Sci.* 15 (12). doi:10.1007/s11629-018-4856-y

Zhao, L., Zou, D., Hu, G., Du, E., Pang, Q., Xiao, Y., et al. (2020). Changing climate and the permafrost environment on the Qinghai–Tibet (Xizang) plateau. *Permafr. Periglac. Process.* 31, 396–405. doi:10.1002/ppp.2056

Zhao, L., Hu, G. J., Zou, D. F., Wu, X. D., Ma, L., Sun, Z., et al. (2019). Permafrost changes and its effects on hydrological processes on Qinghai-Tibet Plateau. *Bull. Chin. Acad. Sci.* 34, 1233–1246. doi:10.16418/j.issn.1000-3045.2019.11.006

Zheng, D., Wang, X., Velde, R. V. D., Zeng, Y., Wen, J., Wang, Z., et al. (2017). L-band microwave emission of soil freeze–thaw process in the third pole environment. *Remote Sens. Environ.* 55, 5324–5338. doi:10.1109/TGRS.2017.2705248

Zhou, J., Kinzelbach, W., Cheng, G., Zhang, W., He, X., and Ye, B. (2013). Monitoring and modeling the influence of snow pack and organic soil on a permafrost active layer, Qinghai–Tibetan Plateau of China. *Cold Reg. Sci. Technol.* 90-91, 38–52. doi:10.1016/j.coldregions.2013.03.003

Zhou, J., Pomeroy, J. W., Zhang, W., Cheng, G. D., Wang, G. X., and Chen, C. (2014). Simulating cold regions hydrological processes using a modular model in the west of China. *J. Hydrol.* 509, 13–24. doi:10.1016/j.jhydrol.2013.11.013

Zhou, J. X., Wu, J. K., Liu, S. W., Zeng, G. X., Qin, J., Wang, X. N., et al. (2015). Hydrograph separation in the headwaters of the shule river basin: combining water chemistry and stable isotopes. *Adv. Meteorol.* 2015, 1–10. doi:10.1155/2015/830306

Zhou, J., Zhang, W., Pomeroy, J., Cheng, G. D., Wang, G. X., Chen, C., et al. (2013). Simulating the cold regions hydrological processes in Northwest China with modular modeling method. *J. Glaciol. Geocryol.* 35, 389–400. doi:10.1016/j.jhydrol.2013.11.013

Zhou, X. H., Zhou, J., Kinzelbach, W., and Stauffer, F. (2014). Simultaneous measurement of unfrozen water content and ice content in frozen soil using gamma ray attenuation and TDR. *Water Resour. Res.* 50, 9630–9655. doi:10.1002/2014WR015640

Zou, D., Zhao, L., Sheng, Y., Chen, J., Hu, G., Wu, T., et al. (2017). A new map of permafrost distribution on the Tibetan Plateau. *Cryosphere.* 11, 2527–2542. doi:10.5194/tc-11-2527-2017

Conflict of Interest: The authors declare that the research was conducted in the absence of any commercial or financial relationships that could be construed as a potential conflict of interest.

Advantages of publishing in Frontiers

OPEN ACCESS
Articles are free to read for greatest visibility and readership

FAST PUBLICATION
Around 90 days from submission to decision

HIGH QUALITY PEER-REVIEW
Rigorous, collaborative, and constructive peer-review

TRANSPARENT PEER-REVIEW
Editors and reviewers acknowledged by name on published articles

Frontiers
Avenue du Tribunal-Fédéral 34
1005 Lausanne | Switzerland

Visit us: www.frontiersin.org
Contact us: frontiersin.org/about/contact

REPRODUCIBILITY OF RESEARCH
Support open data and methods to enhance research reproducibility

DIGITAL PUBLISHING
Articles designed for optimal readership across devices

FOLLOW US
@frontiersin

IMPACT METRICS
Advanced article metrics track visibility across digital media

EXTENSIVE PROMOTION
Marketing and promotion of impactful research

LOOP RESEARCH NETWORK
Our network increases your article's readership